Rehabilitation Engineering

Rehabilitation Engineering

Edited by
Tan Yen Kheng

In-Tech
intechweb.org

Published by In-Teh

In-Teh
Olajnica 19/2, 32000 Vukovar, Croatia

www.intechweb.org
Additional copies can be obtained from:
publication@intechweb.org

First published December 2009
Printed in India

Technical Editor: Melita Horvat

Rehabilitation Engineering,
Edited by Tan Yen Kheng

p. cm.
ISBN 978-953-307-023-0

Preface

All around the world, the age distribution of the world population is shifting towards older ages, causing an increase in the world population's mean or median age. The corresponding figures for the world population's mean age as a whole are 23.9 for 1950, 26.8 for 2000, and 37.8 for 2050 (United Nations, 2004). The growing trend of the world population's mean age is largely due to the decline in the fraction of the population composed of children (declining fertility) and the rise in the fraction of the population that is elderly (due to longer life expectancy). The impact of population ageing on developed countries with strong economy strongholds, such as United States of America (USA) and Japan, is even more severe. To a certain extent, Singapore, serving as a Southeast Asia's financial and high-tech hub, is also affected as well. According to statistic, in the year 2013, the percentage of elderly people is forecasted to be 25 percent of the total population in Japan.

Population ageing has major consequences and implications in all areas of our daily life as well as other important aspects such as economic growth, savings, investment and consumption, labour markets, pensions, property and care from one generation to another. Additionally, health and related care, family composition and life-style, housing and migration are also affected. Given the rapid increase in the aging of the population and the further increase that is expected in coming years, an important problem that has to be faced is the corresponding increase in chronic illness, disabilities, and loss of functional independence endemic to the elderly (WHO 2008). For this reason, novel methods of rehabilitation and care management are urgently needed.

Rehabilitation means different things in different cases. For home-based rehabilitation, the new trend is to rely on the virtual reality technology because of its inherent ability to simulate real-life tasks. Virtual reality (VR) is a young and growing field. It allows users to interact with virtual objects in a near natural way through different interface devices using their natural senses of vision, audition and taction. The interaction makes users feel immersed in the virtual environment as if they are surrounded in a real world. With the inheriting simulation capability, virtual reality can bring the physical world into the controlled environment. Therefore, the virtual reality based system can implement performance analysis from different aspects, and give the feedbacks to users in real time. Preliminary analyses and useful results can be stored in the computer as references for specialist. The specialist may then adjust training parameters and levels for appropriate self-practicing according to the need of individual patients. It is also possible to develop a system for tele-rehabilitation to allow services from a remote location, while patients remain in their home settings. The scenario of applications demonstrating the potential for remote diagnosis and treatment through robot-aided telerehabilitation is quite recent. The specialist may provide professional guidance remotely to avoid the drawbacks of self-training in rehabilitation.

Many rehabilitation support systems and robots have been developed for upper limbs, lower limbs as well as visually impaired condition. The advantage using the robots and the systems are that the patients can perform effective rehabilitation trainings and the therapeutic effect can be evaluated quantitatively. Braille alphabet system, created by Louis Braille (1821), for visually impaired or blind people to write and read via touching is one good example of a rehabilitation support system. A Braille character consists of six or eight dots in a rectangular array 3x2 or 4x2. The dot may rise at any position based on a character mapping code. The character mappings are coded differently depended on languages. No matter what the language is, most of written communication today trends to be in electronic forms, for examples, report, manuscript, email, SMS, blog or website. Refreshable electronic Braille display is designed for display those electronic media in the Braille format. Height of the Braille dot is controlled by a piezoelectric bimorph underneath. Electrical signals stimulate the piezoelectric bimorphs to bend up or down, consequently causing the dots to rise or fall, forming the Braille characters. This allows blind users to read by touching as alternative to listening to the screen reading or text-to-speech software, such as WebAnywhere for English language and PPA Tatip for Thai language.

Another rehabilitation support system for various resistance trainings of upper limb motor function is recorded. This system, equipped with the teaching/guided function for personalized rehabilitation, supports the occupational therapy for recovering physical functions. The teaching/guided function enables the therapists to easily make not only training trajectories but also training programs to suit the individual needs of the patients. Other than upper limbs, the lower limb research works are also discussed like motorized foot rest for electric powered wheelchair and standing assistance device.

The editor would like to thank all authors for their contribution and all those people who directly or indirectly helped make this work possible, especially Vedran Kordic who was responsible for the coordination of this project.

Editor

Tan Yen Kheng

Contents

Preface V

1. Virtual Reality in Rehabilitation 001
Xiaoli Yang (Ph.D.), Associate Professor

2. Augmented Reality Musical System for Rehabilitation of Patients with Duchenne Muscular Dystrophy 013
Ana Grasielle Dionísio Corrêa, Adriana Nathalie Klein and Roseli de Deus Lopes

3. Development of a Systems Architecture for Robot-Aided Telerehabilitation 037
Roberto Colombo

4. Analysis and Design of Piezoelectric Braille Display 049
Pruittikorn Smithmaitrie

5. Stereo Vision Utilizing Parallel Computing for the Visually Impaired 063
Pichaya Tandayya, Thanathip Limna and Nikom Suvonvorn

6. Engineering Better Electric-Powered Wheelchairs To Enhance Rehabilitative and Assistive Needs of Disabled and Aged Populations 079
Yen Kheng Tan and Sangit Sasidhar

7. A Rehabilitation Walker with a Standing Assistance Device 109
Daisuke Chugo and Kunikatsu Takase

8. Lower Extremity Joint Moments during Squat and Stoop Lifting 129
Seonhong Hwang, Youngeun Kim and Youngho Kim

9. Acetabular loading in rehabilitation 139
Hana Debevec, Aleš Iglič, Veronika Kralj-Iglič and Matej Daniel

10. The Lognormal Framework in the Context of Human Movement Rehabilitation 157
Christian O'Reilly and Réjean Plamondon

11. Quantitative Evaluation Methods of Therapeutic Effects of Sanding Training in Patients with Hemiplegia 173
Yoshifumi Morita and Hiroyuki Ukai

12. Quasi-3 DOF Rehabilitation System for Upper Limbs, "PLEMO" 187
Takehito Kikuchi and Junji Furusho

13. Wearable Robots in Rehabilitation Engineering Tremor Suppression 203
E. Rocon, J.C. Moreno, J.A. Gallego and J.L. Pons

14. Processing surface electromyographical signals for myoelectric control 223
Sorin Herle and Sergiu Man

15. A 6-DOF Rehabilitation System for Upper Limbs “Robotherapist”and Other Rehabilitation Systems with High Safety 245
Junji Furusho and Ying Jin

1

Virtual Reality in Rehabilitation

Xiaoli Yang (Ph.D.), Associate Professor
Department of Electrical and Computer Engineering, Purdue University Calumet

1. Stroke and rehabilitation

Rehabilitation means different things in different cases. In this chapter, the term is referred to as post-stroke treatment for recovery purposes. According to the World Health Organization, 15 million people suffer stroke worldwide each year [The Internet Stroke Center; and Patient @UK stroke]. In the United States, stroke is the leading cause of serious, long-term disability and also the third leading cause of death [NIH post-stroke rehabilitation]. Though the effect differs on survivors, stroke might leave patients with brain damage, paralysis or some dysfunctions such as limb's stiffness and tightness and losing balance. These effects may seriously weaken survivors' capabilities of controlling movements, using languages, and memorizing, thus, leaving them with residual disabilities. Proper rehabilitation is essential for helping stroke survivors progressively rebuild capability and relearn skills that have been lost due to brain impairment. The aim of rehabilitation is therefore to maximize activity and quality of life. Although short and intensive rehabilitation is critically important following a stroke, continuous and repetitive rehabilitation is essential to help survivors achieve the best possible long-term outcomes with the goal of reaching the highest possible level of independence in daily living activities which require skills of mobility, communication, and social interactions [Stroke and rehabilitation education]. Basically, rehabilitation employs the same technique as that used for teaching new skills.

As an ongoing process, repetition in rehabilitation is to maintain and refine the learned skills for a long period of time typically in months or years after the stroke. The right direction is provided by specialists since symptoms and disabilities following a stroke vary greatly depending on such factors as the part of the brain affected, the time elapsed between the stroke and the treatment, and the extent of the damage. Progress and recovery are therefore unique for each person due to the complexity of individual cases. Although rehabilitation centers with trained professionals and facilities are ideal for stroke survivors to regain their living skills, certain situations, such as transportation and financial problems, may prevent them from accessing to the centers. In such cases, self-directed rehabilitation may be continued at home. However, self-directed exercises at home often lack professional guidance and quantitative feedbacks. To circumvent these problems, an innovative rehabilitation system allowing guided self-training in home settings will be beneficial to many stroke survivors.

2. Virtual reality in rehabilitation

To develop an innovative system of home-based rehabilitation, the new trend is to rely on the virtual reality technology because of its inherent ability to simulate real-life tasks [Adamovich et al., 2005; Boian et al., 2002; Yang et al., 2008]. Virtual reality (VR) is a young and growing field. It allows users to interact with virtual objects in a near natural way through different interface devices using their natural senses of vision, audition and taction. The interaction makes users feel immersed in the virtual environment as if they are surrounded in a real world [Burdea & Coiffet, 2003]. The growing technologies along with concomitant system cost reductions have benefited many fields such as education, medical training and health care, manufacturing, military, and entertainment. An advantage of virtual reality is that it allows individuals to easily vary training parameters and to explore effective scenes that may be difficult or unsafe to construct in the real world. Furthermore, a fully immersive virtual environment mimics reality exceptionally well. VR is especially useful for systems which depend heavily on visualization and experimentation for practicing. As more advanced technologies are developed, new applications ensue. The virtual reality based rehabilitation training is one of the advancing and emerging research fields.

Compared to the traditional rehabilitation method, the VR based system has several advantages, which include the ability for individual setups, ease of adjustment, capability of measurement and performing feedback, and the inclusion of stimulus features. The software based rehabilitation exercises are easier and faster to setup than utilizing the traditional rehabilitation facilities. Individual practice sessions can be customized to suit individual needs according to different dysfunctions and injury levels through computer programming.

Specific software programs may be developed for measuring, quantifying, evaluating, and data storage. With the inheriting simulation capability, virtual reality can bring the physical world into the controlled environment. Therefore, the virtual reality based system can implement performance analysis from different aspects, and give the feedbacks to users in real time. Preliminary analyses and useful results can be stored in the computer as references for specialist. The specialist may then adjust training parameters and levels for appropriate self-practicing according to the need of individual patients. It is also possible to develop a system for tele-rehabilitation to allow services from a remote location, while patients remain in their home settings [Holden et al., 2007]. The specialist may provide professional guidance remotely to avoid the drawbacks of self-training in rehabilitation.

As mentioned earlier, an important factor in rehabilitation is repetition. Users may easily experience boredom for keeping on practicing the same exercise without any stimulus. To attract their attention during the repetitive training session is an important element for increasing the training efficiency and obtaining successful recovery results. It is straightforward to develop either real-life or game-like exercises to attract users by providing interesting scenes and challenging tasks for competing with the computer or other users.

3. Representative work on virtual reality based rehabilitation

Several studies have demonstrated the effectiveness of virtual environments in the treatment of motor skills impairments.

3.1 Upper extremity function rehabilitation by imitation

Holden and colleagues at the Massachusetts Institute of Technology developed a virtual environment based tele-rehabilitation system for improving upper extremity function for patients with stroke [Holden et al., 2007].

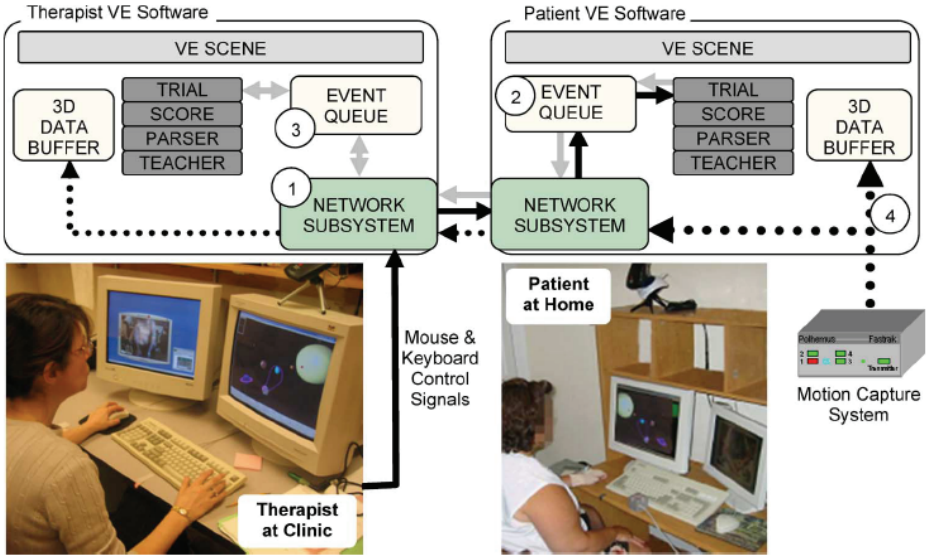

Fig. 1. Schematic of the home-based virtual reality tele-rehabilitation system. Patient and therapist can see and hear each other via a teleconferencing link on a monitor. Motion capture equipment transmits information about patient's arm movements to the virtual reality display. Therapist in the clinic controls the software and views the same virtual scene as that displayed to the patient in her home (second monitor). Video camera allows the therapist to remotely view any part of the patient's workspace. [Holden et al., 2007]

The system (Fig. 1) is to help stroke patients regain upper extremity function through tele-rehabiliation. It employs 2-3 Polhemus sensors attached to the patient with one on the back of the hand, one on the upper arm, and an optional sensor on a held object to capture the motion of the upper extremity. With an algorithm model, the software can generate a "virtual upper extremity" of the arm that infers shoulder, elbow and wrist locations and orientations according to individual setups. The patient can sit in front of a computer with two monitors-one for the virtual environment scene and the other for the videoconference image of the therapist. With the small sized movement parameter data transmitted through the network, the practicing procedure can be synchronously remodeled, viewed and

controlled by the remote therapist. This real-time remodel feature along with the videoconference can provide a rich interactive training program.
The training procedure is to help patients relearn the upper extremity function by imitation. In theory, this should facilitate motor learning by assisting the patient's motor planning process in a natural way. Several "learning by imitation" examples are available [Holden et al., 2001, 2005]. Fig. 2 shows an example of standard training scenes, and Fig. 3 displays additional scenes designed for individual needs. Fig. 4 shows an example of the score calculation and parameters adjustments for different aspects of the patient's performance (e.g., spatial elements, speed, timing, and velocity profile). The score representing the "match" with the teacher's trajectory is displayed in real time for each patient.

The left column shows the virtual reality scene.
The right column shows a schematic of the subject's movement in the real world that the scene is designed for training.
Top panel: Mailbox scene, for learning to reach into into the workspace
Middle panel: SleevePull, training a hand-to-body movement. The score indicator is for showing previous movement at below target performance level.
Bottom panel: Clock, for training repeated reciprocal movement (supination/pronation).

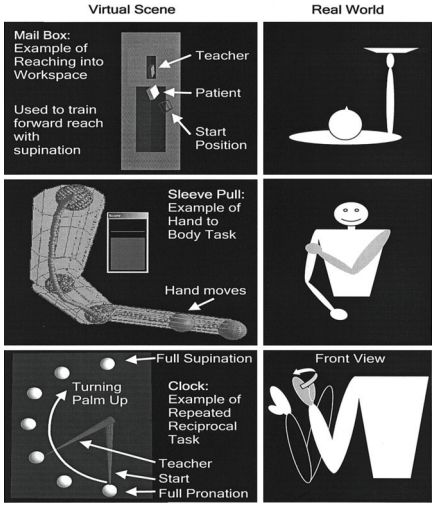

Fig. 2. Examples of three standard training scenes used by all subjects [Holden et al., 2005]

Top panel, scenes used for subject 1 to enhance control of wrist extension, without (left) and with (right) grasp.
Bottom panel, customized scenes used by subject 2. Left: scene allowed practice of elbow extension with shoulder flexion and adduction. Right: practice of isolated shoulder external rotation in neutral flexion/abduction with elbow flexion.

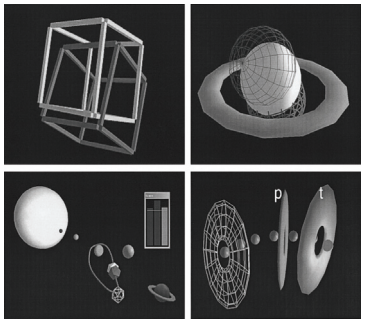

Fig. 3. Examples of additional scenes designed for individual needs[Holden et al., 2005]

Results of the clinical study on subjects with stroke showed significant improvements in upper extremity function following 30 1-h virtual reality treatment sessions as measured by three standard clinical tests: Fugl–Meyer test of motor recovery, Wolf motor test (WMT), and shoulder strength test. Grip strength (GS) showed a trend toward improvement. These changes were maintained, for the most parts, at four-month follow-up.

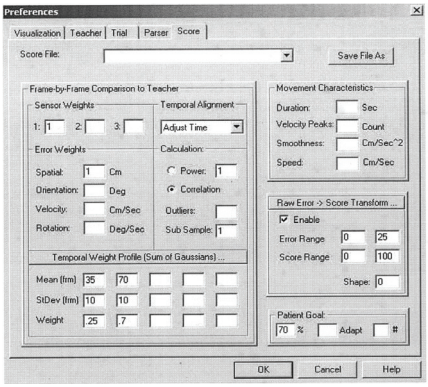

Fig. 4. Score-preferences panel in which all score settings are accessed[Holden et al., 2005]

3.2 Rehabilitation with specially designed hardware

Researchers at Rutgers developed several systems for post-stroke patients. One system is virtual reality based hand manipulation rehabilitation with two versions [Adamovich et al., 2005; Morrow et al., 2006]. The first version utilizes CyberGlove and Rutgers Master II-ND haptic glove. Based on this work, a second version of a low cost hardware is setup with a modified Xbox that runs the training practices. A P5-glove is used to measure the flexion of all fingers as well as the wrist 3D position. The experimental system set up is shown in Fig. 5. Game tasks used for stimulating users' interests are to train finger motions with respect to speed, range, fractionation and strength. Examples of training scenes are displayed in Fig. 6. Their pilot study seems to indicate that this virtual reality based rehabilitation application may improve hand function in chronic hemiplegic patients.

Fig. 5. Overall view of the experimental low-cost finger training system [Morrow et al., 2006]

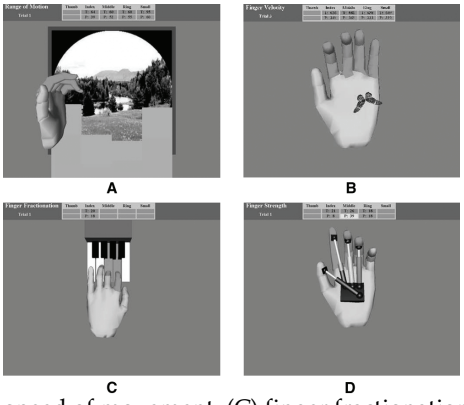

(A) range of motion, (B) speed of movement, (C) finger fractionation, (D) finger strength
Fig. 6. Screen snapshots of four VR exercises [Adamovich et al., 2005]

Another system of "Rutgers Ankle" is for patients with lower-extremity dysfunction [Boian et al., 2002; Deutsch et al., 2001; Lewis et al., 2003; Whitworth et al., 2003]. The main component is a Stewart platform haptic interface that reads foot position and orientation for applying resistant forces. The system also includes the low-level servo control of the platform and the high-level software such as graphical user interface for rehabilitation [Deutsch et al., 2001]. Fig. 7 displays the hardware setup and Fig. 8 shows two virtual reality exercises. From the testing studies taken by chronic post-stroke individuals, it appears that some improvements have been made through the system training.

(a) the rehabilitation system setup showing the PC monitor and the web-based monitoring display

(b) the Rutgers Ankle device

Fig. 7. The VR-based ankle rehabilitation system [Boian et al., 2002]

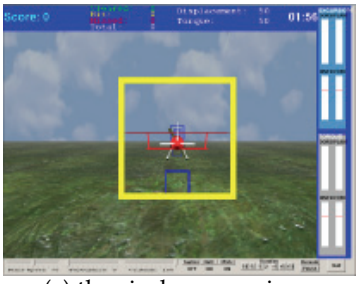

(a) the airplane exercise

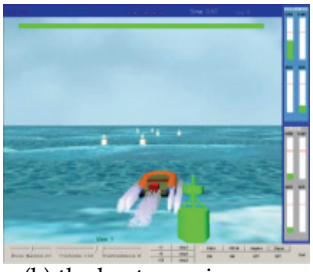

(b) the boat exercise

Fig. 8. Virtual reality exercise simulations [Lewis et al., 2003]

3.3 Hand motor recovery systems with Phantom haptics

Four VR based hand rehabilitation applications (virtual phone dialing, virtual writing, virtual painting, and tele-hockey game) are illustrated below. All were developed by Yang and associates at Purdue University Calumet [Kim et al., 2006, 2007; Yang et al., 2007, 2008].

3.3.1 Virtual phone dialing

Phone dialing is an important part of routine daily life. A virtual phone dialing training application was developed to train users to dial the telephone numbers within a specified period of time [Yang et al., 2008]. The system focuses on training hand movement with precision, speed, and appropriate pressing force. The Phantom premium 1.0 haptic device provides users with feedback as if they were touching the buttons on the real phone. The haptic is represented with a virtual hand along with a virtual phone and other graphic features in the user interface. Once a training session starts, the user needs to press eight buttons chosen by the system randomly within a specified time period. Fig. 9 shows a training scene.

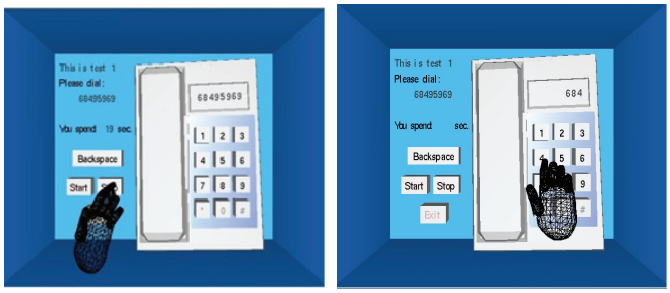

Fig. 9. Virtual phone dialing [Yang et al., 2008]

3.3.2 Virtual writing

Writing requires a fine motor skill which involves hand movement adeptness together with a coordinated hand-eye movement. Different hand-writing training systems have been developed for different purposes such as learning of writing Chinese characters, Japanese calligraphy, or following writing trajectories [Avizzano et al., 2002; Saga et al., 2005; Teo et al., 2002].

The developed virtual writing system is to help recover hand motor skills through real time guiding forces from the Phantom Premium 1.0 haptic device - [Kim et al., 2006, 2007]. The haptic device guides the user's hand to follow the preset English letter trajectory. The guiding force calculated with the developed algorithm is proportional to the distance deviated from the trajectory. The algorithm recognizes the 26 letters based on two categories (straight and curved strokes) and calculates forces accordingly [Yang et al., 2008]. Users may choose any one of the 26-English alphabet letters, and the letter with pre-drawn trajectory will then be displayed on a virtual paper. The system analyzes several training parameters of force, completeness, and correctness in real time. The results are recorded in the database for future reference. Fig. 10 shows a practicing scene of writing letter A in the virtual environments.

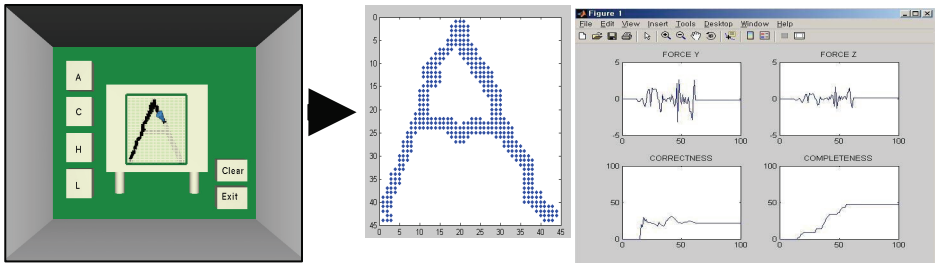

Fig. 10. Virtual writing with real time performance feedbacks [Kim et al., 2007]

3.3.3 Virtual painting

Virtual painting is for improving hand control precision and movement speed. The virtual environment includes mainly a virtual flower composed of thousands of triangle meshes and other graphic user interface features such as buttons, and color options. The Phantom Premium 1.0 haptic device is represented with a virtual pen in the environment. It is developed as a game exercise. Once the user presses the "start" button, a random triangle will be flashing and waiting for the person to paint on the screen and make color changes. The position and time spent on implementing each task is shown to the user as well as recorded in a database for future reference. According to individual needs, levels of tasks can be set with different speed and pedal size. To provide the user with the more realistic touching feeling, a new collision detection algorithm was developed with an efficient triangle management[Yang et al., 2008].

Fig. 11. shows a practicing scene with a virtual flower and a virtual pen. The user is in control of starting and stopping training times. The painted part and the duration of the exercise are shown throughout the training session.

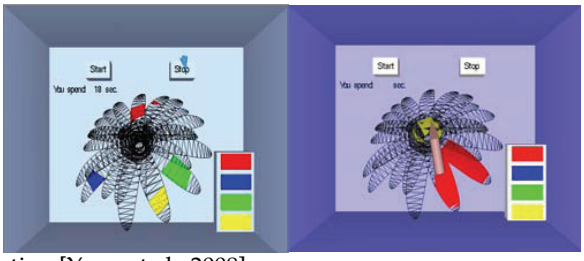

Fig. 11. Virtual painting [Yang et al., 2008]

3.3.4 Tele-hockey game

A tele-hockey game scene was developed for hand motor skill training. It is mainly for stimulating users' interests in a game environment. The virtual scene includes one hockey ball controlled by the system plus two others controlled by users. Each user controls one virtual ball and competes with each other for hitting the ball controlled by system. Two haptic devices-Phantom Omnis are used to give users force feedbacks when they hit the virtual hockey ball. Different levels of difficulty may be set upon request. To avoid accidental scoring by uncontrolled hand shakings from some users, the system is able to filter out the unintentional hitting incident and record only the real practicing results including precision rate and speed [Yang et al., 2007]. Fig. 12 shows a practicing scene.

Fig. 12. Virtual tele-hockey game [Yang et al., 2007]

Volunteered normal human subjects have tested the above four training practices. Based on feedbacks, additional features, such as audio alert, the calculation of guiding force to hand in virtual writing, and adjustment of different levels of difficulties for different needs, have been included in the development. Clinical testing has not been performed for any of these systems, and thus no clinical data are available at this time.

4. Conclusions

In view of the examples presented, it is clear that different virtual reality based rehabilitation systems are useful for different purposes, since no one system can cover all aspects of rehabilitation. For example, a therapeutic environment for gesture analysis and recognition [Camurri et al., 2002] is useful for Parkinson's patients, whereas a web-based tele-rehabilitation system may be suitable for arm and hand therapy for stroke patients [Reinkensmeyer et al., 2002]. Virtual reality is valuable for not only motor rehabilitation but also for others such as psychological and cognitive rehabilitation [Rose et al., 2005; Takacs et al., 2007], as well as orthopedic rehabilitation [Akay et al., 2001; Burdea et al., 2008].
It is encouraging that virtual reality technologies have been successfully employed for helping the skill recovery of post-stroke patients. The advantages of combining virtual reality with rehabilitation have now been realized by the rehabilitation community. However, there is still insufficient clinical testing data to ensure the efficiency and safety of virtual rehabilitation for widespread clinical acceptance. Furthermore, whether virtual reality really influences the nervous system or whether moving within a virtual environment just motivates the individual to perform remains to be answered. Continued efforts and studies are needed for making progresses in this field.

5. References

Adamovich S., A. Merians, R. Boian , M. Tremaine, G. Burdea, M. Recce, and H. Poizner, [2005] "A Virtual Reality Based Exercise System for Hand Rehabilitation Post-Stroke", *Presence, Special Issue on Virtual Rehabilitation*, 14(2), 161-174.

Akay, M., A. Marsh, [2001], "Information Technologies in Medicine, Rehabilitation and Treatment", *Wiley-IEEE Press*, April 2001

Avizzano, C.A., Solis, J., Bergamasco, M. [2002] "Teaching to Write Japanese Characters using a Haptic Interface" in *Proc. of the 10th Symposium On Haptic Interfaces For Virtual Environment & Teleoperator Systems*.

Boian, R., A. Sharma, C. Han, A. Merians, G. Burdea, S. Adamovich, M. Recce, M. Tremaine, and H. Poizner, [2002] "Virtual Reality-Based Post Stroke Rehabilitation," in *Proc. of Medicine Meets Virtual Reality, IOS Press*, Newport Beach CA.

Boian, R.F., C.S. Lee, J.E. Deutsch, G. Burdea and J.A. Lewis [2002], "Virtual Reality-based System for Ankle Rehabilitation Post Stroke", *1st International Workshop on Virtual Reality Rehabilitation (Mental Health, Neurological, Physical, Vocational) VRMHR 2002* Lausanne, Switzerland, November 7-8, 2002, pp. 77-86.

Burdea G., P. Coiffet, "Virtual reality technology (2nd edn)", *Wiley, New York*, 2003. ISBN 0-471-36089-9

Burdea G., D. Fensterheim, D. Cioi and A. Arezki, [2008] "The Rutgers Arm II Rehabilitation System", *Proceedings of Virtual Rehabilitation 2008*, pp. 76, Vancouver Canada, August 25-27, 2008 (poster session).

Camurri, A., E. Cervetto, B. Mazzarino, P. Morasso, G. Ornato, F. Priano, C. Re, L. Tabbone, A. Tanzini, R. Trocca, and G. Volpe, [2002] "Application of multimedia techniques in the physical rehabilitation of parkinson's patients," in *Proc. of 1st. International Workshop on Virtual Reality Rehabilitation*, 65–75.

Deutsch, J., J. Latonio, G. Burdea and R. Boian,[2001] "Post-Stroke Rehabilitation with the Rutgers Ankle System - A case study," *Presence, Vol. 10(4), MIT Press,* August 2001.

Kim, Y.K., X. Yang, [2006] "Hand-writing Rehabilitation in the Haptic Virtual Environment", in *Proc. IEEE International Workshop on Haptic Audio Visual Environments and their Applications (HAVE 2006)*, Ottawa, Canada.

Kim, Y.K., X. Yang, [2007] "Real-time Performance Analysis of Hand Writing Rehabilitation Exercise in Haptic Virtual Reality", in *Proc. 20th Canadian Conference on Electrical and Computer Engineering (CCECE 2007)*, Vancouver, Canada.

Holden, M.K. [2001] "Neurorehabilitation using 'learning by imitation' in virtual environments". In: M.J. Smith et al. (Eds.), Usability Evaluation and Interface Design, Lawrence Erlbaum Associates, Inc. pp. 624-628

Holden, M.K., T.A. Dyar, L. Schwamm, E. Bizzi [2005], "Virtual-environment-based telerehabilitation in patients with stroke" *Presence-Teleoperators and Virtual Environments* 14 (2): 214-233.

Holden, M.K., T.A. Dyar, L. Dayan-Cimadoro, [2007] "Telerehabilitation using a virtual environment improves upper extremity function in patients with stroke", *Transactions on Neural Systems and Rehabilitation Engineering, 15(1): 36-42.*

Lewis, J., R.F. Boian, G.C. Burdea, J.E.Deutsch, "Real-time Web-based Telerehabilitation Monitoring ", *Proceeding of Medicine Meets Virtual Reality 11*, Newport Beach, CA, January 2003, IOS Press, pp. 190-192.

Morrow, K., C. Docan, G. Burdea, and A. Merians, [2006], "Low-cost Virtual Rehabilitation of the Hand for Patients Post-Stroke", *Proceedings of IWVR 2006,* pp. 6-10, August 2006.

NIH post-stroke rehabilitation:
http://www.ninds.nih.gov/disorders/stroke/poststrokerehab.htm
Patient@ UK stroke: http://www.patient.co.uk/showdoc/23068830/

Reinkensmeyer, D.J., C.T. Pang, J.A. Nessler and C.C. Painter, [2002] "Web-Based Telerehabilitation for the Upper Extremity after Stroke," *IEEE Transactions on neural systems and rehabilitation engineering*, Vol. 10, No. 2.

Rose, F.D., B.M. Brooks, A.R. Albert,[2007], "Virtual Reality in Brain Damage Rehabilitation: Review", CyberPsychology & Behavior. June 2005, 8(3): 241-262. doi:10.1089/cpb.2005.8.241.

Saga, S., Kawakami, N., Tachi, S. [2005] "Learning Effect of Haptic teaching using Opposite Force Presentation" in Proc. of the 2005 JSME Conference on Robotics and Mechatronics, Kobe, Japan, 1P2-N-038.

Stroke and rehabilitation education
http://uic.edu/depts/glstrknet/doc/patientEd/life8.pdf

Takacs, B., L. Simon, [2007], "A Clinical Virtual Reality Rehabilitation System for Phobia Treatment," *11th International Conference Information Visualization (IV '07)*, pp.798-806.

Teo, C., Burdet, L.E. and Lim, H. P. [2002] "A robotic teacher of Chinese handwriting" in *Proc. of 10th Symposium on Haptic Interfaces for Virtual Environment and Teleoperator Systems*, 335–341.

The Internet stroke center: http://www.strokecenter.org/patients/stats.htm

Whitworth E., J. A. Lewis, R. Boian, M. Tremaine, G. Burdea and J. Deutsch,[2003] "Formative Evaluation of a Virtual Reality Telerehabilitation System for the Lower Extremity," *Proc. Second Int. Workshop on Virtual Rehabilitation*, pp. 13-20, September 2003.

Yang, X., X. Wu, Z. Zhao, and Y. Li,[2007], "Hand Tele-Rehabilitation in Haptic Virtual Environment," *Proc. IEEE International Conference on Robotics and Biomimetics (ROBIO 2007),* pp. 145-149, Sanya, China, December 15-18, 2007

Yang, X. and Y. K. Kim [2008], "Hand Manipulation Training in Haptic Virtual Environments," *International Journal of Information Acquisition (IJIA),* 5(3): 269-281, 2008.

2

Augmented Reality Musical System for Rehabilitation of Patients with Duchenne Muscular Dystrophy

Ana Grasielle Dionísio Corrêa[1], Adriana Nathalie Klein[2] and Roseli de Deus Lopes[1]
1-Laboratório de Sistemas Integráveis da Escola Politécnica da Universidade de São Paulo
Av. Prof. Luciano Gualberto, trav. 3, n. 158, Cidade Universitária, CEP: 05508-970, São Paulo-SP, Brasil
2-Brazilian Association of Muscular Dystrophy (ABDIM)
Rua Engenheiro Teixeira Soares, 715 - Butantã - CEP: 05505-030 - São Paulo-SP, Brasil

1. Introduction

Human activity is the centralizing and guiding element in construction of the therapeutic process. According to Carlo e Bartalloti (2001), the human activity is constituted by a group of actions that present qualities, demand capacities and establish internal mechanisms for its accomplishment. Therapy then can be understood as life production, which implicates in a multiplicity of interventions.

This therapeutic multiplicity demands a variety of activities that request resources and diversified techniques. In this sense, computers can aid and support several therapeutic exercises, because they provide knowledge and experiences that run into the interests and needs of each patient, providing new possibilities and purposes in intervention (Watanabe et al, 2003). Computers can offer countless benefits to disabled individuals, as for example, communication easiness, personal growth, autonomy, social interaction and cultural inclusion.

Computers make it possible to create applications for therapeutic use adapted to the patient. The individualized treatment can be executed several times without putting in risk patient's safety. Several variables can be modified seeking to increase or to reduce the complexity of therapeutic exercises (Sveistrup, 2004). Besides, the therapist can supervise the treatment progress, quantify evaluations and adapt the treatment plan.

Technological evolution is allowing that computational system answer to touches, gestures and voice. The computer external environment can be captured by hardware through specific software aided by devices as cameras and sensors. Virtual and augmented reality are examples of technologies that make possible to create differentiated virtual environments to disabled users by using conventional devices as keyboard and mouse (Garbin et al, 2006). Through augmented reality, for example, it is possible to add virtual elements in the real world that can be manipulated in a natural way, with the hands,

without use of electronic devices for interaction. This characteristic of augmented reality can provide to individuals with low mobility, access to virtual environment facilitating the education and therapeutic procedures with use of computers.

In literature, several works can be found that make use of a virtual and augmented reality environment in treatment of cognitive and motor disorders (Sveistrup, 2004), (Carvalho et al, 2008), (Richard et al, 2008). However, no work relating technologies with music (applied to rehabilitation treatment) were found to the date of publication of this book. For this reason, for an experiment about use of an augmented reality musical environment (developed to rehabilitation) to be presented, it is necessary to discuss the main differences between virtual environment and mixed environment, pointing their advantages and disadvantages in the therapeutic process. Soon afterwards, a discussion is presented around the possibilities of use of virtual and augmented reality environment in several therapeutic modalities, shown through examples and practical experiences.

Then, a case study will be presented with the augmented reality musical environment GenVirtual applied in rehabilitation of individuals with muscular dystrophy. GenVirtual makes possible to add in the real world, virtual elements capable to simulate sounds of several musical instruments like: wind instruments, strings and percussion. Sounds are played touching virtual elements with hands, without use conventional devices of interaction (mouse, keyboard and joystick) and adapters (to people with physical disability). This way, an individual with hypotonic hands, for example, can use GenVirtual to develop their musical and therapeutic activities. Usually, these individuals cannot keep their fingers bent over the keyboard, or they don't possess enough muscular force to play a tambourine.

Besides resources for musical composition, GenVirtual offers a game of follow sound-and-colors, designed to stimulate attention, concentration and memorization of colors and sounds. Besides cognitive aspects, GenVirtual can provide motor learning through the planning of motor action previously done by the therapist. We hope that the patient can use GenVirtual at home to complement the activities of rehabilitation due to the low cost of this software. With household use, we hope that this software can motivate the family to participate in therapeutic home activities, contributing to their social integration and thus improvement of life quality.

GenVirtual has been evaluated (for specialists in rehabilitation) and experienced (with individuals with motor and cognitive disability) in the Occupational Therapy Division of the Brazilian Association for Muscular Dystrophy (ABDIM). The benefits that GenVirtual offers to therapists and patients with Duchenne muscular dystrophy are being documented and the partial results of this research will be here presented.

It should be noted that this technological introduction doesn't implicates in new theoretical approaches to medical therapies (Carvalho et al, 2008). The objective is to potentiate treatments already existent and to expand the usefulness of techniques already used. This way, the therapeutic relationship and the pertinent use of techniques already established are preserved. As well as other available strategies to the field of therapies, the use of virtual and augmented reality shouldn’t be discriminated, but coherent with patients' needs. For this reason, it should be enhanced the importance of studies in this area that point indications of use of this tool.

2. Mixing Real Environment with Virtual Worlds: perspectives and therapeutic implications

Virtual reality environments make possible total immersion in an artificial three-dimensional world (Kirner & Tori, 2006a). This way, the user can explore and manipulate imaginary virtual worlds as if they were being part of him. Images generated by computer seem to be natural size and scenery modifies starting from the user's interaction with the virtual world. If environment incorporates three-dimensional sounds, then user is convinced the orientation sounds change naturally in agreement with his/her orientation inside the environment. The immersion in a virtual world can be provided through specific technology (Burdea & Coffet, 1994): head-mounted displays (HMD), devices of optical tracking, force-feedback data gloves and joysticks that allow the user to navigate inside a virtual world and to interact with virtual objects (Fig. 1).

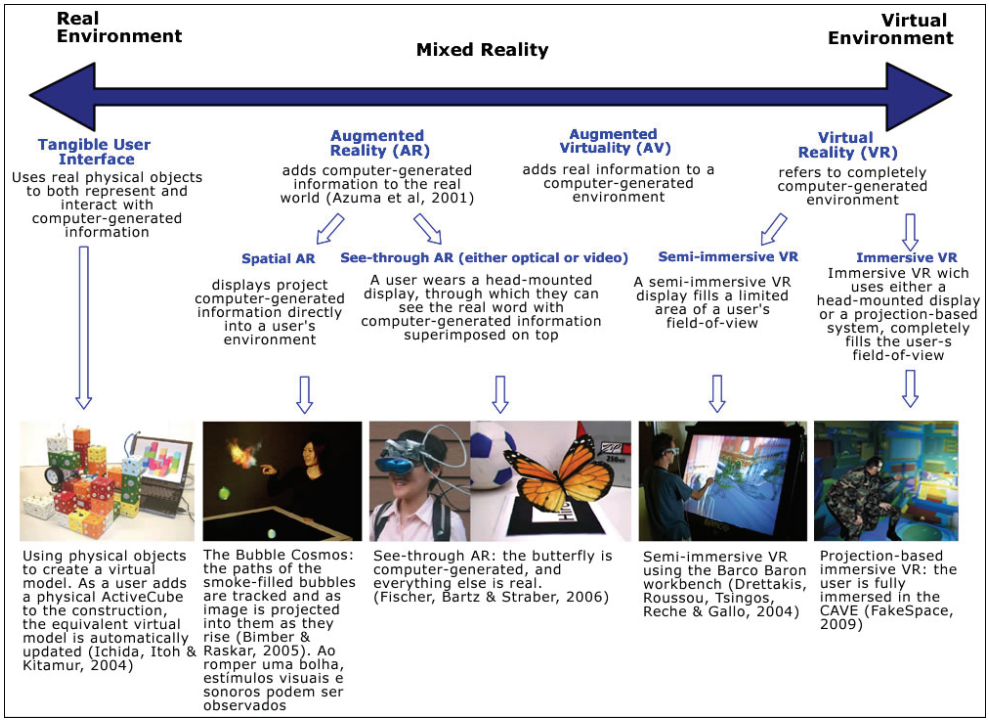

Fig. 1. Continuum of advanced computer interfaces based on Milgram and Kishino (1994).

From the appearance of virtual reality, there was always a separation between real and virtual world. However, technological progress has made possible to mix real environment and virtual worlds (in real time) originating a new concept denominated mixed reality (Kirner & Tori, 2006b). Unlike virtual reality that transports the user inside a virtual world, mixed reality propitiates the incorporation of virtual elements in real environment (the user maintains the presence sense in real world) or it transports real elements for virtual environments complementing the environment. When there is predominance of real over

virtual, the environment is characterized as augmented reality; therefore the real environment is enlarged ("augmented") with addition of three-dimensional objects (Fig. 1). To the opposite, when there is predominance of virtual over real, the environment is characterized as augmented virtuality; therefore real physical objects are captured in real time and inserted in simulated environment by computer.

Augmented reality presents a great advantage on augmented virtuality: allows transport of virtual objects to the real world providing new interaction possibilities to individuals with serious problems of fine motricity (ability) and global motricity (agility). In this case, that the user can manipulate virtual objects happens in a natural way, dragging or touching an object with his/her hands or with his/her feet, without necessarily using devices for interaction or adapters. In case of augmented virtuality or even of virtual reality, training is necessary to use appliances as mouse, keyboard, joystick or other technological devices. Many times, that need generates indifference, fear or even individual's incapacity in interacting with virtual environment.

Augmented reality tends to use devices less perceptible to users, seeking to provide larger naturalness of their actions through tangible interfaces (Azuma et al, 2001). According to Leitener et al (2007), a tangible interface allows manipulation of virtual objects with hands or through physical devices similar to the virtual object. In that way, tangible interfaces unite advantages of physical manipulation and innovative forms of interaction provided by computation, thus enriching the experience of individuals with learning deficiency.

A lot of times, to attend specific needs of individuals with deficiency it is common to develop adaptations for use with computational systems. In function of a specific problem, some individuals can need specific resources hindering the therapeutic process, causing, besides, a higher cost for conception and use. Through tangible interfaces, for example, it is possible to build augmented reality environments, economically viable compared other virtual reality environments. With use of a computer (to process software), a webcam (to capture real environment), a monitor (to visualize mixed environment) and pieces of paper with letters printed on them to create tangible objects, it is possible to develop a simple augmented reality environment, but with a variety potential applications to work with individuals with different deficiencies and incapacities (Garbin et al, 2006).

Presence of a register (paper marker) in the field vision webcam enables the virtual object associated to this marker to be superimposed on it. Manipulation marker in real environment also moves the virtual object: if the individual drags the register with his/her hands, the virtual object associated to that marker is moved together. Besides virtual objects, sounds can be initiated when marker enters in the webcam vision field. Some markers can be created to interfere in associated objects with other markers, making possible to accomplish geometric alterations, change objects, capture or duplication, deletion, etc. Like this, virtual objects can be altered or replaced in agreement with needs, interests and abilities of each individual, generating experiences differentiated with the construction of different sceneries.

This characteristic of augmented reality facilitates the communication process of children with learning difficulties; besides this, allows motor and intellectual development. According to Piaget (1995), cognitive development can be explored through symbols and abstractions of reality, favoring for better understanding of the situation problem and results. In augmented reality environment, children can explore these abilities through

composition; alteration or creation of new situations driven through their autonomous actions impelled by their desire and imagination.
Motricity in an augmented reality environment can be worked through manipulation of tangible objects. This activity can contribute in an expressive way in formation and structuring of the sensorial-motor control, being characterized as education that is done through movement, so that the individual acquires functions more and more elaborated and complex (Leitener et al, 2007). Through this dynamics it is wanted that the individual notices his/her potentiality and identifies the interaction possibilities in augmented reality environment, aiming to overcome harmful subjects in psychomotor development.

3. Used Forms of Virtual and Augmented Reality Environment in Therapeutic Process

Virtual and augmented reality has been used to support medical therapies in a variety of proposals. High degree of realism simulated sceneries for computer and the possibility of mixing real environment with virtual one offer new treatment possibilities to individuals with different deficiencies and incapacities. Among the most common therapies, accomplished with use of virtual reality, considering the context of conducts, can be mentioned live exhibition, that consists of exhibition of the individual to the real situation of his/her phobia, and imaginative, in which the individual imagines the objective of his/her fear in the therapist's clinic (Carvalho et al, 2008). In these cases, fear condition can be introduced to the patient in a virtual way and not in a real way as in conventional treatment.
So much in live exhibitions as in imaginary, it is necessary to build with the patient a list with the hierarchy situations and fearsome stimulus. Starting from that, it is possible to create sceneries with situations and incentives corresponding to reality. The fearsome stimulus are lived in a virtual environment that allows interaction, making it possible to the patient to act in sceneries just as in a real environment (Carvalho et al, 2008). The presence feeling experienced by the patient in a virtual environment and the sensorial-motor involvement (proportionated by different sensorial incentives) provide a larger reality sensation than the individual could feel when constructing sceneries of his/her own imagination (Carvalho et al, 2008).
In the literature can be found works verifying the effectiveness of the virtual environment in treatment of several phobias (Medeiros, 2006). Hoffman et al (2003) investigated the applicability of virtual reality in spider phobia treatment. Juan et al (2005) tested augmented reality environment in individuals with cockroaches and spiders phobia. Results of this researches showed that individuals that received treatment through virtual environment obtained significant improvement, compared to individuals that received conventional treatment.
The main advantages of the virtual treatment of phobias are easiness and variety (North et al, 1998). The enormous range of phobias that can be simulated through virtual and augmented reality explains this variety. The easiness is applied in some phobias that are difficult to be presented in real way, for example, fear of flying. This environment can be easily simulated through virtual reality.
Several works about use of virtual environment for cognitive rehabilitation were found in literature including applications turned to treatment of feeding disorders (Riva et al, 2000), autism (Parés et al, 2005), traumatic cerebral lesions (Bodine & Scherer, 2006), cerebral palsy

(Reid & Campbell, 2006) and also prevention of accidents with senior patients (Alpini et al, 2000). Effects generated by virtual environment stimulate plastic changes in brain, essential for the rehabilitation process, for example, the ARVIC project: virtual integrated environment for cognitive rehabilitation (Costa e Carvalho, 2001).
ARVIC is a virtual reality environment developed to train attention, memory, planning and calculation through recognition of monetary symbols (notes and coins) associated to the products' prices. Environment is constituted of a city containing parkings; stores and a virtual supermarket in a way to mirror situations lived by users in their day-by-day. In ARVIC environment the user can previously buy goods with an amount of money and a list of products established. Products of virtual stores appear located in shelves with price indication in the currency of Brazil. Individual navigates in the virtual world using a mouse for interaction. When clicking with the mouse in a chosen product, a new window opens up showing the user a variety of notes and coins. The user then should choose the exact money amount to accomplish these purchases, considering the amount in money available and the list of items supplied for purchase. ARVIC was tested with several individuals with different pathologies, among them schizophrenic (Costa e Carvalho, 2001) and people with brain lesions (Cardoso et al, 2006). The clinical results proved the effectiveness of this tool in cognitive functions rehabilitation (attention, memory, planning and calculation), verifying patients' most satisfaction with use of a virtual environment to learn.
Another relevant work for cognitive rehabilitation is ARVe (Augmented Reality applied to Vegetal field) (Richard et al, 2008). ARVe is an augmented reality environment (applied to Biology area) for rehabilitation of cognitive disabled children. The virtual environment is constituted of a book containing several registrations (symbols) glued in pages book. Each symbol represents a vegetable component (leaves, flowers, fruits and seeds). The objective is to organize the vegetables components in agreement with their functions. For example, the child should contain all fruits in a book's page, all seeds in another page and so on. Visual cues (red or blue virtual circles) are used to help the child carrying out the task.
Virtual games also present a space of cognitive development exploring basic cognitive functions, such as attention, concentration, memory, planning and calculation, space ability, among other activities that keep relationship to those accomplished in day-by-day (Costa e Carvalho, 2005). Starting from challenges created through games, brain is stimulated to create nervous cells that help to restructure harmed areas. Besides, games can be suitable for different goods, ethnic and age groups and easily they can be found and handled in different contexts as school, clinical hospital, home and other.
Games in augmented reality, for example, allow enriched vision for user and enlarged environment, stimulating perception capacity and space reasoning. Zorzal (2006) presents several models of puzzles games created with augmented reality, for example, game of Words. In this game, markers are cards containing several letters. The user should group the letters to build words that are registered previously in game. When user forms a sequence of letters (registered word), it is possible to visualize a virtual object regarding that word. This characteristic makes this game a source of practical applications like literacy, learning of languages, besides making possible the development of cognitive abilities.

3.1 Motor Rehabilitation Facilitated by Virtual Reality Games

Great rehabilitation centers in the world began to implant its units of virtual rehabilitation whose focus is in computerized games use for intensive rehabilitation (Deutsch et al, 2008),

(Burdea et al, 2008), (Halton, 2008). Patients that suffered a cerebral vascular accident or went through surgical procedures and also for lesions combat, are being benefitted with use of games as an alternative mean for motor rehabilitation. Usually, this patient needs an intensive physiotherapy, which a lot of times can turn into repetitive and painful therapy for the patient. With spreading of games in therapies, the scenery is other. With a game, patients forget that they are in therapeutic intervention. That helps them getting rid of boredom caused by repetitive movements that involve the process of motor rehabilitation.
Virtual reality technologies have been impelling the conception of several computerized games with new entertainment forms (Burdea et al, 2008). It is case of wii, Nintendo videogame that makes use of a remote controller "*wiimote*" sensor based that captures the movements and players' gestures during the game. Players don't need to seat in front of computers or videogame consoles, limited by a joystick. This game allows players to move and interact in different ways in real environment, through different devices and communication technologies without thread.
This characteristic of wii games has shown to be efficient in process of motor rehabilitation, for being a mechanism that requests sensitive and precise movements, similar to activities in daily life. Those movements are made through games that simulate baseball departures, bowling, boxing, tennis, golf, dances, etc. The effort to execute well the movements can provoke positive impacts in the organism as invigoration of musculature, easiness for recovery movements, incentive cerebral activity and increase concentration capacity and balance.

4. A Case Study with an Augmented Reality Musical Environment in Rehabilitation of Individuals with Duchenne Muscular Dystrophy

4.1 GenVirtual: Conception and Description

GenVirtual is an augmented reality musical environment that allows to develop creation activities, improvisation and musical reproduction such as composition and reproduction of melodies, listening to musical and sounds, and musical memory games.
GenVirtual allows to add to the real world, three-dimensional virtual elements (colored cubes) capable of simulating sounds of several musical instruments like wind instruments, strings and percussion. Sounds are executed playing virtual elements with hands, without use of conventional interaction devices (mouse, keyboard, joystick) and adapters for individuals with low mobility (Fig. 2). Some patients have hypotonic hands and cannot keep their fingers bent over the keyboard or do not have enough muscle power to play percussion instruments. In those cases, adapters are necessary, for example, tips in the hands to play the piano (or electronic keyboard) or a support to the tambourine so both hands can be used.

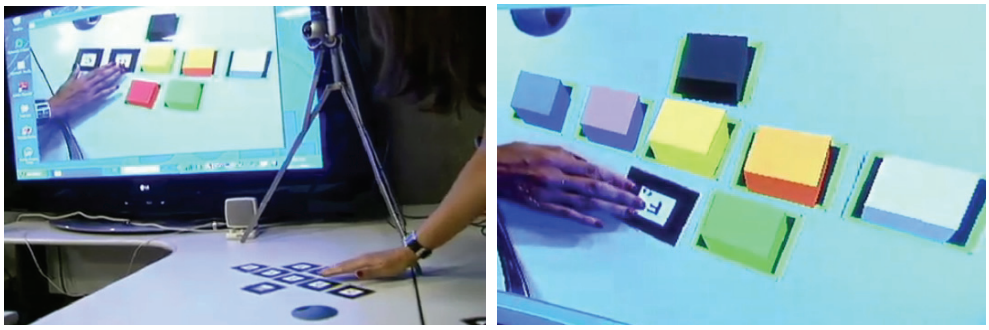

Fig. 2. GenVirtual Interface

Identification of markers (cards) on table happens through processing of images, captured by a webcam, connected to a computer, strategically positioned in the superior part of the table. Symbol card is detected and associated to a sound. The emblem of a piano is the standard sound associated to cards, but there is the possibility to change the emblem of musical notes emitted by cards. For this, simply add a new label in the symbol table containing the desired musical instrument. In this way, same virtual elements emit different sounds, according to instrument defined by new card. It could assume emblems of wind instruments (flute, trombone, trumpet, etc.) or string instruments (violin, guitar, etc). Another possibility is to use cards with symbols corresponding to percussion instruments, as drums, tambourines, triangles, as well as symbols that represent sounds of electronic instruments.

The differential in this music system is the flexibility of cards for interaction. Cards can be printed in different colors and proportions, allowing the therapist to realize a unique motor planning for each individual, in accordance with desired motor challenge. Cards can be organized in different ways on the table, or on the floor, where interaction occurs.

GenVirtual also has a game called "follow sound-and-colors", that makes it possible to stimulate the attention, concentration and memorization of colors and sounds. In this case, GenVirtual generates a musical sequence. Virtual cubes rotate in agreement with the musical sequence to be played, and simultaneously, the musical note regarding that virtual cube is executed. Musical notes are emitted one per time, and system is awaiting the user's interaction that should obstruct the marker regarding the emitted musical note. To each success, sequence wins a new item (musical note), increasing the challenge of memory and retention of information game.

Besides cognitive aspects, GenVirtual can provide the motor learning through the planning of motor action, previously prepared by therapist. According to Nascimento (2006), it is important to have a reference of motor movement to make possible to control movement of that individual, otherwise, motor learning does not occur.

4.2 GenVirtual Implementation

GenVirtual uses techniques of computational vision to generate, to position and to show virtual objects in real world. Basically a webcam (connected to a computer) captures images in real time (video frames). Captured images are analyzed by computational vision software ARToolkit (Geiger et al, 2004). ARToolkit analyzes captured images in search of symbols

registered previously by user. Symbols are printed inside a frame in common and organized paper over the table (tangible objects). When recognizing a symbol, ARToolkit calculates its position and orientation in relation to the real position of webcam and shows in display (monitor) the virtual object super imposed to corresponding symbol (visual feedback). Figure 3 shows necessary components to use GenVirtual.

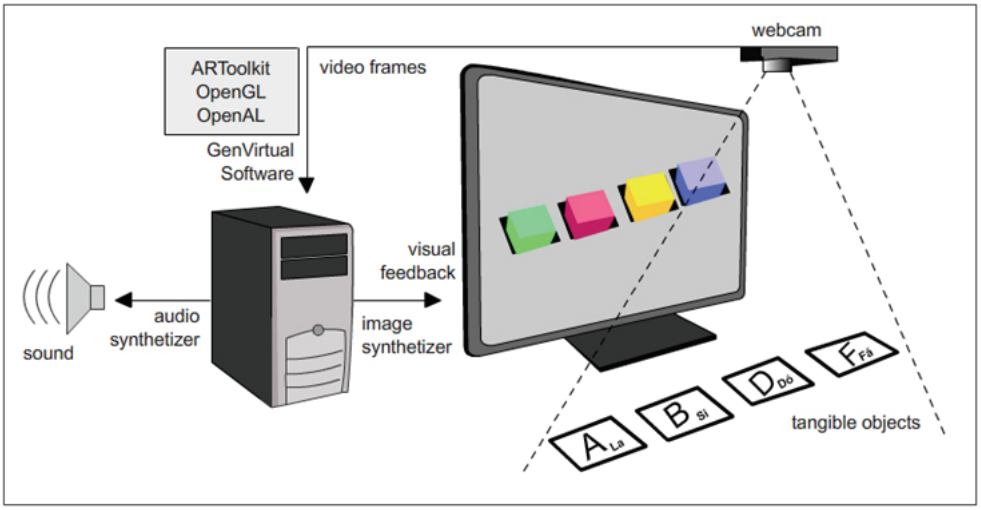

Fig. 3. GenVirtual components

ARToolkit Operation: each video frame captured is transformed in a binary image (black and white) based on an intensity threshold value. Then, it looks in this image for square areas. For each square, the standard drawing inside of it is captured and compared with some forms pre-registered by user. If there is some similarity, ARToolKit considers that it found one reference marker and uses known square size, as well orientation of found pattern, to calculate the real position of camera in relation to real position of marker. A matrix 3x4 will contain real coordinates of camera in relation to marker. This matrix is used to calculate position of coordinates of the virtual camera. If virtual and real coordinates of camera are the same, the graphic computation model can be drawn precisely on real marker. OpenGL library is used to calculate virtual camera coordinates and to draw virtual images. This procedure is illustrated in Figure 4.

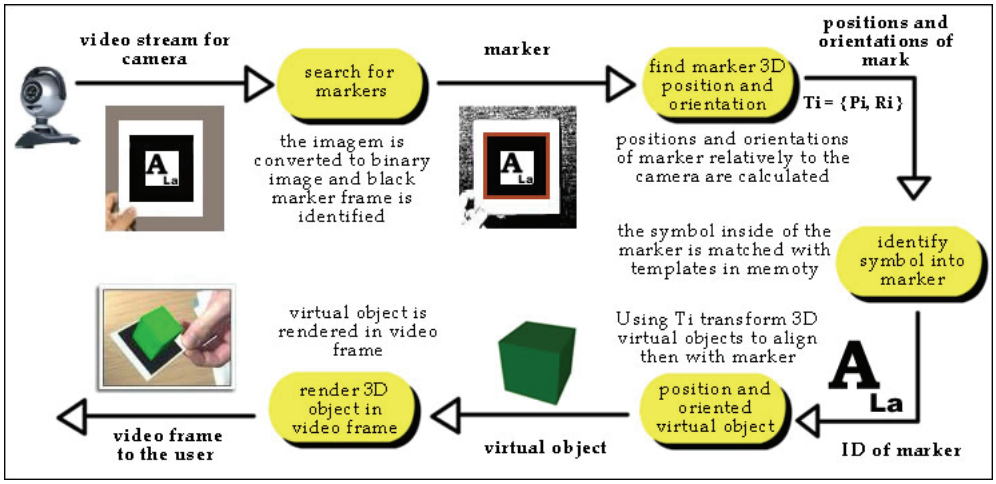

Fig. 4. ARToolkit cicle (Geiger et al, 2004)

Some advantages found in GenVirtual computational vision system:

- Computational vision system can be created in low resolution, making use of just a webcam, which enables a low cost;
- Visualization system is based on monitor or projection screen (indirect vision). Such systems possess inferior cost if compared to other visualization systems as visualization helmets with built-in video cameras;
- Variety of registrations (tangible objects) that allows to diversify musical activities;
- Interaction devices (tangible objects) are easy to use and accessible economically (it can be printed in conventional printer);
- Therapist can create the wanted motor challenge, in agreement with each individual's motor limitation through arrangement of registrations in the table.

4.3 GenVirtual Indications

GenVirtual was applied with patients with muscular dystrophy rehabilitation during occupational therapy at São Paulo Muscular Dystrophy Brazilian Association (ABDIM). The goal was to verify if GenVirtual, applied to a program of superior members exercises, is capable to interfere in motivation, satisfaction and consequent adherence of occupational therapy rehabilitation program of patients with Duchenne muscular dystrophy.

Clinical aspects of Duchenne Muscular Dystrophy (DMD)

Progressive muscular dystrophy (DMP's) form a group of human diseases determined genetically and associated to progressive skeletal muscles degeneration, without compromising central nervous system (Kakulas, 1999). DMP's are characterized by progressive muscular weakness, deterioration and degeneration of muscular fibers, being these of hereditary transmission (Zats, 2002). All of which are characterized equally by a musculature progressive degeneration, whose inheritance can be dominant autosomal, recessive and linked autosomal to X chromosome (Kakulas, 1999). In Brazil, DMP's reach 1 in each 2.000 births (about 100 thousand Brazilians) independent of race or social class.

There are more than 30 dystrophy types, and the more incident and with the worst prognostic is Duchenne muscular dystrophy (DMD) (Zats, 2002), (Stone et al, 2007).
In DMD, clinical signs begin at 3-5 years of age (with frequent falls, difficulties to go up stairways, to run and to get up from ground), retarding normal motor development. Confinement to wheel chair happens before 12 years of age and the affected ones rarely survive after third decade. Studies accomplished in several countries demonstrated a life expectation from 18 to 25 years (Santos et al, 2006). This prognostic has been promising mainly with the introduction of no invasive ventilation (Vianello, 2000). About 30% to 50% of patients with DMD possess mental retardation, whose cause is being investigated (Bach 2004), (Rapaport, 1992).
Muscular compromising is bilateral, symmetrical, proximal musculature is reached previously to distal, and contractures and deformities presence become relentless with natural evolution of the disease (Zats, 2002), (Santos et al, 2006), (Vianello, 2000). These patients start to have a very restricted functional capacity, frequently limited to small mobility of manual extremities.
There isn't any known cure today, or pharmacological treatment that stops or reverts DMP's degenerative process and of a great part of neuromuscular diseases (Santos et al, 2006). In spite of that, there is a series rehabilitation treatment that can stabilize the clinical picture of the pathology, or even reduce the progression speed. Programs of individuals' rehabilitation with DMP present as main purpose to minimize sequels of the pathology, improving quality of life of bearers, through maintenance and prevention of dysfunctions (Zats, 2002), (Santos et al, 2006). For this reason it is necessary to create diversified forms of therapeutic approaches aiming to provide new activities that favor the enlargement of individuals' functional, social, emotional and vocational capacities with DMD.

4.4 Methods

Casuistical: 16 male patients participated in this work, with ages between seventeen and twenty-four. Incorporation of patients to the study depended on authorization of a responsible person expressed through the term of free and illustrious consent. Inclusion criteria were: to possess diagnosis of Duchenne muscular dystrophy; to have accomplished specific rehabilitation program of upper limbs in ABDIM at least for twelve months ago. Exclusion criteria were: to possess some cognitive deficit; illiterate patients.
Participant: 16 individuals with diagnosis of Duchenne muscular dystrophy; they were randomized in two groups, through drawings. 11 patients received exercises programs for active extension of elbow, forearm pronation/supination and wrist extension, using augmented reality resources. Other 5 patients continued accomplishing the active extension of elbow exercises, forearm pronation/supination and wrist extension, using conventional resources of rehabilitation.
Evaluation: using a questionnaire, motivation evaluation and patient's satisfaction - Likert scale (Oliveira, 2001) were measured. In the application of Likert scale, patients indicated agreement degree or disagreement with relative declarations to the accomplishment upper limbs exercises. Punctuation was distributed in the following way 100% (excellent), 80% (very good), 60% (good), 40% (regular), 20% (bad) and 0% (very bad). Questionnaire was applied to the group that used GenVirtual as well as to the group that used the conventional rehabilitation material. Four aspects were selected: 1) easiness of use of GenVirtual or other material during therapy 2) exercise effect 3) motivation degree when accomplishing the

exercise and 4) satisfaction when accomplishing exercise. Therapist's questionnaire was based on three aspects: 1) practicality of equipment use (pre-installation e post-installation) 2) instructions to patient 3) degree of patient's motivation (therapist's vision) when accomplishing exercises.

Intervention: each group received weekly intervention of 30 minutes. Interventions were divided in ten minutes of specific exercises of scapular waist, ten minutes of elbows exercises, forearm and fist wrist and ten final minutes of free activities. Patient stayed positioned at a table, with proportional height of ergonomics of a wheel chair. After the first session a blind evaluator interrogated the patient on his/her satisfaction index. After 4, 8 and 12 sessions the same scale will be reapplied. The same procedure happened with patients of control group that received the conventional intervention, in other words, without using GenVirtual. Therapist's evaluation of technology use was also conducted after the end of each intervention.

4.5 Results and Discussions

Results here presented are regarding the first intervention. After 4, 8 and 12 sessions the same scale will be reapplied and results will be tabulated again and analyzed for futures publications. Figure 5 shows some images of interventions with GenVirtual accomplished in ABDIM.

Fig. 5. Intervention with GenVirtual in ABDIM

Likert Scale applied with patients

Figure 6 and 7 show results obtained after the collection of 16 participants' data: motivation and satisfaction level of patients when accomplishing interventions, degree of easiness use of rehabilitation instruments during therapy and accomplished exercises effect.

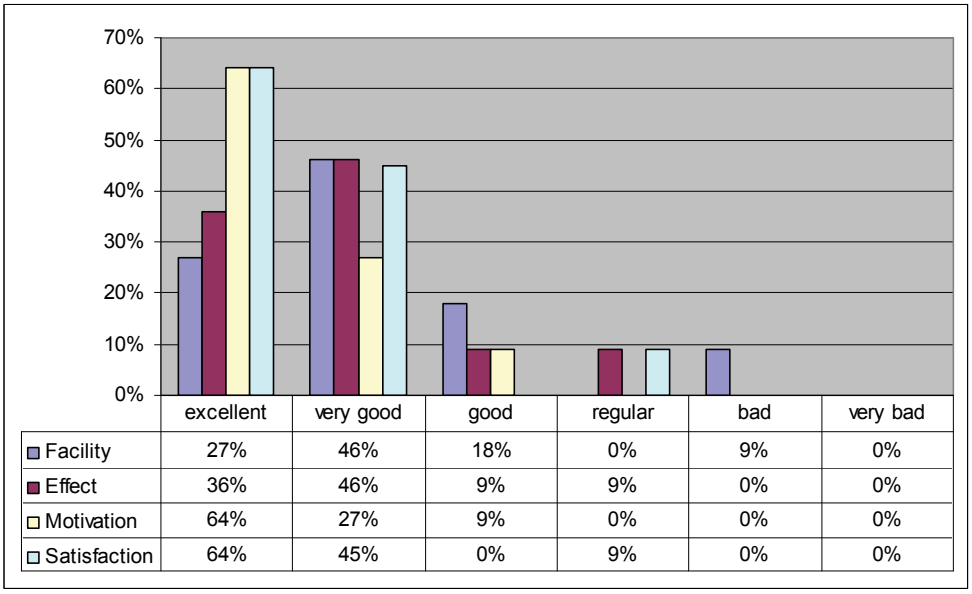

	excellent	very good	good	regular	bad	very bad
Facility	27%	46%	18%	0%	9%	0%
Effect	36%	46%	9%	9%	0%	0%
Motivation	64%	27%	9%	0%	0%	0%
Satisfaction	64%	45%	0%	9%	0%	0%

Fig. 6. Classification levels of easiness, effect, motivation and satisfaction of patients when using GenVirtual in interventions.

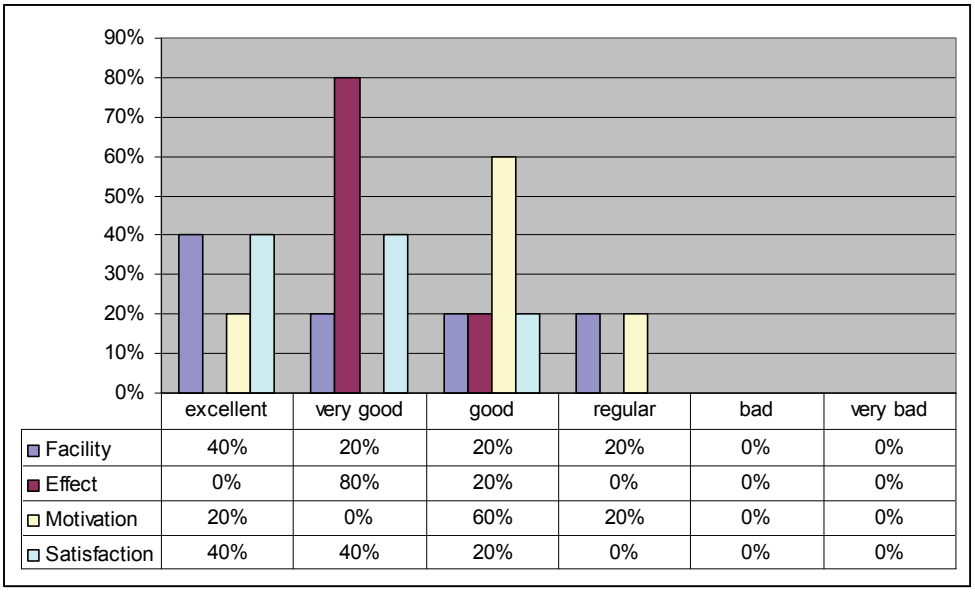

	excellent	very good	good	regular	bad	very bad
Facility	40%	20%	20%	20%	0%	0%
Effect	0%	80%	20%	0%	0%	0%
Motivation	20%	0%	60%	20%	0%	0%
Satisfaction	40%	40%	20%	0%	0%	0%

Fig. 7. Classification levels of easiness, effect, motivation and patients satisfaction when using conventional rehabilitation material (without GenVirtual) during interventions.

To proceed they are discussed the four aspect presented in graphs above: easiness, effect, motivation and patient's satisfaction.
Figure 8 shows a comparison among levels of facility of material used during interventions. In the patients' case that used GenVirtual: 27% found excellent, 46% found very good, 18% found good and 9% found bad. In this last case individuals are framed with little mobility and they had a lot of difficulty in obstructing markers.
In conventional intervention, patients used a stick to accomplish exercises of elbow extension (sliding the stick in table with arms) and modeling mass for exercises of fist extension (touching the mass with hands). Exercises with stick and mass they are equal to the same exercises accomplished with GenVirtual, the one that changes are support materials. The level of easiness of this material varied enough: 40% found excellent, 20% very good, 20% good and 20% regular.

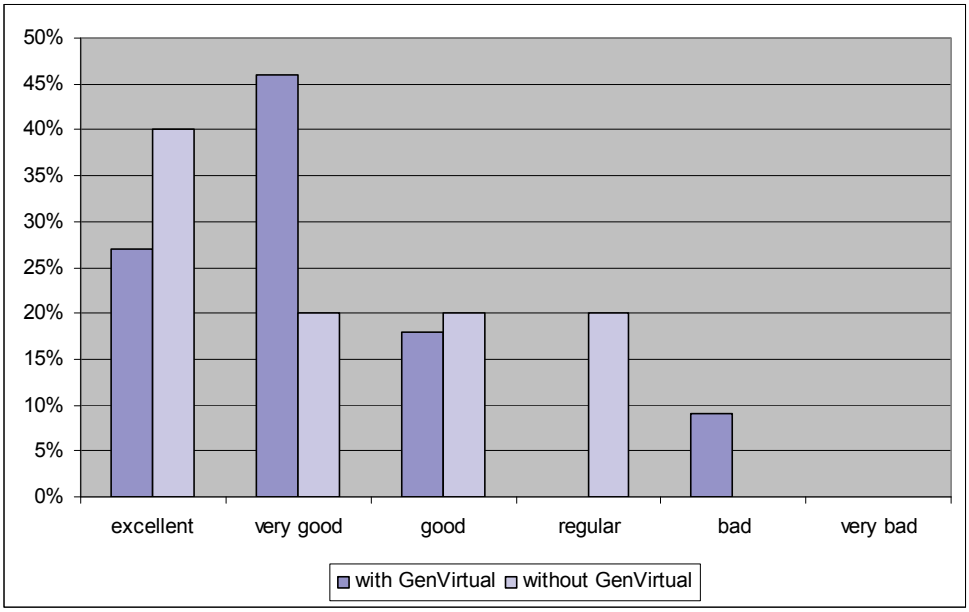

Fig. 8. Classification levels of facility with and without GenVirtual

Figure 9 shows a comparison among levels of effect exercises accomplished with GenVirtual and levels of effect of exercises accomplished without GenVirtual. Results show that effects caused with GenVirtual were proportional to effects caused with conventional exercises: 36% said excellent, 46% very good, 9% good and 9% regular. Negative factor (9% regular) is explained with the deposition of some patient that said that he/she didn't need strength to execute sounds and as a consequence it was not necessary to dissociate or to extend fingers to move and rotate wrist to obstruct the cards in the table. However, exercises' objective was exactly wrist extension, which was verified with GenVirtual. In interventions without GenVirtual, the level of exercises' effects varied among good (20%) and very good (80%).

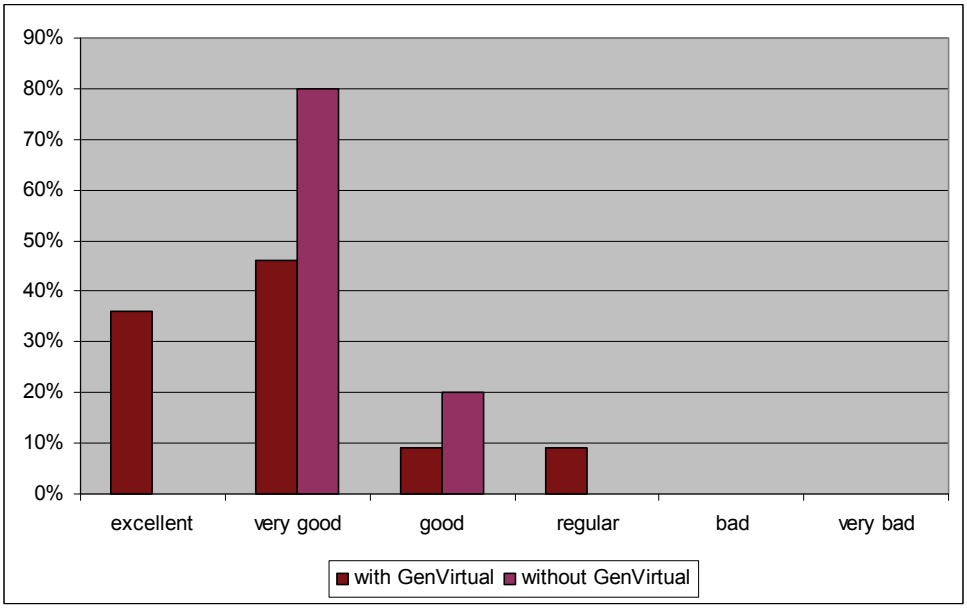

Fig. 9. Classification levels of exercise effect with and without GenVirtual

Figure 10 shows a comparison among levels of patients' motivation that used GenVirtual and the levels of patient's motivation that didn't use GenVirtual. Results demonstrate that motivation level was larger when accomplishing exercises with GenVirtual: 64% of patients said that the motivation degree is excellent, the remaining varied between good and very good. In interventions without GenVirtual, motivation level decreased: 60% of patients said good, 20% found excellent and 20% found regular.

It fits to stand out that results of this experiment in ABDIM are still preliminary and they are just equal to first application of questionnaire Likert. In spite of the fact that all patients use computers, no patient had interacted with an augmented reality environment previously. These patients' first deposition on GenVirtual was positive: all said that environment is very cool, different and stimulating, a different form of doing rehabilitation exercises and that they would like to continue the treatment with GenVirtual. The factor of larger motivation for most patients was the possibility to easily change musical instruments. Many patients wanted to show to their therapist musical knowledge, trying to compose melodies with different instruments.

Figure 11 shows a comparison among satisfaction levels of patients when accomplishing exercises with GenVirtual and levels of patient's satisfaction that made intervention without GenVirtual. Results demonstrate that satisfaction level was larger with GenVirtual: 54% said excellent, 38% said very good and 8% said regular. In interventions without GenVirtual, satisfaction level decreased, however not a lot: 40% found excellent and the remaining varied between good and very good.

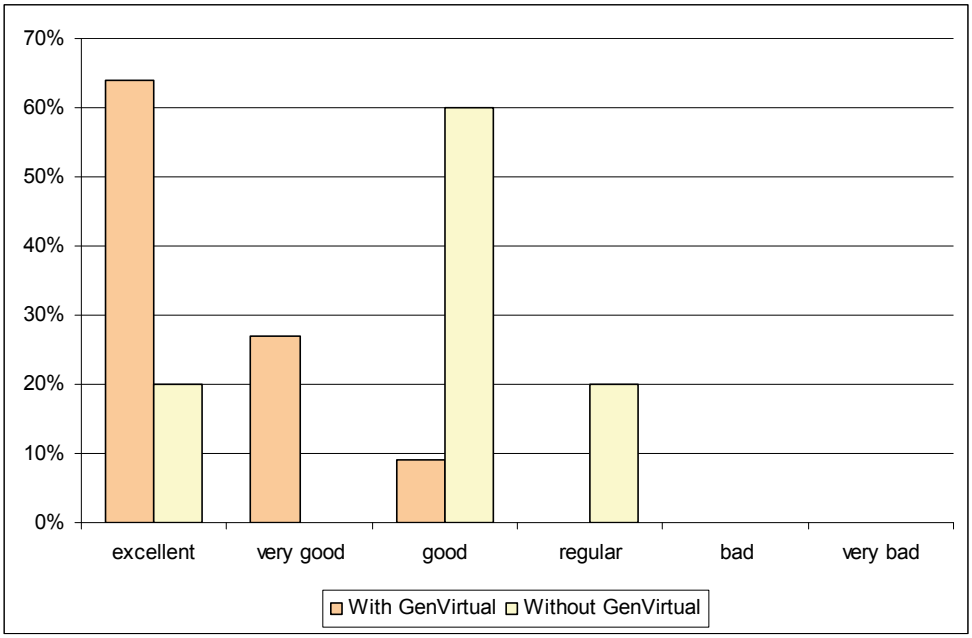

Fig. 10. Classification levels of motivation with and without GenVirtual

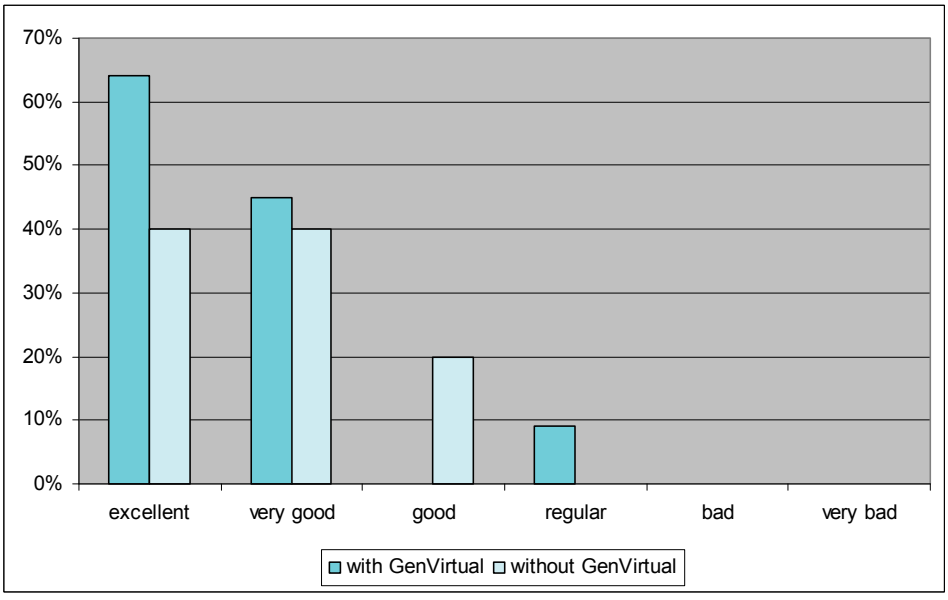

Fig. 11. Classification levels of satisfaction with and without GenVirtual

Likert Scale applied to the therapist:
Figure 12 and 13, show results obtained after the data collection of 2 therapists' involved in these interventions. Results show data as: practicality of equipment use (assembly and desassembly), applicability (use instructions) to patient and degree of patient's motivation (therapist's point view) when accomplishing exercises.

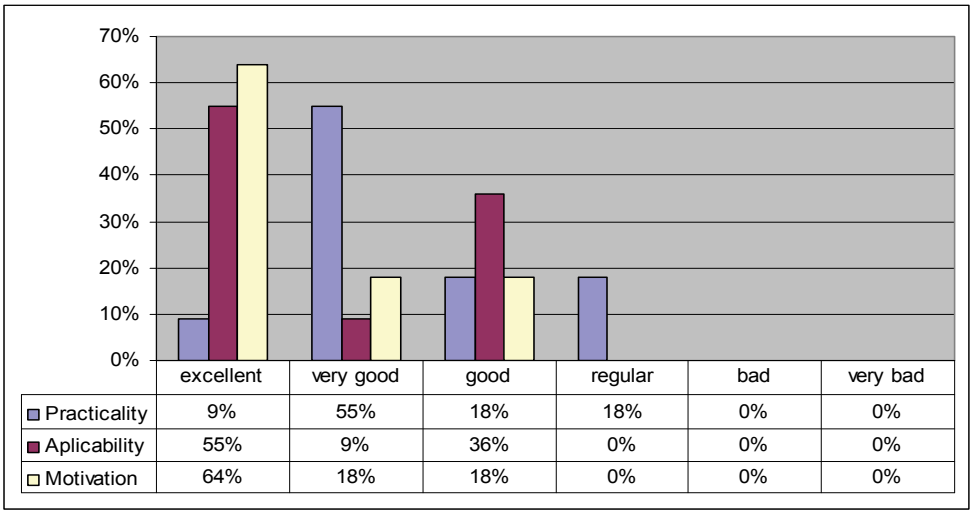

	excellent	very good	good	regular	bad	very bad
Practicality	9%	55%	18%	18%	0%	0%
Aplicability	55%	9%	36%	0%	0%	0%
Motivation	64%	18%	18%	0%	0%	0%

Fig. 12. Classification of practicality, motivation and applicability levels of GenVirtual in interventions (therapist's point of view).

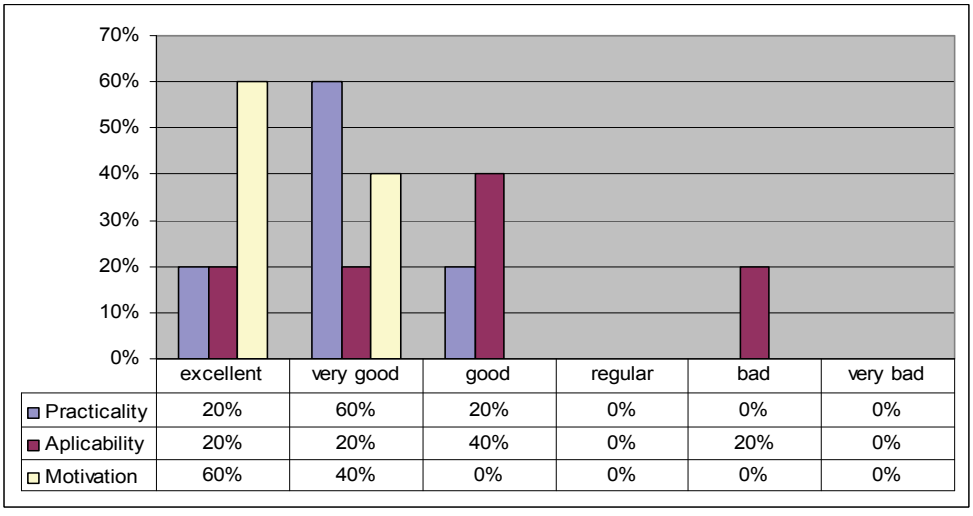

	excellent	very good	good	regular	bad	very bad
Practicality	20%	60%	20%	0%	0%	0%
Aplicability	20%	20%	40%	0%	20%	0%
Motivation	60%	40%	0%	0%	0%	0%

Fig. 13. Classification of practicality, motivation and applicability of conventional rehabilitation material (without GenVirtual) used during interventions (therapist's point of view).

Figure 14 shows a comparison among practicality levels of GenVirtual and conventional material (stick and mass) used to accomplish exercises. Process of materials' assembly was taken into account before beginning interventions as well as disassembly process after concluding interventions. Results demonstrate that the practicality level of both materials was very good. Time of GenVirtual assembly was larger than time with stick and mass. This occurred because it was necessary to adjust the table with the webcam and the patient's posture in relation to table. In general Genvirtual practicality as good: 9% excellent, 55% very good, 18% good and 18% regular. And with stick and mass: 20% excellent, 60% very good and 20% good.

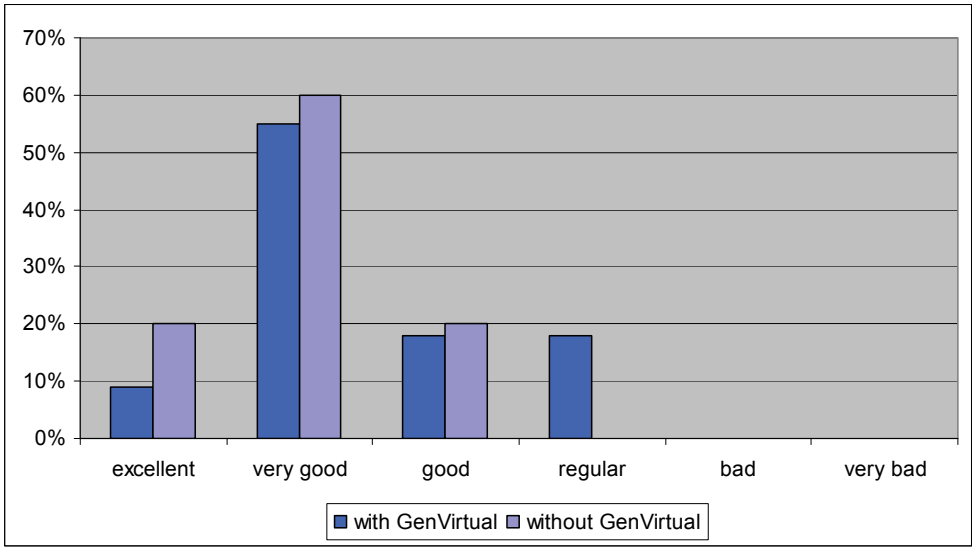

Fig. 14. Classification practicality levels with GenVirtual and with conventional rehabilitation therapy material (without GenVirtual).

Figure 15 shows the comparison among applicability levels of material used to accomplish therapeutic exercises. In case of GenVirtual: 55% found excellent, and the remaining varied among very good and good. Most of therapists found GenVirtual intuitive and of easy assimilation for patients. In case of material with modeling mass and stick: 20% excellent, 20% very good, 40% good and 20% regular.

Finally, figure 16 shows levels of patient's motivation (therapist's point view) when using therapeutic resources in interventions. With GenVirtual: 64% of therapists found patients more motivated during intervention. The remaining varied between good and very good. With use of modeling mass and stick: 60% found excellent and 40% very good. This result demonstrates that the technology doesn't substitute therapeutic practice and yes it complements and it supports already established techniques.

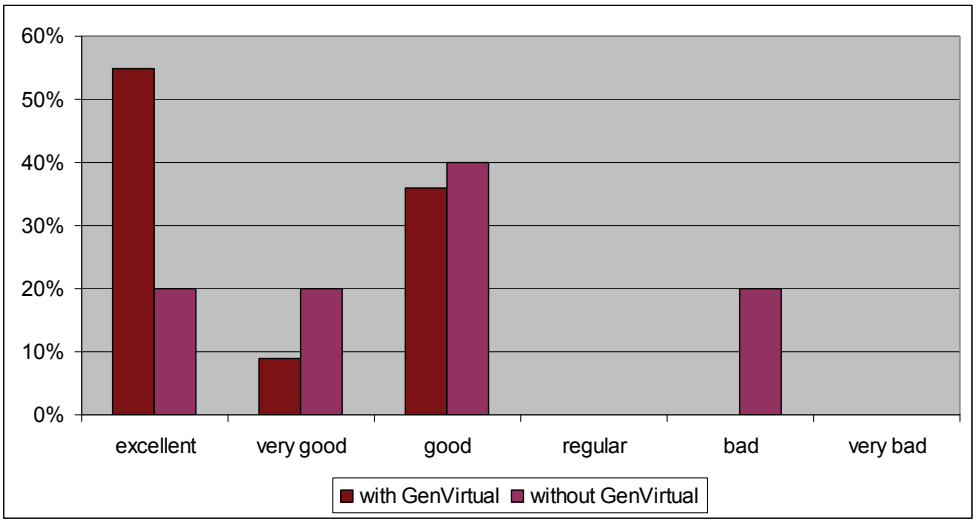

Fig. 15. Classification levels of applicability of therapeutic materials used

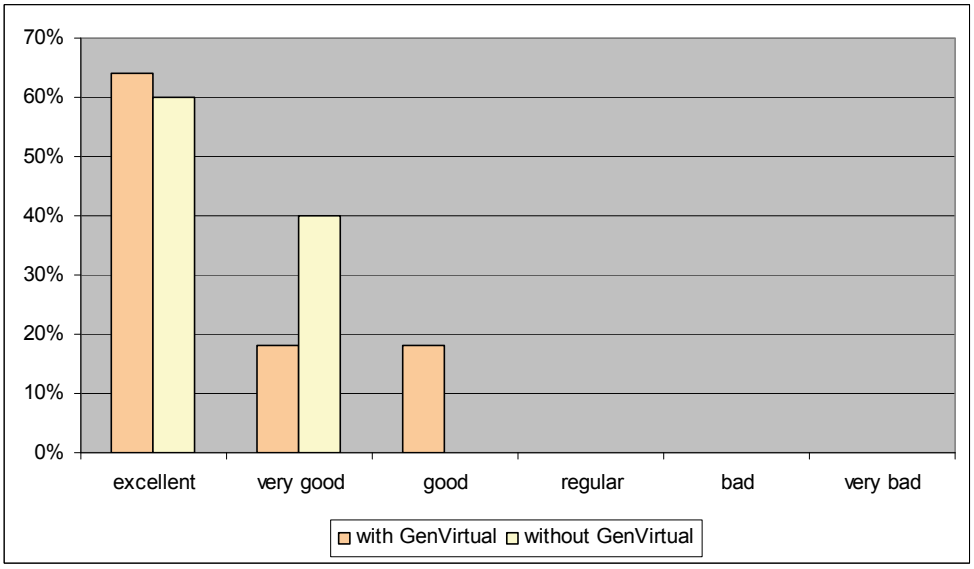

Fig. 16. Classification levels of motivation of the patient's from therapist point of view

4.6 Positive and Negative factors

Some positive points considered:

- Larger motivation: most patients demonstrated more motivation to accomplish upper limbs exercises in a different way making, changing the routine of conventional exercises.

- Differentiated exercises: patients that made exercises with stick and mass found them very repetitive, unlike patients that used GenVirtual, that could make same exercises in diversified ways (changing the cards musical notes and musical instruments).
- Musical stimuli: some patients tried to show their musical knowledge to the therapist. The largest attraction was to change the musical instrument easily;
- Technological Inclusion: none of patients had previous contact with an augmented reality environment.

Some negative points considered:

- Ergonomics: the table used for the accomplishment of exercises needed to be adjusted in a higher position in relation to other interventions with mass and stick, and this a lot of times generated discomfort to patients. Table adjustment was necessary so that the webcam recognized markers on tabletop. The larger the distance of table to webcam, the harder was the cards' identification. This was the main problem reported by therapists when setting up equipment and getting patient's appropriate posture before beginning the exercises.
- Many simultaneous incentives: some patients were very anxious, because there was a lot of incentive (visual and auditive) simultaneously.
- Little effect for individuals with low mobility: when a patient has low mobility, exercises didn't have a lot of effect in relation to conventional treatment.

4.7 Future perspectives

As a continuity of this work, we intend to conclude tests with patients of ABDIM and starting from that, to investigate relative subjects to the appropriate use of results of evaluations for improvement of GenVirtual.

Rehabilitation treatment protocol (with GenVirtual) is being defined in other rehabilitation centers with individuals with other deficiencies for future investigations: children with cerebral palsy in music therapy section and children with other types of muscular dystrophy in occupational therapy section of Association of Attendance to Deficient Child (AACD). In these protocols we will define the number, frequency and duration of interventions and will evaluate the treatment effectiveness. This research was previously approved by São Paulo Research AACD Ethics Committee under supervision of the music therapist section.

We intended to create new scenarios so patients can get involved in other therapeutic activities, as for example, new musical games. An investigation is being made to create a collaborative environment. This way the therapist can follow activities that the patient accomplishes at home. We also intend to investigate the possibility to create mechanisms for the therapist: observation, registration and evaluation activities.

5. Final considerations

In last years there has been some software development for treatment of several motor and cognitive disorders of people with disability. Especially, virtual and augmented reality technologies present an attractive interface generating larger motivation and consequently larger acceptance and participation in therapeutic treatment.

Virtual environments can adhere to therapeutic interventions. Multidisciplinary teams need to be involved during conception of such environments. This way, it is necessary to analyze characteristics or patients' abilities considering their limitations. For this reason, this

research was accomplished by engineers together with therapy specialists of ABDIM considering patients treated in the occupational therapy section taking into account the motive conduct, cognitive characteristic, motivation aspects and individual characteristics.
Results showed that GenVirtual can help therapeutic interventions for contemplating cognitive learning, motor, psychological-social, besides stimulating musicality. Given that it is based on a conventional computational platform, the prototype is already in condition of being used in home environments. This can propitiate family involvement in complementary activities.
It is appropriate to stand out that virtual environments presented here don't substitute conventional medical therapies. These tools empower existing treatments with pertinent use already established therapeutic process and rehabilitation techniques.

6. Acknowledgments

We would like to thank Núcleo de Trabalho, Aprendizado e Entretenimento of Laboratório de Sistemas Integráveis (NATE-LSI) team for the support on the conception and implementation of this project. We thank ABDIM for they daily work, and kind cooperation with this work. We also thank Fundação de Amparo à Pesquisa do Estado de São Paulo (FAPESP).

7. References

Alpini, D.; Cesarani, A.; Pugnetti, L.; Mendozzi, L.; Cardini, R.; Kohen-Raz, R.; Hahan, A. & Sambataro, G. (2000). Preventing mobility-related accidents in elderly and disabled. *Proceedings of International Conference on Disability, Virtual Reality and Associated technologies*, pp. 249-254, ISBN: 07 049 11 42 6, University of Reading, UK, Set. 2000, Alghero, Italy.

Azuma, R.; Baillot, Y.; Behringer, R.; Feiner, S.; Julier, S. & MacIntyre, B. (2001). Recent Advances in Augmented Reality. *Proceedings of IEEE Computer Graphics and Applications*, Vol. 21, No 6, Nov/Dec. 2001, pp 34-47, ISSN : 0272-1716.

Bach J. R. (2004). *Guia de exame e tratamento das doenças neuromusculares*. Ed. Santos, ISBN: 8572884238, São Paulo.

Bimber, O. & Raskar, R. (2005). *Spatial Augmented Reality: A Modern Approach to Augmented Reality*. ISBN: 1568812302, A K Peters, Los Angeles, California.

Bodine, C. & Scherer, M. (2006). Technology for improving cognitive function. *Journal of the International Society of Physical and Rehabilitation Medicine,* Vol. 1, No 4, Set. 2006, pp 257-261, ISSN 1748-3115.

Burdea, G. & Coffet, P. (1994). *Virtual Reality Technology*. 2ª Ed. Washington: Wiley-IEEE Press, ISBN 978-0-471-36089-6.

Burdea, G.; Blois, T.; Ching, E.; Halton, J.; Lopetinsky, B. & Drysdale, V. (2008). Nintendo Wii-based rehabilitation. *Proceedings of Virtual Rehabilitation*, ISBN: 978-1-4244-2700-0, Vancover Convention & Exibition Centre, Ago. 2008, Canada.

Cardoso, L.; Costa, R. M.; Piovesana, A.; Carvalho, J.; Ferreira, H.; Lopes, M.; Crispim, A. C.; Penna, L.; Araujo, K.; Paladino, L.; Sancovschi, R.; Moura, R. & Brandão, G. (2006). Utilização de Ambientes Virtuais na Reabilitação de Pacientes com Lesão Cerebral

por AVC e TCE, *Anais do X Congresso Brasileiro de Informática em Saúde*, Rio de Janeiro.

Carlo, M. P. & Bartalloti, C. (2001). *Terapia Ocupacional no Brasil - Fundamentos e Perspectivas*. Plexus, 2ª Ed., ISBN : 8585689617, São Paulo.

Carvalho, M. R.; Freire, R. C. & Nardi, A. E. (2008). Realidade virtual no tratamento do transtorno de pânico. *Jornal Brasileiro de Psiquiatria*, vol.57, No 1, Mar. 2008, pp. 64-69, ISSN 0047-2085.

Costa, R. M. & Carvalho, L. A. (2001). Experimentando um Ambiente Virtual com Pacientes Neuropsiquiátricos. *Anais da II Conferência Internacional de Tecnologias de Informação e Comunicação na Educação*, pp 529-546, ISBN: 972-98456-1-1, Centro de Competência Nónio Século XXI da Universidade do Minho, Braga-Portugal.

Costa, R. M. & Carvalho, L. A. (2005). O Uso de Jogos Digitais na Reabilitação Cognitiva. *Anais do Workshop de Jogos Digitais na Educação: XVI Simpósio Brasileiro de Informática na Educação*, pp 19-21, ISBN: 85-99925-01-6, Nov. 2005, Ed. ludensarts, Juiz de Fora – MG.

Deutsch, J.; Borbely, M.; Filler, J.; Huhn, K. Guarrera-Bowlby, P. (2008) Use of a Low-Cost, Commercially Available Gaming Console (Wii) for Rehabilitation of an Adolescent With Cerebral Palsy. *Journal of the American Physical TherapyAssociation*. Vol. 88, No 10, Out. 2008, pp. 1196-1207, ISSN 0031-9023.

Drettakis, G.; Roussou, M.; Tsingos, N.; Reche, A. & Gallo, E. (2004). Image-based Techniques for the Creation and Display of Photorealistic Interactive Virtual Environments. *Proceedings of Eurographics Symposium on Virtual Environments,* pp. 157-166, Jun. 2004, The Eurographics Association.

FakeSpace. *CAVE: The Most Widely Installed Fully Immersive Visualization System in the World*. Acessado em Março de 2009, Disponível em: http://www.mechdyne.com.

Fischer, J.; Bartz, D. & Strasser, W. (2006). Enhanced Visual Realism by Incorporating Camera Image Effects. *Proceedigns of International Symposium on Mixed and Augmented Reality*, pp 205-208, ISBN : 1-4244-0650-1, Oct. 2006, Washington: IEEE Computer Society Press.

Garbin, T. R.; Dainese, C. A. & Kirner, C. (2006). Sistema de Realidade Aumentada para Trabalho com Crianças com Necessidades Especiais. In: *Fundamentos e Tecnologias de Realidade Virtual e Aumentada : Livro do Pré-Simpósio, VIII Simposium on Virtual Relaity*. Tori, R.; Kirner, C. & Siscouto, pp. 289-297, Editora SBC, ISBN 85-7669-068-3 Belém-PA.

Geiger, C.; Schmidt, T. & Stocklein, J. (2004). Rapid Development of Expressive AR Applications. *Proceedings of the Third IEEE and ACM International Symposium on Mixed and Augmented Reality*, pp 292- 293, ISBN: 0-7695-2191-6, Nov. 2004.

Halton, J. (2008). Virtual rehabilitation with video-games: A new frontier for occupational therapy. *Occupational Therapy Now,* Vol 10, No 1, Fev. 2008, pp 12-14, ISSN 1481-5540.

Hoffman, H. G.; Palacios, A. G.; Carlin, C.; Furness, T. A. & Botella, A. C. (2003). Interfaces that heal: Coupling real and virtual objects to cure spider phobia. *International Journal of Human-Computer Interaction*, Vol. 16, No 2, Jul. 2003, pp 283-300, ISSN**:** 1532-7590.

Ichida, H.; Itoh, Y.; Kitamura, Y. & Kishino, F. (2004). ActiveCube and its 3D Applications. *Proceedings of IEEE Virtual Reality 2004 Workshop Beyond Wand and Glove Based*

Interaction, ISBN 0-7803-8415-6, Mar. 2004, Washington: IEEE Computer Society Press, Ilinois, Chicago.

Vianello A.; Bevilacqua M.; Arcaro G.; Gallan F. & Serra E. (2000). Non-invasive ventilatory approach to treatment of acute respiratory failure in neuromuscular disorders. A comparison with endotracheal intubation, *Intensive Care Medicine*, Vol 26, No 4, Abr. 2000, pp 384-390, ISSN: 1432-1238.

Juan, M. C.; Alcañiz, M.; Monserrat, C.; Botella, C.; Baños, R. M. & Guerrero, B. (2005). Using Augmented Reality to Treat Phobias. Moving Mixed Reality into the Real World. *Proceedings of IEEE Computer Graphics and Applications,* Vol. 25, No 6, pp. 31- 37, ISBN: 0272-1716, Dez. 2005, IEEE Computer Society.

Kakulas B. A. (1999). Problems and solutions in the reabilitation of patientes with progressive muscular dystrophy. *Scandinavian journal of rehabilitation medicine*, No 4, pp 23-37, ISSN: 0346-8720.

Kirner, C. & Tori, R. (2006a). Fundamentos de Realidade Virtual. In: *Fundamentos e Tecnologias de Realidade Virtual e Aumentada. Livro do VIII Simposium on Virtual Relaity*. Tori, R.; Kirner, C. & Siscouto, pp. 02-21, SBC, ISBN 85-7669-068-3 Belém.

Kirner, C. & Tori, R. Fundamentos de Realidade Aumentada. (2006b). In: *Fundamentos e Tecnologias de Realidade Virtual e Aumentada. Livro do VIII Simposium on Virtual Relaity*. Tori, R.; Kirner, C. & Siscouto, pp. 22-38, SBC, ISBN 85-7669-068-3 Belém.

Leitner, M.; Tomitsch, T.; Költringer, K. & Kappel, T. (2007). Designing Tangible Tabletop Interfaces for Patients in Rehabilitation. *Proceedings of Conference & Workshop on Assistive Technologies for People with Vision & Hearing Impairments: Assistive Technology for All Ages*, ISBN: 1613 0073, Vol 415, Ed. M. Hersh, Ago. 2007, Spanha.

Louro, V. S.; Ikuta, C. Yoko S. & Nascimento, M. F. (2005). Música e Deficiência: Levantamento de adaptações para o fazer musical de pessoas com deficiência. *Arquivos Brasileiros de Paralisia Cerebral*, Vol. 1, No 2, pág 11-17, ISSN: 1807-4456.

Medeiros, G. A. (2006). Sistema de Realidade Virtual para Tratamento de Fobia. *Dissertação de Mestrado. Departamento de Engenharia de Sistemas e Computação - Universidade do Rio de Janeiro*, Rio de Janeiro.

Milgram, Paul. & Kishino, Fumio. (1994). A taxonomy of mixed reality visual displays. *Transactions on Information and Systems Special Issue on Networked Reality,* Vol. E77-D, No.12, Dez. 1994, pp. 1321-1329, ISSN: 1994-1225.

Nascimento, M. F. (2006). Musicoterapia – Princípio e Prática. In: *AACD Medicina e Reabilitação: Princípio e Prática,* Fernandes, A. C.; Ramos, A. C. R.; Casalis, M. E. P. & Hebe, pp. 853-864, Ed. Artes Médicas, ISBN : 8536700556, São Paulo.

North, M. M.; North, S. M. & Coble, J. R. (1998). Virtual Reality Therapy: an effective treatment for phobias. *Studies in health technology and informatics*, Vol. 58, pp 112-119, ISSN: 0926-9630, Amsterdam.

Oliveira, T. M. V. (2001). Escalas de Mensuração de Atitudes: Thurstone, Osgood, Stapel, Likert, Guttman, Alpert. *Administração On Line : Prática - Pesquisa – Ensino*, Vol. 2, No 2, Abr-Mai – 2001, ISSN: 1517-7912.

Parés, N.; Carreras, A.; Durany, J.; Ferrer, J.; Freixa, P.; Gómez, D.; Kruglanski, O.; Parés, R.; Ribas, I.; Soler, M. & Sanjurjo, A. (2005). Promotion of creative activity in children with severe autism through visuals in an interactive multisensory environment. *Proceedings of the 2005 conference on Interaction design and children*, pp 110 – 116, 2005, ISBN:1-59593-096-5, Jun. 2005, Colorado.

Piaget, J. (1995). *Abstração Reflexionante: Relações lógico-aritméticas e ordem das relações espaciais*. Ed. Artes Médicas, Porto Alegre.

Rapaport D. (1992). A deletion including the brain promoter of the Duchenne muscular dystrophy gene is not associated with mental retardation. *Neuromuscular Disorders : NMD,* Vol 2, No 2, mes e ano, pp 117-120, ISSN : 0960-8966.

Reid, D. & Campbell, K. (2006). The use of virtual reality with children with cerebral palsy: a pilot randomized trial. *Therapeutic Recreation Journal*, Vol. 40, No 4, Out. 2006, pp 255-268, ISSN : 0040-5914.

Richard E.; Billaudeau V.; Richard P. & Gaudin G. (2007). Augmented Reality for Rehabilitation of Cognitive Disabled Children: A Preliminary Study. Proceedings of *Virtual Rehabilitation 2007*, pp. 102-108, ISBN: 978-1-4244-1204-4, Set. 2007, Venice.

Riva, G.; Bachetta, M.; Bafurri, M. & Molinari, E. (2002). Virtual Reality Environment for Body Image Modification: A Multidimensional Therapy for the Treatement of Body Image in Obesity and Realated Pathologies. *Journal CyberPsychology & Behavi*our, Vol. 3, No 3, pp 421-431, ISSN : 1557-8364.

Santos M. N.; Rezende M. M.; Terni A.; Hayashi M. C. B.; Fávero F. M.; Quadros A. A. J.; (2006). Perfil Clínico e Funcional dos Pacientes com Distrofia Muscular de Duchenne Assistidos na Associação Brasileira de Distrofia Muscular (ABDIM). *Revista. Neurociências*, Vol 4. No 1, pp 15-22, ISSN : 1984-4905.

Stone K.; Tester C.; Howarth A.; Johnston R.; Traynor N.; & Mc Andrew H. (2007). *Occupational therapy and Duchenne muscular dystrophy*. Chichester-England: John Wiley & sons Ltd, ISBN : 0470510307.

Sveistrup, H. (2004). Motor rehabilitation using virtual reality. *Journal of Neuroengineering and Rehabilitation*, Vol.1, No 1, Dez. 2004, pp. 1-10, ISSN: 17430003.

Watanabe, M. K. F.; Tsukimoto, D. R. & Tsukimoto, G. R. (2003). Terapia Ocupacional e o uso do computador como recurso terapêutico. *Revista Acta Fisiátrica Vol*. 10, No 1, pp 17-20, ISSN: 0104-7795.

Zatz M. (2002). Molecular biology contribution to the understanding and prevention of genetic disorders. *Ciência e Saúde Coletiva*, Vol. 7, No 1, ISSN 1413-8123.

Zorzal, E. R.; Cardoso, A.; Kirner, C. (2006) Lamounier, E. (2006). Realidade Aumentada Aplicada em Jogos Educacionais. *Anais do V Workshop de Educação em Computação e Informática*, Nov. 2006, Ouro Preto - MG.

3

Development of a Systems Architecture for Robot-Aided Telerehabilitation

Roberto Colombo
Service of Bioengineering, Fondazione Salvatore Maugeri, IRCCS
Rehabilitation Institutes of Veruno and Pavia
Italy

1. Introduction

Given the rapid increase in the aging of the population and the further increase that is expected in coming years, an important problem that has to be faced is the corresponding increase in chronic illness, disabilities, and loss of functional independence endemic to the elderly (WHO 2008). For this reason novel methods of rehabilitation and care management are urgently needed. Among the various health problems affecting the elderly, there is no doubt that stroke shows no sign of relinquishing its status as the leading cause of adult disability. After the acute phase all patients require continuous medical care and labour intensive rehabilitation. Arm therapy is used in the neurorehabilitation of patients with upper limb paresis due to lesions of the central nervous system (Riener et al., 2005). Besides traditional physical therapy, task oriented repetitive movements can help patients recover motor function, improve motor coordination, learn new motor strategies and avoid secondary complications, as many studies using robot-aided therapy attest (Krebs et al.,1998; Volpe et al., 2000; Lum et al., 2002, Colombo et al., 2005; 2008). Over the past decade, computer and information technologies have become increasingly available and cost-effective as a means of providing educational and health care services. Telerehabilitation is the delivery of rehabilitation services through a telecommunication network and the internet (Russel, 2009; Telerehabilitation – Wikipedia). A recent study that performed a systematic review of clinical outcomes, clinical process, healthcare utilisation and costs associated with telerehabilitation (Kairy et al., 2009) found, apart from experiments in various disciplines pertaining more to the field of telemedicine, only 28 studies that were strictly classifiable as telerehabilitation applications. Although these studies were heterogeneous in terms of study design, type of patients, settings and outcomes measured, a consistent trend was found in terms of their support for the effectiveness of telerehabilitation. The majority of them implemented programs of physical therapy remotely supervised by means of standard videoconferencing low-bandwidth systems.

The scenario of applications demonstrating the potential for remote diagnosis and treatment through robot-aided telerehabilitation is quite recent. In particular, the feasibility of remote training of arm movement using force feedback devices in stroke patients was first

demonstrated by Reinkensmeyer et al. (2002) using the so-called Java Therapy system and successively updated with the T-WREX device (Sanchez et al., 2006). Another laboratory application successfully tested the use of a virtual reality-based telerehabilitation system in five post-stroke patients (Piron et al., 2004). The Rutgers master II (RMII), developed by Popescu et al. (2000) was used to increase hand strength in stroke patients using teletherapy. Lum et al. (2006) developed a device called AutoCite that automates the intensive training component of constraint-induced movement therapy, and evaluated its effectiveness in a telerehabilitation setting under remote supervision by a therapist. Recently, Carignan et al. (2006) evaluated the potential application of the InMotion2 Robot (the commercial version of the MIT-Manus) for cooperative telerehabilitation in which the therapist and patient interact directly with each other over the internet both visually and kinesthetically. All these studies demonstrated the feasibility of the telerehabilitation approach and, in addition, Lum's study demonstrated that the gains in motor ability obtained with remote supervision were comparable with those obtained with direct supervision. None of these experiences tried to base their architecture on more than one type of rehabilitation device, i.e. none aimed to apply a modular combination of devices that can cover a larger population of patients.

Telerehabilitation may well be able to optimize the therapeutic intervention, despite the fact that the patient does not directly interact with the therapist . This is so not only in the home care setting, but also in the clinical setting where it makes it possible for a therapist to monitor several patients at once, at their training stations located in different laboratories. The connected devices can be diversely configured in order to target the rehabilitation of different joints and motor tasks.

The main advantages of telerehabilitation are that it allows:

- improved continuity of care, through a choice of technological services designed to assist patients as their needs change;
- increased exercise time and intensity for a quicker recovery of the patient, obtained without a corresponding increase in resources allocation and possibly through a more cost-effective application of intensive treatments;
- continuous, real time monitoring of the effects of the treatment session, using video and physiological signal transmission;
- on-line tuning of exercise parameters;
- concurrent monitoring of multiple treatment stations.

This chapter presents a preliminary experience carried out in our Rehabilitation Institute to verify the feasibility of implementation of a telerehabilitation approach based on the application of robotic devices developed in our research laboratories.

2. System Design

2.1 Rehabilitation Devices.

Although virtually any robotic device developed for upper or lower limb rehabilitation can be employed for remote supervised training, in practice the larger, more complex, more expensive devices are reserved mainly for the clinical setting, while the home care setting calls for smaller, cheaper and easy to use devices.

The systems architecture implemented in our experiments consisted of three devices developed for upper limb rehabilitation that can be employed in either setting:

1) a one degree of freedom (DoF) wrist manipulator specifically designed for the rehabilitation of wrist flexion and extension movement.
2) a two DoF shoulder elbow manipulator called MEMOS which allows robot-aided therapy by administering a sequence of reaching movements in the horizontal plane [6].
3) a graphic tablet-based device developed to improve the quality of movement (accuracy, efficiency and smoothness) in patients with mild impairment.

The systems are based on the execution of repeated voluntary movements and on the consequent motor learning phenomenon. The patient is facing a video screen that provides visual feedback in the form of three coloured circles as follows: 1) a yellow circle indicates the task's starting position; 2) a red circle indicates the task's target position; 3) a green circle indicates the current position of the handle. The first two devices are admittance control based; this means that the patient exerts a force on the handle of the device which in turn produces a displacement. Three possible control strategies were implemented: a) completely servo-assisted movements; b) shared control of the movements (i.e. the system will help the subjects to carry out the part of the task they are not able to do autonomously); c) completely voluntary movements. Seamless transition among the control strategies was applied, in the sense that if a time period of more than 3 s. elapsed in which the patient was unable to move the handle, the device would 'take over' and complete the motor task. Details of the systems can be found in Colombo et al. (2005; 2008). The tablet-based device shares the same user interface and features as the two DoF devices but, of course, does not provide assistance when the patient is not able to complete the assigned motor task. This system is applied in a different laboratory where patients practise activities of daily living (ADL) to improve the quality of their movements. This type of practice might be very useful in post-stroke, TBI patients and subjects with ataxia.

2.2 Systems Architecture

The systems architecture implemented is represented in figure 1. It consists of a number of rehabilitation stations (a maximum number of 16 was selected) and a supervision station, located in different laboratories. They are all interconnected by means of a standard Ethernet II network. The supervision station includes also connection to the internet in order to connect remote rehabilitation stations in the home setting. In this preliminary presentation only the in-clinic subnet will be discussed.

Rehabilitation Station: it consists of a rehabilitation device (robot or tablet) and web cam directly connected to the network (IP camera). This configuration enables both video/audio and exercise monitoring. It exchanges information with the supervision station in order to implement the following functions:

a) activate the exercise by means of a program interface easily manageable by the patient; b) allow remote setting of the exercise parameters (protocol, duration, maximum speed, duration of rest, etc.); c) manage exercise execution during each session; d) collect and store data from the rehabilitation device; e) compute evaluation parameters in order to quantitatively measure patient performance during exercise execution; f) compute and display in real time, during the task execution, scores providing visual feedback to the patient of their performance; g) allow video/audio communication with the supervision station.

Supervision Station: it represents the central node of the network, where the therapist manages all the activities of each rehabilitation station. Consisting of a remote workstation,

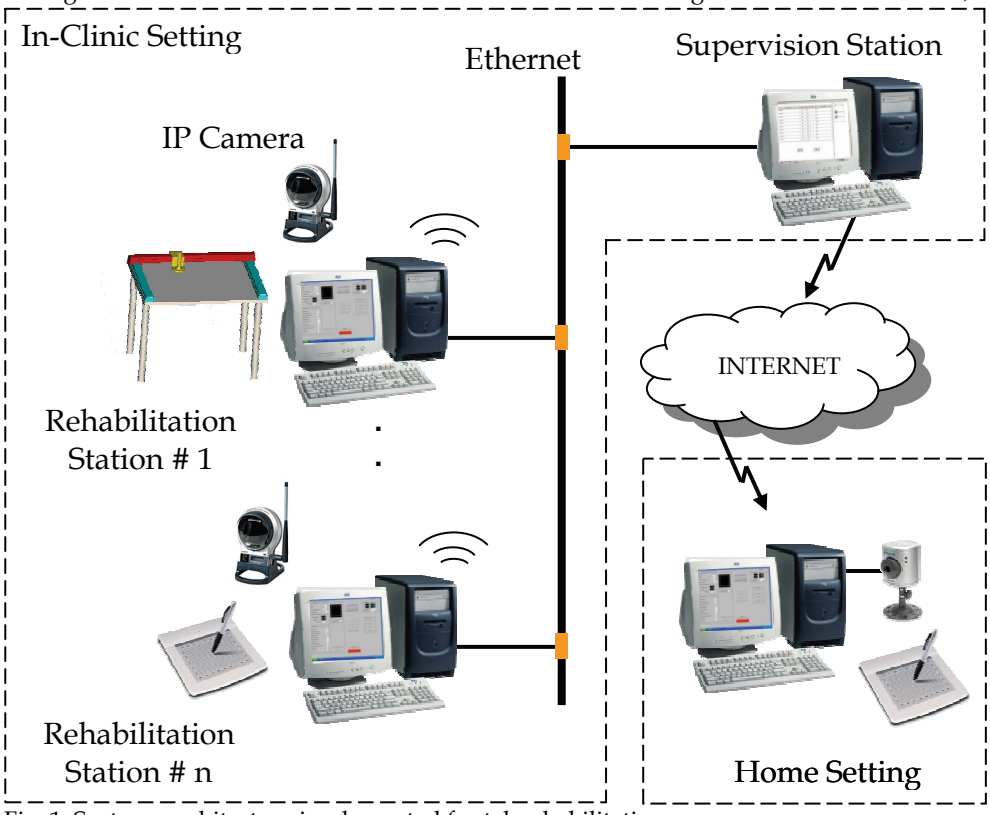

Fig. 1. Systems architecture implemented for telerehabilitation.

it: a) selects the patients to be supervised; b) sets up the rehabilitation protocol and, if required, modifies the exercise parameters; c) monitors in real time the patient's performance by means of specific charts; d) transfers and archives the data and parameters acquired by the rehabilitation station; e) stores the collected data in a central data base; f) post-processes the collected data; g) reviews performance charts and allows comparison of charts; h) prints performance reports; k) allows audio/video communication with the rehabilitation station, in order to implement one-to-one and one-to-many therapist to patient interaction.

Audio/Video monitoring: diverse audio/video features are possible depending on the type of video camera selected. Two-way video conference-like communication using a webcam with pan, tilt and zoom functions can be selected to carry out full audio and video one-to-one interaction (figure 2a). This feature is crucial when the therapist needs to monitor fine movements, like finger movements, with an appropriate resolution. In this pilot study we tested a network-camera (Linksys WVC200) which allowed full videoconferencing with the patient during the motor task execution. With this implementation we could also monitor several patients at the same time so allowing one-to-many telemonitoring (figure 2b).

2.3 Software Implementation

Both the Rehabilitation and Supervision stations were developed using LabWindows CV/I software development environment (National Instruments, Austin-TX,USA). The features of the former have been described elsewhere (Colombo et al., 2005). The application program of the Supervision Station has the following main features:

a) it monitors the current status of the configured devices (device on-line/off-line, patient active/non-active);

b) it remote-configures the exercise. This is typically done by the supervising therapist when a new motor task needs to be configured or the difficulty level of the exercise adjusted. This function (implemented through the UltraVNC program, http://www.uvnc.com) allows the therapist to use the mouse and keyboard of the supervision station to control the rehabilitation station remotely. It means that the therapist can work on a remote computer, and from this location control the rehabilitation station as if seated in front of it.

c) it displays patient performance charts. These display the time course of some parameters measured by the robot. For example for the shoulder and elbow manipulator the charts display the performance score and the parameters measuring the efficacy, accuracy, efficiency and mean speed of movement (see next paragraph for more details). On demand, raw data can be transferred and stored in the supervision station data base.

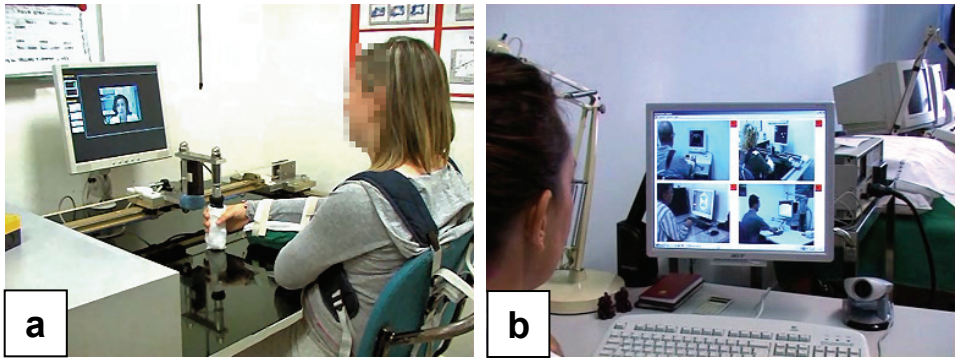

Fig. 2. a) One-to-one and b) One-to-many therapist to patient interaction examples.

3. Telerehabilitation Example

This systems architecture was tested during the rehabilitation of four patients after chronic stroke. The testing was preceded by a learning phase in which patients were trained in order to be autonomous in the phase of connection to the device and start of the exercise. If the patient could not attain autonomy for this task the caregiver was instructed to attach the patient to the device.

Thanks to the remote control program the therapist could take complete control of the remote device and select a new motor task when a change in difficulty level was required. The values of the exercise parameters were logged into a file of the rehabilitation station. In

this way the settings of the previous session could be used as default for the following exercise session.

Figure 3 shows the patients' performance charts obtained during the telerehabilitation preliminary study. Top panels present the charts of two patients during treatment with, respectively, the tablet-based device (left panel) and the shoulder-elbow manipulator (right panel). Bottom panels present respectively the charts of a patient during the course of treatment with the wrist manipulator device (left panel) and those of a patient taken from our patient files. Each chart reports the mean value of some performance parameters measured during the training. Blue points and lines represent the values obtained for each parameter during previous training sessions. The point in red represents the current value during the ongoing session. Current values were updated on the supervision station every 10 s by means of a polling operation. The rehabilitation station acquired and collected the raw data including the position of the robot handle, the patient's exerted force, and the robot status. On demand, raw data could be transferred and stored in the supervision station data base.

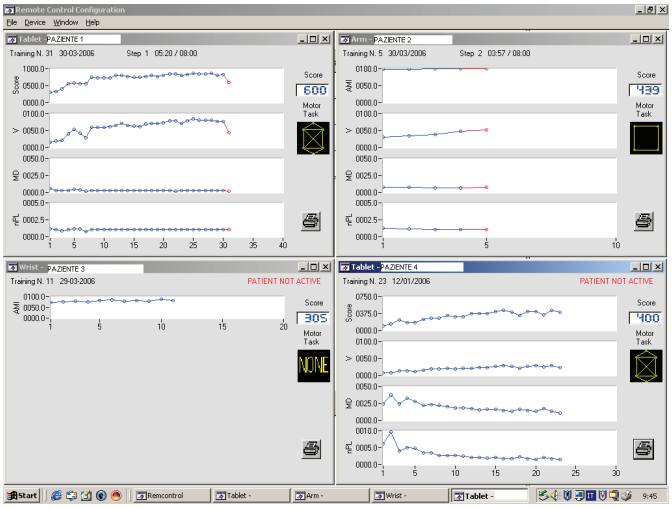

Fig. 3. Patients' performance charts obtained during the telerehabilitation test.

Figure 4 presents a typical example of the time course of the device measured parameters during the treatment of a patient after chronic stroke. In particular, the shoulder-elbow manipulator included the following parameters:

Movement efficacy. The movement efficacy was measured by computing what we called the active movement index (AMI) that quantified the patient's ability to execute the assigned motor task without robot assistance. A score termed 'robot score' was displayed on the video screen facing the patient during task execution. It increased only during the patient's voluntary activity, reflecting the proportion of theoretical path (i.e. the straight line connecting the starting point and the target) travelled by the handle thanks to the patient's force. The robot score was expressed as a tenth of the total distance between the starting point and the target. The AMI was calculated as the ratio between the robot score obtained by the patient and the theoretical score, i.e. the score obtained if the patient completed all

tasks of the training session by means of his voluntary activity. In order to obtain a normalized index it was expressed in percentage units.
Movement speed. The training device allowed to record the current position of the handle. In this way the mean value of the velocity (VM) of the handle during the task execution could be computed.
Movement accuracy. The accuracy of the movement was assessed by measuring the mean absolute value of the distance (MD) of each point of the path from the theoretical path. When this parameter approximates zero movement accuracy will be very high. It is actually a measurement of the error of accuracy; hence a decrease in this index during training indicates an improvement of accuracy in the motor task execution.
Movement efficiency. The movement efficiency was obtained by computing the path length (nPL) of the trajectory travelled by the patient in order to reach the target. This parameter is virtually the line integral of the trajectory over the time taken to reach the target. In practice it was obtained by summing the distances between two consecutive points of the patient's path; it was normalized to the straight line distance between the starting point of the task and the target. Also this parameter is a measure of the error of movement efficiency; hence decreasing values during training should reflect an improvement of efficiency of the motor task execution.

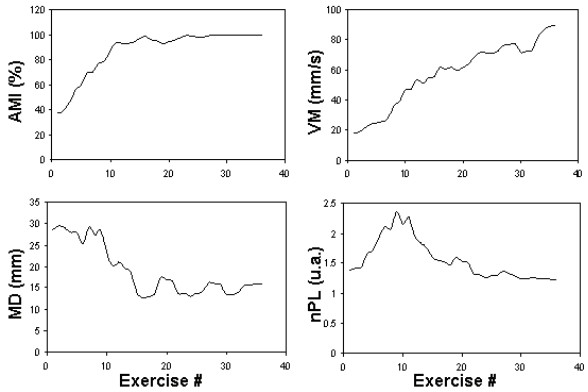

Fig. 4. Example of the time course of the device measured parameters during the treatment of a patient after chronic stroke.

In this example one can note that the AMI increased up to half-way through treatment, at which point the patient was able to complete the motor task. The mean speed VM was constantly increasing, indicating continuous improvement of the patient's performance throughout the treatment. The mean distance (MD) and the normalized path length (nPL) errors decreased, thus showing an improvement in both accuracy and efficiency of the movement.

4. Human factors in robot-aided telerehabilitation

Despite the fact that telerehabilitation is strongly based on technology, it is essential that all telerehabilitation services are designed and implemented with the users in mind. We must consider as users both sides of the communication channel, i.e. the patient and the therapist. It is thus extremely important that human factors are considered in the planning and implementation of the telerehabilitation programmes and in the design of new devices (Brennan DM et al., 2008). In particular, the technology employed should be easy to use both for the therapist and patient. A simple user interface, an easy way to interact with the system and an environment that does not distract the patient are fundamental prerequisites. The systems should be flexible enough to support the diverse requirements due to the different age, education, technology experience and level of impairment of patients, so as to maximize patients' acceptance and motivation and minimize the effects of their disabilities. Another key factor is training. Patients should receive clear, detailed information about the technology in view of the fact that the home care setting will be a reduced supervision environment. The possibility to implement both videoconference communication and remote management and monitoring of the devices should be considered an add-on value of our architecture able to soften the impact of technology.

IMI subscale	*Score (Mean ± S.D.)*
Interest/Enjoyment	6.00 ± 1.49
Perceived Competence	4.59 ± 1.89
Effort/Importance	6.70 ± 0.72
Value/Usefulness	6.15 ± 1.38
Pressure/Tension	2.26 ± 2.07
Pain	2.39 ± 2.28

Table 1. Subscale findings of the Intrinsic Motivation Inventory questionnaire evaluated in patients treated with the elbow-shoulder rehabilitation device (subscale range= 1–7).

Motivation is an important factor in rehabilitation and frequently used as a determinant of rehabilitation outcome. Several factors can influence patient motivation and so improve exercise adherence. In a previous study (Colombo et al., 2007) our research group assessed patient motivation in a group of post-stroke patients who underwent treatment by means of robot-aided neurorehabilitation in an in-hospital setting. Patients' motivation was assessed by means of the Intrinsic Motivation Inventory (IMI) questionnaire (17-item version). The results are reported in Table 1.

The interest/enjoyment subscale, that is considered the self-report measure of intrinsic motivation, obtained a high score. This means that our patients found the robot therapy very interesting. The perceived competence subscale resulted in a mid score. This result is not surprising given the different level of disability of our patients. In fact, less compromised patients should obtain better results than more compromised patients. Also the effort/importance and value/usefulness subscales obtained a high score, demonstrating that patients were really motivated in doing this type of treatment and were satisfied with the results obtained. In particular, they perceived that the treatment had a positive result in terms of improving their disability. The pressure/tension and pain subscales obtained a low

score. This means that the majority of patients did not experience tension or pain during the training with the robot device.
Recently Piron and colleagues (2008) measured the satisfaction with telerehabilitation care in post-stroke patients. They compared the degree of satisfaction of two groups of patients undergoing a virtual reality (VR) therapy programme: at home versus in a hospital setting. Patient satisfaction was measured through a 12-item questionnaire administered at the end of treatment. The questionnaire included items assessing the usability of the VR system, the relationship with the therapist and overall satisfaction with the treatment. Patients treated at home with the telerehabilitation approach showed median values equal to or higher than those obtained in the in-hospital group. In addition the first group improved significantly their motor performance, while the latter group showed no significant change.

Question	*Score (Mean ± S.D.)*
1. I need to monitor patient performance during remote supervision.	5.9 ± 1.7
2. I need to modify the exercise parameters (duration, difficulty level, task shape, etc.) during remote supervision.	6.6 ± 0.8
3. I would like to be able to remotely feel the patient's exerted force during the exercise execution.	5.2 ± 2.0
4. I think that robot-aided telerehabilitation can be useful in the home setting.	5.1 ± 2.0
5. I think that robot-aided telerehabilitation can be useful in the in-hospital setting.	4.6 ± 2.3
6. I think that robot-aided telerehabilitation can reduce rehabilitation costs.	4.4 ± 2.7

Table 2. Mean score and standard deviation obtained in six questions assessing therapists' opinions about the telerehabilitation architecture. (Score range= 1 -7; 1= not at all true; 7= very true).

To assess therapists' opinions about the architecture presented here and general issues regarding telerehabilitation, we surveyed a group of 18 therapists. They underwent a 1 h briefing session in which they received detailed information about robot aided rehabilitation and telerehabilitation. They were then divided into three groups and underwent a 1 h practice session in which they could conduct a complete telerehabilitation training session using the robots. At the end of the practice session the therapists were asked to fill in an ad-hoc questionnaire. Table 2 reports the results (mean score ± standard deviation) obtained for six specific questions.
The therapists thought it very important to monitor specific exercise parameters (such as accuracy, efficiency, speed, etc.). This means that they consider it important not only to communicate with the patient but also to measure the patient's performance. They expressed the need to be able to remotely modify the exercise (e.g. change the difficulty level of the task, the exercise duration, etc.). They also stated that they would like to feel the patient's exerted force during the exercise performance. This is a feature unsupported by our system at present but we hope to introduce it in future extensions.

Questions 4 to 6 regard general opinions about the telerehabilitation approach. The scores were lower than those obtained for questions 1 to 3, but in any case mid-scale values were obtained. This is due to the fact that there were two main attitudes in favour and against the telerehabilitation approach and consequently high and low scores. It is expected that a longer practice period during real treatment sessions could positively change this result.

5. Discussion and Conclusion

The study presented in this chapter shows the feasibility of implementing a telerehabilitation approach based on the application of robotic devices to increase training intensity in post-stroke patients. The robot-assisted teletherapy was well accepted and tolerated by all patients. The assessment by means of ad-hoc questionnaires of patient and therapist satisfaction with the telerehabilitation approach confirmed a high degree of satisfaction with this type of approach. In addition, the new technological context facilitated therapy planning for the medical professionals and therapists, including the possibility to continue the rehabilitation program in the home setting. Of course, extended application in a consistent group of patients is required to evaluate if the improvement of patients' motor ability obtained through telerehabilitation is similar to that obtained in controlled laboratory conditions. In particular, evidence is needed to show that learning in a telerehabilitation environment can be generalized to a community setting.

Circuit class therapy is a mode of delivering rehabilitation services with a reduced therapist-to-patient ratio. The advantage of this approach is that it offers increased intensity of treatment while at the same time reducing health care costs. However, only patients who can safely perform the required motor tasks may be eligible for this type of therapy. The architecture we implemented can be considered as a sort of technological circuit class therapy to be used with more compromised patients.

A key goal of future research will be to quantitatively evaluate patients' adherence to the prescribed regimen. The remote supervision and the possibility of administering appealing motor tasks specifically adapted to the patient's ability/disability should contribute to enhance their motivation, so improving adherence and involvement.

Some applications have explored the feasibility of using "interactive telerehabilitation" and "cooperative telerehabilitation" (Carignan & Krebs, 2006) i.e. the situation in which both therapist and patient interact directly with each other through the Internet, without any direct force feedback interaction in the former case and both visually and kinesthetically in the latter (patient and therapist have the feeling of being in direct contact with each other through the device). This type of approach involves a one-to-one interaction; thus it would be economically justifiable mainly in situations of long distance between the patient's home and the rehabilitation centre. In addition, it requires the solution of problems of time delay in the control loop due to the network; this delay is not negligible in the case of Internet communication and is highly variable.

The application of one-to-many remote-supervised therapy implies a reduction in the therapist to patient interaction. Such contact could take place at the beginning and end of each session or less frequently. This would allow the patient to concentrate on performing the assigned motor task without being distracted by the technology. Real time video/audio communication might be useful mainly at the beginning of training to provide suggestions for an optimal task execution, and subsequently just for reporting feedback about the

obtained performance and sustaining patient motivation. Such approach would have more chances of a successful application because it would combine an increase in the intensity of treatment with a contemporary reduction of health care costs.
Finally, future studies should address the development of new devices such as wearable robotics and wireless sensors in order to give patients the chance to be trained through a telerehabilitation approach directly in activities of daily living.
In addition, further research is needed to set minimum technical specifications and standards, provide safe and fault-tolerant technology, validate clinical protocols, investigate the effectiveness of interventions and establish the cost-effectiveness of robot-aided telerehabilitation. Thus, with a rapid increase in the speed and quality of the telecommunication services, the future should hold bright prospects for the spread of telerehabilitation.

6. References

Brennan, D.M. & Barker, L.M., (2008). Human factors in the development and implementation of telerehabilitation systems. *Journal of Telemedicine and Telecare*, 14(2), 55-8.

Carignan, C.R. & Krebs, H.I., (2006). Telerehabilitation robotics: bright lights, big future? *Journal of Rehabilitation Research and Development*, 43(5), 695-710.

Colombo, R. et al., (2008) Assessing mechanisms of recovery during robot-aided neurorehabilitation of the upper limb. *Neurorehabilitation and Neural Repair*, 22(1), 50-63.

Colombo, R. et al., (2007). Design strategies to improve patient motivation during robot-aided rehabilitation. *Journal of Neuroengineering and Rehabilitation*, 4, 3.

Colombo, R. et al., (2005). Robotic techniques for upper limb evaluation and rehabilitation of stroke patients. *IEEE Transactions on Neural Systems and Rehabilitation Engineering,* 13(3), 311-24.

Kairy, D. et al., (2009). A systematic review of clinical outcomes, clinical process, healthcare utilization and costs associated with telerehabilitation. *Disability and Rehabilitation*, 31(6), 427-47.

Krebs, H.I. et al., (1998). Robot-aided neurorehabilitation. *IEEE Transactions on Rehabilitation Engineering*, 6(1), 75-87.

Lum, P.S. et al., (2002). Robot-assisted movement training compared with conventional therapy techniques for the rehabilitation of upper-limb motor function after stroke. *Archives of Physical Medicine and Rehabilitation*, 83(7), 952-9.

Lum, P.S. et al., (2006) A telerehabilitation approach to delivery of constraint-induced movement therapy. *Journal of Rehabilitation Research and Development*, 43(3), 391-400.

Piron, L. et al., (2004). Motor tele-rehabilitation in post-stroke patients. *Medical Informatics and the Internet in Medicine*, 29(2), 119-25.

Piron, L. et al., (2008). Satisfaction with care in post-stroke patients undergoing a telerehabilitation programme at home. *Journal of Telemedicine and Telecare*, 14(5), 257-60.

Popescu, V.G. et al., (2000). A virtual-reality-based telerehabilitation system with force feedback. *IEEE Transactions on Information Technology in Biomedicine*, 4(1), 45-51.

Reinkensmeyer, D.J. et al., (2002). Web-based telerehabilitation for the upper extremity after stroke. *IEEE Transactions on Neural Systems and Rehabilitation Engineering*, 10(2), 102-8.

Riener, R., Nef, T. & Colombo, G., (2005). Robot-aided neurorehabilitation of the upper extremities. *Medical & Biological Engineering & Computing*, 43(1), 2-10.

Russell, T.G., (2009). Telerehabilitation: a coming of age. *The Australian Journal of Physiotherapy*, 55(1), 5-6.

Sanchez, R.J. et al., (2006). Automating arm movement training following severe stroke: functional exercises with quantitative feedback in a gravity-reduced environment. *IEEE Transactions on Neural Systems and Rehabilitation Engineering*, 14(3), 378-89.

Telerehabilitation - *Wikipedia*, the free encyclopedia. Available at: http://en.wikipedia.org/wiki/Telerehabilitation

Volpe, B.T. et al., (2000). A novel approach to stroke rehabilitation: robot-aided sensorimotor stimulation. *Neurology*, 54(10), 1938-44.

WHO. - *The World Health Report 2008*. Available at: http://www.who.int/whr/2008/en/index.html

4

Analysis and Design of Piezoelectric Braille Display

Pruittikorn Smithmaitrie
Department of Mechanical Engineering, Faculty of Engineering,
Prince of Songkla University
Thailand

1. Introduction

Braille alphabet system was created by Louis Braille in 1821 for visually impaired or blind people to write and read via touching. A Braille character consists of six or eight dots in a rectangular array 3×2 or 4×2 (Tiresias, 2009). The dot may rise at any position based on a character mapping code. The character mappings are coded differently depended on languages. No matter what the language is, most of written communication today trends to be in electronic forms, for examples, report, manuscript, email, SMS, blog or website. Refreshable electronic Braille display is designed for display those electronic media in the Braille format. This allows blind users to read by touching as alternative to listening to the screen reading or text-to-speech software, such as, WebAnywhere for English language and PPA Tatip for Thai language (Bigham et al., 2008; PPA, 2009).

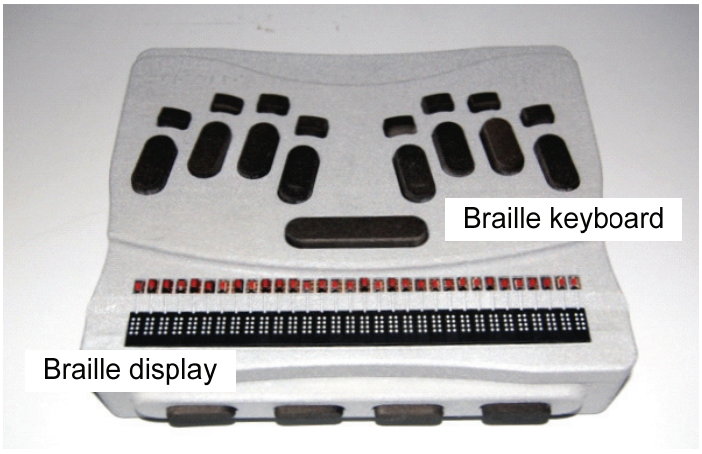

Fig. 1. Portable Braille Note.

The Braille display is an electronic device that displays refreshable Braille characters. Height of the Braille dot is controlled by a piezoelectric bimorph underneath. Electrical signals stimulate the piezoelectric bimorphs to bend up or down, consequently causing the dots to rise or fall, forming the Braille characters. The piezoelectric Braille display unit is an electrical control system. Thus, it can be connected to a computer, mobile phone or Braille Note, as shown in Fig. 1, to transform on-screen information into the Braille character form (Braille and Assistive technology, 2009). This provides access to blind users for reading or checking the electronic media by touching the Braille display.
Refreshable Braille cell is a single unit of a Braille character that can be display and refresh itself to any Braille character depended on a command input. The refreshable Braille cells have been continuously developed for several decades. Beginning in the 1980s, solenoids were used as actuators to control movement of the Braille dots (Frisken-Gibson et al., 1987; Fukuda et al., 1997). Later, in the 1990s, relay-control Braille cells were proposed (Sriskanthan & Subramanian, 1990). Meanwhile, piezoelectric Braille cells were also proposed (Linvill & Bliss, 1966; Linvill, 1969) and continuously developed. At present, the piezoelectric Braille cell (Fig. 2.) is a common type of refreshable Braille cells and commercially available (HumanWare, 2009) because it has relatively lightweight and a small size. In addition, there are some actuators that can be applied to control the Braille dots such as pneumatic (Yobas et al., 2001; Yobas et al., 2003), piezoelectric polymer (Linvill, 1986), shape memory alloy (Taylor et al., 1998; Velazquez et al. 2006; Velazquez & Pissaloux, 2006), ultrasonic motor (Shinohara et al., 1998; Cho et al., 2006) and electrorheological (ER) fluid (Taylor et al., 1998), but most of them are not commercially available due to their limitations.

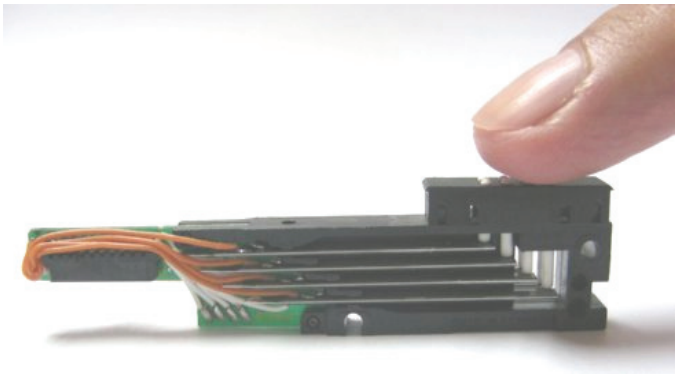

Fig. 2. The piezoelectric Braille cell.

The aim of this study was to implement the piezoelectric actuator for designing the Braille display. The results of this work would facilitate product designers or engineers to apply the design procedure and parameters to achieve a suitable electronic Braille display that uses the piezoelectric actuator as a driving mechanism. The piezoelectric Braille display has many advantages, i.e., compact size, lightweight and direct-electrical control.
In this chapter, physical behaviour of the piezoelectric bimorph inside the piezoelectric Braille display is analyzed. The governing equation of the piezoelectric Braille system is presented. Then, survey data of visually impaired people using a Braille Note is reported as design information and a reference input for calculation of the piezoelectric Braille response

under the touching force. Based on the mathematical model, relationship betweens the key design parameters (free length of the piezoelectric bimorph, dot height and applied voltage) are studied. The result gives well understanding of the piezoelectric Braille cell behaviour under both touching force and electrical excitation simultaneously. This is the important issue for development of piezoelectric Braille display in senses of controlling Braille dot displacement or force-feedback display unit in the future.

2. Design of the Piezoelectric Braille Display

The piezoelectric Braille display consists of a structural base, piezoelectric bimorphs, a printed circuit board (PCB), a cap and pins as illustrated in Fig. 3. A Braille dot is a part of the pin which is controlled by the piezoelectric bimorph underneath. The active dot rises up when the corresponding piezoelectric bimorph is excited by the electrical control signal. The height of the dot is an important parameter that must be designed to rise up to a specific sensible height above the reference surface or the cap.

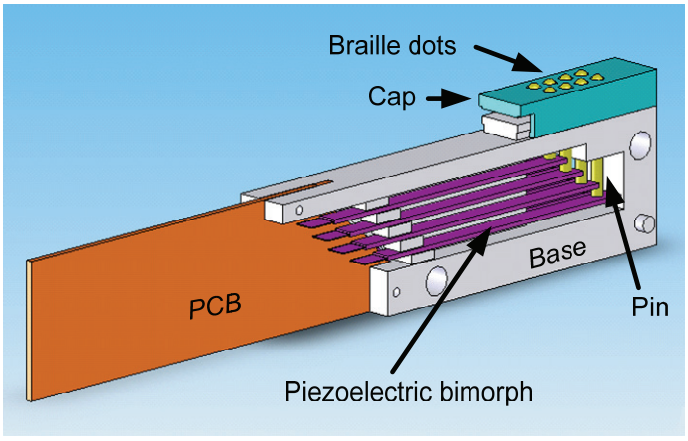

Fig. 3. Assembly drawing of the piezoelectric Braille cell.

As shown in the driving mechanism (Fig. 4.), the pin is supported and controlled by the piezoelectric bimorph, and the other end of the bimorph is fixed to the base. The free length of the bimorph is L. The tip displacement is d. The bimorph is a straight beam when there is no electrical excitation (normal position). If there is an electrical signal causing the bimorph to bend up, the dot will be raised up. This rise position is used when the dot is active. On the other hand, if there is an electrical signal causing the bimorph to bend down, the dot will fall down under the reference surface. This fall position is used when the dot is inactive. Thus, the total pin movement (full stroke) is two times of the tip displacement. Because of this two-state action, i.e., bending up and down, it is so called the bimorph.

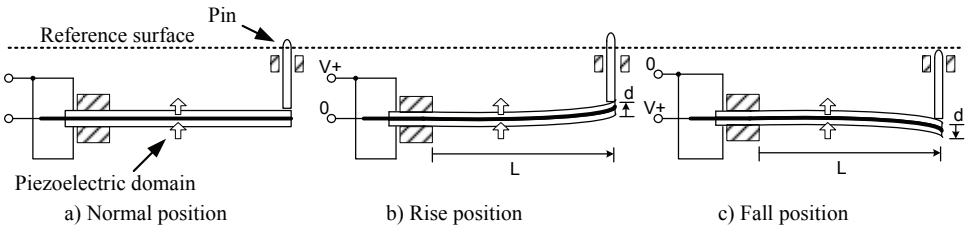

Fig. 4. Actuation mechanism of the piezoelectric Braille cell.

The piezoelectric actuator layers are laminated on the top and bottom surfaces of the beam. There are many configurations to arrange piezoelectric domains of the actuators in order to control the beam position according to the electrical input. One suggestion of the piezoelectric domain arrangement and corresponding electrical control input is shown in Fig. 4. Next, the governing equation of the piezoelectric bimorph is determined to analyze relationship between the free length of the bimorph, tip displacement, electrical excitation and external pressing force.

3. Analysis of the Piezoelectric Bimorph

The piezoelectric actuators are fully bonded with a flexible beam on both sides as shown in Fig. 5. During operation, the electrical signal excites the piezoelectric bimorph causing the dot to rise or fall, as previously illustrated in Fig. 4. In this research, movement of the pin is investigated when the electrical control signal is applied.

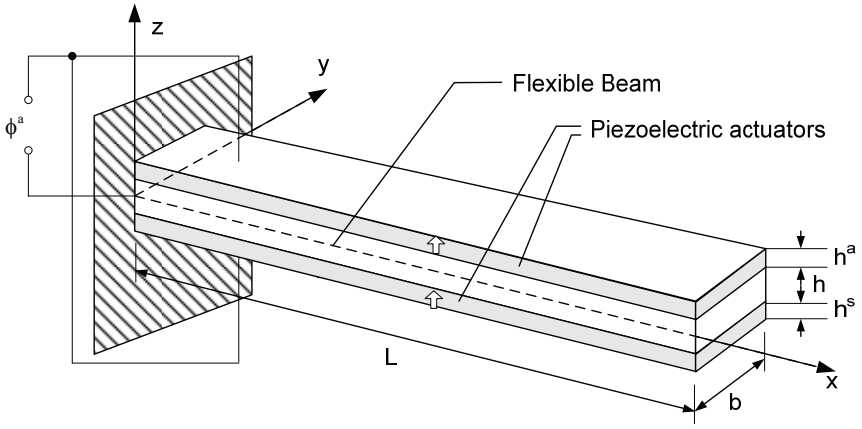

Fig. 5. The piezoelectric bimorph.

The actuator area is from x_1 to x_2 in the x-direction and has the same width as the beam b. Thus, the effective actuator area S^e is $b(x_2-x_1)$. The piezoelectric bimorph is assumed to be an elastic thin beam. Hence, the equation of motion of an Euler-Bernoulli beam is (Tzou, 1993)

$$YI\frac{\partial^4 u_3}{\partial x^4}+\rho A\frac{\partial^2 u_3}{\partial t^2}=bq_3 \tag{1}$$

where Y is Young's modulus; $I = bh^3/12$ is the area moment of inertia; b is the beam width, h is the beam thickness; u_3 denotes the transverse displacement; A = bh is the cross-section area; and q_3 is the transverse excitation. The piezoelectric actuator induces control moment M_{xx}^c and it is added into the governing equation of the beam. Thus, the equation of motion of the system becomes

$$YI\frac{\partial^4 u_3}{\partial x^4}+\rho A\frac{\partial^2 u_3}{\partial t^2}-b\frac{\partial^2 M_{xx}^c}{\partial x^2}=bq_3\,, \tag{2}$$

where the actuation control moment M_{xx}^c relates to the piezoelectric actuation force as follows,

$$M_{xx}^c=r^a d_{31} Y_p \phi^a\,, \tag{3}$$

where r^a is the effective moment arm (distance from the neutral surface of the beam to the mid-plane of the actuator layer); d_{31} is the piezoelectric strain constant; Y_p is Young's modulus of the laminated piezoelectric layers; and ϕ^a is the electrical control voltage. The displacement of the pin is assumed to be equal to the displacement of the beam tip. Therefore, the displacement of the pin is the transverse displacement u_3 at x = L where L is the free length of the beam.

It is assumed that only a transverse voltage is applied. If the electrode resistance is neglected, the voltage on the piezoelectric actuator is constant. Thus, an actuation voltage $\phi^a(x,y,t)$ applied to the piezoelectric actuator is

$$\phi^a(x,y,t)=\phi^a(t)[u_s(x-x_1)-u_s(x-x_2)][u_s(y-y_1)-u_s(y-y_2)]\,, \tag{4}$$

where u_s represents a unit step function, $u_s(x\text{-}x_i) = 1$ when $x \geq x_i$, and = 0 when $x < x_i$. Hence, the control moment M_{xx}^c in the x-direction induced by the piezoelectric actuator can be defined as

$$M_{xx}^c=r^a Y_p d_{31}\phi^a(t)[u_s(x-x_1)-u_s(x-x_2)][u_s(y-y_1)-u_s(y-y_2)], \tag{5}$$

The system governing equation, Equation (2), is a partial differential equation (PDE) (Strauss, 1992). In the numerical analysis, derivatives are formulated by a finite difference technique. That is, $\partial u/\partial x=\lim_{\Delta x\to 0}(\Delta u/\Delta x)$. By definition of central differences, the fourth order derivative can be represented as follows (Wang, 1966; Mathews & Fink, 2004),

$$\partial^4 u/\partial x^4 \approx \left(\frac{u_{n+2}-4u_{n+1}+6u_n-4u_{n-1}+u_{n-2}}{\Delta x^4}\right), \tag{6}$$

where u_n is the displacement of the n^{th} node; and $\Delta x = L/m$ is the element size and m is the total number of differences. Thus, the finite difference beam equation at the n^{th} node can be expressed as

$$YI\left(\frac{u_{n+2}-4u_{n+1}+6u_n-4u_{n-1}+u_{n-2}}{\Delta x^4}\right)+\rho A\frac{\partial^2 u_n}{\partial t^2}-b\frac{\partial^2 M_{xx}^c}{\partial x^2}=bq_3\,. \tag{7}$$

Accuracy of the nodal transverse displacement u_n depends on the difference size. The smaller difference size yields the better solution. The electrical signal excites the piezoelectric actuator causing the control moment to deform the beam as written in

Equation (5). For this reason, displacement and dynamic response of the piezoelectric bimorph is controlled by the electrical excitation. The piezoelectric control force and moment depend on the actuator locations, actuator thickness, modal characteristics, actuator material properties and control voltage (Smithmaitrie et al., 2007; Smithmaitrie et al., 2008b). In case of two piezoelectric actuator layers laminated on a beam, the total displacement response of the piezoelectric beam can be determined by superposing the responses induced by respective actuators.

Recent studies of structural systems laminated with piezoelectric actuators have shown that the system governing equations yield reasonable estimation when the mechanical properties of the piezoelectric structures are treated as composite structures (Smithmaitrie et al., 2007; Smithmaitrie et al., 2008b). Therefore, to analyze the system response of this piezoelectric Braille cell, equivalent mechanical properties of the bimorph are considered as elastic properties of the composite lamina (Daniel & Ishai, 1994; Jones, 1999). For a thin beam fully bonded with piezoelectric actuators, the modulus of elasticity of the structure Y is approximated by (Smithmaitrie et al., 2008b)

$$Y = \frac{Y_b Y_p}{(v_p Y_b + v_b Y_p)}, \tag{8}$$

where v_p is the volume fraction of the piezoelectric actuator, v_b is the volume fraction of the thin beam, Y_p is the modulus of elasticity of the piezoelectric material and Y_b is the modulus of elasticity of the thin beam. The density of the composite structure ρ is

$$\rho = v_p \rho_p + v_b \rho_b, \tag{9}$$

where ρ_p is the density of the piezoelectric material and ρ_b is the density of the beam. The effective thickness of the system is calculated based on the increased volume of the laminated actuators. Next, the Braille display usage condition is investigated in order to determine practical input for design the Braille cell.

4. Usage Condition of the Braille Display

To acquire information for design of the piezoelectric Braille cell, a field study is conducted at Tammasakon School, a school of visually impaired people in Hat Yai, Songkhla, Thailand. All subjects in the investigation are voluntarily participants. Twelve visually impaired people (5 males and 7 females) are selected from the blind people who daily read Braille books. The age range is from 10 to 36 years. The selection is based on the following criteria to ensure the optimal touching force: 1) experienced Braille reader, 2) equality numbers between males and females, and 3) wide range of age.

In this survey, touching force of the blind people when sensing Braille characters on a Braille Note is measured. In addition, preference of the blind people to roundness of the Braille dots is studied by letting them read the same characters but different dot shapes. The roundness of the dots is defined by the fillet radius R of the pin, as illustrated in Fig. 6.

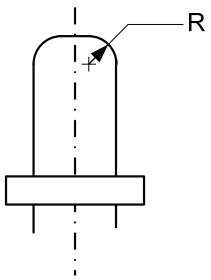

Fig. 6. The fillet radius of the Braille dot.

Diameter of the pin is set at 1.3 mm. Thus, the larger fillet radius means the sharper dot. There are three different dot roundness offered to the blind people at the fillet radius of 0.75, 1.2 and 1.5 mm. The survey data is reported in Table 1. (Smithmaitrie et al., 2008a)
The touching force of the Braille note is in the range of 0.05-0.39 N. The average touching force is 0.17 N. However, the amount of touching force is individual preference which depends on many factors, for examples, age and frequency of usage which implies Braille reading skill (Way & Barner, 1997). For the dot contour, most of them prefer the round dots (the least fillet radius) because it has smooth touch feeling and ease to read. Due to the limited number of subjects who are skilled Braille readers in the area, increasing number of subjects would be suggested for more accurate and reliable interpretation. However, the presented study yields primary information of the touching force and dot shape that can be taken to consider in the design of piezoelectric Braille cell.

Age (years)	Sex (M/F)	Touching Force (N)	Roundness Preference (Fillet radius R in mm)		
			0.75	1.2	1.5
10	M	0.03	✓		
12	M	0.24	✓		
15	F	0.14			✓
16	F	0.09	✓		
16	M	0.08	✓		
16	F	0.39		✓	
17	F	0.05		✓	
20	F	0.37	✓		
30	M	0.17	✓		
32	F	0.22	✓		
33	F	0.20		✓	
36	M	0.08	✓		

Table 1. Touching force and roundness preference of Braille readers.

5. Design Parameter Variation

The Braille cell should be designed to meet the Braille standard and able to operate under conditions according to the survey data. Free length of the bimorph, dot height and applied voltage are the key parameters for designing the Braille cell. The relationship of these parameters is studied based on material properties of the piezoelectric bimorph as shown in Table 2. The presented piezoelectric bimorph is also used as the actuator of a commercial Braille cell.

	Piezoelectric actuator (PZT-5)	Carbon fiber beam	Unit
Young's modulus	Y_{xx}= 61 Y_{zz}= 43	100	GPa
Density	ρ_p = 7400	1770	Kg/m^3
Thickness	$h^a = 0.25\times10^{-3}$	$h=0.1\times10^{-3}$	m
Poisson's ratio	0.35		
Width	$b=2.1\times10^{-3}$	2.1×10^{-3}	m
Free length	$L=20\times10^{-3}$-35×10^{-3}	20×10^{-3}-35×10^{-3}	m
Dielectric constant	4500		
Piezoelectric constant			
d_{31}	-320×10^{-12}		C/N
d_{33}	750×10^{-12}		C/N

Table 2. Properties of the piezoelectric bimorph.

Responses of the piezoelectric Braille cells are simulated based on the proposed mathematical model. The piezoelectric bimorph is designed by using the material selection and dimension presented in Table 2. The relationships among the key design parameters are investigated as follows.

5.1 Free length of the bimorph

According to Fig. 4, the relationship between the tip displacement d and the free length of the bimorph L is investigated. Moreover, the applied voltage is set at 150, 200, 250 and 300V, which are in the typical range for exciting the piezoelectric Braille actuator. The displacement of the bimorph tip implies the height of the Braille dot since the bimorph directly controls the pin movement. The result shows that the tip displacement increases as the free length of the bimorph increases. Also, the more applied voltage yields the higher tip displacement.

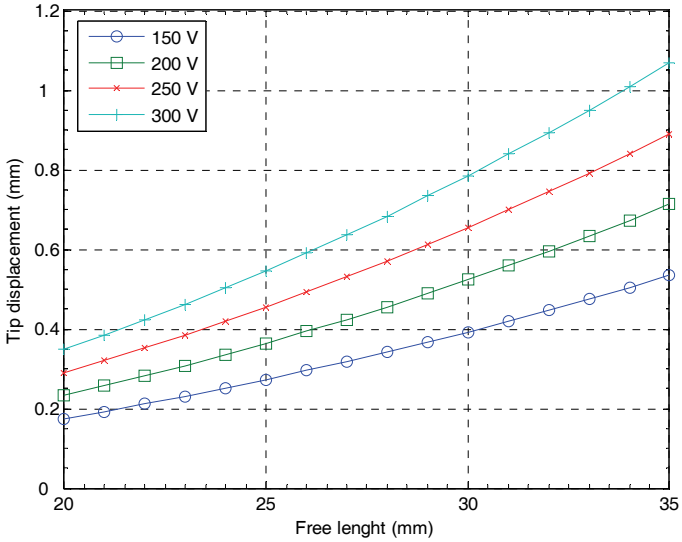

Fig. 7. The relationship between the free length of the bimorph and the tip displacement.

Based on the relationship shown in Fig. 7, product designers can select the free length of the bimorph according to the specific dot height and applied voltage. This relationship is a useful guidance for designing the dot height to meet the Braille standard and able to operate under a specific voltage supply. But it should be notice that the longer bimorph causes the larger size of the Braille display.

5.2 Applied voltage

The tip displacements of bimorphs with the free lengths of 20, 25, 30 and 35 mm are studied when the applied voltage is varied from 150 to 300 V. The result shows that relationship between the applied voltage and tip displacement is linear. Besides, the longer bimorph allows more tip displacement at a specific applied voltage as shown in Fig. 8.

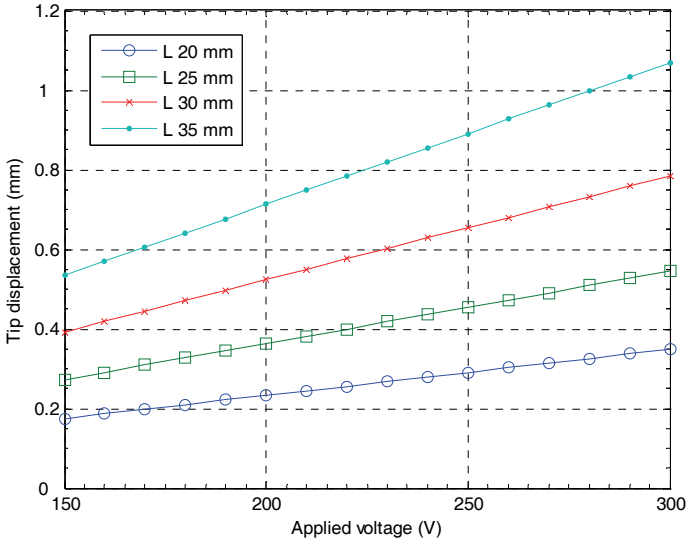

Fig. 8. Relationship between the applied voltage and the tip displacement.

The simulation shows that the displacement linearly increases as the applied voltage increases because the increased applied voltage linearly increases the bending moment as expressed in Equation (3). However, this is based on the assumption of the small deflection. In fact, piezoelectric bimorphs show nonlinear and hysteresis behaviors when they are operate over the wide range of the applied voltage. Though, for the piezoelectric Braille application, the applied voltage is set at a specific value during operation. Hence, the operating displacement is maintained at a constant height. In any case, this result helps the designers to select the applied voltage that suitable for the Braille dot height.

5.3 Touching force

While touching the active Braille character, the underneath piezoelectric beam is simultaneously subjected to both touching force and applied voltage which are mechanical and electrical excitations, respectively. In this section, displacement of the Braille dots is studied when it is pressed during operation. The response of the Braille dots is investigated when the touching force is varied from 0-0.32 N which is the common range for Braille readers based on the presented survey data. In the first case, relationship between the touching force and the tip displacement is studied when the voltage is set at 200V and applied to the different bimorphs (L = 20, 25, 30 and 25 mm). The result in Fig.9 shows that the touching force reduces the tip displacement or dot height even though the piezoelectric bimorph is activated. In addition, the piezoelectric bimorphs with different free lengths have different resistance to the touching force. That is, when the touching force increases, the short bimorph is capable of maintain its tip displacement closed to the initial no-load displacement better than the long bimorph does. In some cases, the bimorphs are pressed

down under the normal position (d < 0) for certain amount of touching forces, depended on the free length.

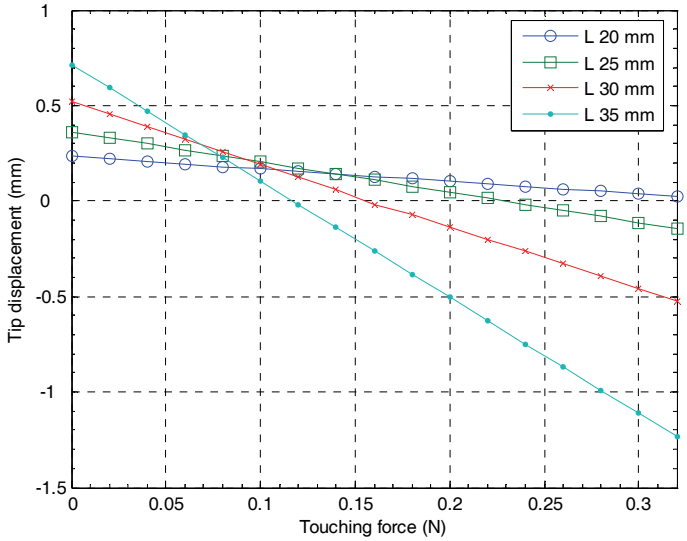

Fig. 9. Relationship between the touching force and the tip displacement of different bimorphs at the 200-V applied voltage.

In the second case, the 25-mm length bimorph is subjected to the applied voltages at 150, 200, 250 and 300 V, respectively. Figure 10 shows the tip displacement of the pressed piezoelectric beam when the touching force increases. The result implies that the tip displacement decreases as the touching force increases. The dot is able to maintain its position above the normal position for certain amount of force depended on the applied voltage. In this case, the resistance forces at the normal position are 0.11, 0.17, 0.22 and 0.28 N at the supplied voltages of 150, 200, 250 and 300 V, respectively. The result reveals behavior of the piezoelectric Braille cell when it is subjected to the touching force during the operation. The touching load lessens the height of the Braille dot. However, the result also implies that increasing of applied voltage is able to rise up the dot height as compensation to the touching load. Hence, closed loop control is an alternative approach to overcome the problem of the decreased displacement as the touching force increases.

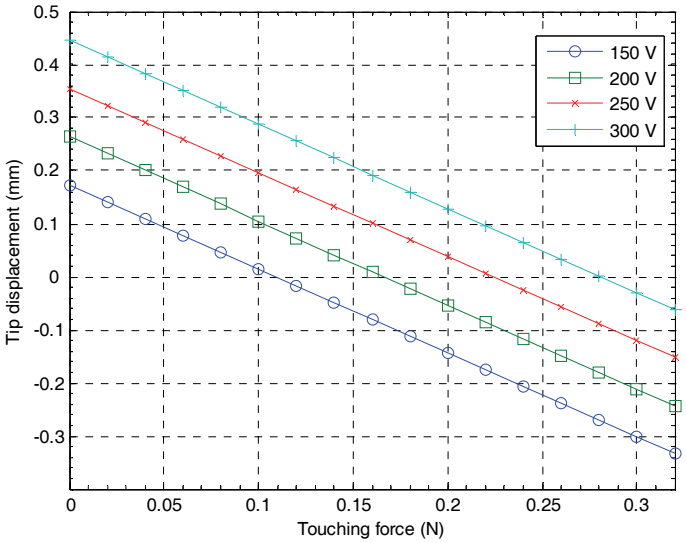

Fig. 10. Relationship between the touching force and the tip displacement of the 25-mm bimorph at various applied voltages.

In summary, tip displacement, free length, applied voltage and touching force are the key parameters for design the piezoelectric Braille display. Based on the design parameter variation of this section, the designers should be able to layout the piezoelectric bimorph dimensions and select material properties of the bimorph cell that meets the Braille standard. According to the literature review, the Braille dot height should be in the range of 0.2-0.5 mm (Way & Barner, 1997; Tiresias, 2009). In addition, the survey data provides primary information showing that the touching forces are in the range of 0.05-0.39 N and the preference of dot roundness is 0.75-mm fillet. Along with these usage conditions, dimension of the piezoelectric bimorph and the material selection can be designed to meet the requirement by following the procedure shown in this chapter. Moreover, the governing equation can serve as a general model for design of piezoelectric Braille displays.

6. Conclusion

In this chapter, analysis and design of a piezoelectric Braille display is presented. The analysis and mathematical model of the piezoelectric Braille cell are proposed and discussed. The survey data of the Braille Note usage condition is reported as primary design information of the piezoelectric Braille cell, i.e., touching force and dot roundness. Based on the usage condition and commercially available material, relationships of the key design parameters (tip displacement, free length, applied voltage and touching force) are studied. The relationship between these design parameters shows that 1) the tip displacement increases as the free length of the bimorph increases, 2) the tip displacement linearly increases as the applied voltage increases, 3) While touching the Braille dot, the short piezoelectric bimorph is capable of maintain its tip displacement closed to the initial no-load

displacement better than the long bimorph does, and 4) the touching force lessens the tip displacement even though the piezoelectric bimorph is activated but this can be compensated by increasing of the applied voltage. The design, analysis, mathematical model, material selection and design parameter relationship presented in this work can serve as a useful guideline for design of piezoelectric Braille display systems.

7. Acknowledgement

This research is supported by the department of Mechanical Engineering, Faculty of Engineering, Prince of Songkla University. This support is gratefully acknowledged.

8. References

Bigham J.P.; Prince, C.M. & Ladner R.E. (2008). WebAnywhere: A screen reader on-the-go, *Proceedings of the 2nd Cross-Disciplinary Conference on Web Accessibilit,* pp. 73-82, ISBN: 978-1-60558-153-8, Beijing, China, April 2008, ACM, New York, NY.

Braille and Assistive technology. (2009) Braille and Assistive technology. Accessed 20 April 2009 from the website: braille.coe.psu.ac.th

Cho, H.C.; Kim, B.S.; Park, J.J. & Song, J.B. (2006). Development of a Braille display using piezoelectric linear motors, *International Joint Conference SICE-ICASE*, pp. 1917–1921, ISBN: 89-950038-4-7, Oct 2006.

Daniel, I.M. & Ishai, O. (1994). *Engineering Mechanics of Composite Materials,* Oxford University Press, ISBN: 0195097386, New York, NY.

Frisken-Gibson, S.F.; Bach-Y-Rita, P.; Tompkins, W.J. & Webster, J.G. (1987). A 64-solenoid, four-level fingertip search display for the blind, *IEEE Transactions on Biomedical Engineering BME*, Vol. 34, No. 12, pp. 963–965, ISSN: 0018-9294.

Fukuda, T.; Morita, H.; Arai, F.; Ishihara, H. & Matsuura, H. (1997). Micro resonator using electromagnetic actuator for tactile display, *Proceedings of the 1997 International Symposium on Micromechatronics and Human Science*, pp. 143–148, ISBN: 0-7803-4171 -6, Oct 1997.

HumanWare. (2009). BrailleNote Notetakers for the Blind and Visually Impaired: BrailleNote. Accessed 20 April 2009 from the website: www.humanware.com/en-asia/products/braille_and_speech/braillenotes

Jones, R.M. (1999). *Mechanics of Composite Materials,* Taylor & Francis, ISBN: 156032712X, Philadelphia, PA.

Linvill, J.G. & Bliss, J.C. (1966). A direct translation reading aid for the blind, *Proceedings of the IEEE,* Vol. 54, No. 1, pp. 40–51, ISSN: 0018-9219.

Linvill, J. (1969). Development progress on a microelectronic tactile facsimile reading aid for the blind, *IEEE Transactions on Audio and Electroacoustics,* Vol. 17, No. 4, pp. 271–274, ISSN: 0018-9278.

Linvill, J.G. (1986). Piezoelectric Polymer Transducer Arrays, *6th IEEE International Symposium on Applications of Ferroelectrics*, pp. 506–510.

Mathews, J.H. & Fink, K.D. (2004). *Numerical methods using MATLAB*, 4th ed, Pearson Prentice Hall, ISBN: 0130652482, Upper Saddle River, NJ.

PPA. (2009). PPA Thai Text-to-Speech. Accessed 3 April 2009 from the website: www.ppainnovation.com/text-to-speech%20PC/index_en.html

Shinohara, M.; Shimizu, Y. & Mochizuki, A. (1998). Three-dimensional tactile display for the blind, *IEEE Transactions on Rehabilitation Engineering*, Vol. 6, No. 3, pp. 249–256, ISSN: 1063-6528.

Smithmaitrie, P.; DeHaven, J.G.; Higuchi, K. & Tzou, H.S. (2007). Vibration response and harmonic wave propagation of ultrasonic arc drivers, *Mechanical Systems and Signal Processing*, Vol. 21, No. 2, pp. 1174-1187, ISSN: 0888-3270.

Smithmaitrie, P.; Kanjantoe, J. & Tandayya, P. (2008a). Touching force response of the piezoelectric Braille cell, *Disability and Rehabilitation: Assistive Technology*, Vol. 3, No. 6, pp. 360-365, ISSN: 1748-3107.

Smithmaitrie, P.; Suybangdum, P.; Muensit, S. & Tzou, H.S. (2008b). Wave propagations of curvilinear motors driven by partially laminated piezoelectric actuators, *Smart Materials and Structures*, Vol. 17, No.6, 065015(10pp), ISSN: 0964-1726.

Sriskanthan, N. & Subramanian, K.R. (1990). Braille display terminal for personal computers, *IEEE Transactions on Consumer Electronics,* Vol. 36, No. 2, pp. 121–128, ISSN: 0098-3063.

Strauss, W.A. (1992). *Partial differential equations: An introduction*, John Wiley & Sons, ISBN: 0470054565, Chichester, UK.

Taylor, P.M.; Moser, A. & Creed, A. (1998). A sixty-four element tactile display using shape memory alloy wires, *Displays*, Vo. 18, No. 3, pp. 163–168, ISSN: 0141-9382.

Taylor, P.M.; Pollet, D.; Hosseini-Sianaki, M.A. & Varley, C.J. (1998). Advances in an electrorheological fluid based tactile array, *Displays,* Vol. 18, No. 3, pp. 135–141, ISSN: 0141-9382.

Tiresias. (2009). International Information on Visual Disability Braille Cell Dimensions [Internet]: Scientific and Technological Report, Braille Cell Dimensions. Accessed 22 April 2009 from the website: www.tiresias.org/research/reports/braille_cell.htm

Tzou, H.S. (1993). *Piezoelectric shells (distributed sensing and control of continua)*, Kluwer Academic Publishers, ISBN: 0792321863, Boston/Dordrecht.

Velazquez, R. & Pissaloux E. (2006). Design and optimization of crossbar architectures for shape memory alloy actuator arrays, *International Symposium on Micro-NanoMechatronics and Human Science*, pp. 1–5, ISBN: 1-4244-0718-1, Nov 2006.

Velazquez, R.; Pissaloux, E.E. & Wiertlewski, M. (2006). A compact tactile display for the blind with shape memory alloys, *Proceedings 2006 IEEE International Conference on Robotics and Automation (ICRA 2006)*, pp. 3905–3910, ISBN: 0-7803-9505-0, May 2006.

Wang, P.C. (1966). *Numerical and matrix methods in structural mechanics*, John Wiley & Sons, ISBN: 0471919500, Chichester, UK.

Way, T.P. & Barner, K.E. (1997). Automatic visual to tactile translation: I. Human factors, access methods and image manipulation, *IEEE Transactions on Rehabilitation Engineering,* Vol. 5, No. 1, pp. 81–94, ISSN: 1063-6528.

Yobas, L.; Huff, M.A.; Lisy, F.J. & Durand, D.M. (2001). A novel bulk micromachined electrostatic microvalve with a curved compliant structure applicable for a pneumatic tactile display, *Journal of Microelectromechanical Systems,* Vol. 10, No. 2, pp. 187–196, ISSN: 1057-7157.

Yobas, L.; Durand, D.M.; Skebe, G.G.; Lisy, F.J. & Huff, M.A. (2003). A novel integrable microvalve for refreshable Braille display system, *Journal of Microelectromechanical Systems*, Vol. 12, No. 3, pp. 252–263, ISSN: 1057-7157.

5

Stereo Vision Utilizing Parallel Computing for the Visually Impaired

Pichaya Tandayya, Thanathip Limna and Nikom Suvonvorn
Intelligent System (iSys) Research Team, Department of Computer Engineering
Faculty of Engineering, Prince of Songkla University
Thailand

1. Introduction

Many technologies have been developed to help the visually impaired. For example, a walking stick with an ultrasonic sensor can detect whether there are obstacles ahead, but cannot judge the distance, size, and position of the objects. A Differential Global Position system (DGPS) (Hashimoto et al., 2001 and Helal et al., 2001) with a mobile phone Electronic Sensory System for the visually impaired (ESSVI) (Ando, 2003) can find a destination, but says nothing about the safety of the surrounding area.

Ultrasonic or infrared devices can be attached to walking sticks or glasses, to detect obstacles in the environment and calculate distances, but do not provide size and position information for continuing a journey.

Stereo vision technology can help by finding the distance between an object and the stereo cameras, and also its size and position.

In a stereo vision system, two cameras represent the 3D view as seen by human eyes. Stereo disparity and depth estimation are determined by the difference in the positions of two corresponding points in the stereo images.

Stereo matching algorithms can be classified into two categories: Intensity-based Stereo Matching (ISM) using the intensity profile of each image for finding the disparity (Owens 2009), and Feature-based Stereo Matching (FSM) for finding the disparity using features in each image, such as edges, lines, and corners (Owens 2009). Generally, FSM cannot provide a proper disparity for images with featureless surface objects such as whiteboards, doors, and television monitors, while ISM fares much better. The tradeoff is that ISM requires intensity information for each pixel, which demands longer processing time.

The Electro Neural Vision System (ENVS) is a stereo vision application which presents obstacles and distances via signal alerts sent to the fingers (Meers & Ward 2004). If an object is close by then a signal with a high frequency is sent, while a signal with a lower frequency is sent for a distant object. However, ENVS employs FSM which cannot detect objects with featureless surfaces.

The ISM technique can detect objects with featureless surfaces, but applying the technique in real time requires complex and time consuming image processing, especially when accuracy is required. However, PCs are getting more powerful, often having 2-core or 4-

core CPUs. Unfortunately, sequential processing cannot fully utilize the maximum performance of multi-core CPUs, and parallel processing techniques are therefore necessary. This chapter describes a stereo vision system for the visually impaired, employing ISM to detect objects with almost any kind of surface.
Most image processing algorithms for stereo vision can be categorized as Single Instruction Multiple Data (SIMD), often utilizing threads and processes. With threads, it can be very difficult to predict the order of tasks and the number of run-time tasks. Alternatively, parallel programming using a Message Passing Interface (MPI) has better process management, follows mature standards, and offers robust implementations (MPI standard, 2009).
MPICH is an MPI implementation using shared memory which naturally maps to the Symmetric Multiple Processors (SMPs) architecture (MPI CH, 2009) used in our stereo vision system. The code can be easily recompiled on other device configurations and architectures.
Our work is novel in that parallel computing has never previously been combined with the ISM technique to reduce computing time. This chapter investigates the computing time reductions possible when applying the parallel computing approach to a Depth Discontinuities Pixel-to-Pixel stereo (P2P) algorithm (Birchfield & Tomasi, 1998), running on a 2-core PC and an 8-core server.
Our work applies parallel computing using MPI, ISM techniques, and off-the-shelf multi-core computers to reduce computing time. We also investigate the calibration of low-cost stereo cameras using webcams.
The next section will present background on stereo vision, depth discontinuities algorithms, and the message passing interface. Section 3 describes the system design, including a system overview, low-cost stereo cameras, object distance estimation, and enhanced P2P using MPI. Experiments are described, and results analyzed.

2. Background

We provide some background on stereo vision using ISM, and parallel computing using MPI. Also, the sequential computing performance of P2P is investigated.

2.1 Stereo vision using intensity-based stereo matching (ISM)

In FSM, features of the matching process are applied to features extracted from the stereo images. In ISM, the matching process is directly applied to the intensity profiles of two images.
We are interested in the ISM technique since it can find a disparity even in featureless surface objects. In particular, we employ Depth Discontinuities by Pixel-to-Pixel Stereo (P2P), developed by Birchfield and Tomasi, and available within OpenCV, an open source framework for computer vision (CVAUX, 2009).

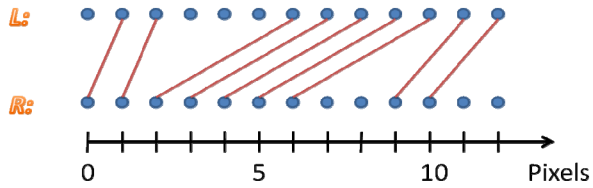

Fig. 1. Example of the P2P scan line matching - matching pixels from left and right images (Birchfield & Tomasi, 1998).

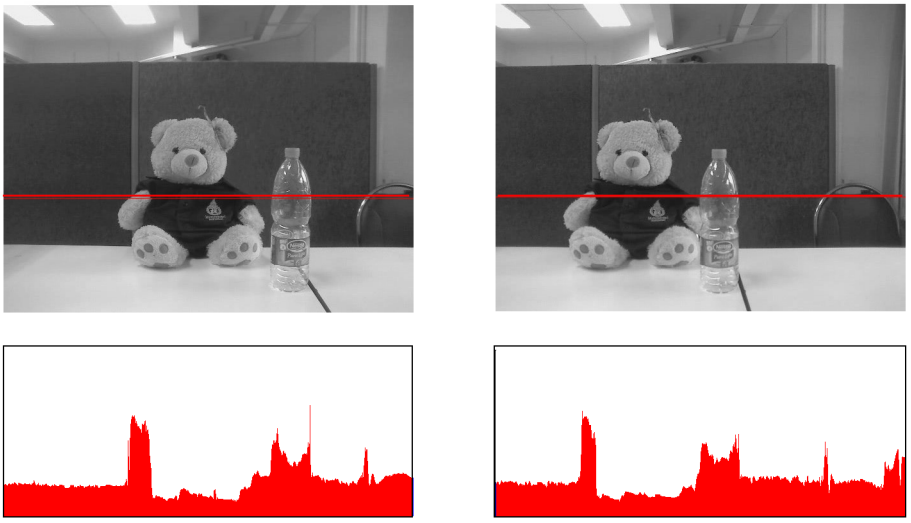

Fig. 2. Intensity of a pair of scan lines.

The P2P algorithm processes left and right images projecting on the same scan lines (Figure 1) in such a way that the processing of each pair of scan lines is independent and also relatively easy to parallelize. Figure 2 shows an example of an intensity comparison of a pair of scan lines. However, the post-processing algorithm needs to combine data from both rows and columns, which is harder to parallelize. P2P matches pixels on paired scan lines by applying a cost function (Birchfield & Tomasi, 1998) (given as Equation 1) to find an M sequence that represents the scan line being considered.

$$\gamma(M) = N_{occ} K_{occ} - N_m k_r + \sum_{i=1} d(x_i, y_i) \tag{1}$$

K_{ooc} is an occlusion penalty constant, k_r the match reward constant, $d(x_i,y_i)$ the distance between pixel x_i and pixel y_i, N_{occ} is the occlusion, and N_m is the number of related pairs.

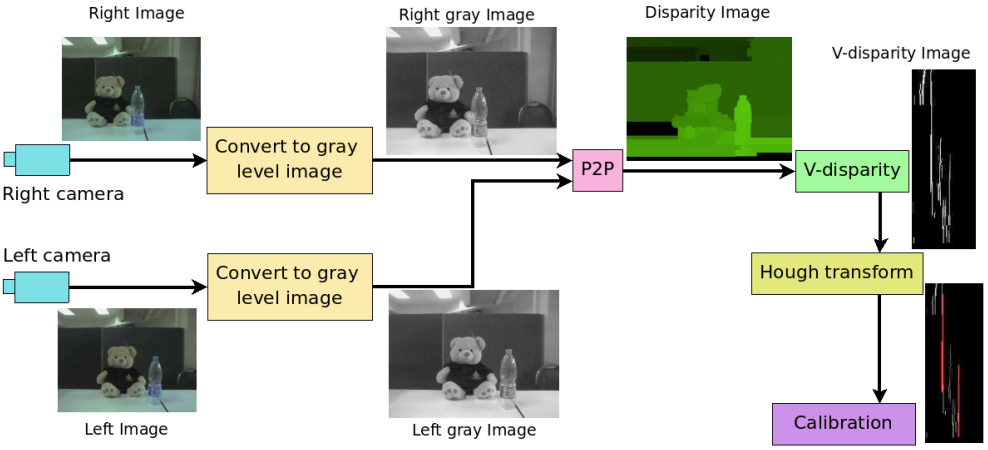

Fig. 3. Stereo vision processes (Limna et al., 2009).

Figure 3 shows the stereo vision processes. First, the color images from the left and right cameras are transformed into gray-level images to speed up subsequent processing and remove unnecessary information. The disparity image created by the P2P algorithm is a binary image containing pixels that define a relationship between the left and right images. The disparity image (see Figure 4) is used to calculate a summary of the disparity values in each scan line (called a V-disparity image). Then, depth lines are extracted from the V-disparity (Labayrade et al., 2002) using a Hough transform, and compared with the V-disparity to obtain object distances.

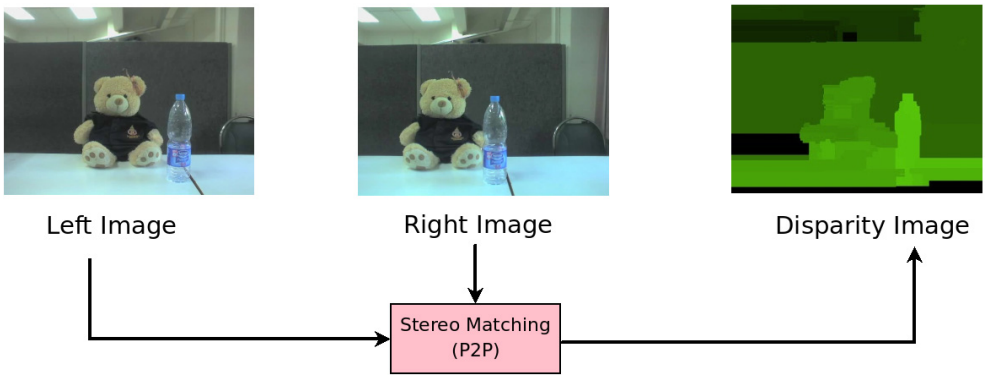

Fig. 4. Example left, right, and disparity images. (Limna & Tandayya, 2009)

Parallel computing can help reduce the processing time at several stages, such as for edge detection and scan line matching.

2.2 Parallel computing using message passing interface (MPI)

The Message Passing Interface (MPI) is a specification which facilitates parallel processing by distributing tasks and data amongst distributed processing units or processors (MPI standard, 2009). MPI is applied widely in computational sciences, where the efficient analysis of high quantities of data is required; e.g., finding the relationships between base sequences in human DNA, preparing a drug formula for destroying cancer cells, animation, and image processing.

MPICH is an MPI implementation (MPICH Document, 2009) that supports several different computer architectures by providing a variety of devices:

- a ch_p4 device for Workstation Networks;
- a ch_p4mpd device for Workstation Networks and Clusters;
- a ch_shmem device for Shared Memory Processors;
- a globus2 device for Grids.

The most suitable device for our work is ch_shmem for multi-core CPUs which share memory, including PCs, laptops, and multi-core servers.

2.3 Sequential computing performance of P2P

There are two processes in the P2P algorithm: scan line matching and post-processing. Scan line matching matches corresponding pixels in the left and right images on the same scan lines. In each scan line, processes match corresponding pixels independently from one another. Post-processing exchanges data between the scan lines in order to select the best disparity image. This requires data across rows and columns, and is not suitable for parallelization. We tested the sequential P2P algorithm on an Intel® Core™ 2 Dual 6320 1.86 GHz 1010.7 MB RAM, running Linux kernel 2.6.26. With a maximum disparity of 100 and an image size of 320x240 pixels, the average computing times was 1.168 seconds for scan line matching and 0.165 seconds for post-processing. Figure 5 **Fig.** shows the experimental results of the sequential P2P algorithm. The scan line matching requires about 70% of the computing time, so its parallelization should benefit the P2P algorithm.

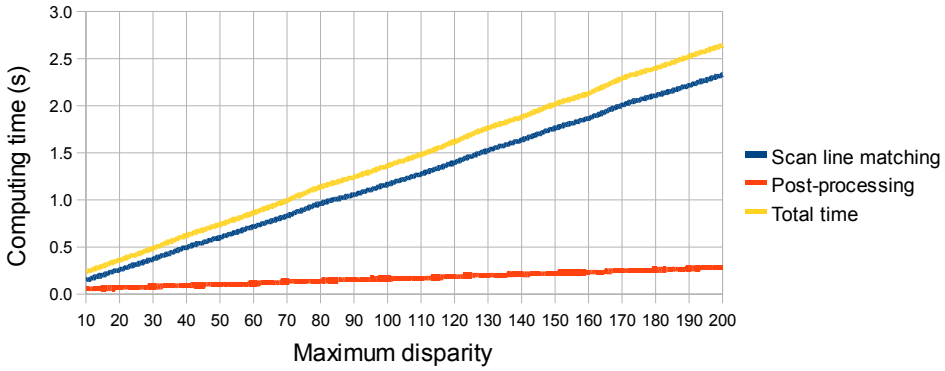

Fig. 5. The relationship between the computing time and the maximum disparity of the sequential computing P2P algorithm, running on a 2-core computer. The image size is 320x240 pixels (Limna & Tandayya, 2009).

3. System design and implementation

This section describes our stereo vision system including system overview, low-cost stereo cameras, and object distance estimation with V-disparity.

3.1 System overview

Our object detection system should issue a warning when there are obstacles 10 meters ahead, as shown in Figure 6**Fig.** . However, the most critical range is between 1 and 6 meters, which is outside a walking stick's range. Our aim is not to replace the walking stick but to augment it.

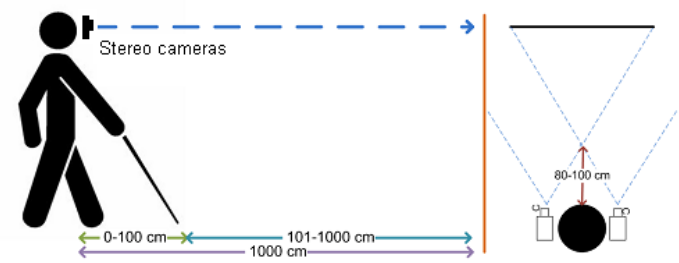

Fig. 6. System usage (Limna et al., 2009).

3.2 Low-cost stereo cameras

Normal stereo cameras are rather expensive, so we utilized cheaper web-cams instead-Logitech QuickCam web-cams for Notebooks Pro (Clark, 2009). On the downside, they are less accurate than normal cameras, and may produce more noise.

We plan to attach the cameras to a helmet, so their base line was 12 centimetres, which is an average head diameter. The design of the stereo cameras is shown in Figures 7 and 8.

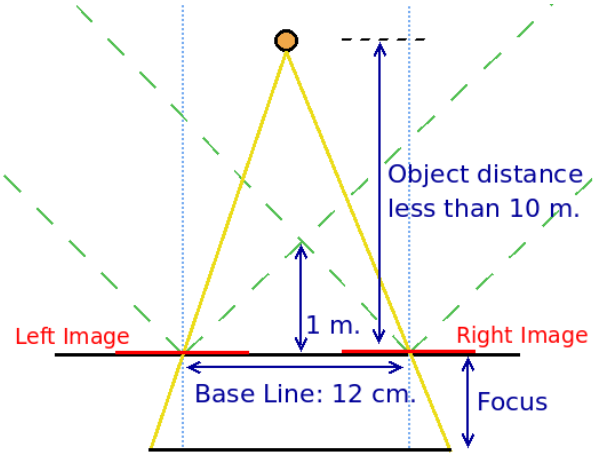

Fig. 7. Design of our stereo cameras (Limna et al., 2009).

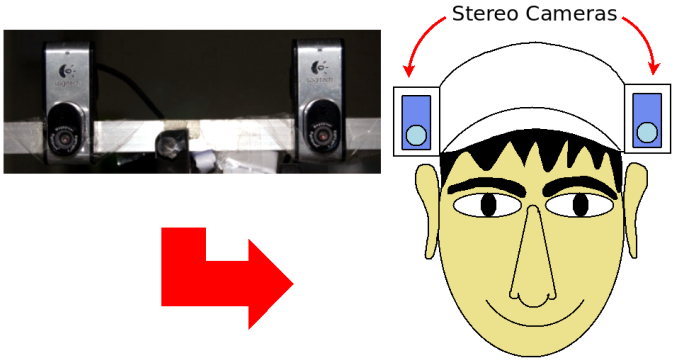

Fig. 8. Our stereo web-cams.

3.3 Object distance estimation with V-disparity

An object's depth information can be calculated from slight offsets of projections of the object in both images (the disparity), the relative positions of both cameras (the base line), and the image resolution focal length.

The disparity image created by the P2P algorithm is a binary image that contains corresponding pixels from the left and right images. The V-disparity image is calculated from the summation of the disparities in each scan line. Each vertical straight line in the V-disparity image represents a depth distance. A Hough transform is used to find the depth lines in the V-disparity image, and the distance information in the depth lines are then compared with the V-disparity to find the object distance.

4. Parallel P2P algorithm

The scan line matching algorithm is suitable for parallelism because it independently computes each scan line. Figure 9 shows an example of MPI data distribution in the scan line matching. In each image frame, we divide the left and right image into two segments and distribute them to two processes. The first process computes the top parts of the left and right images, and the second process computes the bottom halves of the images. We then combine the outputs and create a disparity image.

The program is designed to run on a computer with more than two processors, and the user can specify the number of processes at run time. The MPI Scatter command is used for distributing portions of the left and right images to the processes, and each process manages the same number of scan lines. For example, if an image size of 320x240 pixels is assigned to 4 processes, then each process will match 80 rows of scan lines from the left and right images. After the matching is finished, the disparity image and depth discontinuities will be gathered together in process 0 before moving to the next step of the calculation.

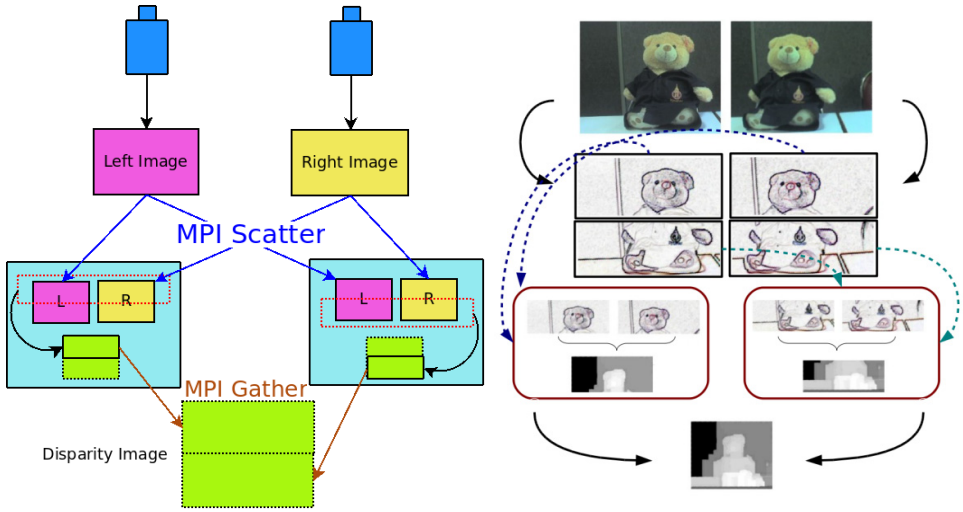

Fig. 9. Data distribution using parallel computing across two processes. (Limna & Tandayya, 2009)

We compared the sequential and parallel algorithms by testing them both on a 2-core PC and an 8-core server. The 2-core machine is an Intel® Core™ 2 Dual 6320 1.86 GHz 1010.7 MB RAM running Linux kernel 2.6.26. The 8-core server is an Intel® Xeon© E5440 2.83 GHz 8200 MB RAM also running Linux kernel 2.6.26.
The pseudo code for the parallel algorithm (Limna & Tandayya, 2009):

```
ROWS : number of rows in the image
id : process id
numProcs : number of processes
startIndex := ROWS*id/ numProcs;                    //starting scan line
endIndex := ROWS*(id+1)/numProcs;                   //finishing scan line

//scatter left and right images at Process 0 to other processes from startIndex to ROWS/
numProcs
MPI::Scatter(imgL[startIndex],COLS*ROWS/numProcs,...);
MPI::Scatter(imgR[startIndex],COLS*ROWS/numProcs,...);

for (scanline = startIndex; scanline < endIndex; scanline++)
scan line matching code

//gather disparity images and depth discontinuities images from all the processes into
Process 0
MPI:: Gather(disparity_map[startIndex],...);
MPI:: Gather(depth_discontinuities[startIndex],...);
```

The MPI Scatter and Gather commands handle data distribution and collection (MPI 2009). MPI Scatter divides an array into smaller parts equal to the number of processes and sends each to a process. MPI Gather collects data stored in all the processes into a receiving array.

5. Result and discussion

This section provides experimental results, a discussion of calibration and distance estimation, and describes the effectiveness of the P2P enhancement using MPI.

5.1 Calibration and distance estimation

This subsection concerns stereo camera calibration and object distance estimation using the V-disparity image.

5.1.1 Stereo camera calibration

The V-disparity image obtained from the disparity image contains several straight lines. Each line's length is the height of the associated object from the disparity image. Also its distance from the left edge is an inverse variation of the distance from the stereo cameras to the object. We can find the distance to the object from a V-disparity straight line by comparing it with the distances of the object measured in prior experiments.

Object distance (meters)	Pixel Position		
	Minimum	Medium	Maximum
1	42	43	44
1.5	31	32	34
2	26	26	27
2.5	21	23	24
3	20	21	21
3.5	19	19	20
4	18	18	18
4.5	17	17	17
5	16	16	16
5.5	16	16	16
6	15	15	15
6.5	15	15	15
7	15	15	15

Table 1. Matches between real object distances and pixel positions from the V-disparity by finding the medium (Limna et al., 2009)

Table 1 and Figure 10 show the relationship between the object distances and V-disparity line pixel positions (minimum, medium and maximum). Each distance range refers to the prior testing dataset, and the data is processed to find the medium for distance estimation. The matches between object distances and pixel positions in the V-disparity can be estimated by the 6^{th} order polynomial equation shown in Equation 2.

Figure 11 shows a graph plot of Equation 1 using the medium dataset. In Equation 2, d is the distance to the obstacle and x the length of the vertical line from the x-axis in the V-disparity.

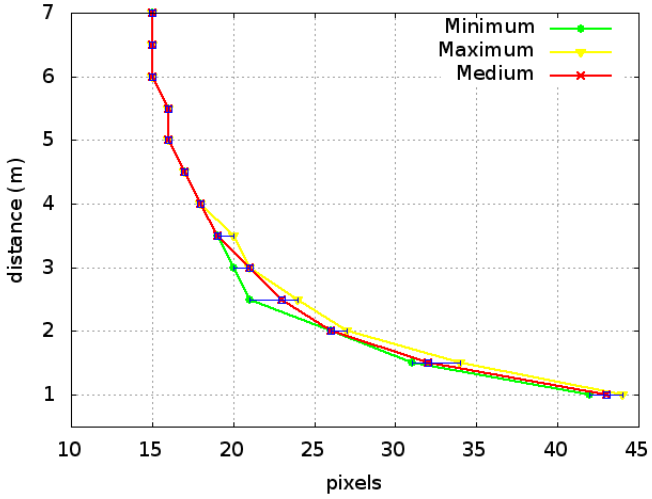

Fig. 10. V-disparity results.

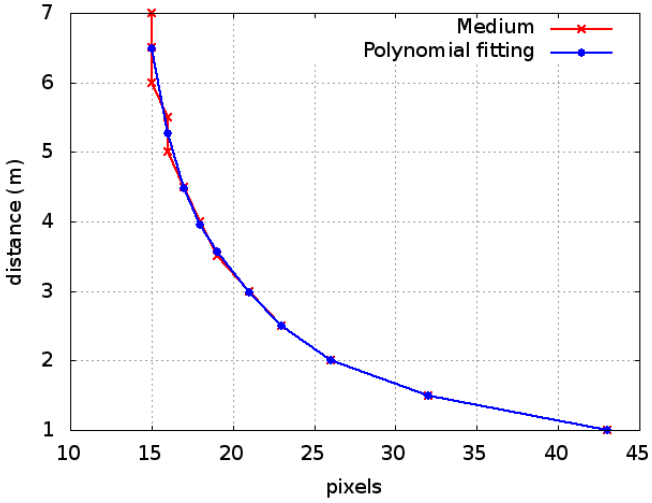

Fig. 11. Medium dataset fits for a 6th order polynomial equation. (Limna et al., 2009)

$$d = 1.7938 \times 10^{-6} x^6 - 2.9101 \times 10^{-4} x^5 + 1.9294 \times 10^{-2} x^4 \\ -0.67064 \times x^3 + 12.925 x^2 - 131.57 x + 559.10 \quad (2)$$

5.1.2 Object distance estimation

We use the V-disparity from the P2P algorithm to find straight lines by employing an OpenCV function, cvHoughLine. It returns two sequence pairs, which are the beginning and ending points of the straight line. The x-axis value represents the object depths, and replaces the x in Equation 2 to obtain the object distance. Currently, our system can find object distances within 5 meters of the stereo cameras.

5.2 Enhancing P2P using MPI

The results for the sequential algorithm in Figure 5 shows that scan line matching takes up most of the computing time. The results for the parallel algorithm using MPICH with a shared memory device are shown in Figures 12 and 13.

5.2.1 Running on a 2-core computer

The parallelized algorithm reduces the total response time to 0.79 seconds at a maximum disparity of 100, applied to 320x240 pixels using two processes on a 2-core PC. By comparison, the total time of the sequential algorithm is 1.365 seconds per frame, indicating that the parallelized version can reduce the time by about a half.

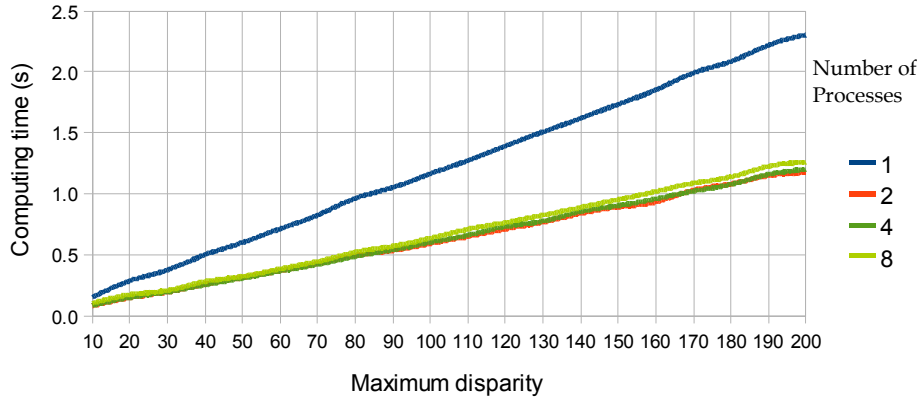

Fig. 12. The relationship between the computing time and the maximum disparity. The graph lines are the number of processes employed in the parallel computing scan line matching of the P2P algorithm using MPICH and a 2-core computer. The image size is 320x240 pixels. (Limna & Tandayya, 2009)

Figure 12 shows that data distribution on the scan line matching algorithm reduces the computing time if more than one process is used. However, when there are more than two processes, the computing time becomes longer than that for two processes. Using more processes than the number of CPU cores does not increase the speed of the parallel algorithm. The computing time for scan line matching at a maximum disparity of 100 is significantly reduced by 49.23%, or 0.575 seconds, which makes the algorithm suitable for use at run time.

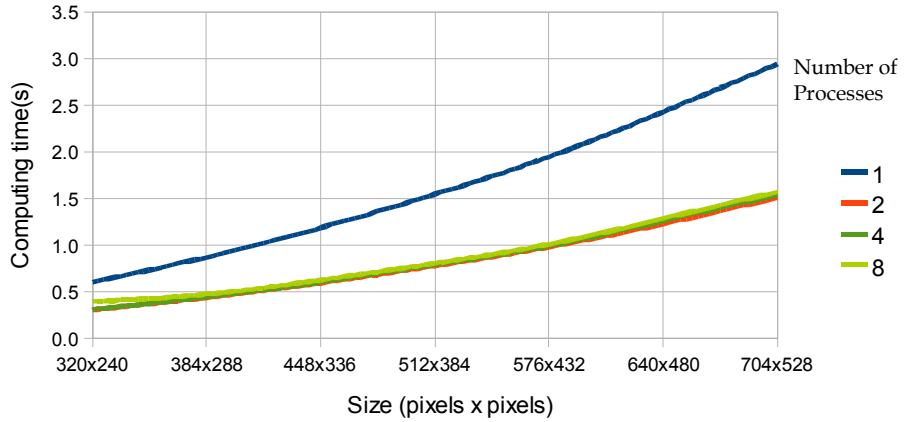

Fig. 13. The relationship between the computing time and the size of images. The graph lines are the number of processes employed in the parallel computing scan line matching of the P2P algorithm using MPICH and an 8-core server (Limna & Tandayya, 2009).

In Figure 13, we vary the image size and number of processes and investigate the computing time when the image size and number of processes increases. The results show that the bigger the image size, the better the efficiency, and that the relationship between the speedup and number of processes remains the same.

5.2.2 Running on an 8-core computer

The results when running the sequential algorithm on the 8-core machine are shown in Figure 14. The results are similar to those on the 2-core computer - scan line matching is the main computing load. Figures 15 and 16 show the results for the parallel algorithm. The computing time is less when the number of processes is increased. From Table 2, the computing time for the parallel algorithm at a maximum disparity of 100 is reduced by 0.7792 seconds, or 88.21%, compared to the sequential algorithm on two processes.

Type of computer	Computing time (s)			
	Sequence algorithm	Parallel algorithm with		
		2 processes	4 processes	8 processes
2-core	1.1683	0.5932	0.6028	0.6369
8-core	0.8833	0.1041	0.0554	0.0285

Table 2. Average computing time of the serial and parallel algorithms at a maximum disparity of 100 on a 2-core computer and an 8-core server (Limna & Tandayya, 2009).

On the 2-core computer, at a maximum disparity of 100 and an image size of 320x240 pixels, the average sequential computing time of scan line matching is 1.168 seconds, while the average parallel computing time with two processes is 0.593 seconds. For the 8-core server, the average sequential computing time of scan line matching is 0.883 seconds, while the average parallel computing time with two processes is 0.104 seconds. Increasing the number

of processes above two processes in the 2-core computer does not reduce the computing time. By contrast, increasing the number of processes in the 8-core server up to 8 significantly reduces the computing time.

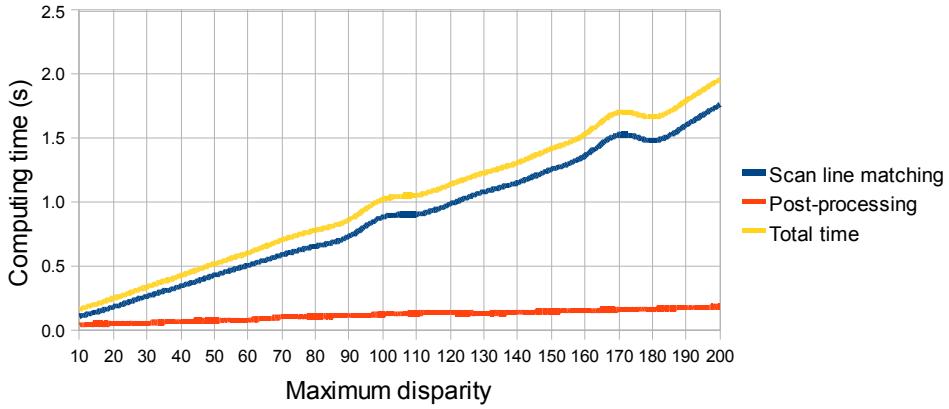

Fig. 14. The relationship of the computing time and maximum disparity of the sequential computing P2P algorithm on an 8-core server. The image size is 320x240 pixels (Limna & Tandaya, 2009).

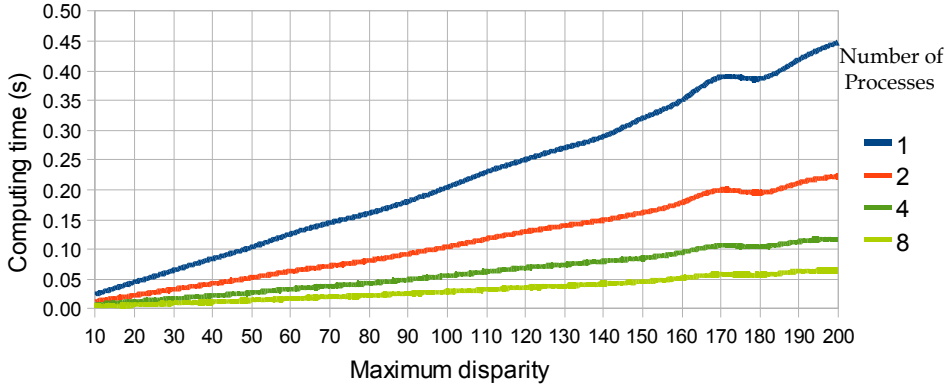

Fig. 15. The relationship between the computing time and the maximum disparity. The graph lines are the number of processes employed in the parallel computing scan line matching of the P2P algorithm using MPICH and an 8-core server. The image size is 320x240 pixels (Limna & Tandaya, 2009).

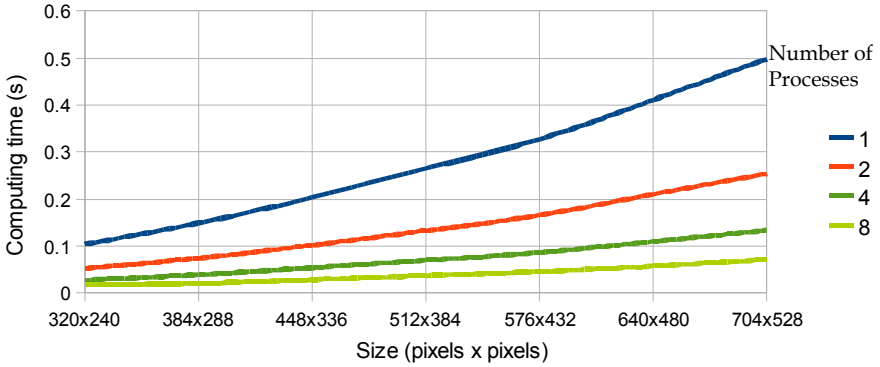

Fig. 16. The relationship between the computing time and the image size. The graph lines are the number of processes employed in the parallel computing scan line matching of the P2P algorithm using MPICH and an 8-core server (Limna & Tandaya, 2009).

5.3 Result analysis

In order to apply the parallel P2P algorithm in real-time, there are three factors to consider: the response time, the image size, and the disparity. A response time of less than 1 second is preferable. To detect obstacles within 1-6 meters of the cameras requires that the disparity is in the range of 100-150 so it can be computed within that response time. The best image size for this disparity lies between 320x240 and 512x384 pixels.

The results show that the number of processes run on a multi-core computer should not exceed the number of cores, corresponding to parallel computing theory.

5.4 Limitations

The P2P algorithm employs ISM techniques, which requires multiple parallel images so it can accurately detect obstacles. Our prototype utilizes stereo web-cams that have a maximum base line diameter of about 12 centimeters so they can be attached to a helmet (or glasses). Consequently, the prototype can accurately detect obstacles within a 5 meter range. For distances beyond 5 meters, the system's accuracy is variable. It can detect an object of 65x65 centimeters at a distance of 10 meters, but the image is so small that it may be lost amongst noise. Better quality cameras would increase the detecting distance and accuracy.

The application response time is 0.790 seconds for an image of 320x240 pixels at the maximum disparity of 100. It can detect slowly moving objects such as people walking, but cannot reliably detect quickly moving objects, such as cars, in real time.

6. Conclusion

Our obstacle detection system for the visually impaired uses stereo vision and parallel computing to reduce the response time of a depth discontinuities P2P stereo algorithm, by re-implementing scan line matching using MPI on a 2-core computer and an 8-core server. The object distances are found by employing V-disparity.

Our system can accurately detect slowly moving objects within a 5 meter range, using 12-centimeter base-lined low-cost web-cams. More development and detailed experiments will improve these results.
Our work shows that parallel computing using MPI on multi-core computers significantly reduces the computing time of the P2P depth discontinuities ISM algorithm, making it possible to detect obstacles in real time.
Planned future work includes a suitable interface for the visually impaired user, and a proximity warning system for dangerous objects. Applying stereo vision with pattern recognition can provide more details about the environment. When prices allow, increasing the number of cores on the computer, to 4 or 8, will reduce the computing time even further.

7. Acknowledgements

The authors are grateful for the support of the PSU Grid Center of Prince of Songkla University, the Thai National Grid Center, and the Intel Corporation. The authors are also thankful for Dr. Andrew Davison for proof reading.

8. References

Ando, B. (2003). Electronic Sensory Systems for the Visually Impaired. *Instrumentation & Measurement Magazine*, IEEE Vol. 6, Issue 2, (June 2003) page numbers (62-67)

Birchfield, S. & Tomasi, C. (1998). Depth discontinuities by pixel-to-pixel stereo, *Proceedings of the Sixth IEEE International Conference on Computer Vision*, pp. 1073-1080, Mumbai, India, Jan. 1998

Birchfield, S. & Tomasi, C. (1998). A pixel dissimilarity measure that is insensitive to image sampling, *IEEE Transactions on Pattern Analysis and Machine Intelligence*, pp. 401-406, Apr. 1998

Clark, S. (2009). Logitech QuickCam for Notebooks Pro. *http://www.everythingusb.com/logitech_quickcam_for_notebooks_pro.html*, Available on 4 Jan. 2009

CvAux, *http://opencv.willowgarage.com/wiki/CvAux#FindStereoCorrespondence*, Available on 4 Jan. 2009

Hashimoto, H.; Magatani, K. & Yanashima, K. (2001). The development of the navigation system for visually impaired persons. *Proceedings of the 23rd Annual International Conference of the IEEE Engineering in Medicine and Biology Society,* vol. 2, pp. 1481 - 1483, Istanbul, Turkey, Oct. 2001

Helal, A., Moore, S.E., Ramachandran & Drishti B., (2001). An integrated navigation system for visually impaired and disabled. *Proceedings of the Fifth International Symposium on Wearable Computers*, pp. 149 - 156, Zurich, Switzerland, Oct. 2001

Labayrade, R., Aubert, D. & Tarel, J.-P., Real time obstacle detection in stereo vision on non flat road geometry through "v-disparity" representation. *Proceedings of IEEE Intelligent Vehicle Symposium*, vol.2, pp. 646- 651, June 2002

Limna, T., Tandayya P. & Suvanvorn N., Low-cost Stereo Vision System for Supporting the Visually Impaired's Walk, *Proceedings of 3rd international Convention on Rehabilitative Engineering & Assistive Technology (i-CREATe 2009)*, Singapore, Apr. 2009

Limna, T. & Tandayya P., Enhancing the Pixel-to-Pixel Depth Discontinuities Algorithm Using MPI, *Proceedings of 6th International Joint Conference on Computer Science and Software Engineering (JCSSE2009)*, Phuket, Thailand, May. 2009

Meers, S. & Ward, K. (2004). A vision system for providing 3D perception of the environment via transcutaneous electro-neural stimulation. *Proceedings of the Eighth International Conference on Information Visualisation*, pp. 546 - 552, ISBN 0-7695-2177-0, London, UK, July 2004, IEEE Computer Society

MPICH-A Portable Implementation of MPI, *http://www-unix.mcs.anl.gov/mpi/mpich1/*, Available on 4 Jan. 2009

MPICH Documents, *http://www-unix.mcs.anl.gov/mpi/mpich1/docs.html*, Available on 4 Jan 2009

Nicolescu, C. & Lecture, P. (2000). Parallel low-level image processing on a distributed-memory system, *Proceedings of the 15 IPDPS 2000 Workshops on Parallel and Distributed Processing*, pp. 226 - 233, Cancun, Mexico, May 2000, Springer

Owens, R., (2009). Stereo, *http://homepages.inf.ed.ac.uk/rbf/CVonline/LOCAL_COPIES/OWENS/LECT11/lect11.html*, Available on 4 Jan. 2009

Stereo vision start with two views, *http://www.vision3d.com/stereo.html,* Available on 4 Jan. 2009

The Message Passing Interface (MPI) standard. *http://www-unix.mcs.anl.gov/mpi/*. Available on 4 Jan. 2009

6

Engineering Better Electric-Powered Wheelchairs To Enhance Rehabilitative and Assistive Needs of Disabled and Aged Populations

Yen Kheng Tan and Sangit Sasidhar
National University of Singapore
Singapore

1. Introduction

All around the world, the age distribution of the world population is shifting towards older ages, causing an increase in the world population's mean or median age. The corresponding figures for the world population's mean age as a whole are 23.9 for 1950, 26.8 for 2000, and 37.8 for 2050 (United Nations, 2004). The growing trend of the world population's mean age is largely due to the decline in the fraction of the population composed of children (declining fertility) and the rise in the fraction of the population that is elderly (due to longer life expectancy). The impact of population ageing on developed countries with strong economy strongholds, such as United States of America (USA) and Japan, is even more severe. To a certain extent, Singapore, serving as a Southeast Asia's financial and high-tech hub, is also affected as well. Population ageing has major consequences and implications in all areas of our daily life as well as other important aspects such as economic growth, savings, investment and consumption, labour markets, pensions, property and care from one generation to another. Additionally, health and related care, family composition and life-style, housing and migration are also affected.

According to a published report titled "Singapore's population ageing" (CAI, 2006), it is found that the number of seniors will increase from 8.4% in 2005 to 18.7% in 2030 as illustrated in Chart.1. In absolute terms, seniors will increase from about 296,900 in June 2005 to 873,300 in 2030. The report continues to elaborate that "the first batch of post-war baby boomers will reach 65 years of age by 2012. Today, one out of every twelve Singaporeans is aged 65 or above. By 2030, this ratio will become one out of five". These figures indicate that our ageing population in Singapore is esclating at a fast rate. Other than the aged population issue, the numbers of disabled people with mobility difficulties are expected to increase over the years. Mr. Heng Chee How, Minister of State for National Development and Mayor of Central Singapore District, backs up this statement for Singapore context and he believes that the key driving forces behind this expected increase are, "the proportion of a growing population who use the wheelchair as a result of medical conditions and accidents and the rate of ageing of the population itself." Similarly, in

worldwide context, an estimated 100-130 million people with disabilities need wheelchairs. Experts predict that the number of people who need wheelchairs will increase by 22 percent over the next ten years (R.A. Cooper & R. Cooper, 2003). Due to the increasing population of mobility impaired people in the world, there is an overwhelming need for wheelchairs and the research and development required to make these wheelchairs safer, cheaper, more comfortable and effective and widely available.

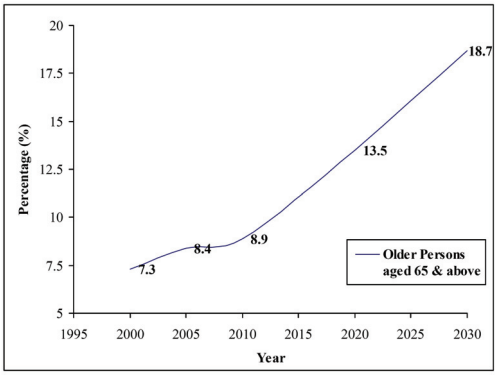

Fig. 1. Proportion of Resident Population Aged 65 & Over From 2000 – 2030
Source: Singapore Department of Statistics (DOS), 2005

Some advanced technologies can be explored for engineering better wheelchairs to enhance the rehabilitative and assistive needs of the disabled and aged populations. Assistive technology (AT) is defined as any technology that is developed to assist people with disability or old age to perform tasks that are too difficult for them to complete. It promotes greater independence for people with disabilities by enabling them to perform tasks that they are formerly unable to accomplish, or has great difficulty accomplishing, by providing enhancements to or changed methods of interacting with the technology needed to accomplish such tasks. By doing so, the daily needs of the disabled and aged populations can be better taken care of without any extra assistance. As mentioned earlier, the aged and disabled populations are rising at a fast pace, hence a lot of research efforts have been poured into the AT field. Many researchers are devoting their time and attention on AT research work so as to improve the lifestyle of the aged and disabled peoples (Cooper et al., 2008).

Wheelchair technology is one of the most favourable technologies to be investigated because the demand for electric powered wheelchairs has been increasing very rapidly due to ageing populations. The introduction of wheelchairs allows individuals to complete daily tasks with greater independence and to access school, work, and community environments. More individuals are able to benefit from the new options and sophisticated wheelchair-related technologies. For examples, Nanyang Technological University (NTU) in Singapore has developed a wheelchair with wheelchair gap enabler, which allows wheelchair users to board a bus faster and easier and also clear low steps, such as roadside curbs, with ease and efficiency. The iBOT developed in USA can engage four-wheel drive to maneuver rough terrain, go up slopes, or climb 4-inch curbs. These improvements have given great helps to the disabled people sitting in the wheelchairs to overcome many difficulties. Since

wheelchairs have been in use for several hundred years, it is going to continue to evolve in their design and use; much remains to be learned about optimum design and safe use of wheelchairs (Cooper et al., 2006).

Electric-powered wheelchairs (EPWs) have gained increasing popularity among the disabled as well as aged populations because they provide functional mobility for people with both lower and upper extremity impairments. They are becoming increasingly important as more users transition from manual mobility to powered mobility. This shift is especially true for individuals with progressive conditions and people with high levels of impairment (Cooper, 1998). Advances have been made in the design of EPWs over the past 20 years, yet there are some aspects in these wheelchairs which have not improved substantially since the early 1980s. These include adequate mobility and comfort with enhanced control methods (Ding & Cooper, 2005), proper leg and foot support (Lei et al., 2005), advanced maneuver and navigation techniques (Aissaoui et al., 2000).

In this chapter, the three main features to be incorporated onto electric-powered wheelchair are discussed. These features include 1) voice-activated control and closed-loop current control for electric-powered wheelchair, 2) personal navigation system based on wireless sensor network and 3) motorized foot rest which give a way of mobility for handicapped and elderly people to move around in indoor condition easily and to perform rehabilitative excersies without being dependent on someone else.

2. Existing Electric-Powered Wheelchair Technology

Electric-powered wheelchairs available in the market provide much functionality for the user and are composed of many different sub-systems. Each of these sub-systems and their functions can be tailor made for catering to a specific target user group.

The basic system of a wheelchair is the drive system which usually consists of a two wheel drive type or a four wheel drive type. The mid wheel drive power wheelchair is maneuverable in small spaces and provides for a tighter turning radius but the wheelchair may get stuck on uneven terrain. The front wheel drive system is very stable for uneven terrain and for inclined mobility but they are slower as compared to the rear wheel drive system. The most common type is the rear-wheel drive wheelchairs. The chair is stable and can achieve high speeds. The only drawback of this system is the large turning radius of the wheelchair (Ding & Cooper, 2005). External all-terrain wheelchairs typically use the four wheel drive system as they are easier to maneuver and control. Wheelchairs with special functions such as stair climbing or dynamically balance function use a wheel-cluster system (Ding & Cooper, 2005). Stair climbing is done by balancing the centre of gravity of the chair between the front and the rear wheels at all times. Dynamically balancing the wheelchair on two wheels, mimicking the human balance model, enables the user to move around at eye level. Our system uses a rear wheel drive system as the stability of the wheelchair is an important criterion when designing for elderly users or for users with limb disabilities.

Portable power is an important aspect of the wheelchair. The study by Beno et al. (2002) explores the feasibility of flywheel batteries for vehicles in general. Another study by Cooper & Tai (1998) discusses the feasibility of flywheel batteries for electric-powered wheelchairs and explores the safety issues such as fragmentation failure or touch-down failures of the flywheel. Typically, electric powered wheelchairs use chemical batteries as their energy source but it makes the wheelchair bulkier and difficult to transport.

There are many ways for the user to input information into the wheelchair control system. The joystick is the most commonly used mode of input for the wheelchair. Cooper et al. (2000) have designed an isometric joystick and compared its performance standards to a position sensing joystick while Diciano et al. (2007) developed a digital isometric joystick and studied the force applied by the user on an isometric joystick and motion sensing joystick. Jones et al. (1998) studied the performance of wheelchairs using a performance sensing joystick and a force sensing joystick. Oskoei & Hu (2008) propose a myoelectric based virtual joystick, which utilizes myoelectric signals from the forearm of the user to navigate the wheelchair. The advantage of this methodology is that users with severe motor disabilities find it easier to maneuver the wheelchair. Another mode of input for such users is voice recognition. The user trains the system to recognize simple commands such as "GO" or "STOP" and uses them for navigating the wheelchair. Pacnik et al. (2005) and Stanton et al. (1990) have both devised intelligent wheelchairs with voice recognition control. A combination of joystick input and voice recognition input is utilized in the wheelchair designed by us to help users with motor disabilities and to navigate in close-spaced environments.

A navigation system for wheelchairs would require the user not to worry about the path taken and concentrate only on commanding the wheelchair. The Brunel Navigation System for the Blind (BNSB) (Cecelja et al., 2006) is developed by integrating three main technologies: Global Positioning System (GPS), Geographical Information System (GIS) and Mobile Communication System (MCS). The BNSB uses GPS as the main navigational systems which operates in assisted GPS (AGPS) mode and fixes the users' position. The same system can be used for wheelchair users as well but implementing it in indoor environment may not be efficient. Wheelchair users in a fixed indoor environment like a shopping centre or the user's house would benefit much with an indoor navigation system. The Power-Line Positioning (PLP) Indoor Location System (Patel et al., 2006) uses the residential powerline for finding the location of the user. The PLP uses fingerprinting of tone detectors in different parts of the house and the room to localize them and find their location. Use of Wireless Sensor Networks for navigation has been done by (Lei et al., 2005) who have designed a wireless assisted pedestrian system using magnetic compass and accelerometers. Jirawimut et al. (2003) propose a method for dead reckoning correction in pedestrian navigation system while Usui et al. (2005) evaluate the position accuracy of pedestrian navigation systems using 3-dimensional maps in lieu of 2-dimensional maps. For us, wireless sensor network is used for the wheelchair navigation system in known indoor environments along with a digital compass for direction mapping.

Commercial foot rests available for wheelchairs are manual and they have very bare minimal functionalities. These conventional foot rests are manually adjustable to some preset heights and positions which are then locked at that position by an external locking mechanism. The problem with such conventional foot rest is that the old age or disabled user who is normally quite weak needs a lot of strength to lift up his/her legs onto the resting pad of foot rest. Another alternative is to ask someone besides the user to provide the assistance. Additionally, prolong sitting on the wheelchair causes a set of problems to the user as mentioned by Aissaoui et al. (2000). At present, there is next to negligible literature regarding the motorized foot rest and therefore the related work is presented in this chapter.

3. Microcontroller Based Voice-Activated Powered Wheelchair Control

This part of the chapter describes the design of a microcontroller based voice-activated powered wheelchair supplementary with joystick control. Most of the conventional electric powered wheelchairs use a joystick as a user input mode of control to maneuver the powered wheelchairs (Nisbet, 1996). The major drawback of joystick control is that users with upper limb disability would find it difficult to maneuver the wheelchair. Moreover, elderly users with weak and jerky hands would be more comfortable giving verbal instructions than navigating the wheelchair using a joystick. The proposed voice-activated powered wheelchair supplementary with joystick control would allow users with weak and disabled upper limb to maneuver the wheelchair easily without the need to use hands. Referring to Fig. 2, the electric powered wheelchair consists of three main building blocks viz. the user interface, the control system and the drive system.

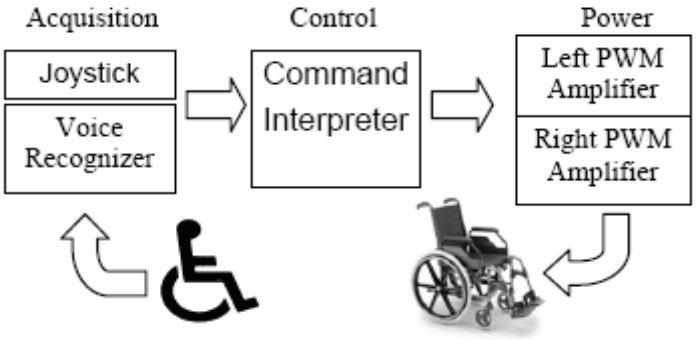

Fig. 2. Block Diagram of an Electric Powered Wheelchair

3.1 User Interface (Acquisition)

This electric-powered wheelchair is targeted for elderly users and users with disability hence, both joystick and voice recognition are used as user interface for acquisition. The supplementary joystick gives a better control of speed for better manoeuvring in confined areas. During the research work, a standard HFX magnetic joystick is used for joystick control. The joystick utilises Hall Effect Sensors to measure the physical movement of the joystick's handle. When the handle is moved, magnets attached to the shaft of the joystick (one for each axis) link the Hall Effect sensors causing a fluctuation in the magnetic field. This causes a voltage change that is interpreted by the integrated microcontroller. Both X and Y axes sensors are placed in series with a resistor and a fixed bias of 5 V is used to power the sensors, and the centre voltage output is 2.5V. The output voltage of the joystick can't be 0V or 5V due to additional resistance, but varies between 0.8V and 4.6V.

The voice processing module, as shown in Fig. 3, consists of a HM2007 voice recognition chip which processes the input voice signals fed through a microphone. The microphone is capable of noise cancellation and voice amplification. The voice recognition chip uses a supervised training method for classification. The voice chip is initially trained by the user. Once the system is programmed with the required commands, the chip operates in the hearing mode i.e. the chip listens continuously and tries to match the words spoken by the

user to the words programmed earlier. If there is a match, it sends an output corresponding to the match; otherwise the module continuously waits and keeps listening. The words recorded by the system are recognized by their frequencies, and different people speak may the same words at different frequencies. Hence, only the user's voice must be used for training the module. The accuracy rate and the ability to work even in noisy environment are very important for the safety and the ease of use of the wheelchair.

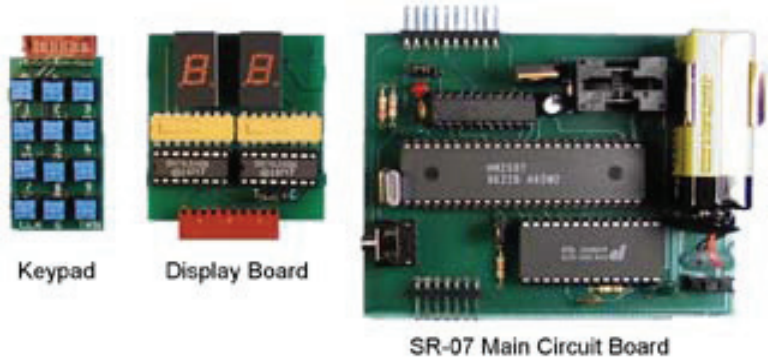

Fig. 3. Components of the SR-07 Voice Recognition Module

The user trains the chip using the included keypad. One of the keys is pressed and the voice command is spoken into the microphone clearly. For example, pressing the number of "01" would train the word number 01 and assign the voice command spoken to it. The LED in the main circuit board blinks off momentarily, signalling the successful acceptance of the word and the number used for this command is displayed. Further commands can be programmed in a similar way.

3.2 Control System

The microcontroller chosen for the implementation of the control system is an Infineon XC886 high performance 8-bit Microcontroller with on-chip flash memory for enhanced motor control. It has automatic code generation provided by the software DavE , and can be programmed using C programming language with Keil compiler and debugger. The microcontroller has several peripheral features required by the control of the power wheelchair, such as Capture/Compare Unit (CCU6) with two independent 16-bit timers dedicated for PWM generation for AC and DC motor control, providing 4 compare channels with 7 outputs, and 8-bit ADC with high accuracy, providing 8 channels, to convert the analog input signals to digital signals respectively.

There are two modes of control possible for the drive system viz. the open loop control and closed loop control. In open loop control as there is no feedback from the motor, the microcontroller will not be able to detect any increase or decrease in speed and take corrective action. This may result in a jerk effect that may cause discomfort to the wheelchair user. Providing a closed loop current control using a PI controller, as shown in Fig. 4, would ensure that any abrupt change in the load torque would not result in an abrupt change in the motor torque resulting in close to zero acceleration and negligible jerks during wheelchair operation.

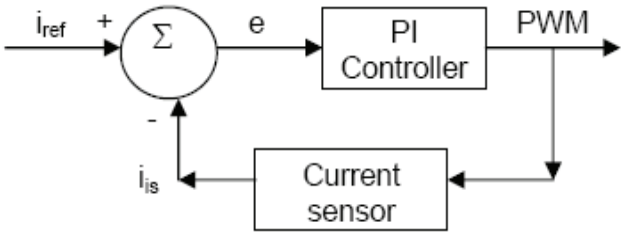

Fig. 4. Closed-Loop Feedback Current Control

The motor torque, T_{em}, is proportional to the armature current, I, across the motor.

$$T_{em} = k\phi I \tag{1}$$

$$T_{em} = T_l + J\frac{d\omega}{dt} \tag{2}$$

$$V = iR + k\phi\omega \tag{3}$$

If the current is controlled such that there are no sudden changes, then the motor torque, T_{em}, would also not have any sudden changes. The acceleration, $d\omega/dt$, of the motor is dependent on the difference between the motor torque, T_{em}, and the load torque, T_l. Since there is no abrupt change in the motor torque, the wheelchair moves at a constant speed with zero acceleration, hence there is no jerk at all. Hence a good control of current can lead to a much better performance of wheelchair. Furthermore, with the use of current sensor HXS 50-NP/SP2, it is possible to determine if the load current exceeds the current limit. With over current protection implemented, problems like overheating or damage of the motor are limited.

The microcontroller receives analog signals from the joystick, converts them to digital format and interprets and processes them. The voice recognition system processes the voice commands and sends the digitized signal to the microcontroller. The feedback from the current sensors is compared with the reference current and the speed of the motor is determined according to the error between the signals received from user interface and current sensors feedback. The microcontroller outputs the corresponding PWM signals to the motor drive circuit to drive the DC motor. The joystick control and the voice recognition control are further discussed below.

3.2.1 Joystick Control

The motion of wheelchair depends on the position of joystick. The duty cycle of PWM signals is generated according to the analog inputs from joystick, and the PWM signals determine the speed of the motors. The frequency of PWM operation is 20 kHz. The analog signal acquired from joystick is converted into digital format in the microcontroller which is used as the reference current signal for the closed-loop current control. X-axis and Y-axis of the joystick are used to describe the position of joystick knob. Different reference currents are assigned to each position. As shown in Fig. 5, the numbers (0 – 10) represent the strength of the reference current signal. The number on the left hand side indicates the left motor whereas the number on the right hand side indicates the right motor. If the reference

number is larger than 5, the motor rotates forward; when the given reference current number is less than 5 (0-4), the motor rotates in the reverse direction.

					10,10					
				9,10	9,9	10,9				
			8,10	8,9	8,8	9,8	10,8			
		7,10	7,9	7,8	7,7	8,7	9,7	10,7		
	6,10	6,9	6,8	6,7	6,6	7,6	8,6	9,6	10,6	
5,10	5,9	5,8	5,7	5,6	5,5	6,5	7,5	8,5	9,5	10,5
	4,8	4,7	4,6	4,5	4,4	5,4	6,4	7,4	8,4	
		3,6	3,5	3,4	3,3	4,3	5,3	6,3		
			2,4	2,3	2,2	3,2	4,2			
				1,2	1,1	2,1				
					0,0					

Fig. 5. Left and Right Motor Current Reference (I_{ref}) Distribution over Joystick

3.2.2 Voice Recognition Control

The control signal flow diagram of the voice recognition circuit is illustrated in Fig.6. The voice recognition circuit is continually listening. When repeating a trained word into the microphone, the number of the word is displayed. For instance if the word "GO" was trained as word number 01, when saying the word "GO" into the microphone, the number 01 would be displayed. This number is sent to the microcontroller and logic corresponding to it would generate the appropriate duty cycle for PWM generation.

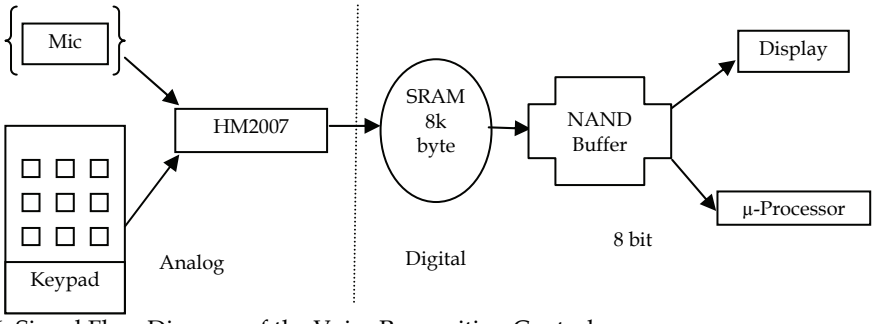

Fig. 6. Signal Flow Diagram of the Voice Recognition Control

The current sensor feedback signal corresponding to the load current drawn by the motor is first checked to see if it is larger than the preset current limit. This is the over-current protection feature. If the load current is within the normal operating range, the feedback current is compared with reference current, generating an error signal. The error signal is then injected into the PI controller to generate the output PWM control signals.

3.3 Drive System

The wheelchair has 2 DC motors attached to each of the left and right wheels. By controlling the individual speeds of both motors, the motion, i.e. the speed and direction of the wheelchair can be controlled. For example, the wheelchair turns left if the right wheel rotates faster than the left wheel and vice versa. A DC chopper not only allows adjustable speed control, but it also eliminates discontinuous conduction mode and allows bi-directional rotation. It consists of an H-bridge circuit which allows the direction and speed of the motor to be controlled by the power semiconductor switches. The switches are required to withstand a high current drawn by the motor under load conditions. The PWM outputs to adjacent switches are complimentary to ensure that there is no shoot-through effect resulting in a short circuit of the power supply.

The drive system is made up of two high current PN half bridge (BTS7970B) devices which amplify the input PWM signals to drive the DC motor. The designed PCB drive circuit board can provide a maximum driving current of 37.5A. The control system provides the PWM output signals to the drive system based on the command input signals from the user on the wheelchair. The output voltages are determined by the PWM signals. Fig. 7 shows the PCB layout of the H-bridge and its associated electronic circuit designed for the wheelchair.

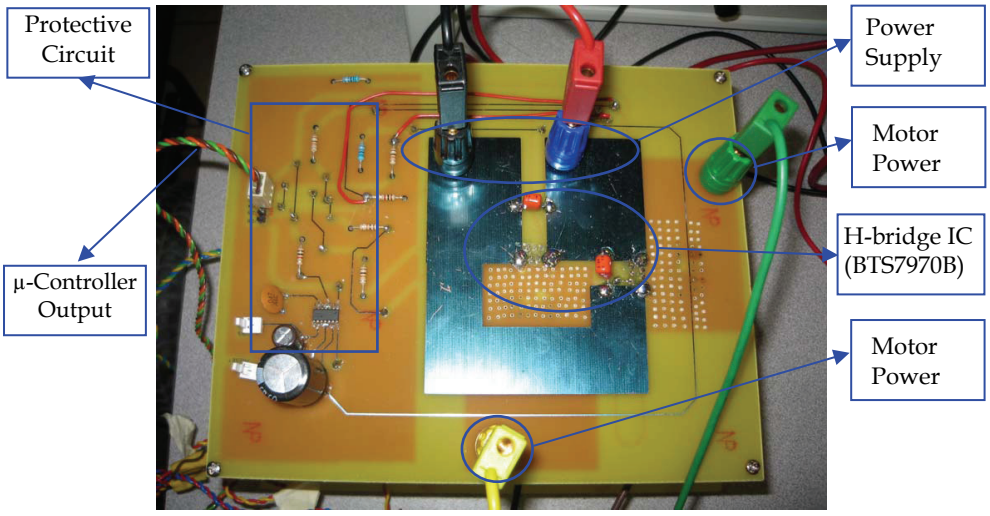

Fig. 7. PCB Layout of the H-bridge and its Associated Electronic Circuit

A 12V 36AH lead acid battery is used as the power supply for the electric-powered wheelchair. Lead acid battery is chosen over a flywheel battery as the wheelchair is designed for users with upper limb disability and elderly users and the risk of any damage due to the flywheel breaking or fragmenting is much higher (Cooper & Tai, 1998).

3.4 Prototype Wheelchair

Fig. 8 shows the schematic of the motor drive system and the control system of the prototype while Fig. 9 shows the prototype wheelchair.

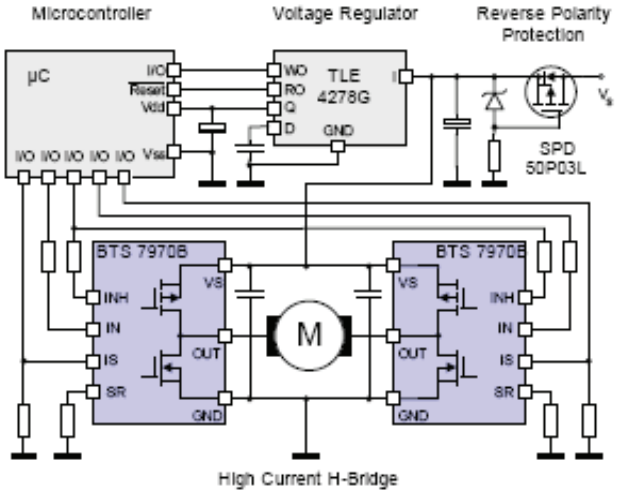

Fig. 8. Schematic Diagram of Prototype Motor Drives and Control System

Fig. 9. Prototype of Electric-Powered Wheelchair

The technical specifications of the wheelchair are given below:

Parameters	Value
Battery	12V , 36AH
Motor	24V DC
Charging Time	9 Hrs
Max. Driving Speed	Forward: 6.0Km/Hr Backward: 3.0Km/hr
Max. Weight Capacity	120 Kg
Total Weight of the Chair	77.29 Kg

Table 1. Technical Specifications of the Prototype

3.5 Experimental Results

The speed of the motor is determined by the voltage across the motor armature, as shown by equation (3), as the voltage drop across the armature resistance is negligible at steady state. To vary the voltage of the motor, a pulse width modulator (PWM) circuit is used. The PWM circuit varies the duty cycle of the output voltage and hence changes the average DC link voltage across the motor terminals.

The prototype electric-powered wheelchair has been tested with human load between 60 kg to 120 kg moving on a flat surface. The starting current of the DC motor is much higher than the rated full load current due to the negligible back emf across the motor armature. If the driver circuit is incapable of supporting the starting current it will fail, resulting in the breakdown of the whole system. The starting current drawn by the DC motor is observed to be about 20A. Our designed motor driver circuit board which can deliver up to 37.5A is able to meet this requirement. Fig. 10 shows the output voltage and the load current for a stationary wheelchair with a load of 100 kg. According to Fig. 5, the reference current for this joystick position is (5, 5) or a PWM duty cycle of 50% as evident from Fig. 10.

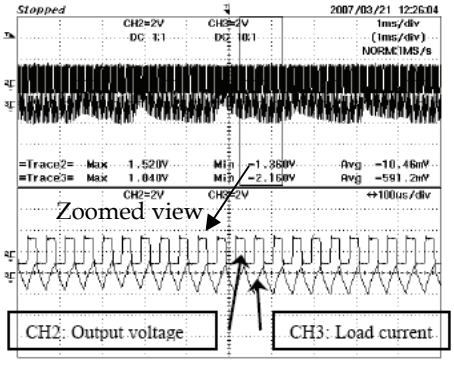

Fig. 10. Wheelchair in still position

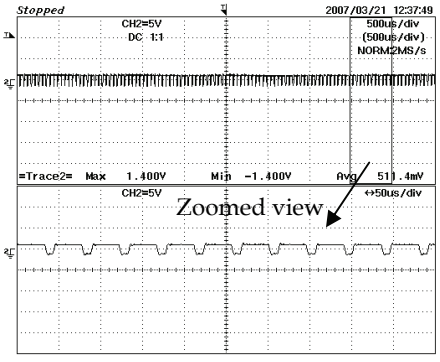

Fig. 11. Output Voltage in Steady State with Load for Forward Motion

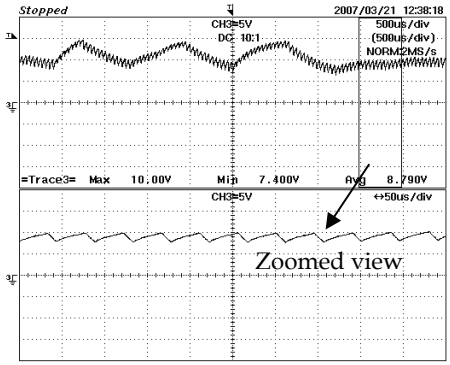

Fig. 12. Load Current in Steady State with Load for Forward Motion

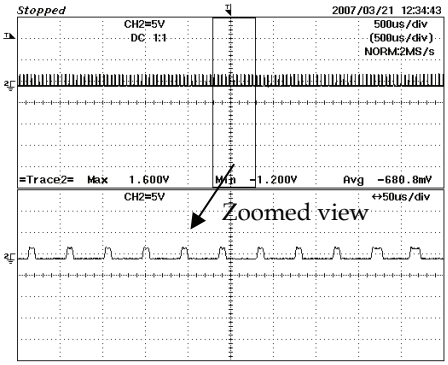

Fig. 13. Output Voltage in Steady State for Reverse Motion

From Fig. 12 it can be observed that the load current can be controlled to a certain level with stable performance. The fluctuating parts are due to the position change of the joystick, which is not fixed at one point due to manual control. Fig. 11 indicates the output voltage with a duty cycle of about 80% corresponding to a speed of 5 km/hr in the forward direction. Fig. 13 shows a PWM duty cycle of about 20% indicating reverse motion corresponding to a speed of 2.5 km/hr. The response time of the voice recognition system is calculated from Fig. 14 and Fig. 15 and is found out to be 672ms for the 'GO' command and 824ms for the 'STOP' command.

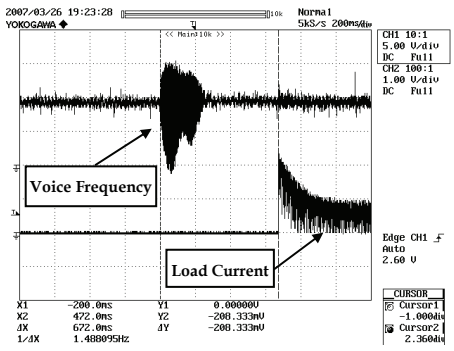

Fig. 14. Voice Frequency and Load Current with "GO" command

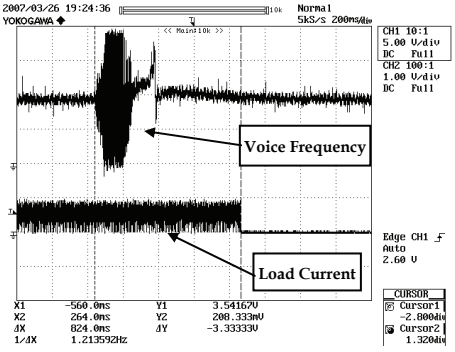

Fig. 15. Voice Frequency and Load Current with "STOP" command

This section of the chapter describes the design for a microcontroller based voice-activated powered wheelchair supplementary with joystick control. The voice recognition system helps the elderly users or users with upper limb disability in commanding the wheelchair. The next section deals with the design of a personal intelligent navigation system for known indoor environment using wireless sensor networks.

4. Personal Navigation System Based Wireless Sensor Network Technology

4.1 Introduction on Wireless Personal Navigation System

The objective of this section is to illustrate the development of a wireless indoor navigation system for the disabled and aged, particularly the wheelchair bounded, through the achievement of both location and direction determinations. A commonly used method of navigation for wheelchair patients in an indoor setting is the line tracking system, where light sensors are used to differentiate white and dark lines that are attached onto the ground surface. While this method has areas for further improvements (unsightly and inflexible navigation), hence a better wireless alternative is proposed in achieving the same motives. In recent years, the Global Positioning System (GPS) is widely used in many modern navigational applications. However, GPS technology is ineffective in indoor settings due to obstructions in buildings that hinder transmissions. Other possible location determining methods include using infrared, ultrasonic or radio signals and optical tracking systems.

A literature study was conducted to understand some of the research papers that were published regarding wireless indoor navigation systems. For instance, the Brunel Navigation System (Cecelja et al., 2006) for the Blind (BNSB) is developed by integrating three main technologies: Global Positioning System (GPS), Geographical Information System (GIS) and Mobile Communication System (MCS). The functional components of the BNSB are accommodated into two remotely linked terminals: Mobile Navigation Unit located at the remote site of the visually impaired pedestrian and the Navigation Service Centre, which is the sighted guide. The Mobile Navigation Unit is a wearable terminal that includes a digital video camera, a GPS receiver and a mobile network interface. A dead reckoning system, used to position the user when the GPS is not available, is also placed in the unit. The Navigation Service Centre is a stationary computer terminal running a GIS database and a display system to visualize video image and the user's location on a digital map. Navigation information includes real time transmission of the video image, GPS or dead reckoning positioning data and voice communication between the user and the guide.

Another research area for indoor navigation systems is the Mobile Ad Hoc Network (MANET). MANET (Latiff et al., 2005) is a collection of wireless mobile nodes that cooperatively form a network without specific user administration or configuration. All nodes contribute and maintain connectivity in the network since all of them can both communicate and also relay packets to other nodes. When nodes move, the topology of the network also changes and hence previously computed routes to a specific node has to be recomputed. Nodes can either determine location either by itself or rely on other nodes. The self-positioning system uses at least three signal strength measurements extracted from messages that are being broadcast by pre-determined nodes at intervals. These pre-determined nodes, also termed anchor nodes (AN), are stationed strategically in order to be received by all mobile nodes in the network. Distance of the mobile node (MN) to the ANs will be determined from the signal strength received based on a propagation path loss model of the environment. If the distance and location of these ANs are known, mobile nodes can triangulate its coordinates. The system to be developed will not require additional hardware since it uses the existing wireless communication hardware which is based on IEEE 802.11b standards. Another special feature of this self-positioning system is that it does not use signals from GPS.

A wireless pedestrian dead reckoning system (Lei et al., 2005) that combines inertial sensing and sensor network technology, called the NavMote is also in the research for indoor

positioning. The NavMote gathers information about pedestrian motion from an integrated magnetic compass and accelerometers. When the NavMote comes within range of a sensor network, it downloads the compressed data to the network. The network relays the data via a RelayMote to an information center where the data are processed into an estimate of the pedestrian trajectory based on a dead reckoning algorithm. Static and dynamic calibrations of the compass data are crucial to compensate the heading errors. The dead reckoning performance is further enhanced by wireless telemetry and map matching. It was also shown in research that indoor navigation is possible with the aid of augmented pictures (Merico et al., 2007), i.e. pictures with a very wide aspect-ratio that have been dynamically annotated with navigation information. Each picture is the result of automatically stitching together regular photos that have been taken under control of a "mapping" application. The mapping application starts from building plans in standard format and a list of points-of-interest and identifies where pictures should be taken from. The whole process is almost completely automatic and makes it possible to "map" a new building in a few days. Photos are processed in order to create a set of scrollable pictures that are augmented in real time with markers that indicate the direction to take and the position of "relevant locations" that can be used to recalibrate the dead-reckoning position.

Despite that many research works have already been carried on realizing the concept of wireless navigation system, local positioning system is still more favourable over GPS for indoor context. In similar approach as NavMote discussed by Lei et al., 2005, the target is for wheelchair-bounded aged and disabled people. In the implementation setup, radio frequencies of 433.98 MHz are used to set up a simple location determining network. As for direction determination, a 1490 digital compass sensor manufactured by Robson Company is being used. The sensor is a solid state Hall-effect device that is sensitive enough to detect the Earth's weak magnetic field and when rotated, outputs 4-bit digital signals that represent the compass' cardinal points to the microprocessor. Apart from the RF navigation system, a voice-activated powered module is also proposed to be incorporated with a joystick enabled wheelchair. The voice recognition system as described in the previous section recognizes voice commands and compares to those in the pre-stored memory; the respective coded digital signals would then be sent to the microcontroller which provides the relevant outputs to the wheelchair accordingly. With a voice-activated system, more convenience is hence brought to the disabled people. Additionally, a recent survey indicates that almost all of the people are not able to control the EPW by conventional methods and these users could benefit from the automated navigation system. Moreover, there are situations in which the user wants to travel from one location to another within a building either at home or at workplace repeatedly several times in a day (for example going to the toilet) (Pačnik et al., 2005). These users would benefit if a learning mechanism can be built into the wheelchair control system such that it would learn the path in an iterative manner and after few trials/iterations the controller would be able to take care of the navigation system making the user free to do something else or even relax. This is accomplished by integrating the Wireless Sensor Network (WSN) technology based on Zigbee protocol onto the EPW. The user first selects the destination he/she targets to go, through the WSN information; the indicator will guide the user on the EPW accordingly.

4.2 Navigation Methodology

Generally, in any navigation techniques, there are two possible ways widely used in directing a user from the starting point to the desired destination: The first method is to provide a general direction for the navigator to travel upon (unplanned routes) and the second method is to guide the user from one section to another (planned routes); Both techniques would eventually lead the user to his final destination. The illustrations and explanations of the navigation methodology are shown in the two figures in Figs. 16 and 17:

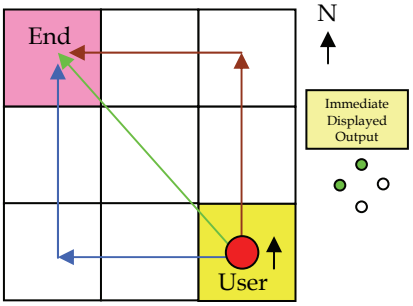

Fig. 16. Illustration on Unplanned Routing Methodology

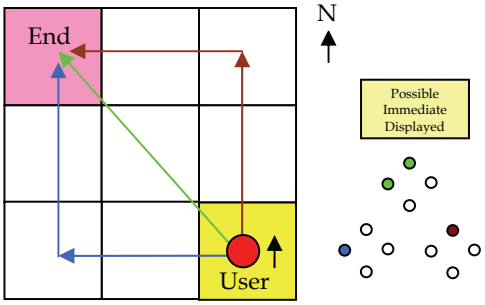

Fig. 17. Illustration on Planned Routing Methodology

Initially, the user starts from a random location, say the yellow grid, and he is facing the north direction as shown in Fig. 16 The final destination is to travel to a facility that is located in the pink grid. If the navigation system is programmed according to the unplanned routing methodology, the immediate displayed option would be as that shown in the diagram – directing him NorthWest with respect to where he/she is facing. This output direction indicates that his destination is somewhere along the NorthWest line, hence the user can choose to travel in the green line (fastest route), blue line, brown line or any other variations because all options would still lead him to his end point. In summary, the output directions given through the unplanned routing system always point the user DIRECTLY towards his destination. Consider the same scenario as seen in Fig. 17 but this time round, the output could be either the green, blue or brown route. This is dependent on how the route was planned beforehand and the user can make the choice out of the three options. In summary, the output directions given through the planned routing system need not always point to the destination directly. The user has to follow the navigation outputs accordingly to reach his destination, since he is not aware of where his endpoint lies.

Table.2 summarizes the comparisons between the two navigation methods. Based on the comparisons made between the unplanned and planned routing methodologies tabulated in Table.2, it can be concluded that adopting the planned routing method would be more appropriate for the aged and disabled people. The most important advantage of planned route over the unplanned route is that it can serve as an obstacle avoidance director. The scenario illustrated in Fig. 17 summarizes all the key benefits of planned routing methodology

	Unplanned routing	Planned routing
Output	Always point to end destination	Not necessarily point to end destination
Degree of freedom	High	Low
Distance traveled	Minimum	Varies
Time required	Varies	Varies
Ease of navigation	Low	High
Programming complexity	High	Low
Suitability for disabled	Low	High

Table 2. Comparison between the Unplanned and Planned Routing Methodologies

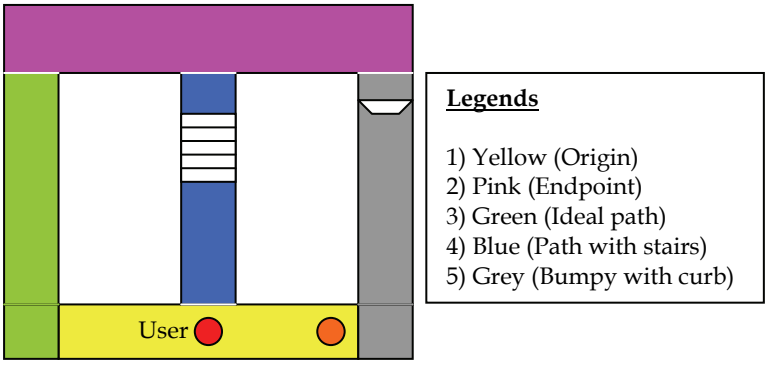

Fig. 18. Illustration to Show Key Benefits of Planned Routes Methodology

Consider a wheelchair user (red dot) who wishes to navigate to the pink region. There are three different paths for the user to choose of which the green path is the safest and easiest to cross. If the navigation system is adopting the unplanned routing method, the immediate output would be pointing the user straight ahead to the blue path, which is undesirable. However, if the planned routing method is to used, the output would direct the user to turn left instead, towards the green route away from the blue and grey paths, so as to avoid the obstacles along those routes. When the user is in the green region facing his destination point, the output would be simply move forward. Likewise, for the user at the orange dot, it would be his immediate instinct to choose the grey path since the unplanned routing system would simply tell him that his destination is 'somewhere' straight ahead. However, the planned routing system would instruct the orange user to take the extra mile towards the green path because the path is the safest possible way for the user. A set of software codes has been developed to compute the relevant directions that are used to guide the user to the intended destination. The corresponding true navigation charts, depicting the respective outputs at different locations and directions, have to be prepared beforehand as well.

Function 1 (Current location = Yellow, Destination = pink)

Progress	A	B	C	D
*Current direction	N or NE	W or NW	S or SW	E or SE
Immediate output				

Function 2 (Current location = Grey, Destination = pink)

Progress	A	B	C	D
*Current direction	N or NE	W or NW	S or SW	E or SE
Immediate output				

Function 3 (Current location = Blue, Destination = pink)

Progress	A	B	C	D
*Current direction	N or NE	W or NW	S or SW	E or SE
Immediate output				

Function 4 (Current location = Green, Destination = pink)

Progress	A	B	C	D
*Current direction	N or NE	W or NW	S or SW	E or SE
Immediate output				

* Possible directions faced by user at the instance in time

 : For example: Turn back

 : For example: Turn right

 : Destination reached

The 4 functions demonstrated as shown above aim to navigate the user residing in any of the locations to the pink destination region. Using the four functions, the sequences of the routing paths can be planned as the followings: -

Function 1 to 4 or Function 2 to 1 to 4 or Function 3 to 1 to 4

where Function 4 is the last function in all the 3 sequences, which is termed as the end function of the whole sequence. In the programming terms, regardless of the user's current location, the ultimate aim is to direct him to the end function eventually. In bigger and more complex layouts, there can be multiple end functions that lead the user to the same destination.

4.3 Location Determining System

System name	Signal	Method	Absolute positioning	Relative Positioning	Positioning	Tracking	Geometrical	Symbolic	Costs	Positioning Accuracy [m]
Active Badge	IR	CoO	X			X		X	Low	Room
WIPS	IR	CoO	X		X			X	Low	Room
Active Bat	US	ToA	X			X	X		Low	0,1
Cricket	US	ToA	X	X	X			X	Low	1,2
GSM	RS	TDoA/AoA	X			X	X		Low	50-100
A-GPS	RS	ToA	X		X		X		High	20-25
Locata	RS	ToA	X		X		X		High	0,1-1
Radar	RS	SS	X		X	X	X		High	3-4
IMST ipos	RS	SS	X			X	X		High	1-3
Ekahau	RS	SS	X				X		High	1-3
Wi-Fi	RS	SS			X	X	X	X	High	N/A
WhereNet	RS	SS	X				X			N/A
UWB	RS	ToA/TDoA	X		X	X	X		High	0,2
Bluetooth	RS	CoO	X		X	X	X		Aver	10
SpotON	RS	SS	X	X	X	X	X		Aver	1
RF sensor network	RS	CoO		X				X	Low	1-20
Cybercode	VL	DI		X	X			X	Aver	Variable
Ubitrack	VL	DI		X		X	X		N/A	N/A
Easyliving	VL	DI	X			X	X		High	Variable

Table 3. Examples of Location Determining Systems

In the field of indoor positioning, it can be observed in Table.3 that many different location determining systems have been developed over the years; and signals such as infra red (IR), ultrasonic (US), radio signals (RS) and visible light (VL) are employed widely within them. Methods for position determination include Cell of Origin (CoO) where the location of the user is described in a certain cell area around the transmitter; Time of Arrival (ToA) where the travel time of a signal between a transmitter and receiver is obtained; Time Difference of Arrival (TDoA) where the time difference of signals sent from a transmitter is determined at two receiving stations and Signal Strength (SS) measurement for location determination using fingerprinting. These methods are employed in various systems of Wireless Fidelity (Wi-Fi), Assisted Global Positioning System (A-GPS), Bluetooth and Radio Frequency Sensor Networks such that location determination can be achieved. Among them, radio signals within the radio frequency (RF) refers to the electromagnetic field that is generated for wireless broadcasting and communications over a significant portion of the RF spectrum - from about 9 kilohertz (kHz) to thousands of gigahertz (GHz) is used. The idea is to develop a network of sensors, comprising of multiple transmitters, each of which emitting a

common frequency carrying different sets of data. Although this method does not offer absolute positioning, it is effective enough, for a close indoor setting, in providing general directions to the user towards his destination. In addition, the price of setting up a RF network is low compared to the above proposed suggestions. Because of all these factors, the RF sensor network is hence adopted as the location determining system.

4.4 Direction Determining System

With the location determining system in place, it is time to move on to the next vital component necessary in every navigation application: the setting up of a direction determining system. The most common method in determining direction is to make use of the Earth's weak magnetic field. However this entails the use of certain magnetic techniques and devices. Table.4. gives the relative attributes of the four most widely used technologies: Hall effect, magnetoinductive, flux-gate and magnetoresistive.

Comparison of magnetic sensor technologies					
Technology	**Sensitivity**	**Size**	**Cost**	**Power consumed**	**Comments**
Magnetoinductive	High	Small	Low	Low	Provides digital (frequency) output, temperature compensation
Flux-gate	High	Medium	Medium	Medium	Provides analog output, temperature compensation
Magnetoresistive	High	Small	Medium	Medium	Provides analog output
Hall-effect	Low	Very small	Low	Medium	Provides analog output, subject to drift and high noise, amenable to IC-fabrication techniques

Table 4. Comparison of Magnetic Sensor Technologies

Hall-effect devices are the smallest and least expensive with the lowest sensitivity of the four magnetic sensor technologies. Their low cost and small size stem from their adaptability to monolithic-IC processing. The drawback of low sensitivity is overcome by the Dinsmore digital compass sensor by magnifying the earth's field in order to bring it within the range of the sensor – by means of increasing its Hall coefficient, R_H. The Hall coefficient which measures the resulting Hall field is defined as:

$$R_H = \frac{E_H}{B * J} \tag{4}$$

$$V_H = \frac{-IB}{d * n * e} \tag{5}$$

where,

R_H is the Hall coefficient
E_H is the Hall field (proportional to Hall Voltage, V_H)
B is the applied magnetic flux density
J is the applied current density
I is the current across the plate length
B is the applied magnetic field
d is the depth of the plate
e is the electron charge
n is the bulk density of the carrier electrons.
According to the above two equations, a high Hall coefficient means that the sensor is able to sense a lower value of B (in this case the Earth's weak magnetic field) and result in a larger Hall field and hence Hall voltage – sufficient to be detectable.

4.5 Hardware Design and Implementation

The overall hardware design and implemented prototype of the navigation system consist of four main parts: 1) User interface which includes a LCD display and three input buttons (commands of 'scroll up', 'scroll down' and 'enter'); 2) One digital compass sensor for direction determining; 3) One receiver and four transmitters which make up the RF sensor network and 4) Output directional pad which consists of 4 LEDs. All these components are interfaced directly to the microcontroller as shown in Fig. 19.

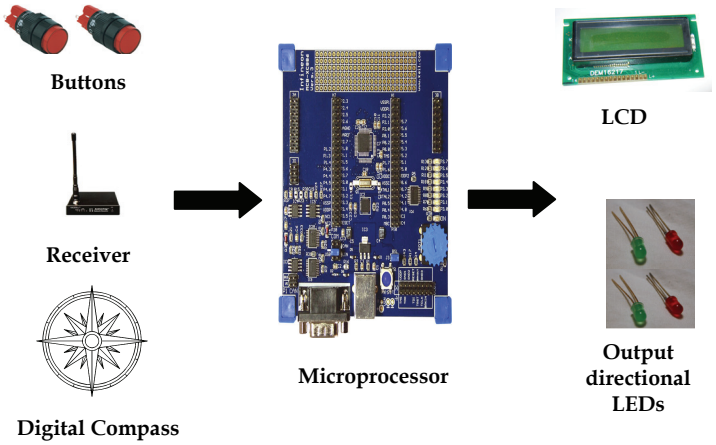

Fig. 19. Overall Block Diagram of the Personal Navigation System

The flow of the program written in the personal navigation system is illustrated in Fig. 20 Initially, the physical location of the user is determined by the location determining system mounted onboard the navigation system. The RF transmitters deployed at various points of the indoor location is set to continuously broadcast the location ID of that particular RF transmitter. Once the RF receiver of the navigation system receives any of the location IDs, the user's location will be known. Take for instance, the user is presently residing in the Linear Lab, the location ID of the lab is 0001 which is broadcasted to the RF receiver to

inform the user of his/her present location as illustrated in Fig. 20 After which, the user then selects the destination point (1/4 – 4/4). With the start point and end point information, the best route to travel between the points can be determined through the true navigation chart. Along the route, the direction determining system enables the indication LEDs accordingly to guide the user towards the selected destination.

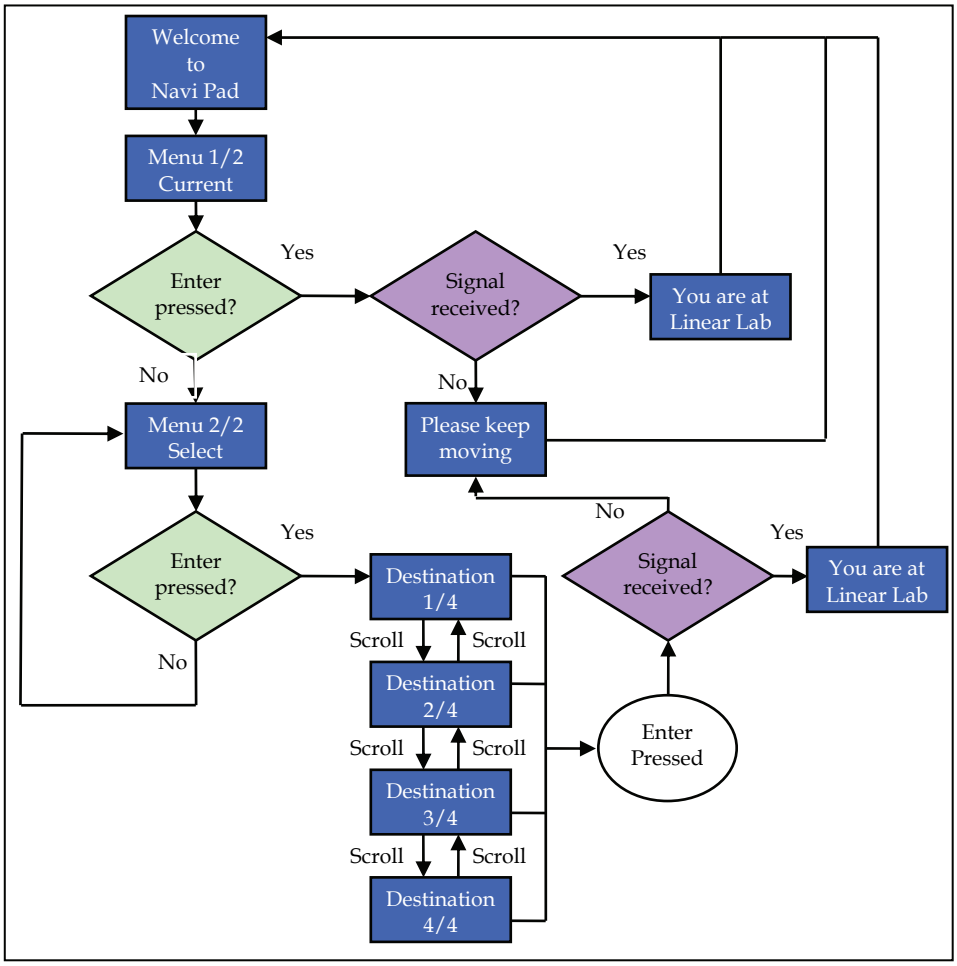

Fig. 20. Flowchart of Graphical User Interface (GUI) with Navigation System

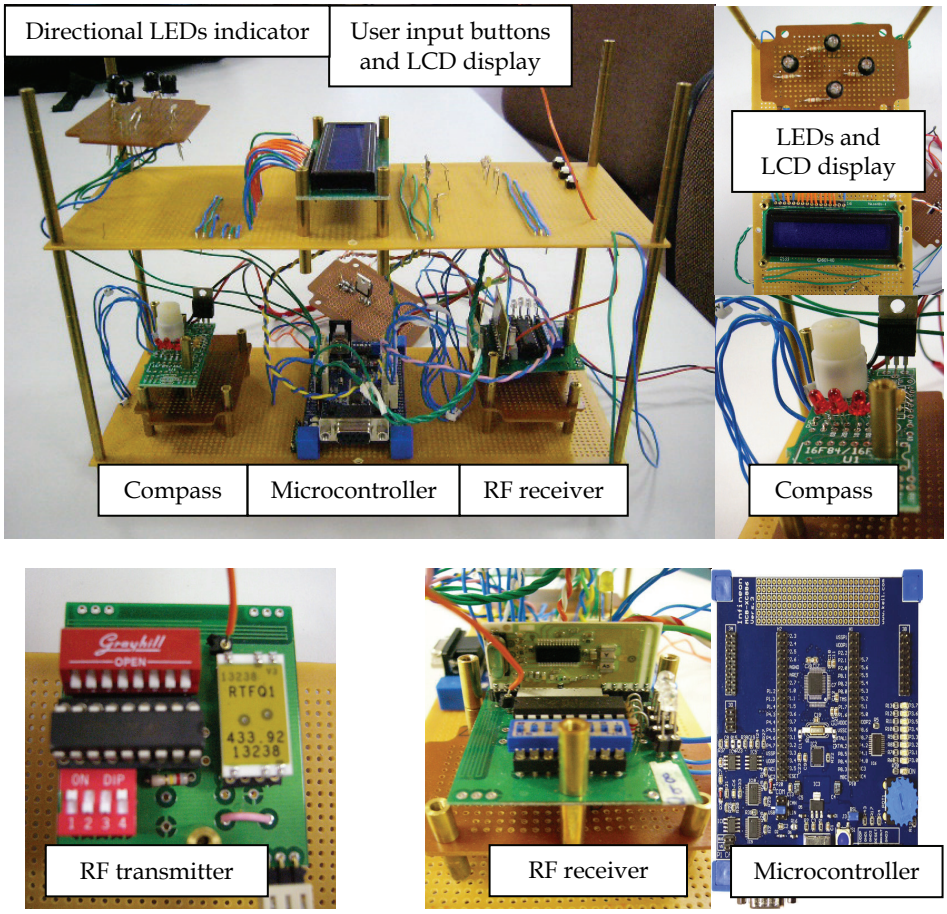

Fig. 21. Hardware prototype of personal navigation system based wireless sensor network

The design of the personal navigation system is implemented based on the WSN technology for indoor application. The system has been developed into hardware prototype for testing as shown in Fig. 21. The RF transmitter acts like a sensor node that keeps broadcasting the location ID via the 433.92 MHz frequency band. The microcontroller is used to process the 4-bit location ID received from the RF receiver as well as the directional signal sensed by the compass unit. The processed information is then conveyed to the user via the LCD display. The user can select his/her choice from the list of destinations recorded in the memory of the microcontroller and the navigation system will then guide the user to the end destination via the most suitable path routed based on the true navigation chart.

5. Motorized Foot Rest for Electric Powered Wheelchair

5.1 Introduction on Wheelchair Foot Rest

Wheelchair foot rests are known by many names including front rigging, foot rest, lower leg support, wheelchair leg supports, or just wheelchair legs to name a few (McLaurin & Axelson, 1990). The foot rests are installed on the wheelchair as the base of support to the lower limbs of the wheelchair user and they prevent excessive sliding motion and discomfort feeling to the lower limbs of the wheelchair-bounded aged and disabled individuals. At present, the conventional foot rests are adjusted manually by some external assistances to meet the desired height and position required by the user. Ironically, the wheelchair users often have limited strength in their arms and torso and thus most of the time they can only depend on the wheelchair in sedentary position. Hence, the users are hardly able to move their legs or feet supported by the conventional fixed foot rest due to weakness in their lower part of their body. In this way, there must be somebody at the side of the user to help in lifting the users' feet from the ground onto the pad of foot rest. This creates some form of inconvenience to both the wheelchair users and the people around them. Both physical and psychological barriers obstruct the wheelchair users from walking out of their homes to enter into the society. Another problem is that if the user's legs are too short and the resting pad is too far down from the seat, it would be very uncomfortable to dangle the legs and feet in the air since the foot rest is very difficult for the user himself/herself to manually adjust to the desired position.

One very severe problem for wheelchair users is the long period of time siting on the wheelchair where they have very minimum chances to exercise and the problem of poor blood circulation and physical inactivity (Cooper et al., 1994) will become critical. With considerations of the few critical problems and limitations related to the conventional foot rest, a motorized foot rest has been designed to overcome those problems and a model prototype is developed to demonstrate the working principles and feasibility of the motorized foot rest for electric powered wheelchair. The motorized foot rest has to be able to assist the wheelchair users to lift up their feet from the ground without any external assistance and adjust the length and angle of the motorized foot rest to provide a most comfortable position for the user to put their feet. The motorized foot rest must also provide the wheelchair users the rehabiliative means to exercise their legs in order to improve blood circulation in the legs.

5.2 Importance of Adjustable Foot Rest for Wheelchair-Dependent Individuals

Lower leg support is a generic term, describing a variety of products, such as legrest pads, calf straps and kneelers. Elevating legrests are generally used to augment venous circulation and reduce depended edema, or to fix the knee in extension as a result of orthopedic deformity, surgical immobilization, or severe hypertonicity in the extensors. The importance of elevating foot-rests for easier patient transfer and wheelchair stability has also been described (Aissaoui et al., 2000). A basic misconception regarding leg position in the wheelchair is that in order to reduce pressure under ischial tuberosities, the feet of a person in a wheelchair should bear little or no weight. The detrimental effects for wheelchair-dependent individuals sitting with the legs hanging freely or with minimal foot support have been described as follows: 1) it is very unstable sitting posture, as the weight of the unsupported legs destabilizes the trunk; 2) it is a fatiguing sitting posture, resulting in an

increase in back muscle activity in an attempt to stabilize the trunk; 3) the weight of the unsupported legs creates a force that causes the pelvis to slide forward on the seat. The individual ends up in a slumped posture, with an increase in pressure and shearing forces over and posterior to ischial tuberosities.

The rationale behind footplate adjustment usually appears to be empirically-based and varies between authors. It was found that proper foot support would reduce 18.4% of the body weight from the seat. Using able-bodied subjects sitting in a wheelchair, Bush found no significant difference on ischial pressure when the feet were hanging freely compared to when the legs were fully extended. Gilsdorf et al. found that the lowest ischial interface pressures on any cushion were with the legs dangling. They acknowledged however, that it is impractical to leave a wheelchair user's legs without support. In the study of Hobson, the foot-rests were adjusted to take approximately 10% of the body weight, while in the study of Koo et al. they are adjusted so that the thighs are horizontal. The influence of foot-rest position on seat pressure distribution was investigated in. Although based on a single subject, this study clearly showed that optimal foot-rest adjustment is essential for minimizing peak pressure on the seat. Rising the footplate height can increase ischial pressure by as much as 100%, compared to when they are as low as possible but still supporting the foot.

All these studies have focused on the length of the foot-rest i.e. the distance from the front seat to the foot supports. Aissaoui et al. (2000) found that peak pressure gradient around ischial tuberosities increased significantly by 20% when the foot-rest angle was changed from 90 to 45 with respect to the horizontal. Moreover, the elevation of the leg supports is directly related to knee extension. In fact, the angulation of lower leg supports can affect the posture of the sitter's hip if the angular modification changed the distance from the seat front to the foot supports. This change results from the fact that the foot-rest's axis of motion is not aligned with the knee joint axis. This interdependency between foot-rest angularity and the distance between the foot support and seat, requires the linear placement of the lower leg and foot support to be adjusted in synchrony with the foot-rest's angular modification. Products that do not address this changing geometry can cause sitter discomfort and soft tissue trauma. For example, if a foot-rest is elevated and the foot support is not lengthened, then the hip and knee joints is forced into flexion, and weight-bearing pressure increases under ischial tuberosities. This risk of pressure increase can be avoided by selecting equipment that allows the foot supports to lengthen as the foot-rest procline. This mechanism has led to a design of a new foot-rest called a compensatory (CMP) foot-rest, in contrast with a conventional (CNV) foot-rest that had a fixed axis of rotation. However, no data exist in literature to corroborate the beneficial effect of the CMP foot-rest. The purpose of this study is to compare the effects of the CNV and the CMP foot-rests on posture and pressure distribution of ten able-bodied subjects while sitting in a manual wheelchair. In this study, we hypothesized that the CMP foot-rest will compensate for the knee joint motion. This compensation will preserve the posture adopted initially by subjects when the legrest is set vertically. Moreover, thigh and pelvic motion will be minimized when extending the knee joint, and pressure distribution at the body-seat interface will be reduced when using the CMP foot-rest. The biomechanics part of the leg and foot rest affecting the user is not going to be the main focus of this section. What we want to discuss in this section of the chapter is the practical implementation of a motorized

foot-rest to help the user to overcome the above mentioned problems arising from prolong sitting and improper leg resting position.

5.3 Design and Prototype of Motorized Foot Rest

The motorized foot rest has to be designed to enhance the assistive and rehabilitative needs of the disabled and aged population. There are several factors to be considered when the motorized foot-rest is designed such as the weight of the foot rest, number of motors used, construction of the design, types of materials needed, overhead and manufacturing costs, etc. The initial stage of prototyping the motorized foot rest was carried out and the model prototype is developed as illustrated in Fig. 22.

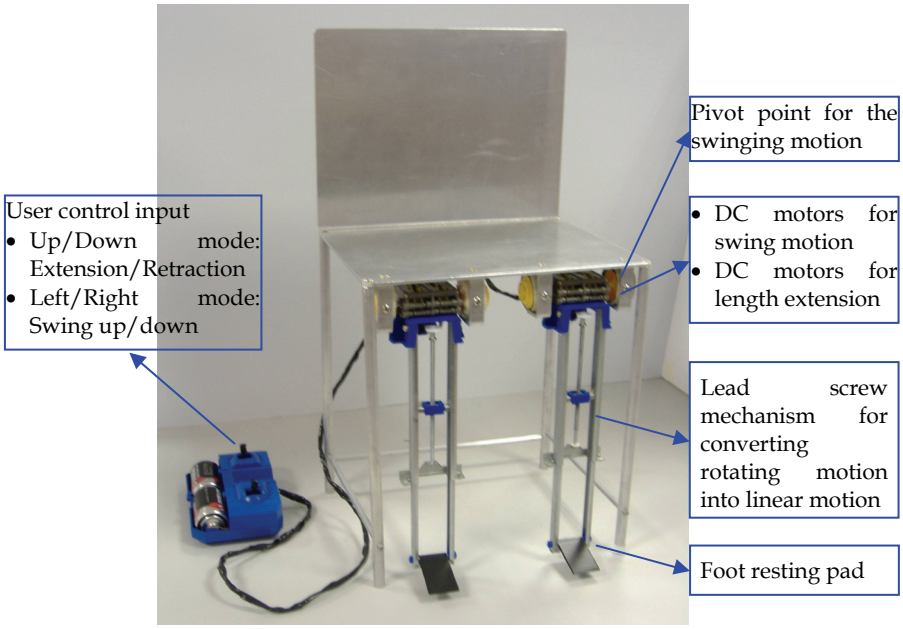

Fig. 22. Prototype of the motorized foot rest

The DC motors are designed to be placed between the top of the entire foot rest and the seating chair as shown in Fig. 22. This is done to minimize the effect of the heavy weight of the motors and its associated mechanisms adding on the foot rest. Less electrical power is needed to lift up the lower moving part of foot rest, hence smaller and low-powered motors can be used which will reduce the overall system cost as well as the power consumption of the motors and its associated drive system. The present design allows two degrees of freedom namely one rotational and one linear movement so as to attain the necessary motions required in the assistive and rehabilitative needs of the disabled and aged population.

During the experiments, several tests were carried out to determine the motion speed, the extension distance and the swing angle attainable. It is found that the motorized foot rest can move up and down in the linear motion at an average speed of 6 mm/sec. The foot rest

can extend as long as to a maximum length of 30 cm with respect to the original length of 18 cm. For the rotational motion, the foot rest is managed to swing a maximum angle of 90 degrees. The whole motorized foot rest system is powered up by an external DC power supply.

Components	Descriptions
Control system	A joystick to control the rotational and linear movements by moving the control stick to the left, right, forwards and backwards.
Rotational and linear drives and motoring	DC motors and gearboxes to control the rotational and linear movements of the foot rest
Movable mast	Movable mast, threaded shaft/lead-screw to convert rotational motion to linear motion. When motor starts to rotate, the lead-screw rotates accordingly to produce the linear motion.

As mentioned above, the motorized foot rest has to be capable of assisting the user to lift up his/her feet from the ground. The assistive process can be explained as follows. Firstly, the user controls the foot rest to extend its length until both the resting pads touch the ground as shown in Fig. 23. The user can then easily dragged his/her feet onto the resting pad by himself/herself or if the user is having severe upper limb problem, somebody besides the user can easily assist. After which, the motor is activated to lift the user's feet up into the air. With the motorized foot rest, the whole process of lifting the wheelchair user's feet onto the foot rest requires very bare minimum help from people around the user. Once the user's feet is resting on the foot rest, he/she can adjust the length and swing angle accordingly as shown in Fig. 24 and Fig. 25 respectively to suit his/her comfortable position.

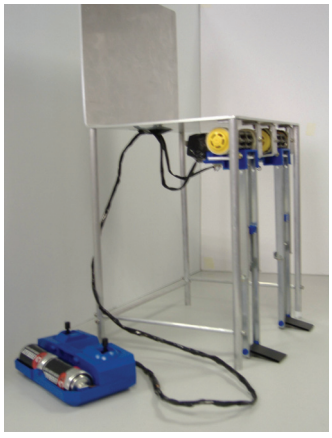

Fig. 23. Motorized foot rest at stationary position

Fig. 24. Motorized foot rest after swing angle adjustment

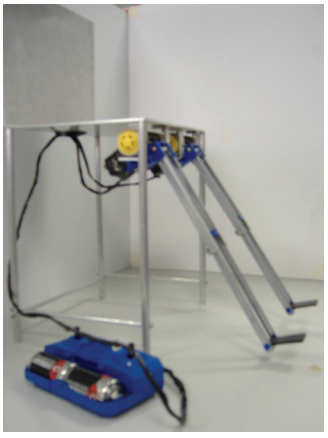

Fig. 25. Motorized foot rest after length adjustment

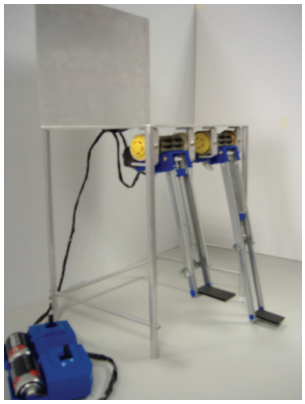

Fig. 26. Illustration of leg lifting exercise (Assistive need)

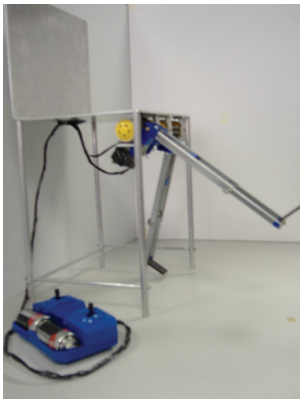

Fig. 27. Illustration of walking exercise (Rehabilitative need)

Having a controllable motorized foot rest, the user can adjust his/her sitting position on the wheelchair to the most comfortable one with the flexibility in adjusting the foot rest position. The user simply manipulates the joystick i.e. up/down or left/right to control both the linear and rotational motions of the foot rest. By doing so, both the vertical length and swing angle can be changed. Take for an example, if the user has long legs, he/she can increase both the length of the foot rest to fit his long leg as well as the swing angle to seek for a comfortable position as illustrated in Fig. 24 to Fig. 25.
Other than supporting the assistive need, the motorized foot rest can be designed to provide some rehabilitative exercises to users so as to move their legs for blood circulation. This can be done by applying the linear or rotational motions continuously; control the foot rest to move up and down (see Fig. 25) or to rotate the swing angle continuously (see Fig.26). This is done by pushing the control sticks forward and backward alternatively to apply linear motion and in the similar way for the rotational motion. The lower limbs including thighs, legs and feet of the wheelchair users are often moving and exercising, just like any healthy person. This encourages blood circulation and physical reaction, which is beneficial to the users' health and recovery.

6. Conclusion

The chapter has discussed about the ageing problem of the world population as well as the increasing amount of disabled people that are wheelchair-bounded. Electric-powered wheelchair is very favourable among people with both lower and upper extremity impairments because EPWs provide excellent functional mobility and comfort as comparable to the manual wheelchairs. However, people with severely impaired physical disabilities are challenged in operating conventional EPWs in some domestic environments. The chapter has introduced three technological solutions to help many aged or disabled people who are dependent on human caregivers to perform daily tasks by themselves. The combined solution of the microcontroller based voice-activated electric-powered wheelchair equipped with the personal navigation system based on wireless sensor network and the motorized foot rest has been described. Experimental results obtained have verified the

solution leads to engineering better EPW to enhance the rehabilitative and assistive needs of the disabled and aged people.

7. Acknowledgements

The authors would like to acknowledge the project works of Mr. David Ang, Ms Jinzhou Yi, Ms Yue Yu, Ms. Hong Wu and Ms Pei Liu, who are students supervised by Associate Professor Sanjib Kumar Panda and Professor Jianxin Xu. Special thanks to be expressed to Associate Professor Sanjib Kumar Panda for his great help in reviewing the chapter.

8. References

Aissaoui R., Heydar S., Dansereau J. & Lacoste M. (2000). Biomechanical analysis of legrest support of occupied wheelchairs: comparison between a conventional and a compensatory legrest, *IEEE Transactions on Rehabilitation Engineering*, Vol. 8, Issue. 1, pp. 140-148

Beno, J., Thompson, R. & Hebner, R. (2002)., Flywheel Batteries for Vehicles, *Proceedings of the Workshop on Autonomous Underwater Vehicles*, pp. 99–101

Cecelja F., Garaj V., Hunaiti Z. & Balachandran W. (2006). A Navigation System for Visually Impaired Pedestrians, *International conference on Instrumentation and Measurement (IMTC 06)*, Sorento, Italy

Chen R.X., Chen L. G., & Chen L. (2000). System Design Consideration for Digital Wheelchair Controller, *IEEE Transactions on Industrial Electronics*, Vol. 47, No. 4, pp. 898-907

Committee on Ageing Issues (CAI) (2006). Report on the Ageing Population, Five-Year Masterplan, *Ministry of Community Development, Youth and Sports (MCYS)*, Singapore

Cooper R.A., Stewart K. L., VanSickle D. P., Albright S. J., Heil T. (1994). Manual wheelchair ISO-ANSI/RESNA fatigue testing experience, *Proceeding of RESNA '94*, Nashville, TN, pp. 324-326

Cooper R.A. (1998). Wheelchairs: A Guide to Selection and Configuration, *NY: Demos Medical Publishers*, New York

Cooper R.A. & Tai C. (1998). Feasibility of flywheel batteries for electric powered wheelchairs, *Proceedings of the 20th Annual International Conference of the IEEE Engineering in Medicine and Biology Society*, Vol. 5, No. 5, pp. 2261-2263

Cooper R A., Widman L. M., Jones D. K., Robertson R. N. & Ster J. F. (2000). Force Sensing Control for Electric Powered Wheelchairs, *IEEE Transactions on Control Systems Technology*, Vol. 8, No. 1, pp. 112-117

Cooper R.A. & Cooper R. (2003). Trends and Issues in Wheeled Mobility Technologies, Retrieved February 5, 2004, from http://www.ap.buffalo.edu/ideaproto/Space%20Workshop/Papers/WEB%20-%20Trends_Iss_WC%20(Cooper).htm

Cooper R.A., Boninger M.L., Spaeth D. M., Ding D., Guo S., Koontz A.M., Fitzgerald S.G., Cooper R., Kelleher A. & Collins D.M. (2006). Engineering Better Wheelchairs to Enhance Community Participation, *IEEE Transactions on Neural Systems and Rehabilitation Engineering*, Vol. 14, No. 4, pp. 438-455

Cooper R.A., Dicianno B.E., Brewer B., LoPresti E., Ding D., Simpson R., Grindle G., Wang H. (2008). A perspective on intelligent devices and environments in medical rehabilitation, *Medical Engineering & Physics*, Vol. 30, No. 10, pp. 1387-1398

Diciano B E., Spaeth D M., Cooper R A., Fitzgerald A. G., Boninger M. L. & Brown K. W. (2007). Force Control Strategies While Driving Electric Powered Wheelchairs With Isometric and Movement-Sensing Joysticks, *IEEE Transactions On Neural Systems And Rehabilitation Engineering,* Vol. 15, No. 1, pp. 144-150

Ding D. & Cooper R. A. (2005). Electric-powered wheelchairs, *IEEE Control Systems Magazine*, Vol. 25, No. 2, pp. 22-34

Institute of Public Affairs, edited by Moran A. (2005). Impact and Outcome of Regulation on the Economy, *Institute of Public Affairs Ltd*, Melbourne

Kuruparan J., Jayanthan T., Ratheeskanth V., Denixavier S. & Munasinghe S. R. (2006). Semiautonomous Low Cost Wheelchair for Elderly and Disabled People, *International Conference on Information and Automation (ICIA 2006)*, pp. 104-108

Jirawimut R., Ptasinski P., Garaj V., Cecelja F. & Balachandran W. (2003). A Method for Dead Reckoning Parameter Correction in Pedestrian Navigation System, *IEEE Transactions On Instrumentation And Measurement*, Vol. 52, No.1, pp. 209-215

Jones D. K., Cooper R. A., Albright S. & DiGiovine M. (1998). Powered Wheelchair Driving Performance Using Force- and Position-Sensing Joysticks, *Proceedings of the IEEE 24th Annual Northeast Bioengineering Conference,* pp.130–132

Latiff L., Ali A., Ooi C., & Fiscal N. (2005). Development of an Indoor GPS-free Self Positioning System for Mobile Ad Hoc Network (MANET), *MICC-ICON 2005*, Malaysia

Lei F., Antsaklis P.J., Montestruque L.A., McMickell M.B., Lemmon M., Yashan S., Fang H., Koutroulis I., Haenggi M., Xie M. & Xie X. (2005). Design of a wireless assisted pedestrian dead reckoning system - the NavMote experience, *IEEE Transactions on Instrumentation and Measurement*, Vol. 54, Issue. 6, pp. 2342-2358

McLaurin C.A. & Axelson P. (1990). Wheelchair standards: an overview, *Journal of Rehabilitation Research & Development*, Vol. suppl, pp. 100-109

Merico D. & Bisiani R. (2007). Indoor Navigation with Minimal Infrastructure, *Proceeding of 4th Workshop Positioning, Navigation and Communication (WPNC 07)*, pp. 141–144, IEEE Press

Nisbet P. (1996). Integrating assistive technologies: current practices and future possibilities, *Medical engineering & physics*, Vol. 18, No. 3, pp. 193-202

Oskoei M. A. & Hu H. (2008). Myoelectric based Virtual Joystick Applied to Electric Powered Wheelchair, *IEEE/RSJ International Conference on Intelligent Robots and Systems*, pp. 2374-2379, Nice, France

Pačnik G., Benkič K. & Brečko B. (2005). Voice Operated Intelligent Wheelchair – VOIC, *IEEE International Symposium on Industrial Electronics (ISIE)*, pp. 1221-1226

Patel S. N., Troung K. N. & Abowd G. D. (2006). PowerLine Positioning: A Practical Sub-Room-Level Indoor Location System for Domestic Use, *Proceedings of 8th International Conference of Ubiquitous Computing*, pp. 441-458, California, USA

Stanton K. B., Sherman P. R., Rohwedder M. L., Fleskes C. P., Gray D. R., Minh D. T., Espinoza C., Mayui D., Ishaque M. & Perkowski M. A. (1990). PSUBOT - A Voice-Controlled Wheelchair For The Handicapped, *Proceedings of the 33rd Midwest Symposium on Circuits and Systems,* Vol. 2, pp. 669 – 672

United Nations (2005). World Population Prospects The 2004 Revision, *Department of Economic and Social Affairs (Population Division)*, New York

Usui S., Tsuji J., Wakimoto K., Tanaka S., Kanda J., Sato F. & Mizuno T. (2005). Evaluation of Positioning Accuracy for the Pedestrian Navigation System, *IEICE Trans Commun.*, Vol. E88-B, pp.2848-2855

7

A Rehabilitation Walker with a Standing Assistance Device

Daisuke Chugo* and Kunikatsu Takase**
*Kwansei Gakuin University
Hyogo, Japan
**The University of Electro-Communications
Tokyo, Japan

1. Introduction

In Japan, the population ratio of senior citizen who is 65 years old or more exceeds 22[%] at January 2009 and rapid aging in Japanese society will advance in the future (Population Estimates, 2009). In aging society, many elderly people cannot perform normal daily household, work related and recreational activities because of decrease in force generating capacity of their body. Today, the 23.5[%] of elderly person who does not stay at the hospital cannot perform normal daily life without nursing by other people (Annual Reports, 2001). For their independent life, they need domestic assistance system which enable them to perform daily life easily even if their physical strength reduces.

Standing up motion is the most serious and important operation in daily life for elderly person who doesn't have enough physical strength (Alexander et al., 1991) (Hughes & Schenkman, 1996). In typical bad case, elderly person who doesn't have enough physical strength will cannot operate standing up motion and will falls into the wheelchair life or bedridden life. Furthermore, if once elderly person falls into such life, the decrease of physical strength will be promoted because he will not use his own physical strength (Hirvensalo et al., 2000). Therefore, we are developing the force assistance system for standing up motion which uses part of the remaining strength of the patient in order not to reduce their muscular strength.

In previous works, many researchers developed power assistance devices for standing up motion. However, these devices are large scale and they are not suitable for family use (Nagai et al., 2003) (Funakubo et al., 2001) (Chuv et al., 2006). Furthermore, these devices assist all necessary power for standing up and they do not discuss about using remaining physical strength of patients. Therefore, there is still a risk of promoting the decrease of their physical strength.

In this paper, we develop a walker system with power assistance device for standing up motion. Our system is based on a walker which is popular assistance device for aged person in normal daily life and realizes the standing up motion using the support pad which is actuated by the manipulator with three degrees of freedom. For using the remaining

physical strength, our system uses the motion pattern which is based on the typical standing up motion by nursing specialist as control reference (Chugo et al., 2006).
Our key ideas are two topics. The first is new assistance manipulator mechanism with four parallel linkages which enables the system to be rigid and compact. The second is the combination of force and position control. Using our control scheme, the patients can stand up with fewer loads and can use their own remaining physical strength during the motion. We verify the performance of our proposed assistance system through simulations and experiments using our prototype.
This paper is organized as follows: we introduce the mechanical design and derive its inverse kinematics of our assistance system in section 2; we analyze the standing up motion by nursing specialist in section 3; we propose the new control scheme and show the result of computer simulations and experiments using our prototype in section 4; section 5 is conclusion of this paper.

2. System Configuration

2.1 Assistive Mechanism

Fig.1 and Fig.2 show our proposed assistance system. The system consists of a support pad with three degrees of freedom and the walker system. The support pad is actuated by our new assistance manipulator mechanism with four parallel linkages. Our prototype can lift up the patient of 180[cm] height and 150[kg] weight maximum.

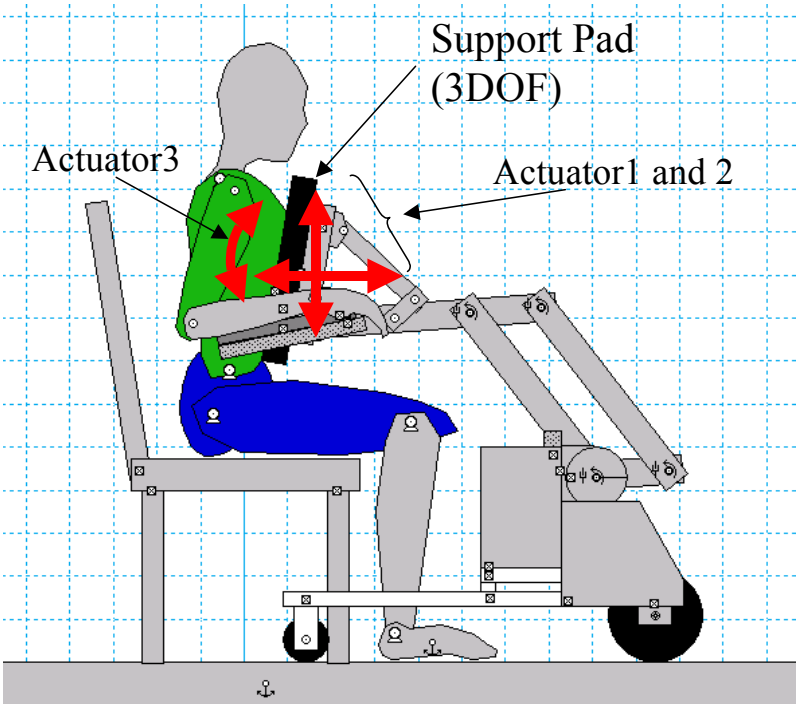

Fig. 1. Overview of our system.

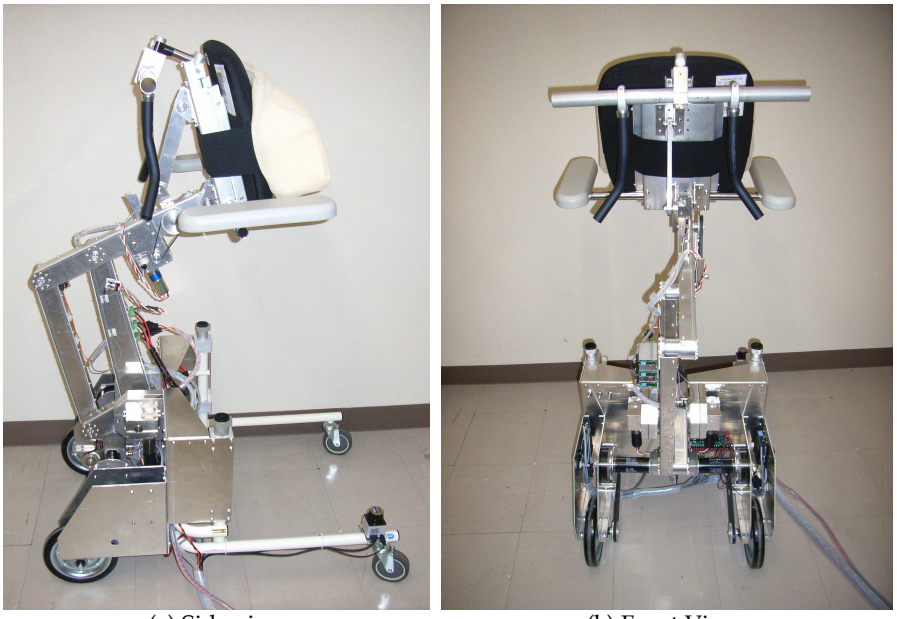

(a) Side view (b) Front View

Fig. 2. Our prototype. Its weight is about 35[kg] without batteries. Our prototype requires an external power supply and control PC. (In future works, we will use batteries and built-in controller.)

Our assistance system assumes the patient leans on the support pad during the standing assistance. We demonstrated our prototype standing assistance system in a welfare event (Chugo & Takase, 2008) and we asked patients, nursing specialists and physical therapist for advice. They indicated the following points.

- Patient's arm should be on the arm holder.
- Handles are required because it helps aged person to fix their arm on the arm holder with his weak grip.
- The support pad should hold the patient body without a slip down to sideways.
- The support pad should hold the patient softly because strong pressure causes obstruction of blood circulation.

Considering with these opinions, we design the support pad as shown in Fig.3(a). The support pad consists of the pad with low repulsion cushion and arm holders with handles. Both sides of this cushion are thick and it holds the patient body without slipping down. The patient leans on the pad, puts the arm holder and grasp the handle during standing up with our assistance system as Fig.3(b). The assistance posture of the patient is based on the assistance scheme of nursing specialist (Kamiya, 2005). (We discuss in section next section.)
In general, a fear of falling forward during standing motion reduces the standing ability of elderly person (Maki et al., 1991). Using this pad, a patient can maintain his posture easily during standing up motion without a fear of falling forward. Furthermore, the pad has force

sensors in its body. Our assistance system can measure its applied force and can estimate a body balance of the patient during standing up motion using these sensors.

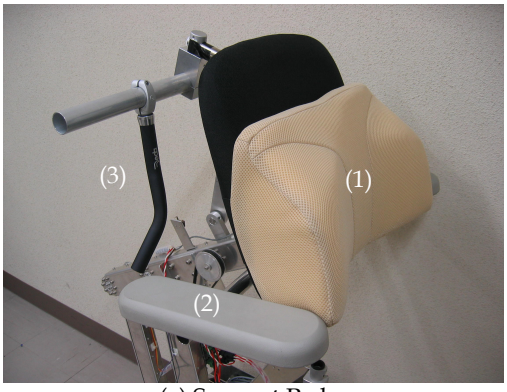

(a) Support Pad

(b) Assistance Posture

Fig. 3. Our proposed support pad. (1) is the pad with a low repulsion cushion, (2) is the arm holder and (3) is a handle. Its diameter is 0.24[m] which is easy to grip for the elderly. Our support pad has force sensors in its body.

Fig.4 shows the frame-kinematic model of our assistance manipulator. The position of the support pad (2DOF) is coordinated by Actuator 1 and Actuator 2 which are equipped on O point. Actuator 1 drives Link1 (α) and Actuator 2 drives Link2 (β). Using four parallel linkages mechanism, two actuators can generate the position of the support pad. The inclination of the support pad (1DOF, θ_3) is coordinated by Actuator 3 which is equipped on P point.

The advantages of our proposed mechanism are two topics. The first is that two main actuators (Actuator 1 and 2) are required to keep only weight of linkages. In general manipulator, the actuator of lower part supports not only weight of linkages but also actuators of upper part. Therefore, the actuators of lower part are required high output traction and tend to be heavy. On the other hand, using our mechanism, main actuators are mounted on the walker body (O point) and they are required to keep only weight of linkages. As the result, we can use smaller actuators for our assistance manipulator.

The second is that the parallel linkage mechanism is strong for a twist load. Using the parallel linkage mechanism, our actuator system can realize same strength with lighter linkages comparing with the general one. Using our proposed mechanism, we can use smaller actuators and lighter linkages, and our system realizes compact design with low cost.

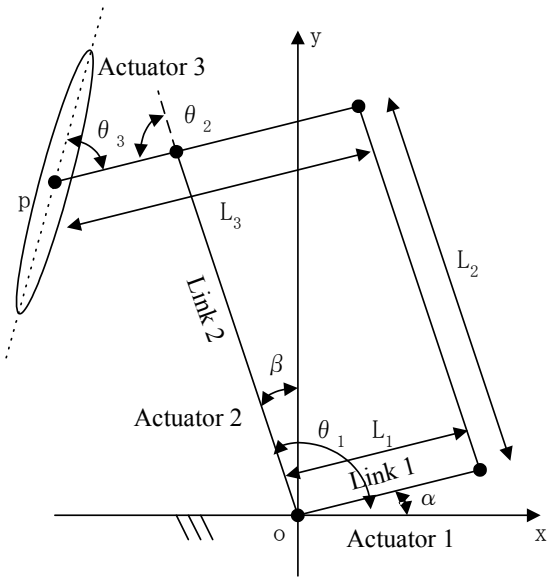

Fig. 4. The flame-kinematic model of developed system.

3.2 Kinematics

In this section, we derive the inverse kinematics of our proposed linkage mechanism. Using our proposed mechanism, the position of P point (We define its coordinates as (x_p, y_p)) is derived as follows;
The first, we set angular values and length of linkages as in Fig.4.

$$\theta_1 = \frac{\pi}{2} + \beta \,,\ \theta_2 = \frac{\pi}{2} + \alpha - \beta \tag{1}$$

$$l_1 = L_2 \,,\ l_2 = L_3 - L_1 \tag{2}$$

where α and β are angular value of Actuator 1 and Actuator 2, respectively. L_1, L_2 and L_3 are length of linkages.
Now, we consider the geometric relationships among the position of P point and these angular values, we can derive (3) and (4).

$$x_p = l_1 \cos\theta_1 + l_2 \cos(\theta_1 + \theta_2) \tag{3}$$

$$y_p = l_1 \sin\theta_1 + l_2 \sin(\theta_1 + \theta_2) \tag{4}$$

From (3) and (4), θ_2 is (5).

$$\theta_2 = \arccos\left(\frac{x_p^2 + y_p^2 - l_1^2 - l_2^2}{2l_1 l_2}\right) \tag{5}$$

We set k_1 and k_2 as (6), (3) and (4) are expressed as (7) and (8).

$$k_1 = l_1 + l_2\cos\theta_2,\ k_2 = l_2\sin\theta_2 \tag{6}$$

$$x_p = k_1\cos\theta_1 - k_2\sin\theta_1 \tag{7}$$

$$y_p = k_1\sin\theta_1 + k_2\cos\theta_1 \tag{8}$$

Furthermore, we set r and γ as (9), k_1 and k_2 are expressed as (10).

$$r = \sqrt{x_p^2 + y_p^2},\ \tan\gamma = \frac{k_2}{k_1} \tag{9}$$

$$k_1 = r\cos\gamma,\ k_2 = r\sin\gamma \tag{10}$$

Using (10), (7) and (8) are expressed as (11) and (12).

$$x_p = r\cos(\gamma + \theta_1) \tag{11}$$

$$y_p = r\sin(\gamma + \theta_1) \tag{12}$$

From (11) and (12), we can derive (13).

$$\tan(\gamma + \theta_1) = \frac{y_p}{x_p} \tag{13}$$

Thus, θ_1 is (14).

$$\theta_1 = \arctan\left(\frac{y_p}{x_p}\right) - \arctan\left(\frac{l_2\sin\theta_2}{l_1 + l_2\cos\theta_2}\right) \tag{14}$$

Using (5) and (14), we can control our manipulator. The lengths of its linkages are L_1 =150[mm], L_2 =450[mm], L_3 =480[mm], and the movable range of the support pad is 520[mm] in horizontal direction (X-axis) and 580[mm] in vertical direction (Y-axis). This range is enough for assisting the standing up motion for the 180[cm] height patient.

3. Standing up Motion

3.1 Motion by Nursing Specialists

In previous study, a lot of standing up motions for assistance are proposed. Kamiya (Kamiya, 2005) proposed the standing up motion which uses remaining physical strength of the patients maximum based on her experience as nursing specialist. Fig.5 shows the standing up motion which Kamiya proposes.

In our previous work, we analyze this standing up motion and find that Kamiya scheme is effective to enable standing up motion with smaller load (Chugo et al., 2006). We assume the standing up motion is symmetrical and we discuss the motion as movement of the linkages model on 2D plane (Nuzik et al., 1986). We measure the angular values among the linkages, which reflect the relationship of body segments. The angular value is derived using the body landmark as shown in Fig.6 (a).

In order to realize the Kamiya scheme, the trunk needs to incline to forward direction during lifting up from chair as shown in Fig.6 (b). Y-axis shows the angular value (Pelvis /trunk, knee, ankle) and X-axis shows the movement pattern (Hughes & Schenkman, 1996) which means the ratio of standing up operation as (15).

$$\hat{s} = \frac{t}{t_s} \tag{15}$$

where t_s is required time to the standing up operation and t is present time.

Generally, inclining the trunk reduces the load of knee during standing up (Fisher et al., 1990) and this motion is useful for elderly person who doesn't have enough physical strength. Therefore, in next section, we derived the control reference for our assistance system which realizes this motion using computer simulations.

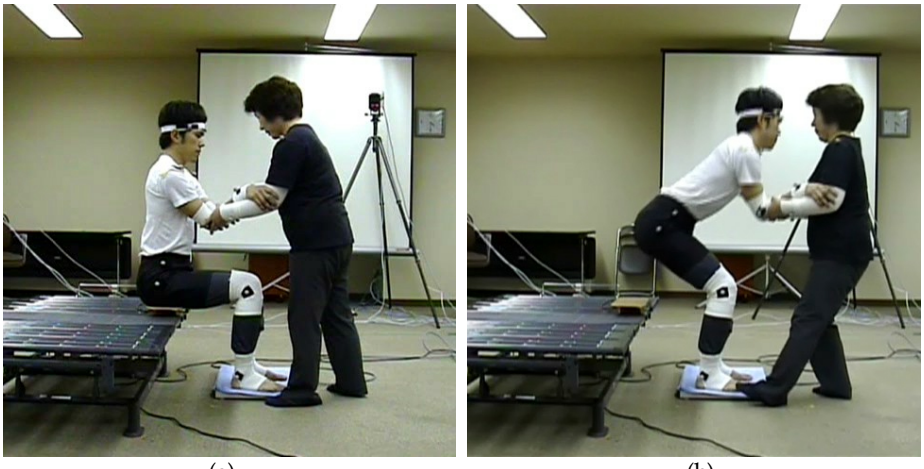

(a) (b)

Fig. 5. Standing-up motion with Kamiya scheme

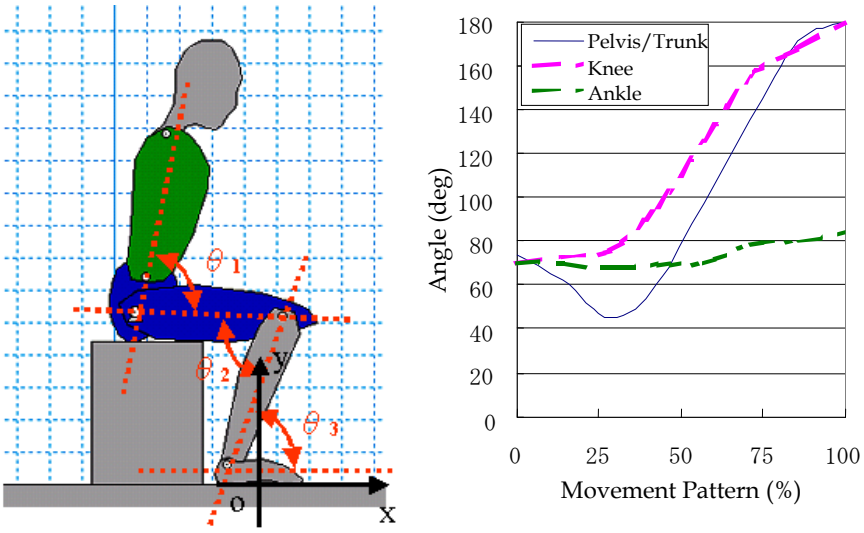

(a) Coordination (b) Angular Value

Fig. 6. Standing-up motion with Kamiya scheme. θ_1 shows the angular of the pelvis and the trunk. θ_2 and θ_3 shows the angular of the knee and the ankle, respectively.

3.2 Derivation of Control Reference

In this section, we derive the control reference of our assistance system which can realize the standing up motion proposed by Kamiya using a computer simulation. Fig.7 shows the simulation setup. The parameters are chosen from a standard body data of adult male (Digital Human) (Okada et al., 1996) as shown in Table 1.

In derivation of the references using the simulation, we assume the following points.

- The human model moves each joints as Fig.6(b).
- The human model puts his forearm on the supporter.
- The human model leans on the pad using his arm with own enough force.
- We assume the height of human model is 170[cm].

Number	Link Name	Mass [kg]	Length [m]	Width [m]
1	Head	5.9	0.28	0.21
2	Trunk	27.2	0.48	0.23
3	Hip	18.1	0.23	0.23
4	Humerus	4.5	0.39	0.12
5	Arm	2.7	0.35	0.08
6	Hand	0.5	0.2	0.07
7	Femur	9.1	0.61	0.17
8	Leg	4.5	0.56	0.16
9	Foot	0.8	0.26	0.11

Table 1. Human Parameters

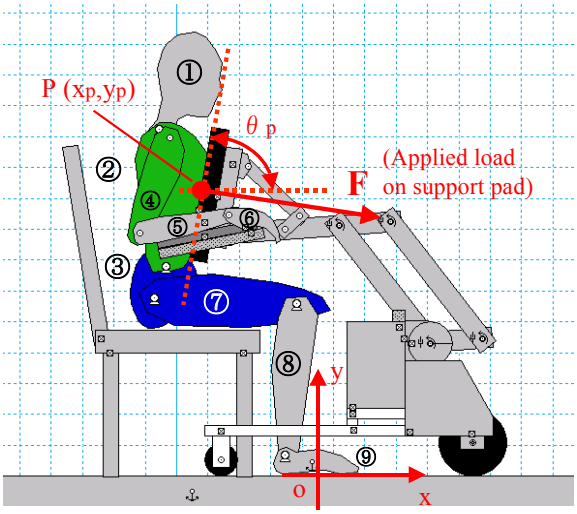

Fig. 7. Simulation setup.

We use the Working Model 2D as a physical simulator and MATLAB as a controller. Both applications are linked by Dynamic Data Exchange function on Windows OS.
From the simulation results, Fig.8(a) shows the position tracks of support pad and Fig.8(b) shows its angle tracks. In Fig.8(b), Y-axis shows the inclination angle of the support pad and X-axis shows the movement pattern $\hat{s}$. The coordination of Fig.8(a) and (b) is defined as shown in Fig.7. In Fig.8(a), the start point is lower left and the end point is upper center. Using these tracks as the position control reference, our assistance system can realize the standing up motion which Kamiya proposes.

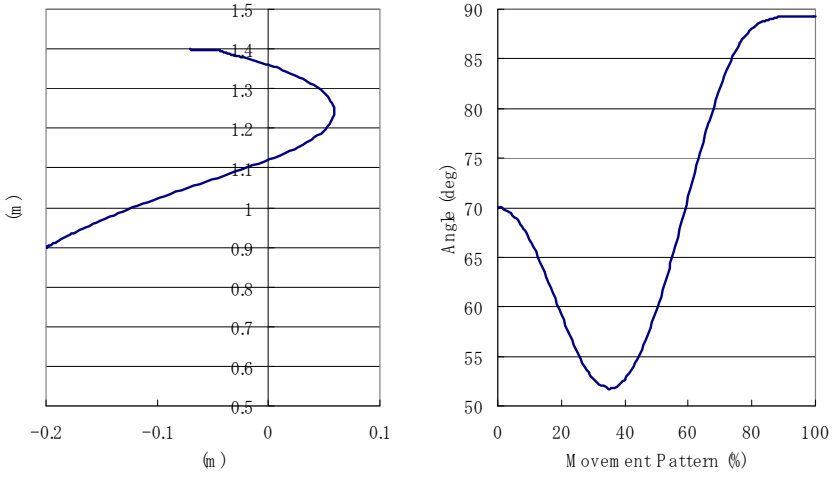

(a) Position (b) Inclination

Fig. 8. Derived control references.

Furthermore, we show the knee load of the patient and applied load on support pad during standing up in Fig.9. The knee load is larger than 0.5[Nm/kg]. In general, if the applied load to each joint is heavier than 0.5[Nm/kg], it is difficult to stand up for the elderly person (Omori et al., 2001). Therefore, it is required to reduce knee load during this standing-up motion.

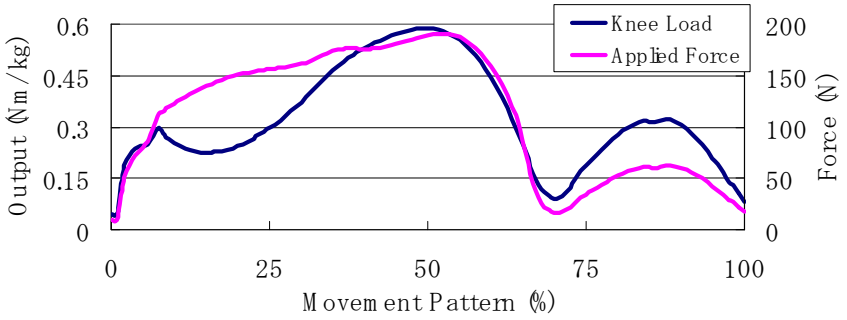

Fig. 9. Applied load on the pad and load of knee joint during human model stands up.

4. Force Control

4.1 Proposed Control Scheme

In general, we can divide the standing up motion into four phases (Schenkman et al., 1990). In first phase, the patient still sits and inclines his trunk to forward direction. In second phase, he lifts off from the chair and in third phase, he lifts the body. In fourth phase, he extends his knee joint completely and ends the standing up motion. From previous research, in third phase, it is required to force assistance because the knee load is heavy. On the other hand, in other phases, it is required to maintain the motion of Kamiya scheme.

Therefore, we propose new control scheme as shown in Fig.10. Proposed control scheme combines dumping control and position control. The dumping control is suitable for the control of the objects with contact (Sugihara et al., 2004). When the required torque of each joint is small enough in first, second and fourth phase, the controller uses the position control. On the other hand, when required torque of knee joint is heavy in third phase, the controller uses the dumping control.

We use the force sensor attached on the support pad for switching condition between the position control and the dumping control. Comparing with the knee load and applied force in Fig.9, the applied force to the support pad shows the same tendency to the applied load of knee joint. Therefore, we can divide the third phase and the other phases using the measuring value of the force sensor as a threshold. Using our proposed control scheme, the controller can select more appropriate control method using the force sensor on the support pad.

Now, we explain our proposed control scheme closely. The reference generator derives the velocity control reference of each actuator from motion reference by Kamiya as Fig.8.

$$\mathbf{v}_i^{ref} = \left[v_i^{ref}(0), \cdots, v_i^{ref}(\hat{s}), \cdots, v_i^{ref}(1) \right]^T \tag{16}$$

where v_i^{ref} is control reference and it is function of the movement pattern $\hat{s}$ as (15).
The output of each actuator is derived from (17).

$$v_i = v_i^{ref} - B\left(F - F_0\right) - K\left(x_i - x_i^{ref}\right) \tag{17}$$

where F is the applied force on the support pad and F_0 is the threshold which selects force or position control. v_i^{ref} is the velocity reference and x_i^{ref} is the position reference derived from track references as shown in Fig.8. v_i is the updated reference which our system uses actually during the assistance motion. B and K are constants.
When F is smaller than the threshold force F_0, the system sets $B = 0$ and selects position control mode. On the other hand, F is larger than the threshold force F_0, the system selects force control mode.

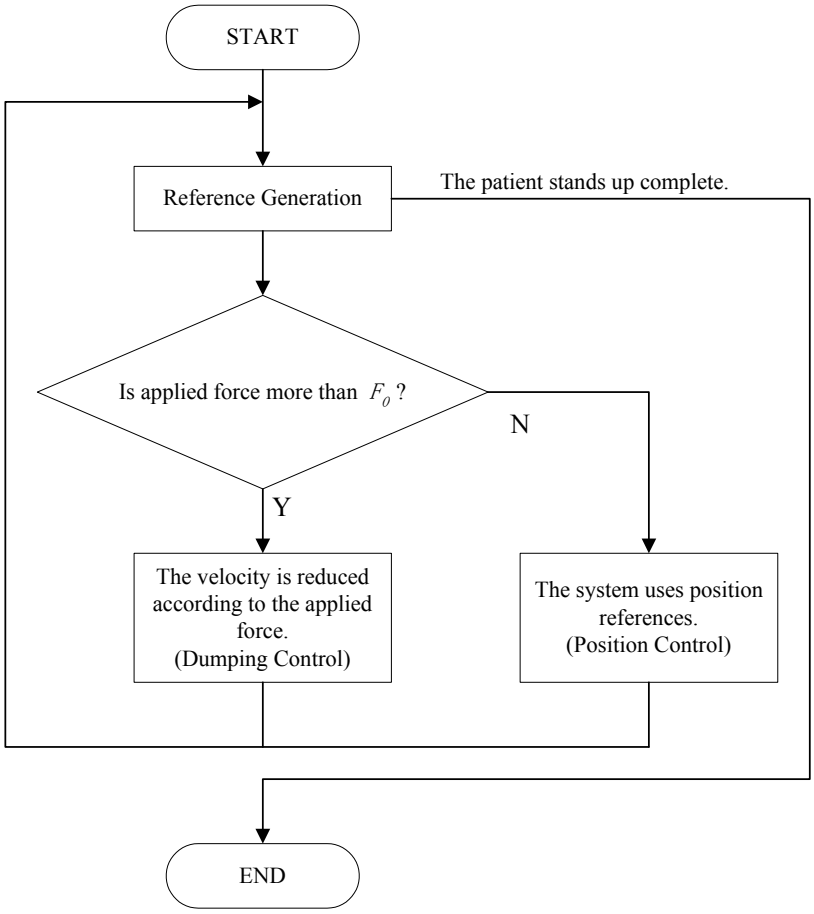

Fig. 10. Flow chart of our proposed control scheme.

4.2 Computer Simulation

We verify the performance of our control scheme by the computer simulation. In this experiment, the human model stands up with Kamiya motion as shown in Fig.6(b). For verifying the performance of our proposed control scheme, we experiment the following mode.

- Position control mode: The system uses only position control. ($B = 0, K = 0.2$)
- Proposed assistance 1: The system uses our proposed control scheme. (Position control mode: $B = 0, K = 0.2$, Force control mode: $B = 0.2, K = 0$)
- Proposed assistance 2: The system uses our proposed control scheme. In this mode, we set strong force control than in case of proposed assistance 1. (Position control mode: $B = 0, K = 0.2$, Force control mode: $B = 0.35, K = 0$)
- Force control mode: The system uses only force control mode. ($B = 0.35, K = 0$)

We use the control references as shown in Fig.8 which is derived from standing up motion with Kamiya scheme in previous section. The simulation parameters are chosen from Table 1. The coordination is defined in Fig.7. To prevent changing the control mode too frequently, we set the threshold as Fig.11. These values are derived experimentally.

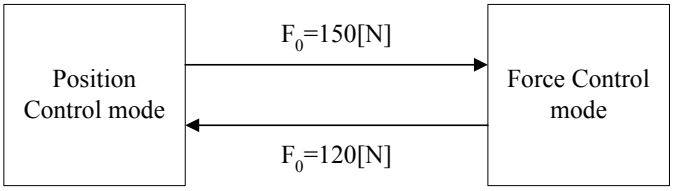

Fig. 11. Threshold.

Fig.12, Fig.13, Fig.14 and Table 2 show the simulation results. Fig.12 is standing up motion using our proposed assistance control. Allows in Fig.12 show the applied assistance force to the patient. The pad applies the force vertically to his body and the arm holder applies the force to his hand. Using our proposed control scheme, we verified that our assistance system realizes the natural standing up motion.

Fig.13 shows the applied force during standing up. During about 25 to 65[%] movement pattern, the force is larger than the threshold and force control mode is selected at our proposed assistance 1 and 2.

Fig.14 shows the output power of each joint. Force control reduces the output power of the patient comparing with the position control. From these results, we can verify that our proposed assistance uses force control mode during only 25 to 65[%] movement pattern (in third phase) and at other time, it uses position control. Our proposes assistance 2 is utilized stronger force control than in case of assistance 1, therefore, the output power of the patient at assistance 2 is less than assistance 1. Using our proposed assistance, system reduces maximum output of the patient into about 0.5[Nm/kg].

On the other hand, Table 2 shows the required workload of the patient for standing up motion. From these results, using our proposed assistance 1, the patients are required about 92[%] workloads for standing up motion comparing with no force assistance. Using force control, the patient uses only 73.1[%] workloads for the standing up motion. Therefore, this means our assistance system can use more part of his remaining strength.

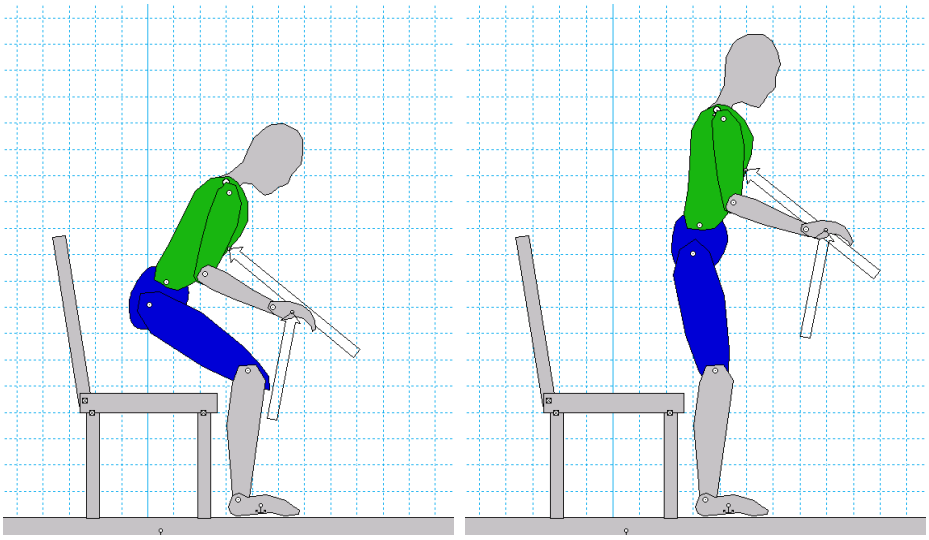

(a) (b)

Fig. 12. Simulation result. Allows show the assistance forces. (Proposed assistance 1)

	Position	Assist1	Assist2	Force
Trunk	29.00	26.75 (92.2%)	24.74 (85.3%)	21.20 (73.1%)
Knee	39.28	35.27 (89.8%)	31.86 (81.1%)	28.70 (73.1%)
Ankle	30.90	28.84 (93.3%)	25.81 (83.5%)	22.60 (73.1%)
Total	99.18	90.86 (91.6%)	82.41 (83.1%)	72.50 (73.1%)

* Values in parentheses are the ratio comparing with the position mode.

Table 2. Workload for standing up. (Ws)

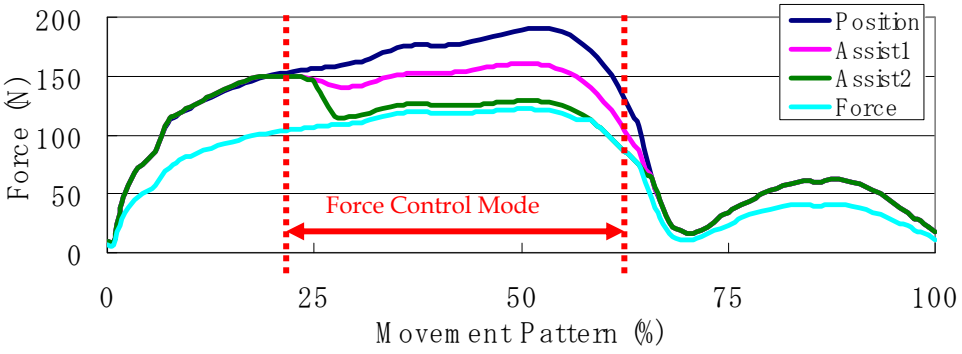

Fig. 13. Applied force.

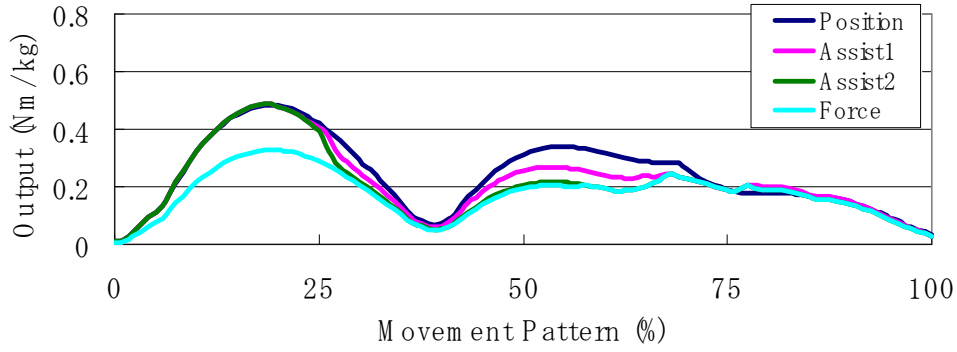

(a) Trunk

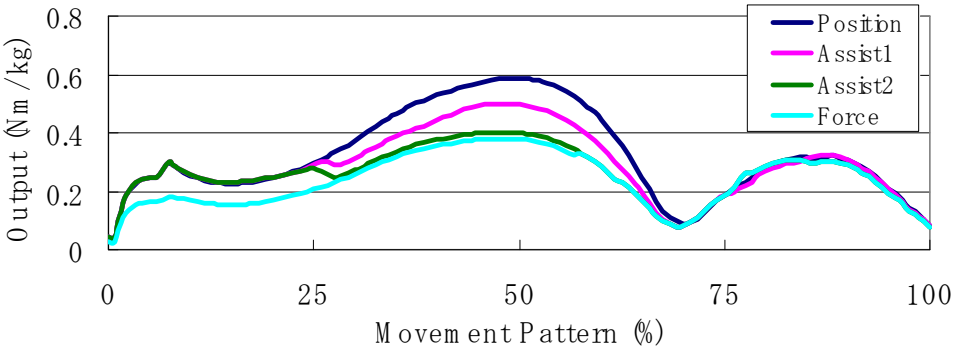

(b) Knee

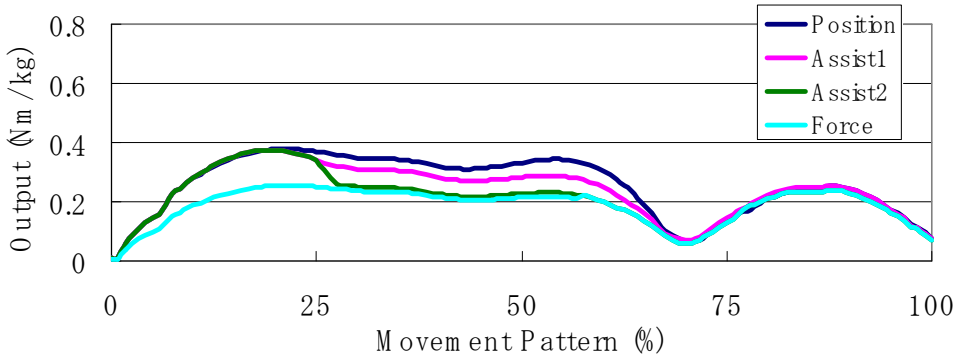

(c) Ankle

Fig. 14. Output force of each joint.

4.3 Experiments

Here, we verify the performance of our prototype system by the experiment. In this experiment, our prototype system assists the patient with our proposed control scheme. For verifying the performance of our proposed control scheme, we experiment the position mode ($B = 0$, always), our proposed mode (In position mode, $B = 0$. In force mode, $B = 0.3$.) and force control mode ($B = 0.3$, always). In order to verify the efficiency of force control clearly, the coefficient k is fixed to zero.

As the result of the experiment, our system can assist the patient as shown in Fig. 15. The height of the patient is 170[cm] and the system lifts him at 14[sec](Position control mode), 17[sec](Our proposed mode) and 23[sec](Force control mode). Our assistance system realizes the natural standing-up motion by nursing specialist.

Fig. 15. Standing up motion with our system. (Our proposed scheme) The tester uses wearing equipment for the experience of the elderly (Takeda et al., 2001).

Fig. 16 shows the control reference and actually position and inclination of the support pad. Fig. 17 shows the applied force to the support pad. During 25 to 65[%] movement pattern (in third phase), system reduces the velocity of standing motion, therefore, the patient can use

won physical strength easily and the applied force to the pad reduces. From these results, we can verify that force control mode works efficiency during 25 to 65[%] movement pattern (in third phase). Furthermore, we can verify that our proposed control scheme switches position control mode and force control mode during motion.

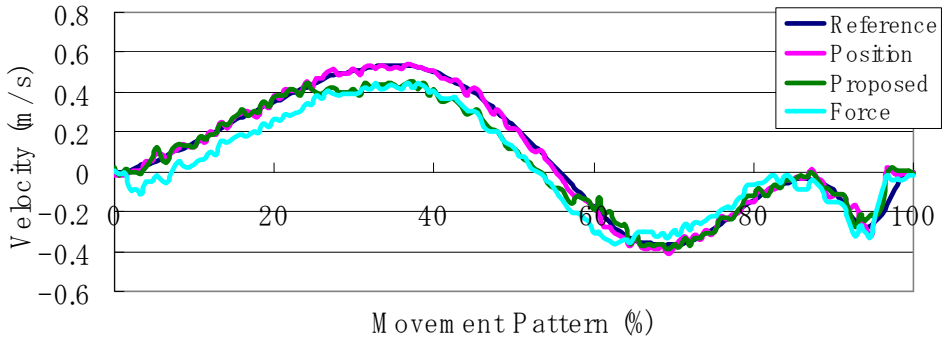

(a) Position (X-direction)

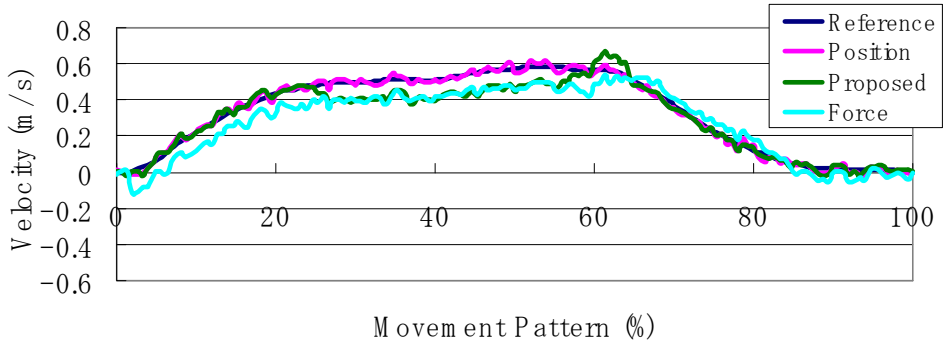

(b) Position (Y-direction)

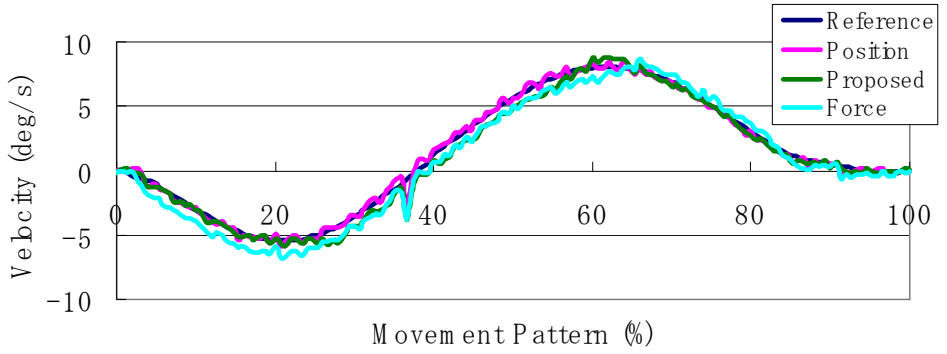

(c) Inclination

Fig. 16. Experimental result.

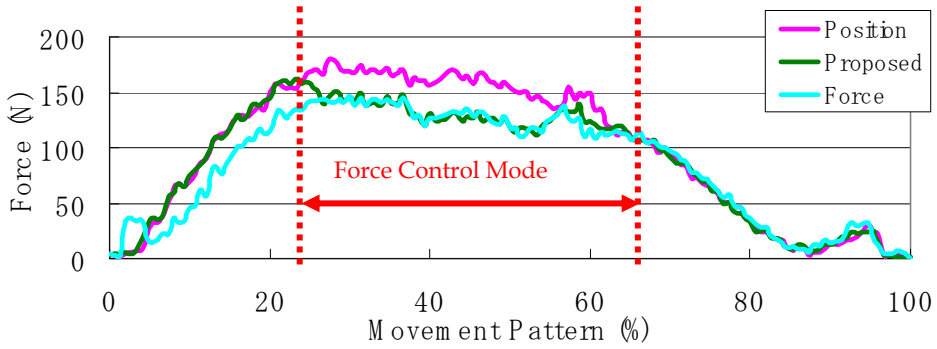

Fig. 17. Applied force.

Fig. 18 shows power output of each actuator during standing assistance. Force assistance mode requires high output comparing with position mode. Total required power of the assistance system and the patient for once standing up motion is constant, therefore, we can evaluate that the load of the patient reduces in force assistance mode. Our proposed assistance mode requires high output during 25 to 65[%] movement pattern and this means our system selects force control and the load of the patient reduces during this period.
Table 3 shows the workload of our system for standing assistance. Force mode requires 147[%] workloads comparing with position mode. On the other hand, our proposed assistance mode requires only 112[%] workloads and this means the patient are required to use more own physical strength.
From these results, our proposed assistance scheme reduces the load of the patient in third phase and uses the physical strength of the patient at a whole assistance motion.

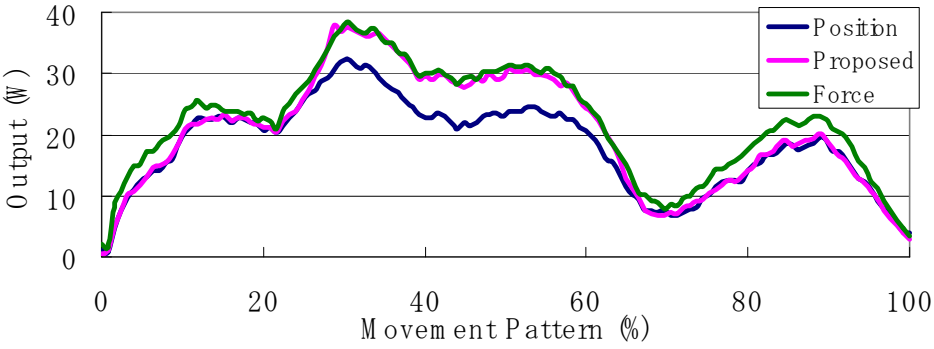

(a) Actuator 1

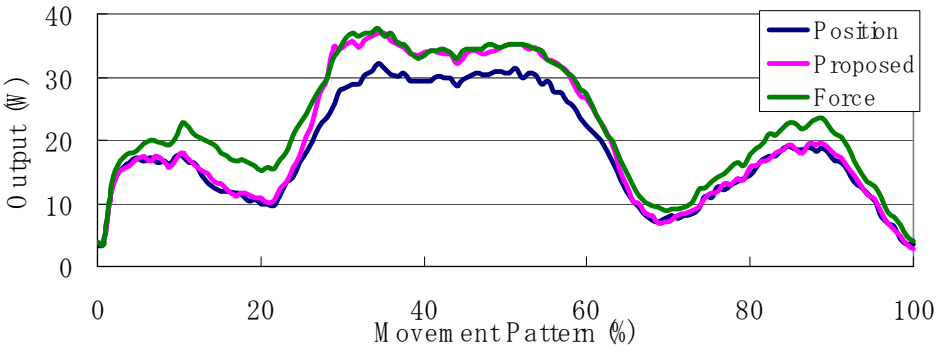

(b) Actuator 2

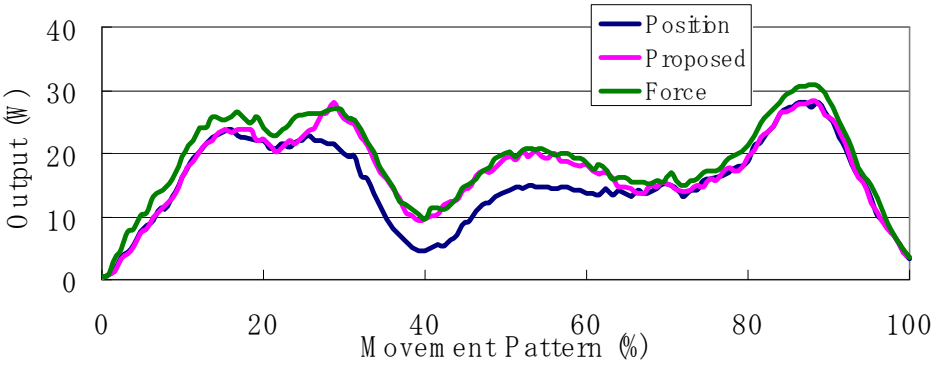

(c) Actuator 3

Fig. 18. Traction output of the assistance system.

	Position	Proposed	Force
Actuator1	68.7	77.7 (113.1%)	100.3 (146.0%)
Actuator2	69.2	76.5 (110.5%)	100.8 (145.7%)
Actuator3	57.5	65.3 (113.6%)	85.2 (148.2%)
Total	195.4	219.5 (112.3%)	286.3 (146.5%)

* Values in parentheses are the ratio comparing with the position mode.

Table 3. Workload of our system (Ws)

7. Conclusion

In this paper, we develop the novel assistance system for the standing up motion. Our system focuses on family use and our system is required to assist the elderly person using part of their remaining strength, in order not to reduce muscular strength.

In order to fulfill this condition, we propose new assistance manipulator mechanism with parallel linkages. Our developed mechanism enables the assistance system to be rigid and compact with low costs.
Furthermore, we design the novel control scheme which combines the dumping and the position control. According to the posture of the patient during standing up motion, our control system can select more appropriate control method from them. Using our assistance system, the load of the patient reduces in third phase, which applies the heaviest load during the motion generally. At the same time, our system requires the patient to use own more physical strength comparing with physical strength without the force assistance. This means our assistance system realizes both reducing the load of the patient and using a part of remaining strength of the patient in order not to reduce muscular strength.

6. Acknowledgement

This work is supported in part by Electro-Mechanic Technology Advancing Foundation.

7. References

Statistics Bureau, Ministry of Internal Affairs and Communications, Japan. (2008). Current Population Estimates as of October 1, 2008, http://www.stat.go.jp/english/data/jinsui/2008np/index.htm

Ministry of Health, Labour and Welfare, Japan. (2001). Annual Reports on Health and Welfare 2001 Social Security and National Life, http://www.mhlw.go.jp/toukei/saikin/ hw/k-tyosa/k-tyosa01/4-3.html

Alexander, N. B.; Schultz, A. B. & Warwick, D. N. (1991). Rising From a Chair: Effects of Age and Functional Ability on Performance Biomechanics. *J. of Geometry: MEDICAL SCIENCES,* Vol.46, No.3, pp.91-98

Hughes, M. A. & Schenkman, M. L. (1996). Chair rise strategy in the functionally impaired elderly. *J. of Rehabilitation Research and Development,* Vol.33, No.4, pp.409-412.

Hirvensalo, M.; Rantanen, T. & Heikkinen, E. (2000). Mobility difficulties and physical activity as predictors of morality and loss of independence in the community-living older population. *J. of the American Geriatric Society,* Vol.48, pp.493-498

Nagai, K.; Nakanishi, I. & Hanabusa, H. (2003). Assistance of self-transfer of patients using a power-assisting device. *Proc. of the IEEE Int. Conf. on Robotics and Automation,* Taipei, Taiwan, September 2003, pp.4008-4015.

Funakubo, A.; Tanishiro, H. & Fukui, Y. (2001). Power Assist System for Transfer Aid. *J. of the Society of Instrument and Control Engineers,* Vol.40, No.5, pp.391-395

Chuv, O.; Hirata, Y.; Wang, Z. & kosuge, K. (2006). Approach in Assisting a Sit-to-Stand Movement Using Robotic Walking Support System. *Proc. of the IEEE Int. Conf. on Intelligent Robots and Systems,* Beijing, China, October 2006, pp.4343-4348

Chugo, D.; Okada, E.; Kawabata, K.; Kaetsu, H.; Asama, H.; Miyake, N. & Kosuge, K. (2006). Force Assistance Control for Standing-Up Motion. *Proc. of the IEEE/RAS-EMBS Int. Conf. on Biomedical Robotics and Biomechatoronics,* Pisa, Italy, February 2006, F132

Chugo, D. & Takase, K. (2008). Walker System with Assistance Device for Standing-Up. *Proc. of JSME Conf. on Bio Mechanics,* AIST, Tsukuba, Japan, September 2008, pp.44-47

Kamiya, K. (2005). Development and evaluation of life support technology in nursing. *Proc. of Proc. of 7th RACE Symp., Research into Intelligent Artifacts for the Generalization of Engineering,* The Univ. of Tokyo, Tokyo, Japan, January 2005, pp.116-121

Maki, B. E.; Holliday, P. J. & Topper, A. K. (1991). Fear of falling and postural performance in the elderly. *J. of Gerontology,* Vol.46, No.4, pp.123-131

Nuzik, S.; Lamb, R.; Vansant, A. & Hirt, S. (1986). Sit-to-Stand Movement Pattern, A kinematic Study. *Physical Therapy,* Vol.66, No.11, pp.1708-1713

Digital Human Research Center, AIST. Human Body Properties Database. http://www.dh.aist.go.jp/bodyDB/index-e.html

Okada, H.; Ae, M.; Fujii, N. & Morioka, Y. (1996). Body Segment Inertia Properties of Japanese Elderly. *Biomechanisms,* No.13, pp.125-139

Omori, K.; Yamazaki, Y.; Yokohama, H.; Aoki, U.; Kasahara, M. & Hiraki, K. (2001). The relationship between strength in the lower extremity and the ability to stand up from a chair in elderly inpatients. *Sogo Rehabilitation,* Vol.30, No.2, pp.167-171

Schenkman, M.; Berger, R. A.; Riley, P. O.; Mann, R. W. & Hodge, W. A. (1990). Whole-Body Movements During Rising to Standing from Sitting. *Physical Therapy,* Vol.70, No.10, pp.638-648

Sugihara, T.; Kawabata, K.; Kaetsu, H.; Asama, H.; Kosuge, K. & Mishima, T. (2004). Development of a Reasonable Force Sensor for a Standing-up and Sitting Motion Support System, *Proc. of Robotics and Mechatronics Conf. 2004,* Nagoya, Japan, June 2004, 1P1-H-11.

Takeda, K.; Kanemitsu, Y. & Futoyu, Y. (2001). Understanding the Problem of the Elderly through a Simulation Experience – Difference in the Effect between Before and After Clinical Practice, *Kawasaki Medical Welfare J.,* Vol.11, No.1, pp.64-73

8

Lower Extremity Joint Moments during Squat and Stoop Lifting

Seonhong Hwang[1], Youngeun Kim[2] and Youngho Kim[1,3]
[1]*Department of Biomedical Engineering, Yonsei University, South Korea*
[2]*Department of Mechanical Engineering, Dankook University, South Korea*
[3] *Institute of Medical Engineering of Yonsei University, South Korea*

1. Introduction

Low back pain(LBP) is a prevalent problem which causes human suffering and cost for workers and their employers. 60~80% of the adult population have experiences of LBP at least once in their lifetimes(Campbell et al., 2005; Stuart McGill, 2002; Koopman et al., 2004). Despite improved working conditions, including progress due to automation, many objects in the industry are still handled manually. Among basic manual material handling (MMH) activities, lifting has most frequently been associated with LBP(Hsiang et al., 1997). Recently, there have been many researches about lifting such as three-dimensional motion analyses, musculoskeletal simulations and medical imaging studies. The most commonly advised lifting technique is the squat technique, in which the knees are flexed(Garg and Moore, 1992). It can easily be understood that compliance with this advice is often low, given the high energetic cost of this technique(Garg and Herrin, 1979; Welbergen et al., 1991; Duplessis et al., 1998). Van Dieen et al. (1997) conducted a comprehensive review on 27 biomechanical studies, comparing stoop and squat techniques, and concluded that no justification existed for advocating squat technique. Jager and Luttman(1989) used a three-dimensional dynamic model to estimate lumbar compression and found that compression was barely influenced by lumbar curvature. By observations of physiologic, psychologic, biomechanical and clinical evidence on three lifting techniques; squat, semi-squat, and stoop, Leon Straker(2003) reported that all those lifting techniques had both advantages and disadvantages depending on circumstances. These recent studies have shown that many variables exist depending on different lifting methods.
In this study, lumbar, hip, knee, and ankle joint motions and lumbar spine curvatures during squat and stoop lifting of three different weights were analyzed using the 3-D motion analysis to find out the function of lower limb motions contributing to the lumbar joint.

2. Methods

Twenty-six young male volunteers who had no problems in both lifting and walking were selected as the subjects in this study (Table 1).Two forceplates(Kistler Instrumente AG,

Switzerland) and a surface EMG system(MA 300, Motion Lab Systems Inc., USA) were synchronized with the 3D motion analysis system(VICON Motion System Ltd., UK). A total of 31 reflective markers were attached on the anatomical locations according to the VICON Plug-in-Gait marker placement protocol. Besides that, additional four markers(V1~V4) were mounted on the back along the spinous processes to define the spinal curvature. The boxes(34×34×27.5cm) weighed 5, 10 and 15kg, and had the same sized handles. Subjects were asked to lift those boxes using two different techniques (squat and stoop) in their comfortable speed. Joint moments and joint powers in the lower extremities were calculated using the inverse dynamics and the support moment was also determined as the summation of all lower extremity joint moments[15]. Paired t-test was used to determine the statistical difference of the maximum lumbar joint moments between the squat and stoop liftings. The Kruskal-Wallis test was used to compare the joint angles and moments with respect to the increase of weights when the lumbar lordosis appears.

	Mean ± S.D			range
Age (year)	23.5	±	0.76	22 ~ 24
Weight (㎏)	66.5	±	6.37	55.6 ~ 74.5
Height (㎝)	172.1	±	6.03	163.4 ~ 183.5

Table 1. Subject information (N=26)

3. Results

3.1 Joint angles

The subjects lifted the objects as their own comfortable speed and the mean speeds were 0.59m/s(±0.14) in squat lifting and 0.60m/s(±0.10) in stoop lifting. Figure 1 represents the lower extremity joint angles on the sagittal plane during lifting. Though different weights were lifted, significant differences were not found in the range of motions(ROMs). However, between two techniques, ROMs for the same joints showed significant difference. The knee joint ROM showed the largest difference between two techniques(Fig. 1).

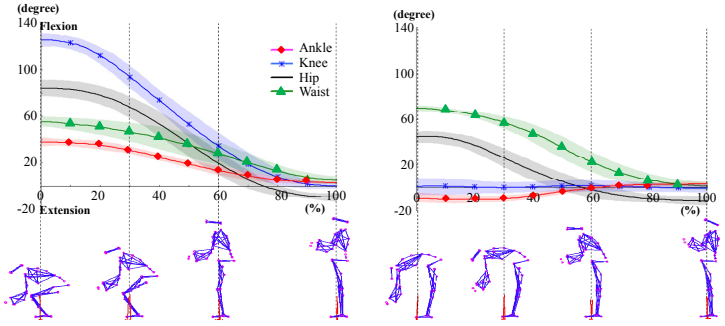

(a) : squat lifting (b) : stoop lifting

Fig. 1. Joint angles of lower extremities during lifting

3.2 Joint moments

Joint moments for the different object weights during squat and stoop lifting were plotted in Fig. 2. The ankle joint moment was larger in the squat lifting than in the stoop lifting. Only the knee flexion moment existed during the whole process of the stoop lifting. However, in the squat lifting, the knee joint moment changed from extension to the flexion moment, and this turn-over occurred earlier as the object weight increased. The hip extension moment increased to its maximum value as soon as lifting started, and then it decreased to nearly zero. For all weights, the maximum hip extension moment in the stoop lifting was always larger than that in squat. The differences of the maximum lumbar extension moments between the squat and stoop were negligible at 5 and 10kg. Rather, it was larger in squat than in stoop when 15kg was lifted ($p<0.05$).

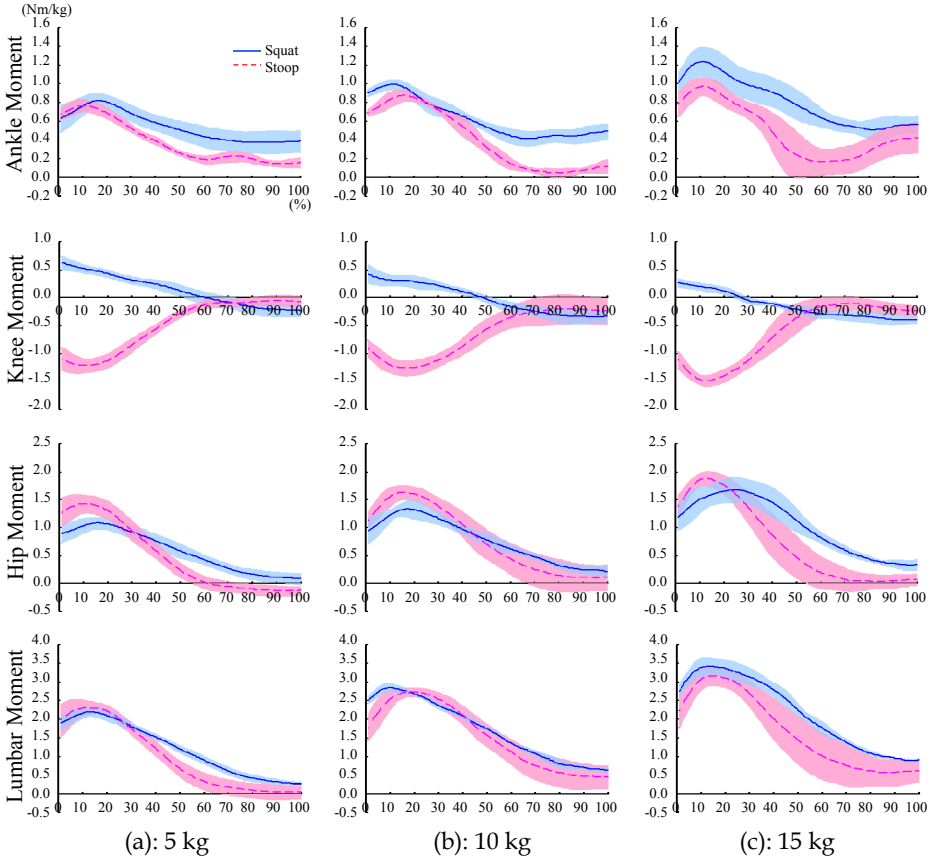

Fig. 2. Joint moments during squat and stoop lifting

3.3 Support moments

Lower extremity joint moment could be analyzed with the concept of 'support moment'(Winter, 1980). Figure 3 shows that the contributions of each lower extremity joint for the support moment in two different lifting techniques. The dashed line in the figure represents the total support moment during lifting, and the height between two curves at any time represents the contribution to the support moment of that joint. At the initial stage of lifting, the hip and ankle joint extension moments were large during the squat lifting. On the other hand, during stoop lifting (the knee joint ROM was nearly zero), there were large knee flexion moments at the initial stage of lifting. Total support moments were larger in squat than in stoop because of the negative values of the knee moment in stoop lifting. Therefore, hip and ankle contributed to the most part of the support moment during squat lifting, and the knee flexion moment played an important role in the stoop lifting.

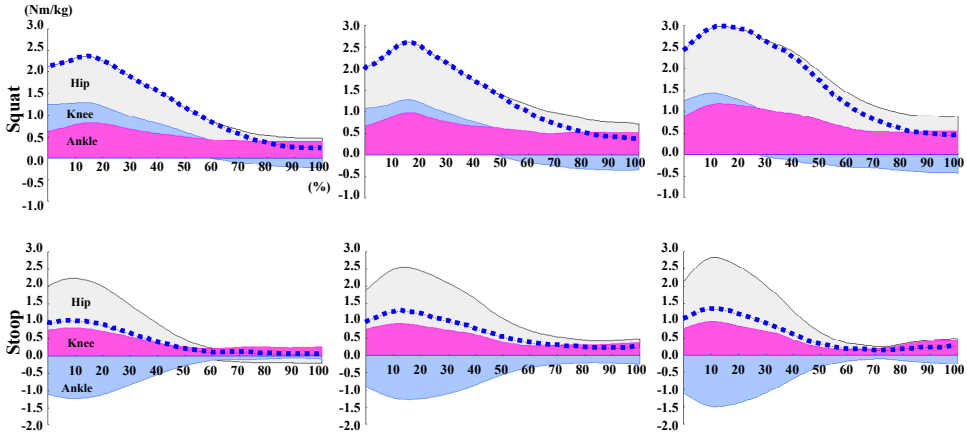

(a): 5 kg (b): 10 kg (c): 15 kg

Fig. 3. Support moments during squat and stoop lifting

3.4 Dynamic EMG

Biceps femoris and rectus femoris showed large variances of activation during the squat lifting. Tibialis anterior, medial gastrocnemius, and biceps femoris showed large variances of activation during the stoop lifting (Fig. 4). Rectus abdominis and lumbar erector spinae had not significant differences between the squat and stoop lifting.

Co-contraction of the bi-articular knee antagonists (rectus femoris and biceps femoris) were observed markedly during the squat lifting. The concentric contraction of the tibialis anterior and the simultaneous eccentric contraction of the gastrocnemius during the stoop lifting also observed in the ankle joint.

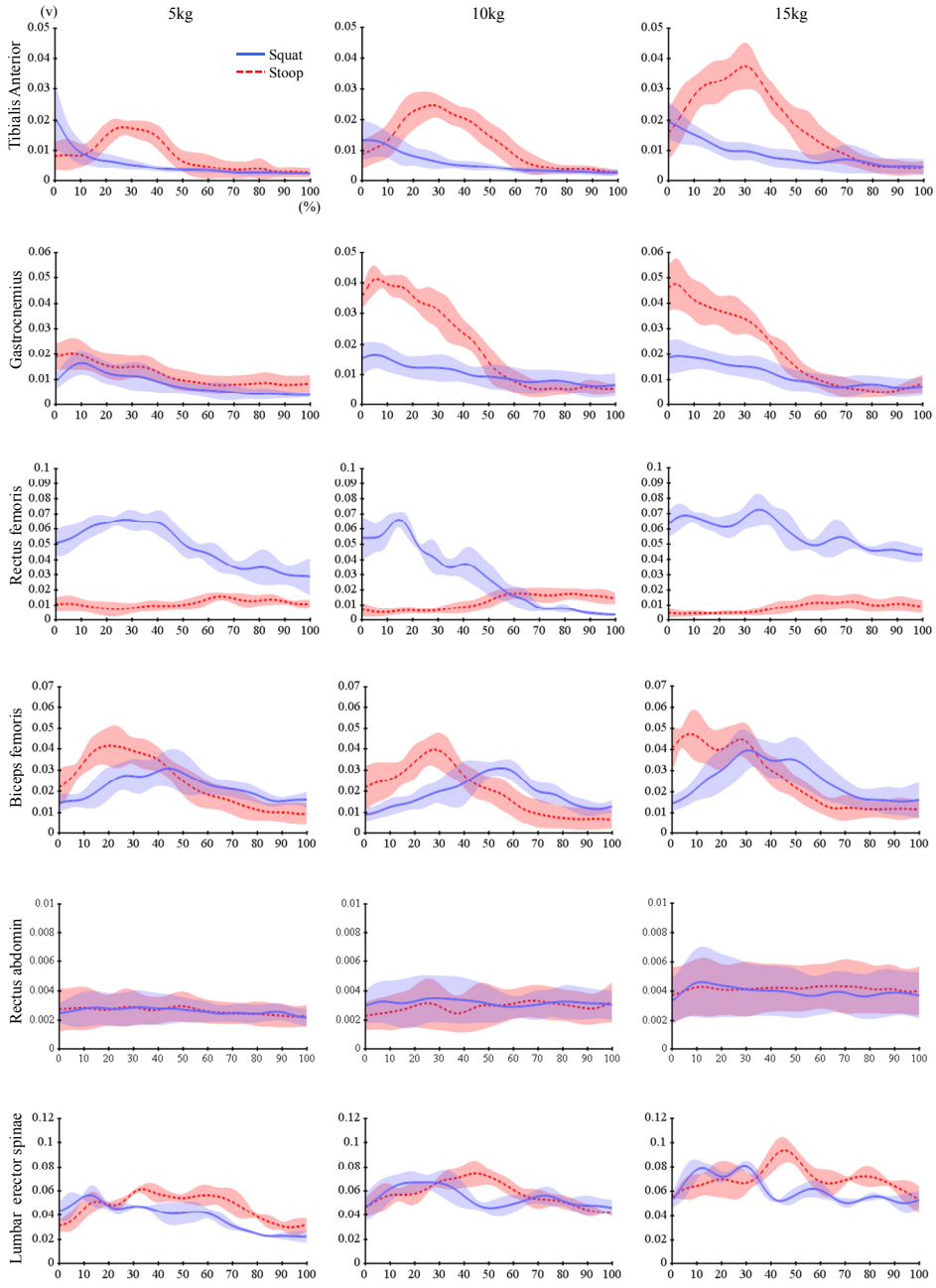

(a): 5 kg (b): 10 kg (c): 15 kg

Fig. 4. Dynamic EMG during squat and stoop lifting

3.5 Lumbar curvature

Fig. 5 represents the spine curvature when the lumbar lordosis appeared. Lumbar curvature was changed from the kyphosis to the lordosis about 50% in the squat lifting, and 60% in the stoop lifting regardless of weights. Lower limb joint angles and moments at that time were showed at Table 2, and its difference among the three different object weights were tested by the nonparametric central tendency test in the three groups (5, 10, 15kg). The knee angle, the ankle angle, the lumbar moment had significant differences as the weight increased in the squat lifting. The lumbar angle, the lumbar moment and the hip moment had significant differences as the weight increased ($p<0.05$) in the stoop lifting. Table 3 shows the correlation coefficients between the "lumbar" and the "lower extremities", comparative parameters were the angles and moments. The knee angle in the squat, the hip and ankle angles in the stoop showed strong correlation with the lumbar angle. All three joint moments(hip, knee, ankle) showed the correlations with the lumbar moment in the squat lifting, however only the hip moment had the correlation with the lumbar moment in the stoop lifting($p<0.01$).

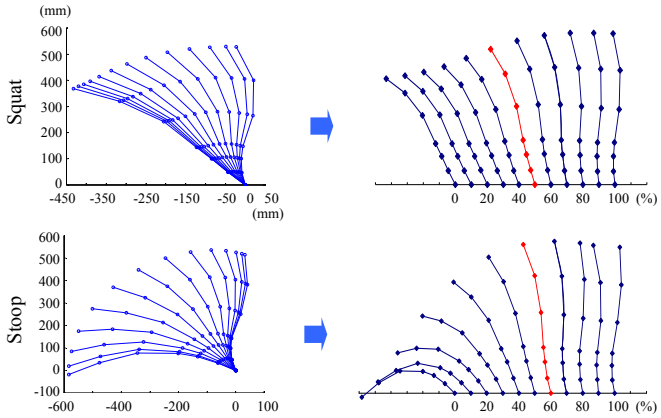

Fig. 5. Lumbar spine curvatures during squat and stoop lifting

4. Discussion

Without limitation of the assumption of biomechanical model used for calculation of kinematic and kinetic results, the limitations of this study were summarized as follows. We just analyzed the representative two lifting techniques on the assumption that they were symmetrical movements. In addition, the movements in the coronal/horizontal plane were not included in this study. Under the in-vitro examination, it was inevitable to keep the subject's motion under control - initial foot position, upper extremity position, knee flexion angle(semi-squat during squat lifting). The objects were not placed close enough to the body because the reflective markers could be hidden. In fact, lumbar could be often damaged mechanically due to the asymmetric or unbalanced lifting movement.

The heavy weight of object is also critical factor to the lumbar damage but 15kg was assumed as heavy weight in this study for the safety of the subjects.

The result of the maximum lumbar joint moment comparison between the squat and stoop lifting corresponded to the previous study that there was no conclusive evidence for advocating the squat lifting(van Dieen, 1999).
The support moment calculated by the summation of the extension moments in the previous study(Grag and Herrin, 1979) however all moments including flexion moments were summated for support moment in this study because the knee flexors could act as supporters.
It was expected that the joint moment results could be supported by the EMG results. However, the normalized EMG data had large variation among subjects and a lot of data excluded for analysis because of its failure of detection therefore we were focused on the activation patterns to interpret EMG data.
The lumbar lordosis appearance time was important during the lifting motion(Mitnitski et al., 1998; McGill et al., 2000; Gracovetsky, 1986; Dolan and Adams, 1993), thus we tried to find out the contributions of the lower extremities in relation to the lumbar joint.
The correlation coefficients between the lumbar and the lower extremity were investigated which were calculated by using the angles and moments at the time of lumbar lordosis appearance. The knee angle had the strong correlation with the lumbar angle in the squat lifting, and the hip and ankle angle had the correlation with the lumbar angle in the stoop lifting. These results showed representative kinematic characteristics of each lifting technique. All three lower extremity joint moments had the correlation with the lumbar joint in the squat lifting, and only the hip joint moment had the correlation with the lumbar joint in the stoop lifting.
There are three important bi-articular muscles in the lower body (rectus femoris, biceps femoris, gastrocnemius), and they affects two joints simultaneously(Doorenbosch et al., 1994; McGinity et al., 2000; Escamilla et al., 1998; Zajac et al., 2003).
In addition, the squat lifting as well as the stoop lifting is the typical closed kinetic chain motion(McGinity et al., 2000; Escamilla et al., 1998) so that the bi-articular muscle function is more complex(Lombard paradox(Lombard, 1903, 1907)). The EMG analysis and the calculation of individual muscle force change using simulation software could be helpful to determine these bi-articular muscle functions.

5. Conclusions

1) There were not significant differences in maximum lumbar joint moments between two techniques. Rather, the maximum lumbar extension moment was larger in squat than in stoop when 15kg was lifted($p < 0.05$). This result advocates the previous study.
2) The hip and ankle joint contributed to the most part of the support moment during the squat lifting, and the knee flexion moment played an important role in the stoop lifting.
3) The ankle, hip and lumbar joints generated power and only the knee joint absorbed power in the squat lifting. The ankle and knee joints absorbed power and the hip and lumbar joints generated power in the stoop lifting.
4) The EMG results summarized that the co-contraction of the antagonists was observed markedly in the both lifting techniques; the tibialis anterior and the gastrocnemius in the ankle joint, the rectus femoris and the biceps femoris in the knee joint.

5) At the time of lordotic curvature appearance in the squat lifting, strong correlations were found in all three lower extremity joint moments with the lumbar joint. On the other hand, in the stoop lifting, strong correlations existed in the hip moment with the lumbar joint.
In conclusion, considering the correlation with the lumbar joint, the kinetic factors generated by the ankle and hip joints (the extensor moment and the power generation) mostly lead the knee extension which is the remarkable kinematics in the squat lifting. The lumbar joint's kinematics (ROM) was the largest in stoop lifting. However, this movement couldn't be done safely without the knee joint's kinetic factors (the flexor moment, the antagonistic co-contraction of bi-articular muscles and the power absorption).

6. References

Campbell, C. & Muncer S.J. (2005). *Social Science and Medicine*, Vol. 60, No. 2, 409~419, ISSN 0277-9536

Stuart McGill. (2002). *Low back disorders: Evidence-based prevention and rehabilitation*. Human Kinetics, ISBN 0-7360-4241-5, Canada.

Koopman, F. S.; Edelaar, M.; Slikker, R.; Reynders, K.; van der Woude L. H. V. & Marco H. J. M. (2004). *American Journal of Physical Medicine & Rehabilitation*, Vol. 83, No. 2, 94-103, ISSN 0894-9115.

Chen, Y. L. (2000). *International Journal of Industrial Ergonomics*, Vol. 25, 611-619, ISSN 0169-8141.

Burgess-Limerick, R.; Shemmell, J.; Barry, B. K.; Carson, R. G. & Abernethy, B. (2001). *Human Movement Science*, Vol. 20, No.4-5, 549-562, ISSN 0167-9457.

Hsiang, S. M.; Brogmus, G. E.& Courtney, T. K. (1997). *International Journal of Industrial Ergonomics,* Vol. 19, 59-74, ISSN 0169-8141.

van Dieen J. H.; Marco, H.J.M. & Toussaint, H. M. (1999). *Clinical Biomechanics*, Vol. 14, 685-696, ISSN 0268-0033.

Jager, M. & Luttman, A. (1989). *Ergonomics,* Vol. 32, No. 1, 93-112, ISSN 0014-0139.

Straker L. (2003). *International Journal of Industrial Ergonomics,* Vol. 31, No. 3, 149-160, ISSN 0169-8141

Burgess-Limerick, R. (2003). *International Journal of Industrial Ergonomics,* Vol. 31, No.3, 143-148.

Garg, A. & Moore, J. S. (1992). *Occupational Medicine*, Vol. 7, No. 4, 629-640, ISSN 0885-114X.

Garg, A. & Herrin, G. D. (1979). *American Institute of Industrial Engineers transactions*, Vol. 11, 293-302, ISSN 0569-5554.

Welbergen, E.; Kemper, H. C. G.; Knibbe, J. J. & Toussaint, H. M. Clijssen, L. (1991). *Ergonomics*, Vol. 34, 613-24, ISSN 0014-0139.

Duplessis, D. H.; Greenway, E. H.; Keene, K. L.; Lee, I. E.; Clayton, R. L. & Metzler, T. (1998). *Ergonomics*, Vol. 41, No. 6, 790-797, ISSN 0014-0139.

Winter, D. A. (1980). *Journal of Biomechanics*, Vol. 13, 923–927, ISSN 0021-9290.

Hof, A. L. (2000). *Gait & Posture*, Vol. 12, 196-199, ISSN 0966-6362.

Lombard, W. P. (1903). The Action of Two-joint Muscles, *American Physics Education Revoluton*, Vol. 8, 141-145, ISSN.

Lombard, W. P. &. Abbott, F. M. (1907). *American Journal of Physics*, Vol. 20, 1-60, ISSN 0002-9505.

Doorenbosch, C. A. M.; Harlaar, J.; Roebroeck, M. E. & Lankhorst, G. J. (1994). *Journal of Biomechanics*, Vol. 27, 1299-1307, ISSN 0966-6362.

McGinity, G.; Irrgang, J. J. & Pezzullo, D. (2000). *Clinical Biomechanics*, Vol. 15, 160-166, ISSN 0268-0033.

Escamilla, R. F.; Fleisig, G. S.; Zheng, N.; Barrentine, S. W.; Wilk, K. E. & Andrews, J. R. (1998). *Medine& Science in Sports & Exercise*, Vol. 30, 556-569, ISSN 0195-9131.

Zajac, F. E.; Neptune, R. R.; Kautz, S. A. (2003). *Gait & Posture*, Vol. 17, 1-17, ISSN 0966-6362.

Mitnitski, A. B.; Yahia, L. H.; Newman, N. M.; Gracovetsky, S. A. & Feldman, A. G. (1998). *Clinical Biomechanics*, Vol. 13, 121-127, ISSN 0268-0033.

McGill, S. M.; Hughson, R. L. & Parks K. (2000). *Clinical Biomechanics*, Vol. 15, 777-780, ISSN 0268-0033.

Gracovetsky, G. (1986). *Journal of Biomedical Engineering*, Vol. 8, 217-223, ISSN 0141-5425.

Dolan, P. & Adams, M. A. (1993). *Clinical Biomechanics*, Vol. 8, 185-192, ISSN 0268-0033.

Welbergen, E.; Kemper, H. C. G.; Knibbe, J. J.; Toussaint, H. M. & Clijssen, L. (1991). *Ergonomics,* Vol. 34, 613-624, ISSN 0014-0139.

Duplessis, D. H.; Greenway, E. H.; Keene, K. L.; Lee, I. E.; Clayton, R. L. & Metzler, T. (1998). *Ergonomics*, Vol. 41, 790-797, ISSN 0014-0139.

David, A. Winter (2004). *Biomechanics and Motor Control of Human Movement*, John Wiley & Sons, Inc., 3rd edition, ISBN 978-0-471-44989-8.

9

Acetabular loading in rehabilitation

Hana Debevec[1], Aleš Iglič[1], Veronika Kralj-Iglič[1] and Matej Daniel[3]
[1]*Laboratory of Physics, Faculty of Electrical Engineering, University of Ljubljana, Ljubljana, Slovenia*
[2]*Laboratory of Clinical Biophysics, Faculty of Medicine, University of Ljubljana Slovenia*
[3]*Laboratory of Biomechanics, Faculty of Mechanical Engineering, Czech Technical University in Prague, Czech Republic*

1. Introduction

Acetabular fractures are produced by high energy injuries that often cause dislocation of the fragments with gaps and steps (Olson et al., 1997). The goal of operative treatment of such fractures is to restore acetabular anatomy with perfect fragment reduction and stable fixation in order to enable early joint movement (Letournel and Judet, 1993). The fixation of the fragments is not strong enough to allow weight bearing before the bone is healed (Goulet et al., 1994; Olson, 2003) and in some patients even physical therapy with initial passive motion and continued active exercises without weight bearing could lead to dislocation of fragments and early posttraumatic osteoarthritis (Letournel and Judet, 1993).
Early physical therapy of patients with acetabular fractures therefore requires careful selection of exercises in order to prevent excessive loading of the injured acetabular region. Current guidelines for nonoperative management of acetabular fractures and postoperative management of surgical procedures in the acetabular region recommend initial bed rest followed by passive motion in the hip joint. Initial active non-weight-bearing exercises commence a few days after surgery and include active flexion, extension and abduction in the hip in the upright position. The same set of exercises in supine or side-lying abduction is usually postponed until 5-14 days postoperatively. Partial weight-bearing with stepwise progression usually starts 6 weeks postoperatively and full weight bearing is eventually allowed at 10 weeks (Maurer et al., 1997).
Recently, interesting information was obtained by direct measurements of acetabular contact pressures during rehabilitation exercises in subject with pressure-instrumented partial endoprostheses where it was found that acetabular pressures may not follow the predicted rank order corresponding to the commonly prescribed temporal order of rehabilitation activities (Givens-Heiss et al., 1992; Tackson et al., 1997). It has been found that hip stress magnitudes in some non-weight bearing exercises can exceed hip stress in weight bearing exercises or even gait.
Due to technical complexity and invasiveness of direct contact stress distribution measurement, various mathematical models for calculation of the contact stress distribution in the hip joint have been proposed (Brand, 2005; Daniel et al., 2008; Genda et al., 2001; Ipavec et al., 1999; 1995; Legal and Reinicke, 1980; Pedersen et al., 1997). Recently, a mathematical model has been developed that enables computation of the contact stress distribution at any given position of

acetabulum and also allows simulation of different body positions and variations in pelvic morphology. However, such estimation of the contact stress distribution necessarily includes determination of the hip joint reaction force magnitude/direction. Non-invasive determination of the localization of dynamic acetabular loading during gait has so far been performed by inverse Newtonian computations based on kinematic measurements of individual body segments and a muscle model (Delp et al., 1990). For slow rehabilitation exercises the loading in the hip joint at a given leg and/or body position approximates to static biomechanical equilibrium and the hip joint reaction force can then be numerically calculated by using a muscle model and a suitable optimization function without kinematic measurements (Crownishield and Brand, 1981; Pedersen et al., 1997).
It has been shown recently, that the acetabular loading is the highest in unsupported supine abduction (Kristan et al., 2007). However, the abduction may be accompanied with flexion and rotation of the hip as well. The aim of this chapter is to present a model for assessing acetabular loading in non-weight-bearing supine exercises by using a muscle model for computation of the hip joint reaction force and a previously developed mathematical model of contact hip stress distribution. Position of the leg with high acetabular loading will be identified. With this knowledge the range of motion and body position during active exercises can be suggested that would prevent excessive loading of particular acetabular regions and displacement of fracture fragments.

2. Hip joint force computation

2.1 Equilibrium equations

In mathematical modelling, the musculoskeletal system of human body is usually modelled as a system of absolutely stiff segments connected by joints and motion of the segments is realized by the muscles spanning the joints (Nigg and Herzog, 1995; Schneck, 1990; Winters, 2000; Zajac and Winters, 1990). From this point of view, the human body is perceived as a multibody mechanical system controlled by the equations of dynamic equilibrium (Rasmussen et al., 2001).
In the supine abduction, the body could be divided into two segments (Iglič et al., 1990). The first segment is the free leg which performs given exercise and the second segment is the rest of the body. In this position, the leg is loaded by its own weight $\mathbf{W}_L$, by the hip joint reaction force $\mathbf{R}$, and by the force of the muscles $\mathbf{F}$. It is taken that the origin of the hip joint reaction force $\mathbf{R}$ lies in the centre of the femoral head (Yoshida et al., 2006).

$$\mathbf{F} + \mathbf{W}_L - \mathbf{R} = 0 \tag{1}$$

The muscle force $\mathbf{F}$ acting on the free leg is the vector sum of the forces of all the muscles $\mathbf{F}_i$ that are active in the particular body position

$$\mathbf{F} = \sum_i \mathbf{F}_i \tag{2}$$

In the modelled two-segment system, it is taken that rotation of the segments occurs with respect to the axis through the centre of the femoral head. Therefore the centre of the femoral head was chosen for the origin of the coordinate system. In the anatomical position, the x-axes point medially, the y-axes point anteriorly, and the z-axis point superiorly (Fig. 1).
When performing slow exercise, inertial forces can be neglected and moment equilibrium of the free leg with respect to the center of the coordinate system can be written as

$$\mathbf{r}_\mathbf{W} \times (\mathbf{W}_L) + \sum_i \mathbf{r}_i \times \mathbf{F}_i = 0 \tag{3}$$

where $\mathbf{r}_W$ is the radius vector from the centre of rotation (centre of the femoral head) to the centre of gravity of the free leg, $\mathbf{r}_i$ is the radius vector from the center of rotation to the attachment of given muscle at the free leg. The index i runs over all muscles that are active in particular leg position.
The weight of the leg is approximated after Clauser, 1970.

$$W_L = 0.161\, W_B \tag{4}$$

where W_B is the body weight. In supine abduction, the weight of the leg points backward

$$\mathbf{W_L} = [0, -W_L, 0] \tag{5}$$

and position of the center of gravity in neutral position of the leg is approximated as

$$\mathbf{r}_W = [0, 0, -b] \tag{6}$$

where b is the z-coordinate of the center of the gravity of lower leg.
In a static biomechanical analysis, whole muscles are usually represented as single vectors with a certain line of action and force magnitude (Crownishield and Brand, 1981). The line of action of a muscle may be considered to go directly from the origin to the insertion site (Schneck, 1990). We can describe these points by their radius vectors: $\mathbf{r}_i$ for the proximal attachment point and $\mathbf{r}_i{}'$ for the distal attachment point. From the position of the muscle attachment points, the direction of the force of the muscle, given by the unit vector $\mathbf{s}_i$, is calculated.

$$\mathbf{s}_i = \frac{\mathbf{r}_i{}' - \mathbf{r}_i}{|\mathbf{r}_i{}' - \mathbf{r}_i|} \tag{7}$$

The muscle force $\mathbf{F}_i$ can be approximated as (Iglič et al., 1990):

$$\mathbf{F}_i = \sigma_i\, PCSA_i\, \mathbf{s}_i \qquad i = 1, \ldots, 9 \tag{8}$$

where $PCSA_i$ is physiological cross-sectional area of the i-th muscle, σ_i is the average tension in the i-th muscle and $\mathbf{s}_i$ is the unit vector in the direction of the the i-th muscle.

2.2 Muscle model

The musculoskeletal geometry defining positions of proximal and distal muscle attachment points in neutral position and cross-sectional areas of the muscles is based on the work of (Delp et al., 1990). Muscles attached over a large area are divided into separate units. Hence, the model includes 27 effectively active muscles of the hip (Tab. 1).

2.3 Muscle force optimization

If all the muscles were included into equilibrium equations, the number of unknown quantities would be much higher than the number of equations. Mathematically, an infinite number of solutions would satisfy the system of equations. It means, there is more muscles than needed to perform given motion and the problem is referred as the muscle redundancy (Prilutsky and Gregor, 2000; Tsirakos et al., 1997).
It has been suggested that the optimal muscle activation can be found by minimization of the sum of muscle stresses cubed (Crownishield and Brand, 1981; Tsirakos et al., 1997). This optimization criterion is based on the experimentally determined nonlinear dependence between the muscle force and the endurance time of muscle contraction and on the idea that muscles

No	Muscle	No	Muscle
1	adductor brevis	15	gluteusminimus3
2	adductor longus	16	iliacus
3	adductor magnus 1	17	pectineus
4	adductor magnus 2	18	piriformis
5	adductor magnus 3	19	psoas
6	gemelli inf. et sup.	20	quadratus femoris
7	gluteus maximus 1	21	biceps femoris long
8	gluteus maximus 2	22	gracilis
9	gluteus maximus 3	23	sartorius
10	gluteus medius 1	24	semimebranosus
11	gluteus medius 2	25	semitendinosus
12	gluteus medius 3	26	tensor fascie latae
13	gluteus minimus 1	27	rectus femoris
14	gluteus minimus 2		

Table 1. Muscles included in the model of the hip.

are activated in a way that maximizes their endurance time (Brand et al., 1986). The optimization criterion was justified by comparison of the resultant hip force calculation with the experimental measurements using an implanted instrumented endoprosthesis (Brand et al., 1994; Stansfield et al., 2003).
The physiology of muscle requires that the muscle forces are non-compressive and do not exceed their physiological limits (Heller et al., 2001; Tsirakos et al., 1997). Therefore additional inequality constraints were defined which restrict the range of the muscle forces F_i. The maximum allowed muscle force of the i-th muscle is directly proportional to the physiological cross-sectional area (Crownishield et al., 1978) and the maximum allowed tensile stress in the muscle (σ_{max}). In our work the value of 1 MPa was taken for σ_{max} (Crownishield and Brand, 1981; Heller et al., 2001). By taking into account equilibrium of the forces and the moments acting on the pelvis in the rehabilitation exercise (Eq. (3)) and definition of muscle force using a straight-line muscle model (Eq. (8)), the optimisation problem can be defined:

$$\begin{aligned} &\text{minimize} && G = \sum_{i=1}^{N} \sigma_i^3 \\ &\text{subject to} && \mathbf{r_W} \times (\mathbf{W}_L) + \textstyle\sum_i \mathbf{r}_i \times \mathbf{F}_i = 0 \\ & && 0 \le F_i \le \sigma_{max}\, PCSA_i \qquad i = 1, \ldots, N \end{aligned} \tag{9}$$

For solving nonlinear optimisation problems the SOLNP module for MATLAB was used. After minor adjustments of the source code, it was possible to use this module in GNU Octave as well (Eaton, 1997). The SOLNP algorithm solves the general nonlinear optimisation programming problem with an augmented Lagrangian objective function using a combination of linear programming and sequential quadratic programming using Broyden-Fletcher-Goldfarb-Shanno's technique (Ye, 1989). The further description of the algorithms used in the module SOLNP is given in Ye, 1989.

3. Hip joint contact stress distribution – HIPSTRESS model

On the basis of known values of the femoral head radius r, the geometry of the acetabulum given by the Wiberg centre-edge angle ϑ_{CE} and the angle of anteversion ϑ_{AV} (Fig. 2) and the

Fig. 1. Muscles of the hip. Cartesian coordinate system with the origin in the centre of the femoral head, xz-plane coincides with the frontal plane, xy-plane coincides with the transversal plane, x-axis points laterally, y-axis points anteriorly and z-axis points superiorly.

resultant hip force **R**, the peak stress on the weight-bearing surface p_{max} can be computed by using subsequent mathematical model (Iglič et al., 2002; Zupanc et al., 2008). The original model adopts cosine stress distribution derived by (Brinckmann et al., 1981).

3.1 Cosine stress distribution

In deriving model equations, following simplifications concerning the geometry of the hip and the mechanical properties of the articular cartilage were introduced: it is assumed that the femoral head has a spherical shape while the acetabulum forms a hemisphere. The gap between these two rigid spherical surfaces is occupied by a cartilage which is considered to be an ideally elastic material, i.e., it is assumed that it obeys Hooke's law. Upon loading, the femoral head is moved toward the acetabulum and the cartilage is squeezed. Due to the assumed sphericity of the bone surfaces there is only one point where the spherical surfaces of

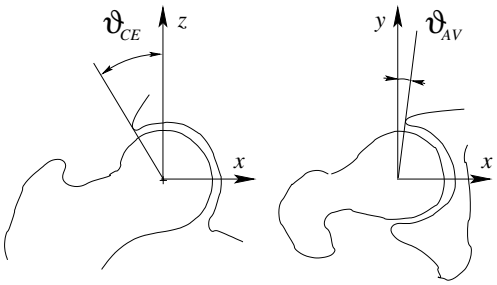

Fig. 2. Position of the acetabular cup is determined by the center-edge angle of Wiberg ϑ_{CE} and angle of anteversion ϑ_{AV}.

the acetabulum and the femur are the closest. This point is called the stress pole (Brinckmann et al., 2002). Since the cartilage completely fills the gap, the deformation of the cartilage is highest at the stress pole. From the sphericity of the bone surfaces it can be derived that the strain in the cartilage layer at any point of the weight bearing area is proportional to the cosine of the angle between this point and the stress pole (Brinckmann et al., 1981; Greenwald and O'Connor, 1971). According to Hooke's law, the contact stress in the cartilage is proportional to the strain in the cartilage, i.e., to the displacement of the femoral head with respect to the acetabulum. The sphericity of the hip surfaces and the ideal cartilage elasticity described above yield the cosine stress distribution function with its maximum at stress pole p_0 (Brinckmann et al., 1981):

$$p = p_0 \cos \nu \tag{10}$$

where ν is the angle between the given point and the stress pole. The area of nonzero contact stress is called the weight bearing area A.

3.2 Equilibrium equations

The stress distribution is described by the position of the stress pole P and value of the stress at it. The sum of the contact stresses over the weight bearing area gives the hip joint reaction force.

$$\int_A p \, \mathrm{d}\mathbf{A} = \mathbf{R} \tag{11}$$

In contrast to the previous work (Ipavec et al., 1999), we present a local coordinate system, which is fixed with respect to the acetabulum instead of global coordinates. The acetabular coordinate system is defined in accordance with Bergmann, 2001. The acetabular coordinate system takes advantage of the symmetry of the acetabular hemisphere.

The hip joint resultant force is calculated in a coordinate system which is fixed with respect to the pelvis. The position of the acetabular cup with respect to the pelvis coordinate system is determined as described in (Bergmann, 2001). The origin of the pelvis Cartesian coordinate system and of the acetabular Cartesian coordinate system coincides with the center of the femoral head. The local coordinate system of the acetabulum is obtained after rotation of the pelvis coordinate system (Bergmann, 2001) for angle β around the x axis and then by angle γ around the z axis (Fig. 3). After the rotation the acetabular xz-plane is identical with the basis of the acetabular hemisphere and the $-y$ axis points to the top of the acetabular shell. After subsequent transformation of coordinate system defined as $x_a = z$, $y_a = z$ and $z_a = -y$, a coordinate system shown in Fig. 4 is obtained. The z_a-axis is the axis of the symmetry of the acetabular hemisphere, y_a-axis points anteriorly and x_a-axis points laterally.

The values of the angles β and γ for a normal hip are computed from position of the acetabulum as:

$$\gamma = \frac{\pi}{2} - \vartheta_{AV} \tag{12}$$

$$\beta = \arctan\left(\frac{\tan(\vartheta_{CE})}{\sin(\gamma)}\right) \tag{13}$$

where ϑ_{CE} is the center-edge angle of Wiberg and ϑ_{AV} is the angle of anteversion defined in Fig. 2.

In the acetabular coordinate system, the hip joint resultant force $\mathbf{R}$ is defined by its magnitude R and by its direction, given by the spherical coordinates $\vartheta_{Ra}, \varphi_{Ra}$. The position of the stress pole is also determined by spherical coordinates Θ_a and Φ_a. The polar angles ϑ_{Ra} and

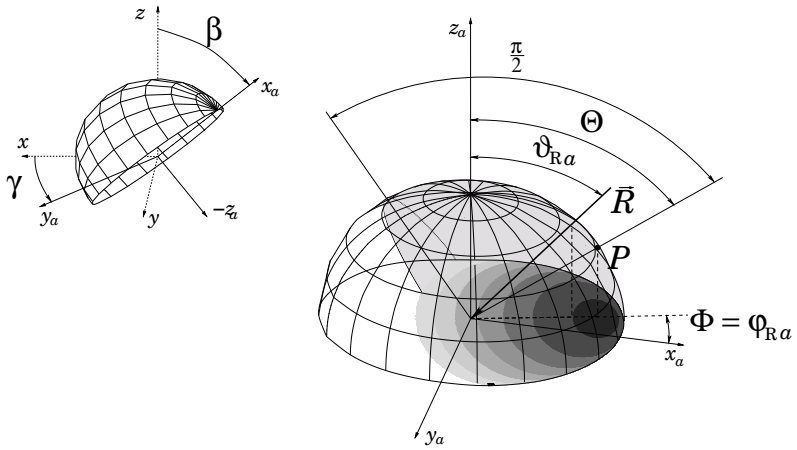

Fig. 3. Position of the acetabular coordinate system (x_a, y_a, z_a) with respect to the pelvic coordinate system (x, y, z) (Bergmann, 2001) (left) and schematic presentation of the acetabular hemisphere and the acetabular coordinate system (right). The weight bearing area is marked by shading, symbol P denotes position of the stress pole (right). The projection of the stress distribution in the xz-plane is also shown.

Θ_a describe the angular displacement from the z_a-axis, while the azimuthal angles φ_{Ra} and Φ_a describe the angular displacement of the pole from the $y = 0$ plane in counterclockwise direction.

Due to the symmetry of the acetabular coordinate system, where the z_a axis is the axis of symmetry of the acetabular shell, angle Φ_a is given by the direction of force φ_{Ra} only as discussed below. Force **R** and the z_a-axis of the acetabular coordinates determine the symmetry plane which divides the acetabular hemisphere into two equal parts. The contact stress distribution should satisfy the condition that integration of p over the area of both halves of the acetabular hemisphere (Fig. 4) gives the resultant hip force (Eq. 11). Since in our model the weight bearing is a part of the acetabular hemisphere, and the stress distribution function (Eq. (10)) is symmetrical with respect to the stress pole, Eq. (11) is fulfilled only in the case if the stress distribution is symmetrical with respect to the plane given by φ_{Ra} and y axis. It means that the stress pole must lie in this symmetry plane defined by R and the y-axis ($\Phi_a = \varphi_{Ra}$).

Using appropriate rotation of the coordinate system around the z_a-axis for angle φ_{Ra} we obtain a new orthogonal coordinate system x'_a, y'_a, z'_a. In the rotated coordinate system the pole of stress P as well as force **R** lie in the $y'_a = 0$ plane. For a force in $y'_a = 0$ plane, method for determination of the position of the stress pole which was developed for the one-leg standing with the force in the frontal plane and acetabulum symmetrical with respect to this plane (Herman et al., 2002; Iglič et al., 1993; 2002) can be used.

In order to solve Eq. (11), the ordinary spherical coordinate system was used in the previous papers (Iglič et al., 1993; Ipavec et al., 1999). Classical spherical coordinates lead to the complex expression for the boundaries of the weight-bearing area. Therefore the corresponding integrals in Eq. (11) are mathematically complicated (Ipavec et al., 1999). If the alternative spherical coordinate system is used the calculation of the integrals in vector Eq. (11) becomes much more simple and transparent (Herman et al., 2002). The alternative spherical coordi-

nates are defined as following:

$$x'_a = r \cos\varphi \sin\vartheta \tag{14}$$
$$y'_a = r \sin\varphi \tag{15}$$
$$z'_a = -r \cos\varphi \cos\vartheta \tag{16}$$

where r is the radius of the articular surface. Angles ϑ and φ are depicted in Fig. 4. In the rotated alternative coordinate system (Fig. 4) force $\mathbf{R}$ and the stress pole will have the spherical coordinates $\varphi'_{Ra} = 0$, $\vartheta'_{Ra} = \vartheta_{Ra}$ and $\Phi'_a = 0$, $\Theta'_a = \Theta_a$, respectively. In the rotated spherical coordinates the angle ν between the radius vector to the stress pole

$$\mathbf{r}_\mathrm{P} = (r \sin\Theta_a, 0, r \cos\Theta_a) \tag{17}$$

and the radius vector to the given point on the articular surface

$$\mathbf{r} = (r \cos\varphi \sin\vartheta, r \sin\varphi, r \cos\varphi \cos\vartheta) \tag{18}$$

can be expressed using the scalar product of $\mathbf{r}_\mathrm{P}$ and $\mathbf{r}$:

$$\cos\nu = \frac{\mathbf{r}\cdot\mathbf{r}_\mathrm{P}}{r^2} = \cos\varphi \cos\vartheta \cos\Theta_a + \cos\varphi \sin\vartheta \sin\Theta_a \tag{19}$$

Then the stress distribution function (Eq. 10) is expressed in the alternative coordinate system with the pole in the $x'_a = 0$ plane, as follows

$$p = p_0 \left(\cos\varphi \cos\vartheta \cos\Theta_a + \cos\varphi \sin\vartheta \sin\Theta_a\right) \tag{20}$$

The elementary infinitesimal integration area in the alternative coordinate system is:

$$\mathrm{d}\mathbf{A} = r^2 \cos\varphi \left(\cos\varphi \sin\vartheta, \sin\varphi, \cos\varphi \cos\vartheta\right) \mathrm{d}\vartheta \, \mathrm{d}\varphi \tag{21}$$

In the new alternative coordinate system, the integration in Eq. (11) can be performed over the fixed boundaries of the weight-bearing area, which considerably simplifies the derivation. The weight bearing area is limited at the lateral border by the acetabular rim ($\vartheta_L = \pi/2$, while the medial border is determined by the curve where the stress vanishes (Eq. 10), i.e., the lateral border consists of points with a constant angular distance $\pi/2$ from the stress pole ($\vartheta_M = \Theta_a - \pi/2$). Since the symmetry plane defined by force $\mathbf{R}$ and the y-axis splits the acetabular hemisphere into two symmetrical parts (Fig. 4), in the new alternative coordinate system angle φ runs from $-\pi/2$ to $\pi/2$ over the whole weight-bearing area.
It follows from Eqs. (20) and (21) that the x'_a and z'_a components of force $\mathbf{R}$ in Eq. (11) can be expressed in the form:

$$R \cos\vartheta_{Ra} = p_0 r^2 \int_{\vartheta_M}^{\vartheta_L} \cos\vartheta \cos(\vartheta - \Theta_a) \, \mathrm{d}\vartheta \int_{-\frac{\pi}{2}}^{\frac{\pi}{2}} p \cos^3\varphi \, \mathrm{d}\varphi \tag{22}$$

$$R \sin\vartheta_{Ra} = p_0 r^2 \int_{\vartheta_M}^{\vartheta_L} \sin\vartheta \cos(\vartheta - \Theta_a) \, \mathrm{d}\vartheta \int_{-\frac{\pi}{2}}^{\frac{\pi}{2}} p \cos^3\varphi \, \mathrm{d}\varphi \tag{23}$$

The integral for the x'_a component of force $\mathbf{R}$ is identically equal to zero due to the symmetry of the rotated coordinate system as discussed above (Fig. 4).

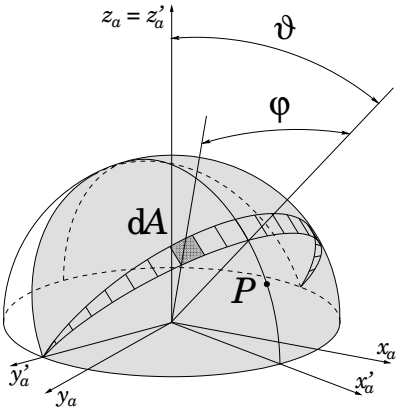

Fig. 4. Rotated acetabular coordinate system (x_a', y_a', z_a') and the alternative spherical coordinate system in the acetabular reference frame. Weight-bearing area is shaded and the elementary area dA is shown. Symbol P denotes the position of the stress pole.

It follows from Eqs. (22) and (23) that the unknown spherical coordinate of the stress pole (Θ_a) can be obtained by solving the nonlinear equation:

$$\tan(\vartheta_{Ra} + \Theta_a) = \frac{\sin^2 \Theta_a}{\pi - \Theta_a + \sin \Theta_a \cos \Theta_a} \tag{24}$$

When the position of the stress pole (Θ_a, Φ_a) is calculated as described above, the value of the stress at the pole is then determined from the expression:

$$p_0 = \frac{3\,R\,\cos(\vartheta_{Ra} + \Theta_a)}{2\,r^2\,(\pi - \Theta_a + \sin \Theta_a \cos \Theta_a)} \tag{25}$$

If the pole of the stress distribution is located within the weight-bearing surface, the location of the p_{max} coincides with the location of the pole (p_{max} equals p_0). When the stress pole lies outside the weight-bearing surface, the stress is maximal at the point on the weight-bearing surface, which is closest to the pole and can be computed after Eq. (10).

4. Modelling rehabilitation exercises

Each specific type of exercise was modeled by rotation of the leg around the center of the femoral head while the pelvis was taken to be fixed in a laboratory coordinate system. Three subsequent rotations were considered: abduction, flexion and internal/external rotation. Abduction angle is defined as rotation of the leg around y-axis, flexion angle is defined as rotation of the leg around x-axis and internal/external rotation is defined as rotation of the leg around z-axis (Fig. 5). Positive values of abduction angle indicate abduction while negative values indicate adduction. Positive values of flexion angle correspond to flexion while negative values correspond to extension. Positive values of rotation angle correspond to external rotation while negative values correspond to internal rotation. The three anatomic angles giving the three rotations corresponds to Euler angles (Kreyszig, 1993). Using these three angles any rotation may be described according to Euler's rotation theorem. For a given set of rotation

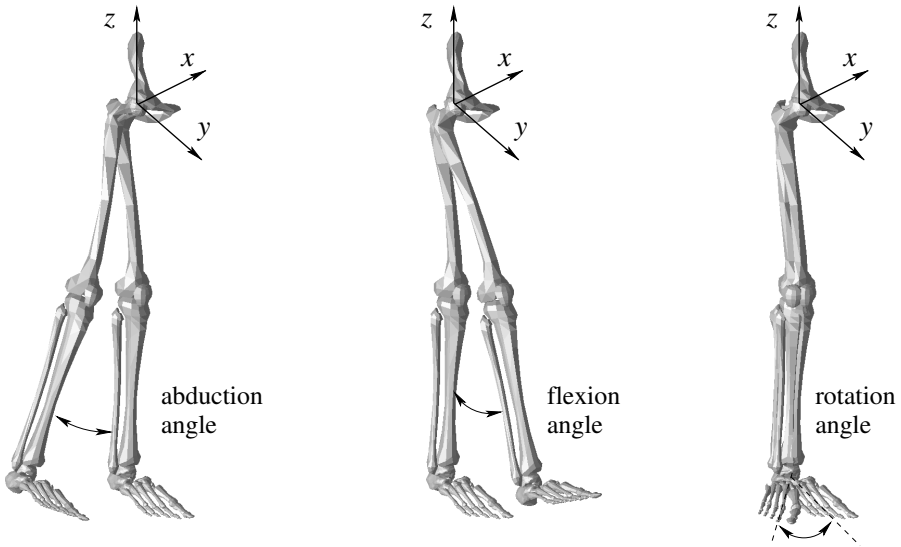

Fig. 5. Angles defining position of the leg with respect to the hip rotation. Positive directions of the angles are depicted.

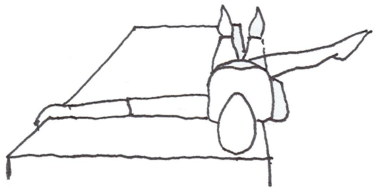

Fig. 6. Unsupported supine exercise.

angles (Fig. 5), the muscle geometry was adapted considering change in the attachment points of muscles on the bones of the leg.

5. Parameters and constants

The range of abduction/adduction was taken from 40 to -10 degrees, respectively, the range of flexion/extension was taken from 70 to -10 degress, respectively and the range of internal/external rotation was taken from -20 to 20 degress, respectively. The z-coordinate of the center of gravity of the leg b was taken to be 42.3 cm. Body weight W_B was taken to be 800 N. Position of acetabulum was defined by angles $\vartheta_{CE} = 30^\circ$ and $\vartheta_{AV} = 15^\circ$. Radius of articular surface r was taken to be 2.5 cm.

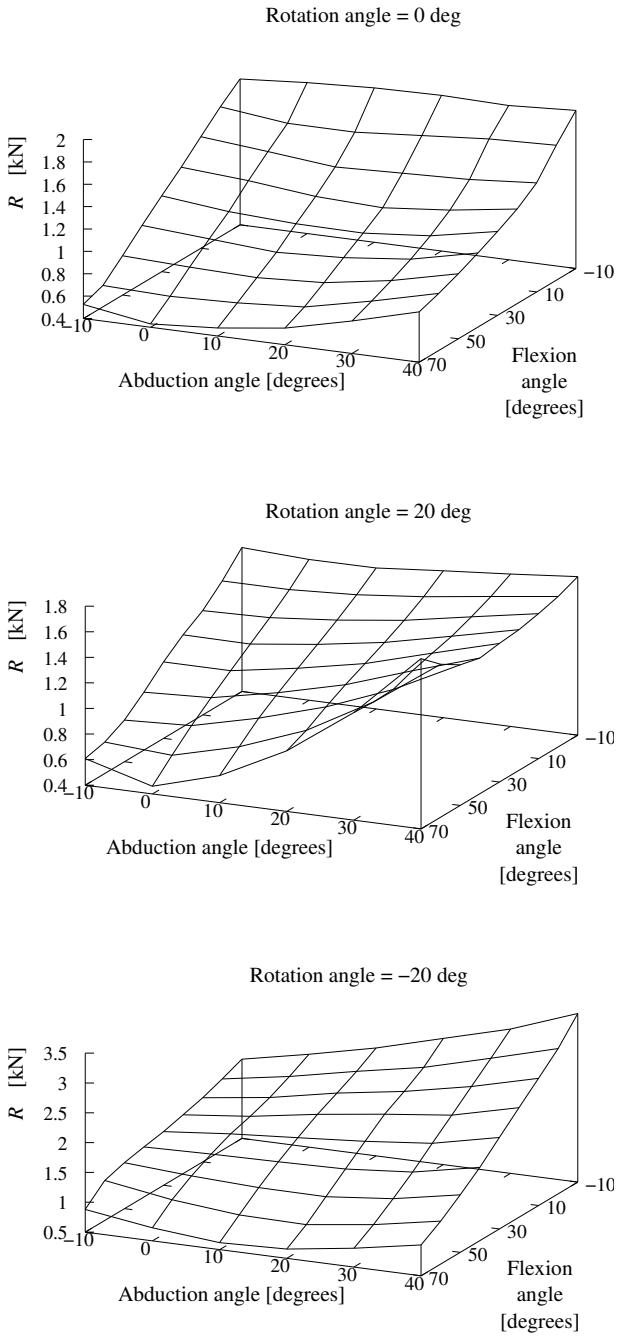

Fig. 7. Magnitude of the hip joint force R in the hip joint for various positions of the leg during supine exercises. No knee flexion is assumed.

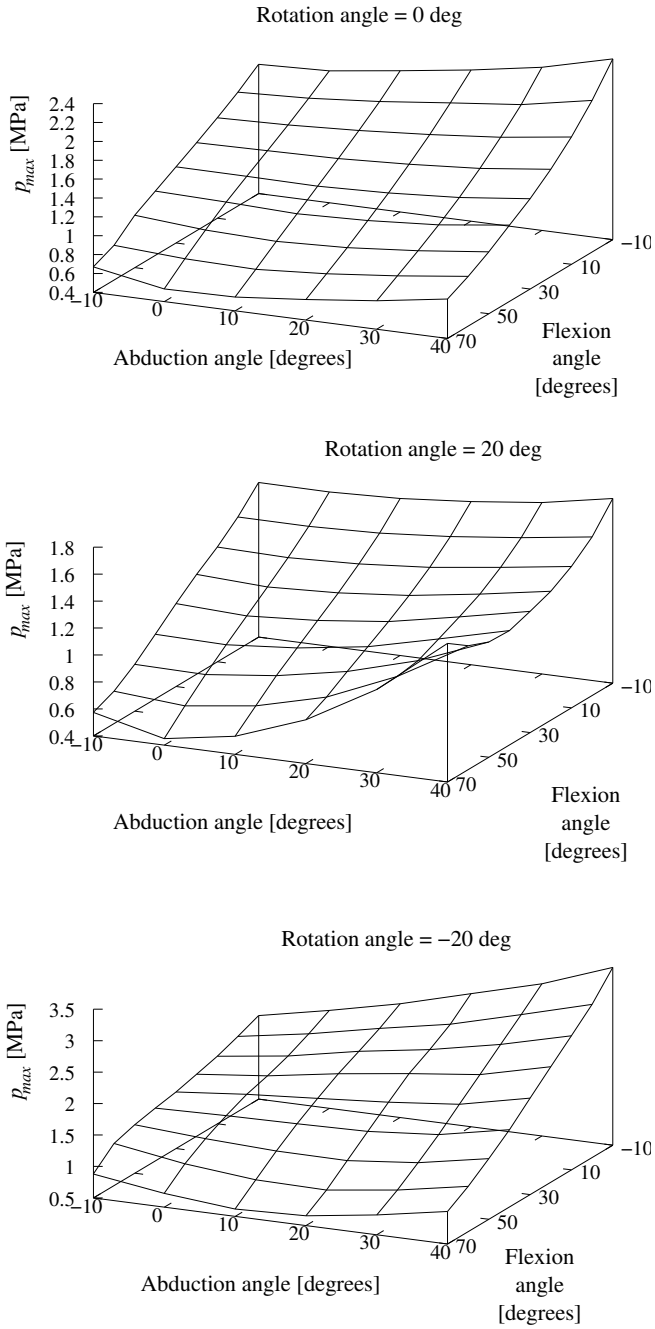

Fig. 8. Peak contact stress p_{max} in the hip joint for various positions of the leg during supine exercises. No knee flexion is assumed.

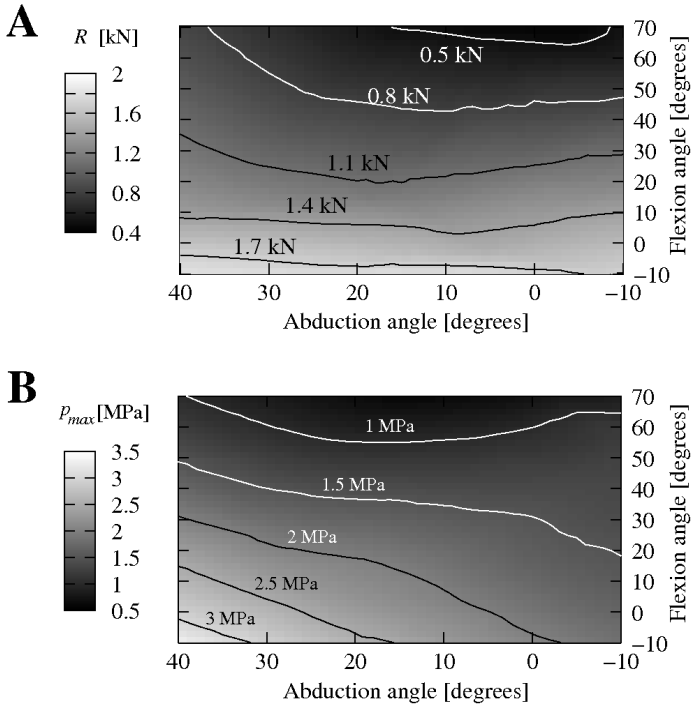

Fig. 9. (A) Magnitude of the hip joint force R and (B) peak contact stress p_{max} in the hip joint for various positions of the leg during supine exercises. No knee flexion is assumed and angle of rotation is taken to be -20 degrees.

6. Results

Previous study shows that the highest acetabular loading was observed in unsupported supine abduction (Kristan et al., 2007) (Fig. 6). Therefore, we have tested the effect of straight-leg exercise about the hip on the hip joint resultant force R and peak contact stress p_{max}.
The magnitudes of the hip joint reaction force **R** and the peak contact stress p_{max} during various positions in rehabilitation exercises in supine body positions are shown in Fig. 7 and Fig. 8 respectively. Fig. 9 shows overview of forces and stresses for rotation angle -20 degrees. Flexion in the hip has greater effect on the resulting loading of the acetabulum than the abduction. The hip joint reaction force R as well as the peak contact hip stress p_{max} is the highest in the unsupported supine extension of the hip. The hip joint loading is the lowest in hip flexion.

7. Discussion

In aggreement with previous studies (Kristan et al., 2007; Tackson et al., 1997), we have found that in the neutral leg position the hip joint reaction force is high for unsupported supine body position. This can be explained by considering the equilibrium of the moments of the gravitational and muscular forces with respect to the center of rotation of the hip joint in different leg positions. In the unsupported supine abduction, the leg has a tendency to extend and hence

the activity of flexors is required. In the supine abduction flexors that are required to maintain this posture have smaller moment arms and thus demand high flexor forces. Therefore the hip joint reaction force magnitude in unsupported supine position is considerably high. Flexion about the hip decreases the moment arm of the weight of the leg and hence decreases loading. Extension of the hip decreases the effective arms of the flexors and it increase the required muscle force as well as the hip joint reaction force.

Computed values of hip joint reaction force and peak contact hip stress reported in this study are of the same order of magnitude as the ones performed in non-weight-bearing exercises measured in vivo (Givens-Heiss et al., 1992; Tackson et al., 1997). Direct measurements of peak contact stress in supine body positions were found to be 2.8 MPa and 3.8 MPa in vivo (Givens-Heiss et al., 1992; Tackson et al., 1997) versus 3.5 MPa in our study. The reports do not specifically mention the amount of vertical leg support in supine adduction, but considering the fast velocities it could be inferred that the abduction was unsupported. It should be noted, however, that these in vivo measurements were performed with angular velocities above 30° and therefore also include the dynamic component of loading.

The limitations of the direct stress measurement method (Morrell et al., 2005) include the facts that the sensors measure the cartilage-on-metal surface and not the cartilage-on-cartilage surface, that the metal prosthesis in contact with natural acetabulum may differ from physiologic morphology of the hip, that sensors were located on the femoral head surface while the values of stress on the acetabular joint surface were estimated from the kinematic data. Further, hip pressure measurements of abduction exercises were performed in one patient only.

On the other hand, our method is limited by the model assumptions. In the calculation of the acetabular loading, it was assumed that the pelvis is fixed. Small rotations of the pelvis are not likely to influence the hip joint reaction force. However, if the rotations of the pelvis were large, this would represent a significant limitation of the study. The muscles were considered as active springs which are able to generate force in order to maintain body position. The passive forces generated by the muscle-tendon unit were not taken into account. To better describe the properties of the muscle, a forward dynamics optimization including activation dynamics and musculo-tendon contraction dynamics could be used Thelen et al. (2003). The static optimization method used in this study to compute muscle forces cannot predict muscle co-contraction Tsirakos et al. (1997). To improve the description of the muscle forces during exercises, a dynamic optimization approach that takes into account dynamic properties of neuromusculoskeletal system could be used. Also, within the static approaches, there are differences according to the choice of the optimization criterion Prilutsky and Gregor (2000). However, comparison of measurements and calculations of the hip joint reaction force showed that the type of the optimization criterion employed does not significantly influence the calculated hip joint reaction force.

In the mathematical model of hip stress calculation, several simplifications were used that could influence the accuracy of the calculated contact stress distribution. For example, in our model the femoral head and acetabulum are taken to be spherical. In normal hips the femoral head and the acetabulum are actually out-of-round by 1-3 mm. It has be shown that in the case of an ellipsoidal articular surface with the semiaxes r and $r + \triangle r$, the cosine stress distribution function (Eq. (10)) can be modified by taking into account the perturbation of the first order in $\triangle r/r$ which yields the stress distribution function in the form $p = p_0 \cos\gamma(1 + 3(\triangle r/r)\sin^2\gamma)$ (Ipavec et al., 1997). Our mathematical model derivation also assumes that the cartilage layer has constant thickness and mechanical properties. The contact stress was assumed to be proportional to the cartilage deformation δ. If the properties of the cartilage

vary along the articular surface, the contact stress at a given point also varies, and this is not taken into account in our model.
The mechanics of cartilage layer in the hip joint obviously cannot be fully described as a homogeneous continuum and a linear elastic material. In order to approach a more realistic description of the stress and force distribution in the cartilage layer, one should take into account the specific molecular structure of the joint articular surface where the two glycoprotein monolayers are adsorbed on the cartilage of both contact surfaces (Nordin and Frankel, 1989). The mechanics of this structure could be realistically described only by using the methods of theoretical physics on the molecular level developed in the field of polymer physics and the statistical physics of interfaces.
We have assumed hip exercises with straight leg only, i.e. no knee flexion was assumed. This assumtion is not fully realistic as the hip flexion is usually acompanied with the flexion in the knee. Also the range of motion in the hip may considerably change if the knee flexion is assumed (Čihák, 2002).
The accuracy of the acetabular loading predicted in this paper could be certainly improved by removing some of the above mentioned simplifications assumed in our mathematical model. However, we believe that the main conclusions would not be changed by using a more advanced mathematical model.

8. Conclusions and further research

We conclude that absolute values of the hip joint reaction force and the peak contact hip stress in unsupported supine abduction are the highest in combination of hip extension, hip abduction and internal rotation. The stresses and force can reach the values observed in weight-bearing exercises or gait (Ipavec et al., 1999). Unsupported Supine abduction in initial rehabilitation phases should be therefore omitted or recommended with ground support (on the bed) or in combination with assisted flexion.
Based on the presented results we suggest that detailed calculations of spatial distribution of the hip joint contact stress is required before starting rehabilitation procedure as to individually design the rehabilitation procedure for a given patient. In the planning, the spatial position of the fracture lines and dislocations of the acetabular fragments should be taken into account.
Our results complement the results of direct measurements of stress during exercises and the experience – based exercise protocols in elucidating the mechanical impacts on the rehabilitation. In further work, stress distributions in other body positions should computed as well in order to select an appropriate therapy for given patient.

9. References

Afoke, N., Byers, P., and Hutton, W. (1987). Contact pressures in the human hip joint. *Journal of Bone and Joint Surgery*, 69B(4):536–541.

Bergmann, G. (2001). *Hip98, Loading of the hip joint.* Freie Universität, Berlin. available online at ftp://ftp.ukbf.fu-berlin.de/pub/biomech/hip98.zip.

Brand, R. (2005). Joint contact stresses: A reasonable surrogate for biological processes? *The Iowa Orthopaedic Journal*, 25:82–94.

Brand, R., Pedersen, D., Davy, D., Kotzar, K., Heiple, K., and Goldberg, V. (1994). Comparison of the hip joint reaction force and measurements in the same patient. *Journal of Arthroplasty*, 9(1):45–51.

Brand, R., Pedersen, D., and Friederich, J. (1986). The sensitivity of muscle force predictions to changes in physiologic cross-sectional area. *Journal of Biomechanics*, 19:589–596.

Brinckmann, P., Frobin, W., and Hierholzer, E. (1981). Stress on the articular surface of the hip joint in healthy adults and persons with idiopathic osteoarthrosis of the hip joint. *Journal of Biomechanics*, 14(3):149–153.

Brinckmann, P., Frobin, W., and Leivseth, G. (2002). *Musculoskeletal biomechanics*. Georg Thieme Verlag, Stuttgart.

Brown, T. (1983). In vitro contact stress distributions in the natural human hip. *Journal of Biomechanics*, 16(6):373–384.

Clauser, C., McConville, J., and Young, J. (1970). Weight, volume and center of the mass of the human body. Technical Report Report AMRL-TR-69-70, National Technical Information Service.

Crownishield, R. and Brand, R. (1981). A physiologically based criterion for muscle force prediction and locomotion. *Journal of Biomechanics*, 14:793–801.

Crownishield, R., Johnston, R., Andrews, J., and Brand, R. (1978). A biomechanical investigation of the human hip. *Journal of Biomechanics*, 11:75–85.

Daniel, M., Iglic, A., and Kralj-Iglic, V. (2008). Hip contact stress during normal and staircase walking: the influence of acetabular anteversion angle and lateral coverage of the acetabulum. *J Appl Biomech*, 24(1):88–93.

Delp, S., Loan, J., Hoy, M., Zajac, F., Topp, E., and Rosen, J. (1990). An interactive graphics-based model of the lower extremity to study orthopaedic surgical procedures. *IEEE Transactions on Biomedical Engineering*, 37:757–767.

Eaton, J. (1997). *GNU Octave Manual*. Network Theory Ltd, Bristol, UK.

Genda, E., Iwasaki, N., Li, G., MacWiliams, B., Barrance, P., and Chao, E. (2001). Normal hip joint contact pressure distribution in single-leg standing – effect of gender and anatomic parameters. *Journal of Biomechanics*, 34:895–905.

Givens-Heiss, D. L., Krebs, D. E., Riley, P. O., Strickland, E. M., Fares, M., Hodge, W. A., and Mann, R. W. (1992). In vivo acetabular contact pressures during rehabilitation, part ii: Postacute phase. *Phys Ther*, 72(10):700–5; discussion 706–10.

Goulet, J. A., Rouleau, J. P., Mason, D. J., and Goldstein, S. A. (1994). Comminuted fractures of the posterior wall of the acetabulum. a biomechanical evaluation of fixation methods. *J Bone Joint Surg Am*, 76(10):1457–1463.

Greenwald, A. and O'Connor, J. (1971). The transmission of load through human hip joint. *Journal of Biomechanics*, 4:507–528.

Heller, M., Bergmann, G., Deuretzbacher, G., Dürselen, L., Pohl, M., Claes, L., Haas, N., and Duda, G. (2001). Musculo-skeletal loading conditions at hip during walking and stair climbing. *Journal of Biomechanics*, 34:883–893.

Herman, S., Jaklič, A., Herman, S., Iglič, A., and Kralj-Iglič, V. (2002). Hip stress reduction after Chiari osteotomy. *Medical and Biological Engineering and Computing*, 40:369–375.

Iglič, A., Kralj-Iglič, V., Antolič, V., Srakar, F., and Stanič, U. (1993). Effect of the periacetabular osteotomy on the stress on the human hip joint articular surface. *IEEE Transaction on rehabilitation*, 1(4):207–212.

Iglič, A., Kralj-Iglič, V., Daniel, M., and Maček-Lebar, A. (2002). Computer determination of contact stress distribution and the size of the weight-bearing area in the human hip joint. *Computer Methods in Biomechanics and Biomedical Engineering*, 5:185–192.

Iglič, A., Srakar, F., Antolič, V., Kralj-Iglič, V., and Batagelj, V. (1990). Mathematical analysis of Chiari osteotomy. *Acta Orthopedica Iugoslavica*, 20:35–39.

Ipavec, M., Brand, R., Pedersen, D., Mavčič, B., Kralj-Iglič, V., and Iglič, A. (1999). Mathematical modelling of stress in the hip during gait. *Journal of Biomechanics*, 32:1229–1235.

Ipavec, M., Iglič, A., Kralj-Iglič, V., and Antolič, V. (1997). Influence of the nonspherical shape of the femoral head on the compressive stress in the hip joint articular layer. In *Proceedings of the 6th Conference of Slovenian IEEE Section*, pages 351–354, Ljubljana.

Ipavec, M., Kralj-Iglič, V., and Iglič, A. (1995). Stress in the hip joint articular surface during gait. *Engineering Modelling*, 8:7–14.

Kreyszig, E. (1993). *Advanced engineering mathematics*. John Willey & Sons, New York.

Kristan, A., Mavcic, B., Cimerman, M., Iglis, A., Tonin, M., Slivnik, T., Kralj-Iglic, V., and Daniel, M. (2007). Acetabular loading in active abduction. *IEEE Trans Neural Syst Rehabil Eng*, 15(2):252–257.

Legal, H. and Reinicke, M. (1980). Zur biostatischen analyse des hüftgelenkes III. *Zeitschrift für Orthopädie und ihre Grenzgebiete*, 118:804–815.

Letournel, E. and Judet, R. (1993). *Fracture of acetabulum*. Springer, New York.

Maurer, F., Mutter, B., Weise, K., and Belzl, H. (1997). [rehabilitation following hip fractures]. *Orthopade*, 26(4):368–374.

Morrell, K. C., Hodge, W. A., Krebs, D. E., and Mann, R. W. (2005). Corroboration of in vivo cartilage pressures with implications for synovial joint tribology and osteoarthritis causation. *Proc Natl Acad Sci U S A*, 102(41):14819–14824.

Nigg, B. and Herzog, W. (1995). *Biomechanics of the musculo-skeletal system*. John Willey & Sons, Chichester.

Nordin, M. and Frankel, V., editors (1989). *Basic biomechanics of the musculoskeletal system*. Lea & Fibiger, Philadelphia.

Olson, S. A. (2003). Biomechanics of acetabular fractures. In Marvin Tile, David Helfet, J. K., editor, *Fractures of the Pelvis and Acetabulum*, pages 46–49. Lippincott Williams & Wilkins.

Olson, S. A., Bay, B. K., and Hamel, A. (1997). Biomechanics of the hip joint and the effects of fracture of the acetabulum. *Clin Orthop Relat Res*, 339(339):92–104.

Pedersen, D., Brand, R., and Davy, D. (1997). Pelvic muscle and acetabular forces during gait. *Journal of Biomechanics*, 30:959–965.

Prilutsky, B. and Gregor, R. (2000). Analysis of muscle cordination strategies in cycling. *IEEE Transactions on Rehabilitation Engineering*, 8(3):362–370.

Rasmussen, J., Damsgaard, M., and Voigt, M. (2001). Muscle recruitment by the min/max criterion - a comparative numerical study. *Journal of Biomechanics*, 34:409–415.

Schneck, D. (1990). *Engineering principles of physiologic function*. New York University Press, New York.

Stansfield, B., Nicol, A., Paul, J., Kelly, I., Graichen, F., and Bergmann, G. (2003). Direct comparison of calculated hip joint contact forces with those measured using instrumented implants. an evaluation of the three-dimensional model of the lower limb. *Journal of Biomechanics*, 26:929–936.

Tackson, S., D.E., K., and Harris, B. (1997). Acetabular pressures during hip arthritis exercises. *Arthritis Care Research*, 10(5):308–319.

Thelen, D., Anderson, F., and Delp, S. (2003). Generating dynamic simulations of movement using computed muscle control. *Journal of Biomechanics*, 36:321–328.

Tsirakos, D., Baltzopoulos, V., and Bralett, R. (1997). Inverse optimization: functional and physiological considerations related to the force sharing problem. *Critical Reviews in Biomedical Engineering*, 25(4&5):371–407.

Čihák, R. (2002). *Anatomie 1*. Grada, 2nd edition.

Winters, J. (2000). Terminology and foundations of movement science. In Winters, J. and Crago, P., editors, *Biomechanics and Neural Control of Posture and Movement*. Springer-Verlang, New York.

Ye, Y. (1989). *SOLNP user's guide: A nonlinear optimization in MATLAB*. Department of Management Sciences, College of Bussoness Administration, University of Iowa.

Yoshida, H., Faust, A., Wilckens, J., Kitagawa, M., Fetto, J., and Chao, E. Y.-S. (2006). Three-dimensional dynamic hip contact area and pressure distribution during activities of daily living. *Journal of Biomechanics*, 39:1996–2004.

Zajac, E. and Winters, J. (1990). Modelling muskuloskeletal movement systems: Joint and body segmental dynamics, muskuloskeletal and neuromuskular system. In Winters, J. and Woo, S. L.-Y., editors, *Multiple Muscle Systems - Biomechanics and Movement Organization*. Spinger-Verlang, New-York.

Zupanc, O., Krizancic, M., Daniel, M., Mavcic, B., Antolic, V., Iglic, A., and Kralj-Iglic, V. (2008). Shear stress in epiphyseal growth plate is a risk factor for slipped capital femoral epiphysis. *J Pediatr Orthop*, 28(4):444–451.

10

The Lognormal Framework in the Context of Human Movement Rehabilitation

Christian O'Reilly and Réjean Plamondon
École Polytechnique de Montréal
Québec, Canada

1. Introduction

For more than a decade, the Kinematic Theory of Rapid Human Movements (KTRHM) has provided researchers insights on the strategies used by the central nervous system to control simple and complex human movements. In the last few years, efforts have been made on exploring its use in the medical field, especially for the diagnosis and the rehabilitation of neuromuscular diseases. The purpose of this chapter is to show how this theory may be used to design neuromuscular tests and to evaluate the motor control condition of stroke-impaired patients by performing an analysis of their upper-limb movements. Toward that goal, the following section presents some related works and discusses how movement modeling could be used to enhance the evaluation aspect of movement rehabilitation.
Subsequently, a special attention is given to the development of two models derived from the KTRHM. First, the Delta-Lognormal model is outlined. This paradigm basic movements such as aiming toward a target. Second, the Sigma-Lognormal model is depicted. This more versatile model can be exploited, for example, to reveal the action plan used at the brain level for preparing and executing tasks requiring complex muscular coordination such as those involved in handwriting production. These two models have been developed rigorously from a mathematical point of view and it is shown that they are firmly underpinned by a sound modeling of the neuromuscular system as well as by their adequacy with empirical observations of movement characteristics.
More details are then given on how these models can be used for the synthesis of human-like movements for explorative purposes in the preliminary stages of a biomedical study. Such an approach shows great promises for the development of a cheaper and more efficient ways to get *a priori* information in the planning of experiments. Moreover this knowledge may be used during data collection to detect failure to respect the experimental protocol and to avoid useless trials. Moving further along the experimentation process, it is then shown how a model-based analysis can be useful once the data collection is completed. Nowadays, this has become a particularly exciting area of applications for the lognormal models since robust algorithms are now available for such a purpose. Finally, this chapter concludes with limitations and perspectives for future developments associated with this work along with a review of the most important topics discussed throughout this chapter.

2. Upper-limb Movement Evaluation for Stroke Patient Rehabilitation

The following section outlines the major aspects of the human movement evaluation. Although many points are general, this overview is particularly focused on the specific case of upper-limb movement rehabilitation in stroke-impaired patients.

In the course of a rehabilitation program, once the prognostic of a given patient is established, many therapies may be proposed to help him regains some of his lost movements (e.g. conventional therapy, constraint-induced movement therapy (CIMT) (Hakkennes & Keating, 2005), robot-assisted therapy (Kwakkel, Kollen, & Krebs, 2008; Riener, Nef, & Colombo, 2005), virtual environment (Holden, 2005), neuromuscular electrical stimulation (Sheffler & Chae, 2007), cognitive strategies such as motor imagery (McEwen, Huijbregts, Ryan, & Polatajko, 2009)) or to help him compensate or develop alternative strategies to regain more freedom in his daily life activities. In this context, the evaluation procedure at the begin of a therapy and all along the rehabilitation process is very important to assess the effectiveness of a given treatment and to establish realistic goals to aim for an optimal recovery of the patient's global quality of life (Perry, 1990).

For such evaluations, many standardized test have been developed over the years. (Rothstein, Roy, Wolf, & Scalzitti, 2005) lists more than 60 tests depending on the subject's age (infant, adult, elder), the aspects of motor control to be assessed (balance, pain, mobility, quality of life, activities of daily life, etc), the affected region (upper extremities, lower extremities, etc) and the origin of the deficit (stroke, spinal injuries, etc). Moreover, the test to adopt may vary depending on to whom the information is collected for (e.g. the patient, the carers, the clinicians, the politicians, the society, etc) (Patel & Rudd, 2004).

Although evaluation tests are numerous, very few use a systematic modeling or a computerized assessment. This is unfortunate given that such tests may have interesting psychometric properties (repeatability, reliability, and sensitivity (Kisacanin, Agarwal, Taber, & Hier, 2000)) as well as interesting practical aspects such as a better potential to be automated. This characteristic may come handy for at-home routine evaluation of patients with or without the supervision of medical staff, in the context of telerehabilitation for example. Moreover, such test could be integrated somehow naturally in therapies using a virtual reality framework or a robotic assisting apparatus. It could also take a greater advantage of more complete human movement tracking system[1] than could conventional testing method mainly based on the evaluation of basic characteristics such as reaction times. Finally, it may be easier to implement these tests in a form which is more interesting for patients, closer to a game than a chore, and therefore, more likely to lead to a higher patient participation.

3. The Lognormal Models

The lognormal models were mainly developed in the context of the analysis of the kinematic signals[2] obtained from the movement of an end effector. Therefore, they are best suited for studying movement characteristics from data obtained with such tool as digitizing tablets. Although particularly well adapted and accurate for fast and simple movement analysis,

[1] See (Zhou & Hu, 2008) for a review of such systems.

[2] The analysis of kinetic signals has also been studied in (Plamondon, 1998).

these models may also be used for complex and slow movement analysis (O'Reilly, C., & Plamondon, R. (2009a)) but this necessitates a more involved analysis. In the following, two particular models are presented - the Delta and the Sigma-Lognormal models – along with a description of their parameters.

3.1 The Delta-Lognormal Model

3.1.1 Definition

The Delta-Lognormal model has been originally developed to devise an analytical and accurate representation of fast pointing human movements. It considers this action has being the result of the synergetic action of two parallel systems, each generating a *neuromuscular component*[3]. The first one is agonistic to the movement, that is, it drives the end effector from its starting position toward its target. The second is antagonistic to the movement and is used as a stopping mechanism to avoid target overshooting. This scheme is depicted in figure 1.

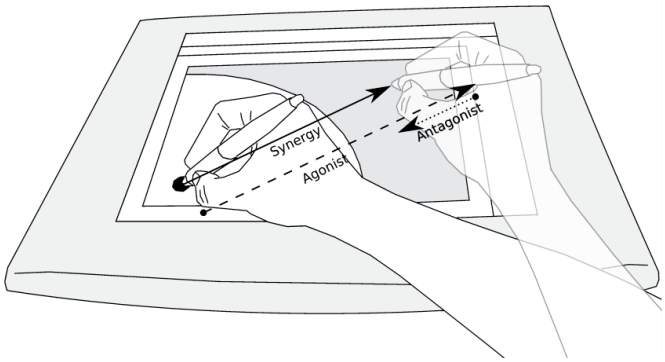

Fig. 1. The production of a pointing movement. The actual movement (solid arrow) is the result of the synergetic combination of an agonistic (dashed arrow) and an antagonistic (dotted arrow) component.

Moreover, the KTRHM considers the components as having a lognormal velocity modulus scaled by a command amplitude parameter (D) and time shifted by the command time occurrence (t_0). Therefore, the Delta-Lognormal model represents the speed profile of a fast pointing movement with the equation (1) where the Λ terms represent the three-parameter form of the lognormal equation as given in (2).

$$v_t = D_1\Lambda(t;t_0,\mu_1,\sigma_1) - D_2\Lambda(t;t_0,\mu_2,\sigma_2) \tag{1}$$

$$\Lambda(t;t_0,\mu,\sigma) = \frac{1}{\sqrt{2\pi}\sigma(t-t_0)}\exp\left(-\frac{\left(\ln(t-t_0)-\mu\right)^2}{2\sigma^2}\right) \tag{2}$$

For reasons that will become more evident latter, the σ and the μ parameters are global timing characteristics of the neuromuscular systems. It should also be noted that the t_0 parameter has the same value for the two components in the Delta-Lognormal model.

[3] Hereafter, referred to simply as component.

3.1.2 Theoretical Underpinning

Two main aspects of the Delta-Lognormal model are discussed in the following paragraphs. The first one is the representation of a target reaching movement as the result of the synergetic interaction of two competing contributions. Beyond the general consideration that most physical system needs equilibrium of opposed forces to remain stable, the plausibility of this assumption is strengthen by the fact that the presence of some cocontraction is known to be a desirable feature to ensure movement stability and precision. Although a large amount of cocontraction may be a sign of some movement disorder (e.g. hemiplegia, spastic cerebral palsy), its presence in a smaller magnitude is a normal phenomenon (Gribble et al., 2003; Winter, 2005).

In this synergetic scheme, the relative importance of the antagonistic component would be expected to increase with a global speed augmentation. To see this, one may think for example about a classic driving ability test: a start-stop test where a given distance has to be covered in the shortest time before making a full stop as close as possible to a target. With a sufficiently slow speed and because of friction, it may be possible to complete this task using almost no braking. However, to increase the performance (i.e. to reduce the required task time T_t) both a stronger acceleration and a stronger braking are needed. That is, if D_1 and D_2 represent respectively the amplitude of the displacement resulting from this acceleration and this braking, we would expect a relation such as shown in (3). This general observation on start-stop movements is well captured by the Delta-Lognormal model which formally predicts a similar[4] relationship (Plamondon, 1995).

$$T_t \propto \frac{D_1}{D_2} \tag{3}$$

The second aspect that needs to be discussed is of paramount importance in both lognormal models. It is the assumption that the speed profile of a component is asymptotically approximated by a lognormal relationship. Using a system engineering point of view, the neuromuscular system generating a given component may be represented as a complex cascaded network of neuronal and muscular subsystems. Given that these subsystems are numerous, locally linear around an operating point and related through a proportional law given in (4), it has been demonstrated using the central limit theorem that the resulting transfer function has indeed a lognormal form as expressed by (2) (Plamondon, Feng, & Woch, 2003).[5]

$$T_j = (1 + \varepsilon_j) T_{j-1} \tag{4}$$

3.1.3 Empirical Evidences

Different experiments tend to support the Kinematic Theory of Rapid Human Movements and its Delta-Lognormal model from a practical perspective. Firstly, it has been shown that the Delta-Lognormal is the model which can represents rapid pointing movement the more accurately and meaningfully (Alimi & Plamondon, 1994; Alimi, 1995). Secondly, experimentation using EMG has strongly supported the proportional effect postulated in

---

[4] The exact relationship have a proportional constant and a power factor, both functions of the neuromuscular parameters (i.e. μ_i and σ_i)

[5] Beside the formal mathematical proof, an experimental illustration of this lognormal genesis scheme is shown by the simulation performed in (Djioua & Plamondon, 2003).

(4). Thirdly, the empirically observed speed/accuracy tradeoff in human fast pointing movement is very well captured by the Delta-Lognormal model (Plamondon & Alimi, 1997). Fourthly, (Landou, 2008) has shown that the occurrence of a command at the time t_0 is observable by an electroencephalography of the brain.

3.2 The Sigma-Lognormal Model

3.2.1 Definition

The Sigma-Lognormal model was developed as a generalization of the Delta-Lognormal one. To that end, two principal elements have been considered. Firstly, the tightly coupled relationship of two opposed components was relaxed. In complex movement like handwriting, the notion of agonist and antagonist neuromuscular systems loose of its interest because the motion is no longer directed at a single and static target. For this kind of movement, it is assumed that a unified command timing of two components, as performed in the Delta-Lognormal model, is no longer an interesting strategy and that the central nervous systems uses instead a sequencing of individual component commands. In other word, no common t_0 is assumed between different components.

Secondly, the one dimensional movement analysis was expended to planar movements[6], using components having circle arc trajectories. This extension requires two additional parameters for each component - a starting angle (θ_s) and an ending angle (θ_e) - and a vectorial combination of individual components. Eq. (5) summarized this combination in a matrix form[7] where the V and Φ symbols are respectively vectors of the velocity modulus and angular variation of individual components (v_j and φ_j) as given formally in (6).

$$\vec{v}(t) = \begin{bmatrix} v_x(t) \\ v_y(t) \end{bmatrix} = V \begin{bmatrix} \cos(\Phi) \\ \sin(\Phi) \end{bmatrix} \quad (5)$$

$$V = \begin{bmatrix} v_1 & v_2 & \dots & v_n \end{bmatrix}^T \quad (6.\text{a})$$

$$\Phi = \begin{bmatrix} \varphi_1 & \varphi_2 & \dots & \varphi_n \end{bmatrix}^T \quad (6.\text{b})$$

$$v_j(t) = D_j \Lambda(t; t_{0j}, \mu_j, \sigma_j) \quad (7.\text{a})$$

$$\varphi_j(t) = \theta_{sj} + \frac{\theta_{ej} - \theta_{sj}}{D_j} \int_0^t v_j(\tau) d\tau \quad (7.\text{b})$$

3.2.2 Action Plan

In the Sigma-Lognormal model, each movement may be represented by an action plan which is hypothesized to be generated at the brain level for the preparation and the execution of a complex motor task. When working with a Sigma-Lognormal representation, this notion is quite useful to better understand the strategy involved in the movement generation process.

An action plan has three constitutive elements: virtual targets, an ordering pattern, and the component trajectories. It may be generated by concatenating the component trajectories in their order of appearance, as specified by their t_{0i}. Component ending points are considered

[6] It may also be generalized to 3D movements (Djioua, 2007; Leduc & Plamondon, 2003).

[7] An alternative formulation in the form of summation equations can be found elsewhere, in (O'Reilly, C., & Plamondon, R. (2009a)) for example.

as being virtual targets which represent the location that would have been reached if no further component had redirected the end effector.
Figure 2 shows two examples of movement action plan, with and without superposition. Without superposition, the trajectory is identical for the action plan and the synthesized movement (It correspond for example to block letter writing). As more superposition is applied, the synthesized movement trajectory starts to depart from the action plan and to show more smoothness.

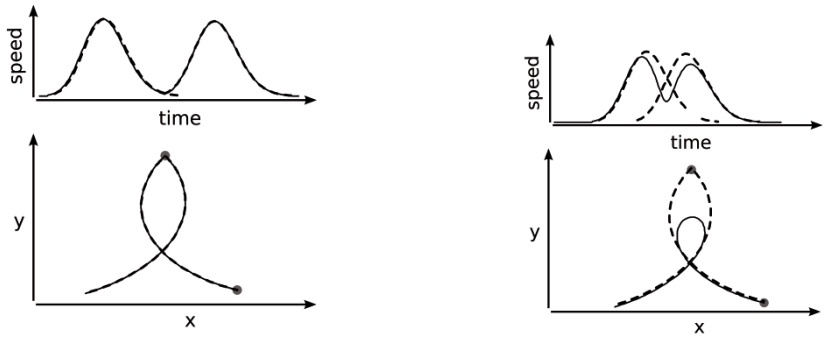

Fig. 2. Examples of movement action plan. Synthesized movements are shown by the solid lines, components by the dashed lines and virtual targets by the grey filled circles. The speed profile is shown on the upper part while the trajectory is on the lower part. The figure shows the case with (a) almost no superposition and with (b) an important superposition.

3.3 Parameter Signification

Lognormal parameters have specific physical meaning in the context of KTRHM. This provides a rich semantic to the lognormal models from a functional point of view. The parameters are further defined in table 1.

4. Lognormal Movement Synthesis

4.1 Advantages of Explorative Synthesis

In research projects where new neuromuscular tasks are designed for defining trials involving the study of an end effector kinematics, it may be interesting to perform some prior synthesis (i.e. simulation) study for at least three reasons.

Parameter	Unit	Meaning
D	meter	Amplitude of the command given for the generation of a neuromuscular component. It also corresponds to the component trajectory length. It is a command parameter.
μ	ln(s)	Time delay of a neuromuscular impulse response on a logarithmic time scale. This parameter is a global characteristic of the neuromuscular systems.
σ	ln(s)	Response time of a neuromuscular impulse response on a logarithmic time scale. This parameter is a global characteristic of the neuromuscular systems.
t_0	second	Time of the command emission.
θ_s	radian	Starting angle of the trajectory. It is a command parameter.
θ_e	radian	Ending angle of the trajectory. It is a command parameter.

Table 1. The Lognormal parameters, along with their unit and meaning.

The first one is that this study may reveal some parameter correlations which are encoded in the task specification (Woch, 2006). It may save time and resources to know these relationships while designing the experiment rather than learning them when analyzing data after the trials are over.
The second reason is that this prior exploration may help in the definition of *a priori* hypotheses. It may also be used to postulate *a priori* classes of movement that are expected or unexpected to be obtained in experimentation (O'Reilly & Plamondon, 2007).
Finally, the third advantage of prior exploration of a neuromuscular test by synthesis experiments is that by defining what kind of movement is expected or unexpected, the experimental protocol may be designed in a more robust way. For example, fast target reaching movements are normally performed in a delta-lognormal fashion featuring two tightly coupled components. The apparition of many more components may generally be associated with one of two main factors: the subject has a poor neuromuscular control (e.g. elder or stroke-impaired subject) or he is performing slow movement (e.g. he has not well understood the importance of making a fast movement or he may be overzealous in reaching precisely the target center). In such situation, it may be adequate to include in the experimental protocol some instructions to make sure that the task will be well understood, avoiding the collection of biased data. For example, it may be specified that, when jerky speed signals are obtained, further instructions should be given to the subject to emphasize more strongly on the importance of performing fast movements. Such a precaution should have no effect on subjects with poor neuromuscular control which would continue to generate unsmooth movements. However, it may help to gather more systematically smooth (i.e. containing a minimum number of components) movements from healthy subjects.

4.2 Example of Lognormal Movement Analysis-by-Synthesis

As an example of the synthesis of a human movement, a motor test using the following protocol will be considered: Starting from target 0, the movement must passes sequentially through target 1 and 2 before making a full stop at target 0. The movement duration must be

as short as possible. The targets are placed at the apexes of an equilateral triangular. Targets have 15mm in diameter and are 90mm apart from each others.
Figure 3.a shows an example of a movement fulfilling the requirement of this task. Three components are used to drive sequentially the movement toward each target and a fourth component is used to stop sharply. Alternative strategies could also be hypothesized. For example, delta-lognormal synergies may be used for each target reaching movement such as shown in figure 3.b. In this example, going from one strategy to the other is a tradeoff between the movement duration and its required resources. The second strategy is faster but necessitates more energy as can be shown by a greater ratio between the trajectory length of the action plan (dashed line) and of the generated movement (solid line).
This kind of analysis may be used to generate research questions. Are these two strategies actually observed in real human movements? Are they consistently associated with different subjects? Is there a shift from one strategy to another along the course of a rehabilitation program? What effect an impairment is expected to have on these strategies? Thinking about such questions before performing the trials may help prepare worthier data collection and guide the researchers in data analysis.

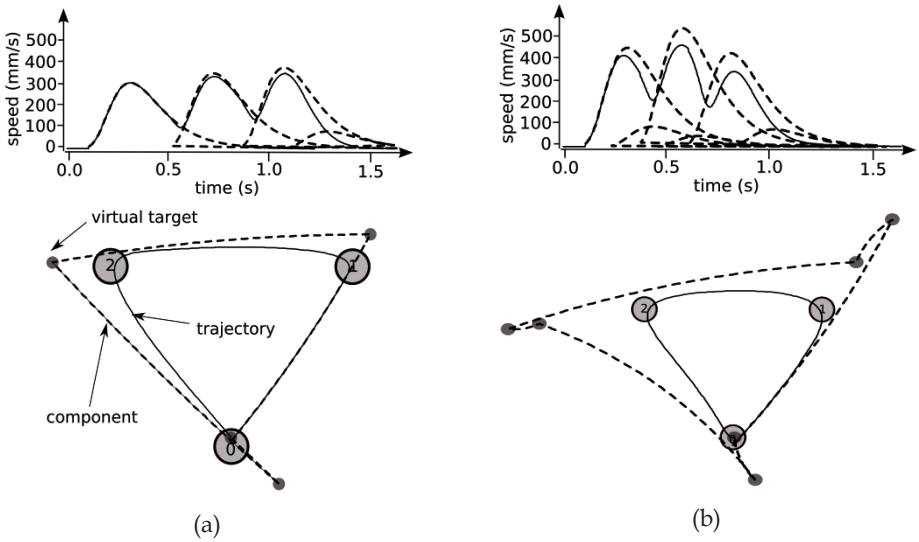

Fig. 3. The synthesis of a fast anti-clockwise triangular movement. The continuous line shows the movement; the dashed line shows its action plan. The upper graphs display the speed profiles associated with the trajectories shown on the lower graphs.

4.3 Synthesis Application: The SimScript Software

Although the synthesis of movement kinematics from the model parameter is somehow straightforward using the mathematical relations (1) to (7), its embedding in a way that is easy to use for exploration purpose is a more cumbersome endeavor. Such a tool has been developed using the Sigma-Lognormal framework and used as a software assistant for the design and the analysis of neuromuscular test (O'Reilly & Plamondon, 2007). In doing so, three objectives were intended: (1) to help to improve the results from rehabilitation for

stroke-impaired patients by enabling a more effective design of neuromuscular tests, (2) to lower the cost of medical care by guiding the development of at-home rehabilitation exercises and (3) to trigger a deeper understanding of the motor system characteristics by allowing an analysis-by-synthesis study of the human movements.
This tool, named SimScript, helps in the interactive synthesis of human movements with Sigma-Lognormal equations. It features a live feedback of the effect on the velocity profiles and on the movement trajectory of any modification of a parameter value. These alterations can be entered through text boxes if a precise value is needed or they can be adjusted through sliders for an explorative approach.

5. Lognormal Movement Analysis

Recent works on Delta-Lognormal and Sigma-Lognormal parameter extraction algorithms has open new possibilities for the analysis of human movements with the lognormal models. From a given movement produced by a subject, it is now possible to recover the parameters that describe its trajectory and so to recover the action plan used by the subject in this specific instance. For completeness, the main aspects of the Sigma-Lognormal parameter extraction have been included in appendix. In the following sub-sections, an example of the study of a neuromuscular test is discussed followed by the presentation of a program developed to perform such an analysis.

5.1 Example of Lognormal Movement Analysis

The experimental protocol presented in section 4.2 has been used in the context of a study on the prevention and the rehabilitation of neuromuscular dysfunction through movement analysis. The Sigma-Lognormal parameters have been extracted from movements gathered from these trials. Figure 4 shows the Sigma-Lognormal representation (i.e. the reconstructed movement (solid line) and its corresponding action plan (dashed line)) obtained for one of these movements. Although, in this particular example, the subject did not fulfill the requirement of passing through both intermediary targets (1 and 2) before stopping at target 0, its action plan is interesting because it shows three typical strategies that are regularly observed on automatic extraction of target reaching movements. At the first target, the strategy used is a simple redirection of the movement without further correction. A strategy of undershooting with subsequent corrective movement is adopted for reaching the second target. Finally, to ensure a sharp stop at the target 0, an overshooting with an antagonistic component has been used.

5.2 Application: The ScriptStudio Software

ScriptStudio has been developed to integrate the SimScript features in a framework that would easily allow the adjunction of more evolved features such as the acquisition and the loading of digitized human movements, the automatic or assisted extraction of Sigma-Lognormal parameters from digitized movements and the non-linear optimization of a whole extraction or of a given component. Such tool is quite useful in Sigma-Lognormal analysis. For an example, it allows displaying a given task guiding sheet at the screen, the acquisition of a movement performed over that sheet and the extraction on-the-fly of this movement parameters. A screenshot of ScriptStudio interface is displayed in figure 5.

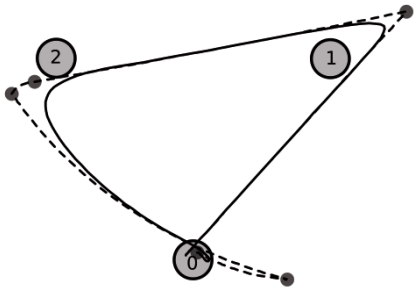

Fig. 4. A fast anti-clockwise triangular movement reconstructed with a Sigma-Lognormal equation (continuous line) along with its action plan (dashed line). The subject was asked to perform a fast movement which would start and end at target 0, passing through both experimental target 1 and 2. Although he failed to meet the precision requirements, the movement action plan reveals an interesting diversity of movement planning strategies.

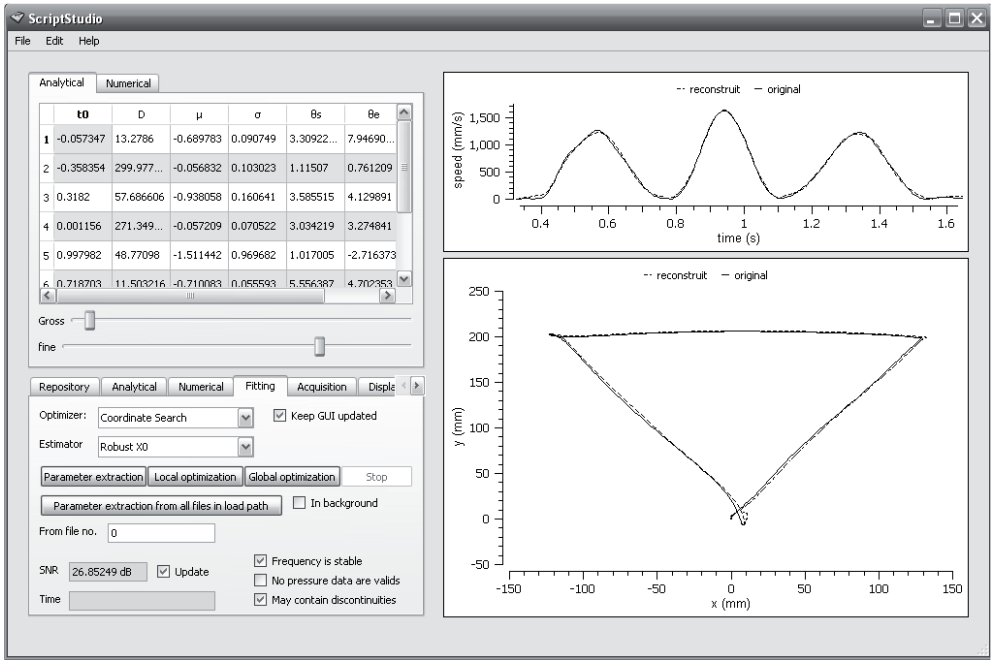

Fig. 5. The ScriptStudio interface. On the upper left, two tabs allow the visualization and the modification of the Sigma-Lognormal parameters of an analytical movement or of the values of the samples of a digitized movement. The lower left part features many tabs allowing managing working repositories, loading and saving analytical and numerical movements, performing fitting operations such as parameter extraction or optimization, acquiring movements and managing the display of both speed signals and trajectory trace. Finally, the interface shows, on its right part, the speed profiles and the trajectory path of a numerical and/or an analytical movement.

6. Final remarks and Future Researches

6.1 Further Medical Application of the Lognormal Models

Although more focused on a preventive perspective, it is worth mentioning that good preliminary results have been obtained using a Sigma-Lognormal analysis for the susceptibility assessment of being victim of a stroke (O'Reilly, C., & Plamondon, R. (2009b)). It may be relevant to consider this kind of measure even in the rehabilitation process since, in disease such as stroke, a first attack is an important risk factor of suffering a subsequent attack. Therefore, rehabilitation should be accompanied by a close monitoring for signs of possible reoccurrence.

Although application of the lognormal models to human movement rehabilitation is still in an early stage of development, works of other research teams on the use of mathematical modeling of human movement for rehabilitation purpose highlights some potential future applications. The work of Rohrer (Rohrer et al., 2002; Rohrer et al., 2004) is a good example of such a thing. In general, movement rehabilitation programs should benefit from the utilization of a formal model such as the Sigma and the Delta-Lognormal models for the analysis of rehabilitation progress and the development of automated neuromuscular characterization test.

However, it should be mentioned that the use of the lognormal models in this area have some limitations. There are some types of study where these models might not, in their current state of development, particularly well adapted for. These include studies concerned with work and energy (e.g. co-contraction, internal forces, joint stiffness study such as in (Gribble, Mullin, Cothros, & Mattar, 2003; Osu et al., 2002), the postural or tremor assessment, and the analysis of multiples simultaneous joints[8] (e.g. study of joint coordination as in (Levin, 1996)).

6.2 Modeling in Motor Rehabilitation

When possible, more formal modeling should be integrated to the various aspects of human movement rehabilitation. This should allow an easier automation of some of the testing and analysis procedures needed in the context of more decentralized rehabilitation cares and in the development of more versatile and robust evaluation techniques. Although it certainly may not and should not replace skilled therapists, it may alleviate some aspects of their work and provide them with a second and objective assessment of the neuromuscular system condition. Moreover, the classical and the automated tests may be used to cover different aspects of patient evaluation. For example, computerized motor evaluation seems more adequate for low level (e.g. characteristics of a given movement) and repetitive (e.g. daily) evaluation than a higher level (e.g. health-related quality of life or quality-adjusted life-year evaluation) and more complete assessment of the impact of a motor control disorder on the patient daily life.

[8] The trajectory of each effector may be analyzed by individual lognormal equations, but there is no specific support for the study of these equation interactions.

6.3 Conclusion and Future Works

This chapter has shown how the lognormal models may be used for the synthesis and the analysis of human movement. It has also presented the programs developed to work with these models in the context of human movement studies and for the development of neuromuscular tests used in the evaluation of motor performances during rehabilitation programs.

Future researches related to these topics include but are not limited to the improvement of the automatic modeling of human movement, the analysis of the characteristics of neuromuscular test based on a Sigma-Lognormal analysis and the development of additional features to ScriptStudio.

7. Appendix - Lognormal Movement Analysis

7.1 Parameter Extraction

Although the synthesis may be quite useful in the planning of trials, the sigma-lognormal representation of real human movements (i.e. extraction of lognormal parameters from movement kinematics signals) becomes a central topic during and after the experimentations because it is necessary to analyze in depth the collected data. However, this is a more involved process than the synthesis. In the following, a short overview of the theory used for parameter extraction is presented for the more general case, that is, for the sigma-lognormal representation of complex movements.[9]

The parameter extraction algorithm implemented so far is of a sequential nature.[10] The parameter extraction of a given component rely on three characteristics point of its velocity modulus which are its maximum point (p_3) and its two inflexion points (p_2 and p_4). Establishing a correspondence between their positions (i.e. their time occurrence (t_i) and their amplitude (v_{ti})) on the numerical signal and their corresponding values on a four-parameter (t_0, D, μ, σ) lognormal curve, we can develop a nonlinear and over determined system of six equations and four unknowns. Taking different subsets of four of the six equations results in different parameter estimations. Nine subsets are solvable with a closed-form solution, corresponding to the case where two amplitude equations and two time occurrence equations are considered. For these cases, the analytical expression of t_0, D and μ is the same regardless of the set of equation considered as describe in equation (8) to (10). However, the form of the σ expression depends on what amplitude equations are considered as stated in equation (11). The a_i variables in these equations are used only for simplification and their expression are given in (12). Note that they depend only on σ.

$$t_0 = t_i - e^{\mu} e^{-a_i} \tag{8}$$

[9] Although the delta-lognormal representation of a rapid pointing movement can be treated as a special case of the sigma-lognormal representation, works have been done especially on the parameter extraction for this particular case (Djioua & Plamondon, 2009). Therefore, if experimental data comes only from simple rapid pointing movements, this specialized extractor should be preferred.

[10] Even though this seems an appropriate strategy for a model that postulates sequential generation of neuromuscular components, some arguments toward a parallel strategy have been formulated (Rohrer & Hogan, 2003).

$$D = \sqrt{2\pi} v_{ti} \sigma \exp\left(\frac{a_i^2}{2\sigma^2} - a_i + \mu \right) \tag{9}$$

$$\mu = \ln\left(\frac{t_i - t_j}{e^{-a_i} - e^{-a_j}} \right) \tag{10}$$

$$\sigma = \begin{cases} \sqrt{-2 - 2\ln\left(\frac{v_{ti}}{v_{t3}}\right) - \left(2\ln\left(\frac{v_{ti}}{v_{t3}}\right)\right)^{-1}} & i \in \{2,4\} \\ \sqrt{2\sqrt{1 + \ln^2\left(\frac{v_{t4}}{v_{t2}}\right)} - 2} \end{cases} \tag{11}$$

$$a_2 = 1.5\sigma^2 + \sigma\sqrt{0.25\sigma^2 + 1} \tag{12. a}$$

$$a_3 = \sigma^2 \tag{12. b}$$

$$a_4 = 1.5\sigma^2 - \sigma\sqrt{0.25\sigma^2 + 1} \tag{12. c}$$

Representing the length of the path travelled (i.e. the time integrated modulus of the velocity) by the letter l, the angular variation of a single component is proportional to l (i.e. $\varphi(t) \propto l(t)$). Knowing the position of the points p_2, p_3 and p_4 along the straight line segment representing a component under the φ-l space, the starting point (p_1) and the ending point (p_5) can be extrapolate to obtain the value of θ_s and θ_e. Formally, these parameters may be computed by (13) and (14). Note that only the sign in the numerator of the last parenthesis changes in these two equations. Also, the expressions of the angular parameters depend only on the estimated value of σ and on the direction of the trajectory at the maximum and at the two inflexion points (i.e. φ_2, φ_3 and φ_4).

$$\theta_s = \phi_3 - (\phi_2 - \phi_4)\left(\frac{1 + erf\left(\frac{-a_3}{\sqrt{2}\sigma}\right)}{erf\left(\frac{-a_2}{\sqrt{2}\sigma}\right) - erf\left(\frac{-a_4}{\sqrt{2}\sigma}\right)} \right) \tag{13}$$

$$\theta_e = \phi_3 + (\phi_2 - \phi_4)\left(\frac{1 - erf\left(\frac{-a_3}{\sqrt{2}\sigma}\right)}{erf\left(\frac{-a_2}{\sqrt{2}\sigma}\right) - erf\left(\frac{-a_4}{\sqrt{2}\sigma}\right)} \right) \tag{14}$$

From these equations, nine different estimations can be made of the six parameters (t_0, D, μ, σ, θ_s, θ_e) of a component. Obtaining the velocity signals (v_x, v_y) as in (5) and computing its departure from the numerical velocity signals (v_{xn}, v_{yn}), the set of parameter which minimize the error of reconstruction (15) can be selected. This set of parameter may be used as a starting estimation to a nonlinear optimization algorithm to further enhance the solution.

$$e(t) = \int_{t_2}^{t_4} \left[\left(v_{xn}(t) - v_x(t)\right)^2 + \left(v_{yn}(t) - v_y(t)\right)^2 \right] dt \tag{15}$$

As mentioned earlier, the extraction process may be performed sequentially. In such a scheme, the first mode in the movement velocity signals would be extracted and its contribution removed from the original signals before extracting the next mode. Of course, many technical details have to be considered in building such an extractor and the reader is referred to (O'Reilly, C., & Plamondon, R. (2009a)) for a more complete treatment of this topic.

7.2 Typical Extraction Results

The figure 6 shows typical results for sigma-lognormal reconstruction of movements acquired from subjects performing the neuromuscular task described in section 4.2. The reconstructed movements (dashed lines) and the original movements (solid lines) are practically identical. This figure shows that the extractor has excellent performances on fast smooth movements (Fig. 6.a) as well then on slower and jerkier movements (Fig. 6.b). Parameter extractions may also be perform on much more complex motions such as handwritten signatures (O'Reilly, C., & Plamondon, R. (2009a)).

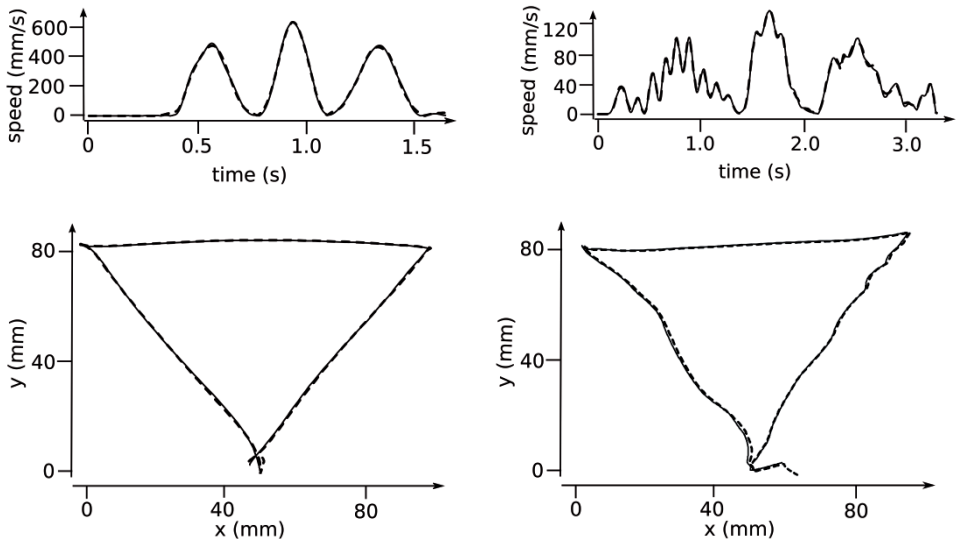

(a) (b)

Fig. 6. Automatic sigma-lognormal parameter extraction and reconstruction of real human movements. The solid lines show the original movements while dashed lines are used to display the sigma-lognormal reconstructions. (a) A fast movement performed by a healthy subject. (b) A much slower movement performed by a subject with a poor health condition.

8. References

Alimi, A., Plamondon, R., 1994. *Analysis of the Parameter Dependence of Handwriting Generation Models on Movements Characteristics*, In Advances in Handwriting and Drawing: A Multidisciplinary Approach, C. Faure, G. Lorette, A. Vinter, P. Keuss (Eds), Europia, Paris, 363-378.

Alimi, A. M. (1995). *Contribution au développement d'une théorie de génération de mouvements simples et rapides application au manuscrit.* École polytechnique de Montréal, Montréal.

Djioua, M. (2007). *Contributions à la généralisation, à la compréhension et à l'utilisation de la théorie cinématique dans l'analyse et la synthèse du mouvement humain.* Unpublished PhD thesis, École Polytechnique, Montréal.

Djioua, M., & Plamondon, R. (2003). *Relationship between Proportionality Law and Lognormality of a Coupled System Response.* Paper presented at the 11th Conference of the International Graphonomics Society (IGS2003), Scottsdale, Arisona, USA.

Djioua, M., & Plamondon, R. (2009). A new algorithm and system for the characterization of handwriting strokes with delta-lognormal parameters. IEEE *Trans Pattern Anal Mach Intell*, 31(11), 2060-2072.

Gribble, P. L., Mullin, L. I., Cothros, N., & Mattar, A. (2003). Role of cocontraction in arm movement accuracy. *Journal of Neurophysiology, 89*(5), 2396-2405.

Hakkennes, S., & Keating, J. L. (2005). Constraint-induced movement therapy following stroke: a systematic review of randomised controlled trials. *Aust J Physiother, 51*(4), 221-231.

Holden, M. K. (2005). Virtual environments for motor rehabilitation: Review. *Cyberpsychology & Behavior, 8*(3), 187-211.

Kisacanin, B., Agarwal, G. C., Taber, J., & Hier, D. (2000). Computerised evaluation of cognitive and motor function. *Medical & Biological Engineering & Computing, 38*(1), 68-73.

Kwakkel, G., Kollen, B. J., & Krebs, H. I. (2008). Effects of robot-assisted therapy on upper limb recovery after stroke: A systematic review. *Neurorehabilitation and Neural Repair, 22*(2), 111-121.

Landou, M. K. (2008). *Potentiels évoqués associés au temps d'occurrence du modèle Delta-Lognormal pour un mouvement volontaire induit.* Master thesis, École Polytechnique, Montréal.

Leduc, N., Plamondon, R. (2001). *A New Approach to Study Human Movements: The Three Dimensional Delta-Lognormal Model*, in Proc. 10th Biennial Conference of the International Graphonomics Society, (IGS' 2001), 6-8 august 2001, University of Nijmegen, The Netherlands, 98-102.

Levin, M. F. (1996). Interjoint coordination during pointing movements is disrupted in spastic hemiparesis. *Brain, 119 (Pt 1)*, 281-293.

McEwen, S. E., Huijbregts, M. P. J., Ryan, J. D., & Polatajko, H. J. (2009). Cognitive strategy use to enhance motor skill acquisition post-stroke: A critical review. *Brain Injury, 23*(4), 263-277.

O'Reilly, C., & Plamondon, R. (2007). *A software assistant for the design and analysis of neuromuscular tests.* Paper presented at the Biomedical Circuits and Systems Conference (BIOCAS 2007), 107-110.

O'Reilly, C., & Plamondon, R. (2009a). Development of a Sigma-Lognormal representation for on-line signatures. *Pattern Recognition, 42*(12), 163324-3337.

O'Reilly, C., & Plamondon, R. (2009b). *Sigma-Lognormal Analysis of a Complex Movements Neuromuscular Test.* Paper accepted for presentation at the 14th Conference of the International Graphonomics Society, Dijon, France.

Osu, R., Franklin, D. W., Kato, H., Gomi, H., Domen, K., Yoshioka, T., et al. (2002). Short- and long-term changes in joint co-contraction associated with motor learning as revealed from surface EMG. *Journal of Neurophysiology, 88*(2), 991-1004.

Patel, M., & Rudd, A. (2004). Evaluating the outcome of rehabilitation interventions. In N. Losseff (Ed.), *Neurological Rehabilitation of stroke* (pp. 67-88): Taylor & Francis.

Perry, J. (1990). Problems and Trends in Rehabilitation. In A. Cappozzo & N. Berme (Eds.), *Biomechanics of human movement : applications in rehabilitation, sports and ergonomics* (pp. 337-350). Worthington, Ohio: Bertec Corporation.

Plamondon, R. (1995). A kinematic theory of rapid human movements. Part II. Movement time and control. *Biol Cybern, 72*(4), 309-320.

Plamondon, R., & Alimi, A. M. (1997). Speed/accuracy trade-offs in target-directed movements. *Behavioral and Brain Sciences, 20*(2), 279-349.

Plamondon, R. (1998). A kinematic theory of rapid human movements: Part III. Kinetic outcomes. *Biol Cybern*, 78(2), 133-145.

Plamondon, R., Feng, C. H., & Woch, A. (2003). A kinematic theory of rapid human movement. Part IV: a formal mathematical proof and new insights. *Biological Cybernetics, 89*(2), 126-138.

Riener, R., Nef, T., & Colombo, G. (2005). Robot-aided neurorehabilitation of the upper extremities. . *Medical & Biological Engineering & Computing, 43*(1), 2-10.

Rohrer, B., Fasoli, S., Krebs, H. I., Hughes, R., Volpe, B., Frontera, W. R., et al. (2002). Movement smoothness changes during stroke recovery. *J Neurosci, 22*(18), 8297-8304.

Rohrer, B., Fasoli, S., Krebs, H. I., Volpe, B., Frontera, W. R., Stein, J., et al. (2004). Submovements grow larger, fewer, and more blended during stroke recovery. *Motor Control, 8*(4), 472-483.

Rohrer, B., & Hogan, N. (2003). Avoiding spurious submovement decompositions: a globally optimal algorithm. *Biol Cybern, 89*(3), 190-199.

Rothstein, J. M., Roy, S. H., Wolf, S. L., & Scalzitti, D. (2005). *The rehabilitation specialist's handbook - 3rd ed.*: F. A. Davis Company.

Sheffler, L. R., & Chae, J. (2007). Neuromuscular electrical stimulation in neurorehabilitation. *Muscle Nerve, 35*(5), 562-590.

Winter, D. A. (2005). *Biomechanics and motor control of human movement* (3rd ed.). Hoboken, New Jersey: Wiley.

Woch, A. (2006). *Étude des primitives bidirectionnelles du mouvement dans le cadre de la théorie cinématique : confirmation expérimentale du modèle delta-lognormal.* PhD thesis, École Polytechnique, Montréal.

Zhou, H. Y., & Hu, H. S. (2008). Human motion tracking for rehabilitation-A survey. *Biomedical Signal Processing and Control, 3*(1), 1-18.

11

Quantitative Evaluation Methods of Therapeutic Effects of Sanding Training in Patients with Hemiplegia

Yoshifumi Morita and Hiroyuki Ukai
Nagoya Institute of Technology
Japan

1. Introduction

In the year 2013, the percentage of elderly people is forecasted to be 25 percent of the total population in Japan. Moreover, the number of elderly people who have a disease or a physical disability is increasing. So, the need of new rehabilitation methods and systems having high therapeutic effect is also increasing.
For this reason many rehabilitation support systems and robots have been developed for upper limbs (Kerbs et al., 1998, Reinkensmeyer, et al., 2000, Jezernik et al., 2003, Colombo et al., 2005, Furusho et al., 2005, Furusho et al., 2007, Kikuchi et al., 2007, Beer et al., 2008). The advantage using the robots and the systems are that the patients can perform effective rehabilitation trainings and the therapeutic effect can be evaluated quantitatively.
We also have developed a rehabilitation support system for various resistance trainings of upper limb motor function as shown in Fig. 1 (Morita et al., 2007a, Morita et al., 2009). This system supports the occupational therapy for recovering physical functions. This system equipped with the teaching/guided function for personalized rehabilitation. The teaching/guided function enables the therapists to easily make not only training trajectories but also training programs to suit the individual needs of the patients. Moreover, we have proposed a quantitative evaluation method of the therapeutic effect of sanding training (Morita et al., 2007b, Morita et al., 2008). This method is used to evaluate the cooperative movement of forearm and upper arm that is one of the therapeutic effects. In the future the final aims of our research are to quantitatively evaluate the therapeutic effect of upper limb motor function during the training from the standpoint of the establishment of EBM (Evidenced Based Medicine) and to develop a new rehabilitation training support system with the quantitative evaluation function of therapeutic effect.
In this chapter three kinds of evaluation methods of upper limbs during sanding training are proposed. These evaluation methods are used to evaluate the achievement level of sanding training, the cooperative movement of healthy and paralyzed arms, and the cooperative movement of forearm and upper arm. In order to verify the effectiveness of the proposed methods, we measure the upper limb motion of healthy people and patients with hemiplegia during the sanding training by using Shape Tape and the force/torque sensor. Then we examine the validities of the proposed evaluation methods using the patients' data, and the relationship between the evaluation results and the Brunnstrom Stage.

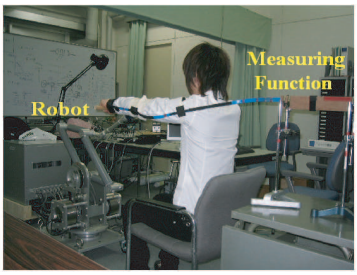

Fig. 1. 3-Dimensional rehabilitation training robot for upper limbs with measuring function

Fig. 2. Conventional sanding training tool

2. Sanding training and measurement

2.1 Measurement of upper limb motion during sanding training

Sanding training, which is one type of resistance training for upper limbs widely performed in occupational therapy in Japan. This training is usually performed using a sanding training tool as shown in Fig. 2. This training is performed for ROM (range of motion) training of joints, muscular reinforcement of upper limbs, improvement of the cooperative movement between flexor muscles and extensor muscles, endurance training and so on.

We evaluate the therapeutic effects of the sanding training by using the data acquired during the sanding training. For this purpose we use two kinds of sensors, namely the 6-axes force/torque sensor (NITTA CORPORATION, IFS-67M25A 15-I 40) and Shape Tape (Measurand Inc.).

As shown in Fig. 3(a), the force/torque sensor is attached to the conventional sanding training tool in order to measure the force and torque exerted by patients. The sensor signal is acquired using a personal computer with the sampling frequency 1[kHz].

By using Shape Tape, we measure the 3-dimensional positions of the wrist, elbow and shoulder joints of the upper limb during the sanding training. In the coordinate system of measurement, let the X, Y and Z axes be horizontal, right-left directions and vertical, respectively as shown in Fig. 3(b). The sampling frequency is 100[Hz]. The measuring points are the styloid process of ulna, olecranon and acromion as shown in Fig. 3(a).

The subjects are ten healthy male students who are between 22 and 25 years old and fifteen patients with hemiplegia. All the healthy persons are right-handed. All patients have one paralyzed arm and one healthy arm. The Brunnstrom Stages (Br.stages) of all the patients are from I to VI. Br.stage I score is the highest of paralysis. Br.stage VI score is the lowest of

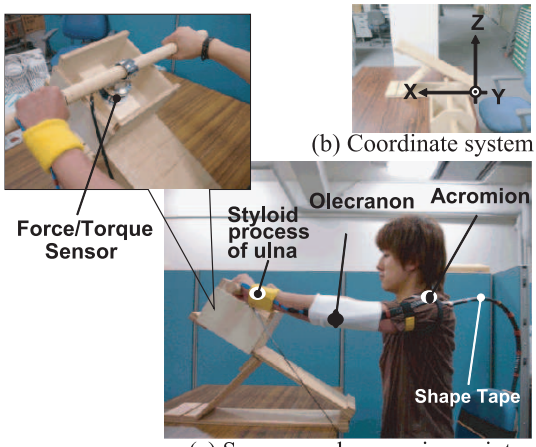

(b) Coordinate system

(a) Sensors and measuring points

Fig. 3. Measurement system

Fig. 4. Sanding training and clinical measurement

paralysis. In the case of patients, Shape Tape is attached to their paralyzed arm as shown in Fig. 4. In the case of healthy persons, Shape Tape is attached to their right arm. All subjects perform the sanding training for 25[sec].

As shown in Fig. 4, the subject takes a seat, holds the grips of the sanding tool with both hands and moves the grips up and down on the slope. If the subject cannot grasp the grip by himself/herself, the subject's hand is fixed to the grip. The range of movement of training is 40cm. The angle of the tilting rotary board is 20[deg]. The therapist chose the loads of training according to the patient's ability from among no weight, 1[Kg] and 2[kg] weight and the angle of inclination of 0[deg], 10[deg] and 20[deg]. The healthy persons performed four cases, namely no weight–10[deg], no weight–20[deg], 2[kg]–10[deg] and 2[kg]–20[deg].

2.2 Measurement data and consideration

For example the time histories of the measured data of a patient of Br.stage II and a healthy person during the sanding training are shown in Fig. 5 and 6. Fig. 5 and 6 show the joint positions of the X axis, the joint velocities of the X axis, the forces of the X, Y and Z axes, and the rotational moment torque of the grip. The joint velocities are obtained by differentiating the joint positions. The conditions of the loads of training are without a weight and the angle of inclination of 10[deg].

The followings are found from the results of the healthy person in Fig. 5. The time necessary for an alternating motion is about 3.0[sec]. The force is large in the upward motion as compared with the downward motion, because the subjects utilize the gravity force in the downward motion. Among the three joint velocities, the amplitude of the wrist joint velocity is large. The shape of the wrist and elbow joint velocities is almost the same. But the shoulder joint velocity is different from them. In the upward motion the shoulder movement starts after the wrist and elbow movements. In the downward motion the shoulder movement finishes before the wrist and elbow movements. This kind of motion can be found in the motion of all the healthy persons. Therefore the characteristic of cooperative movement of upper arm and forearm is found from the three joint velocities.

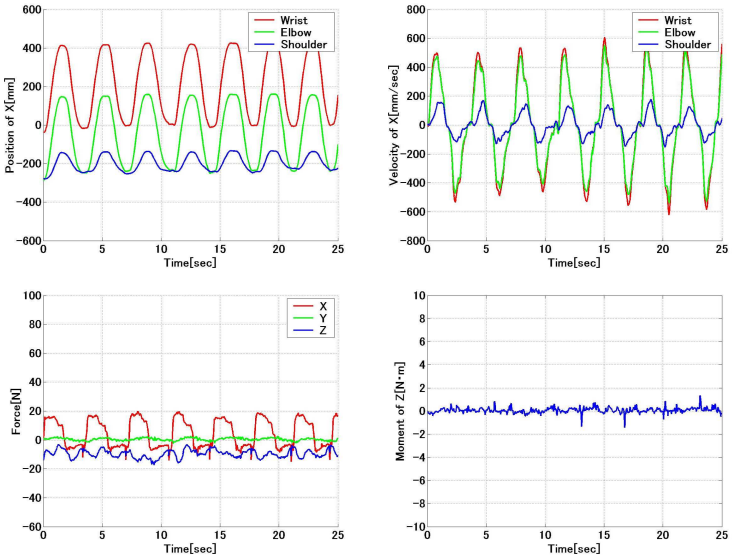

Fig. 5. Time histories of measured data of healthy person during sanding training.

The followings are found from the results of the patient in Fig. 6. It is seen from the time histories of the joint positions and velocities that the motion of upper limbs of the patient is small and the patient can hardly perform the sanding training. The cooperative movement of an upper arm and a forearm found in the motion of a healthy person cannot be found. When a patient with hemiplegia performs the sanding training, the healthy arm pushes the sanding tool and the paralyzed arm is moved along with the healthy arm. In this case the z axis component of the rotational moment torques occurs as shown in Fig. 6, which is called the moment in this chapter. Then the friction between the mover and the board of sanding tool becomes larger due to the moment. Therefore the sanding training becomes more difficult. On the other hand, in the case of healthy persons the measurement of moment is almost zero. The cooperative movement of both arms found in the motion of a healthy person cannot be found in the patient's motion. Therefore the cooperative movement between the healthy upper limb and the paralyzed upper limb of a patient with motor hemiplegia can be evaluated from the measured moment.

3. Evaluation methods and their verification using patients' data

The therapeutic effect of the sanding training can be evaluated quantitatively by analyzing the difference between a healthy person and a patient. In this chapter three kinds of evaluation methods for (1) Achievement level of sanding training, (2) Cooperative movement of healthy and paralyzed arms, and (3) Cooperative movement of forearm and upper arm of the paralyzed arm are proposed.

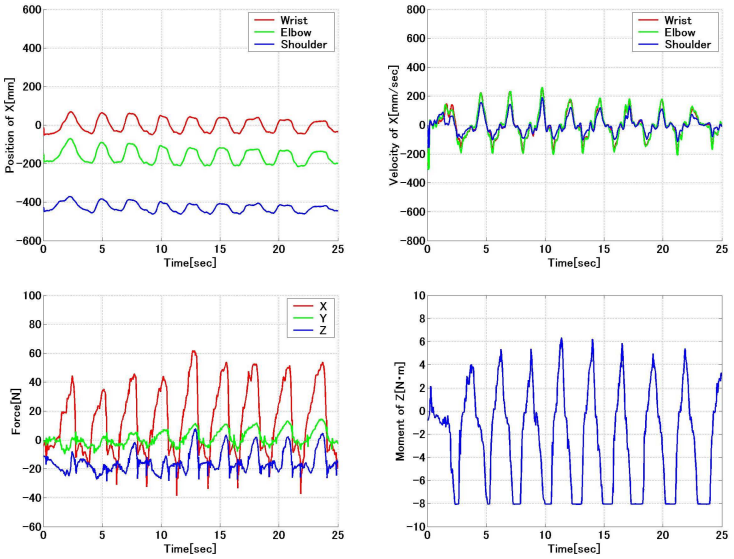

Fig. 6. Time histories of measured data of patient during sanding training.

3.1 Achievement level of sanding training

In order to evaluate the therapeutic effect of the sanding training, the moved distance, the time required for a round trip, the number of round trips per the specified time and so on have been used. In this chapter a new evaluation method is proposed by calculating the three kinds of evaluation indices, namely the moved distance, the time required for a round trip and the number of round trips per 25[sec], from the measurement data and using the classification charts of Fig. 7. The threshold values between healthy persons and patients are determined from the healthy persons' data. The therapeutic effect is evaluated in 5 levels from A to E. Level A is the highest achievement. All the healthy persons are classified in level A. Level E is the lowest achievement. This evaluation index is called achievement level of sanding training. The achievement levels of the fifteen patients and the ten healthy persons are plotted in Fig. 7. The relationship between the achievement level and the Brunnstrom Stage is investigated. The results are shown in Fig. 8. The dashed curve denotes the curve for second order approximation. Although the patient of Br.stage I can not move the paralyzed arm, the patient can perform the sanding training by using only the healthy arm. It is similar to the sanding motion of a healthy person. The paralyzed arm of the patient of Br.stages II and III moves involuntary due to associated movement and stereotyped of motor synergy. So, the patient can not perform the sanding training smoothly, because the paralyzed arm disturbs the smooth motion. Consequently, in the case of Br.stages I, IV, V and VI, the achievement level is high, and in the case of Br.stages II and III, the achievement level is low.

3.2 Cooperative movement of healthy and paralyzed arms

The quantitative evaluation method is proposed for the characteristic of cooperative movement of healthy and paralyzed arms. In the case of a patient with a right paralyzed arm, the

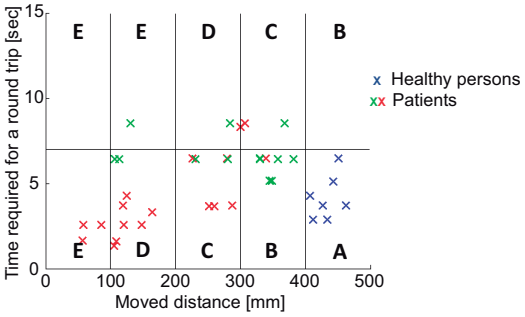

(a) More than 3 round trips per 25[sec]

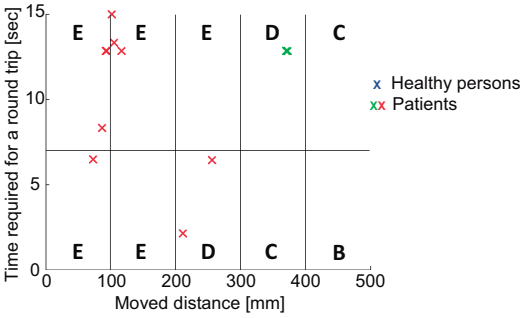

(b) Less than 3 round trips per 25[sec]

Fig. 7. Achievement level

left healthy arm mainly pushes the sanding tool. In the case of a patient with a left paralyzed arm, the right healthy arm mainly pushes the sanding tool. In order to evaluate the cooperative movement of the healthy and paralyzed arms, we measure the moment. The relationship between the peak value of the moment and the Brunnstrom stage are shown in Fig. 9. The higher the level of the paralysis is, the larger the measurement of the moment is. The two dashed lines denote the lines for first order approximation. It is found from Fig. 9 the plus and minus peak values of the moment correspond to the left hemiplegia and the right hemiplegia, respectively. Consequently the cooperative movement of healthy and paralyzed arms can be evaluated using the peak value of the moment.

3.3 Cooperative movement of forearm and upper arm

The quantitative evaluation method is proposed for the characteristic of cooperative movement of forearm and upper arm. The therapeutic effect is evaluated by comparing healthy persons' models with the patient's data. The healthy persons' models are constructed by using the NN (Neural Network) modeling approach(Morita, 2006a).

3.3.1 Evaluation method using Neural Network

The characteristic of cooperative movement of forearm and upper arm of healthy persons is modeled using NN. The three joint velocities of a healthy person are plotted in a 3-dimensional

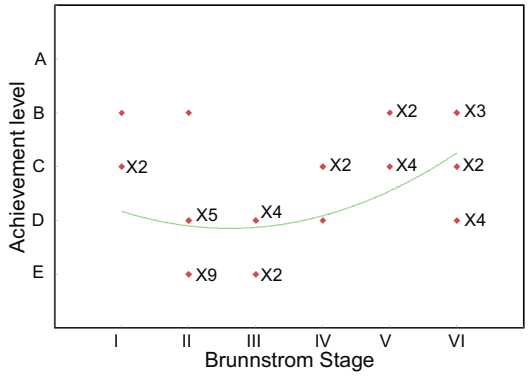

Fig. 8. Relationship between achievement level and Br.stages

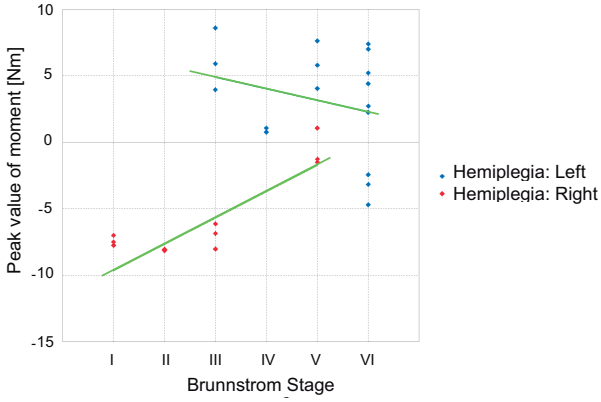

Fig. 9. Relationship between peak value of moment and Brunnstrom stage

phase space as shown in Fig. 10. The mutual relation of the velocities is seen in Fig. 10, as mentioned in Section 2.2.

The structure of NN shown in Fig. 11 is used, where the input signals are the X axis components $(v_W(k), v_E(k))$ of velocities of the wrist and elbow joints, and the output signal is the X axis component $v_S(k)$ of velocities of the shoulder joint. It is important to determine the inputs and outputs. These inputs and the output are determined by comparing the results of all other cases. For example the wrist and shoulder joints are used as input signals and the elbow joint is used as an output signal. The number of the inner layer is one, and the number of neurons is 100.

Since there are individual differences in upper limb motion, it is difficult to model the cooperative movement with only one model. So, the ten healthy persons are classified in two groups on the basis of the individual differences. For this purpose the NN modeling technique and the cluster analysis are used. The dendrogram is obtained as shown in Fig. 12. The horizontal

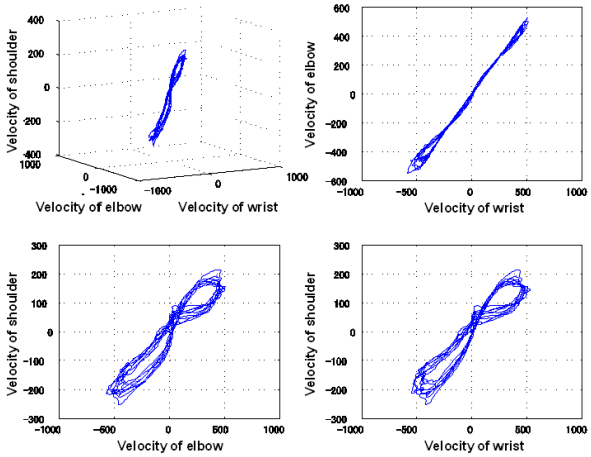

Fig. 10. Joint velocities in 3-Dimensional phase space

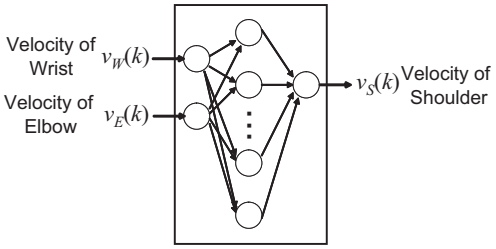

Fig. 11. Structure of neural network

axis is the subject number. The vertical axis is the MSE. The dendrogram shows the similarity between subjects or a subject and subject group. For example, Subject 6 is similar to Subject 10 in upper limb motion. And the group of Subjects 2, 3, 7 and 9 is similar to the group of Subjects 4 and 5. In this study the MSE of 0.015 is used as the threshold of discrimination. As a result, all the subjects are classified into two groups.

Moreover, some patients are not able to move the sanding tool the maximum distance of 40[cm]. So we prepare models of 40[cm] and 20[cm]. We choose one model from the models of 40[cm] and 20[cm] owing to the moved distance performed by a patient.

The difference of the two groups is investigated. We found from the time histories of joint velocities of all subjects that the two groups differ in the amount of shoulder movement in both the cases of the moved distance of 40[cm] and 20[cm]. In one group, the amount of shoulder movement is large, which is called Group 1 and Group 4 in the cases of the moved distance of 40[cm] and 20[cm], respectively. In the other group, the amount of shoulder movement is small, which is called Group 2 and Group 3 in the cases of the moved distance of 40[cm] and 20[cm], respectively. Models 1 to 4 are constructed using the data of Groups 1 to 4, respectively. By using four types of healthy persons' models and by comparing them with the patient's data we can evaluate the therapeutic effect.

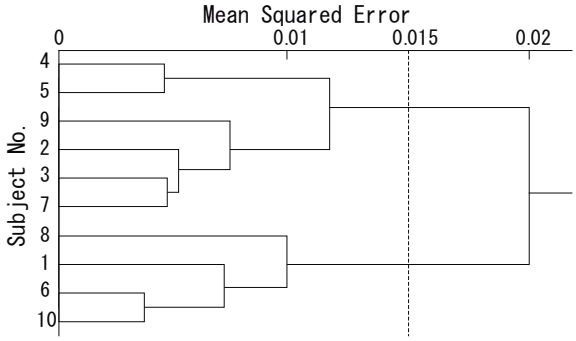

Fig. 12. Dendorogram

The quantitative evaluation method for therapeutic effect of cooperative movement is proposed on the basis of Models 1 to 4 as shown in Fig. 13. The procedure is as follows;
Step 1: The models of 40[cm] or 20[cm] is chosen owing to the moved distance performed by a patient, namely Model 1 and 2 in the case of the moved distance of 40[cm] or Model 3 and 4 in the case of the moved distance of 20[cm].
Step 2: The data of the velocities of wrist and elbow joints of a patient is input to the models chosen in Step 1. The two errors of the velocities of shoulder joint of a patient are output from the two models. The errors, namely $\bar{e}_1$ and $\bar{e}_2$ in the case of the moved distance of 40[cm] or $\bar{e}_3$ and $\bar{e}_4$ in the case of the moved distance of 20[cm] are evaluated using the Mean Squared Error(MSE). The MSE is calculated by

$$\bar{e}_i = \sqrt{\frac{1}{N}\sum_{k=1}^{N} e_i^2(k)}, \quad (i = 1, 2 \text{ or } 3, 4), \tag{1}$$

where $e_i(k) = \hat{v}_{Si}(k) - v_S(k)$, $(i = 1, \cdots, 4)$, N is the number of measured data.
Step 3: The data ($\bar{e}_1$, $\bar{e}_2$) or ($\bar{e}_3$, $\bar{e}_4$) is plotted in the $\bar{e}_1$-$\bar{e}_2$ plane or the $\bar{e}_3$-$\bar{e}_4$ plane, respectively as the quantitative evaluation score.
The data of the ten healthy persons is analyzed. The scores $(\bar{e}_1, \bar{e}_2)$ and $(\bar{e}_3, \bar{e}_4)$ are calculated by applying each subject's data to Models 1, 2, 3 and 4, respectively. The scores $(\bar{e}_1, \bar{e}_2)$ and $(\bar{e}_3, \bar{e}_4)$ of all the subjects are plotted in the $\bar{e}_1$–$\bar{e}_2$ plane and the $\bar{e}_3$–$\bar{e}_4$ plane as shown in Figs. 14 and 15, respectively. The blue marks denote the results of healthy persons. The blue lines denote the threshold between the patients and the healthy persons.
It is seen in Fig. 14 that the marks of healthy persons are in the region ($\bar{e}_1 > 0.006$ and $\bar{e}_2 < 0.006$) and the region ($\bar{e}_1 < 0.006$ and $\bar{e}_2 > 0.006$). The former region contains the subject with short shoulder movement. The latter region contains the subject with large shoulder movement. The similar results are seen in Fig. 15. When the moved distance is smaller, a decreasing tendency is seen in the shoulder movement.

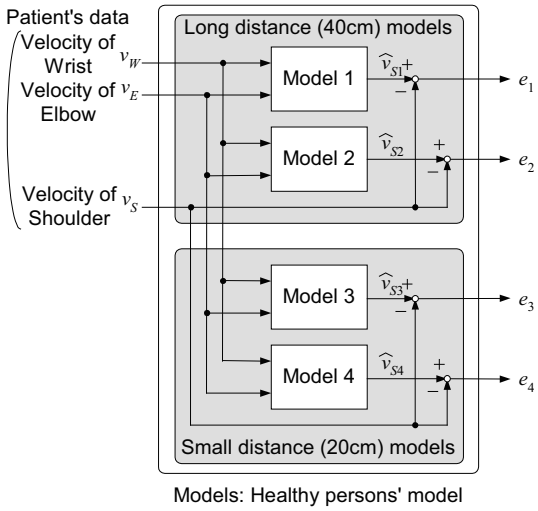

Fig. 13. Block diagram of quantitative evaluation method

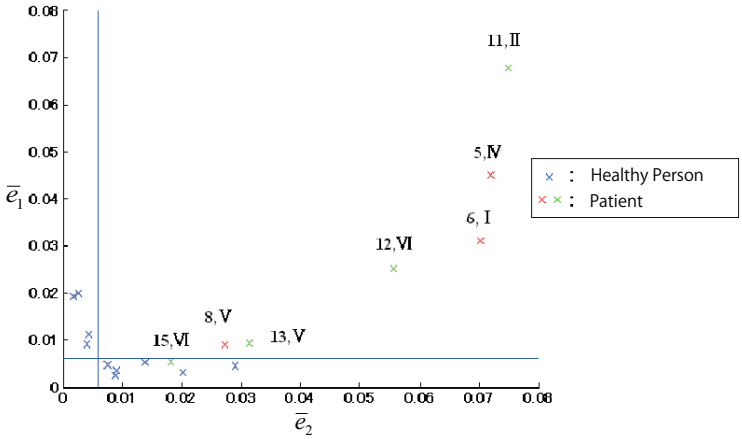

Fig. 14. Distribution charts of quantitative evaluation scores (Moved distance: 40[cm])

3.3.2 Verification of the proposed method using patients' data

Only the data of the achievement level A through D is applied to the proposed evaluation method. The conditions of the loads of training are without a weight and an angle of inclination is 10[deg].

The models of 20[cm] or 40[cm] are chosen owing to the moved distance performed by a patient. The scores of the patients that moved the sanding tool around 40cm and 20cm are plotted in Figs. 14 and 15, respectively. The cardinal number on the left is the patient number.

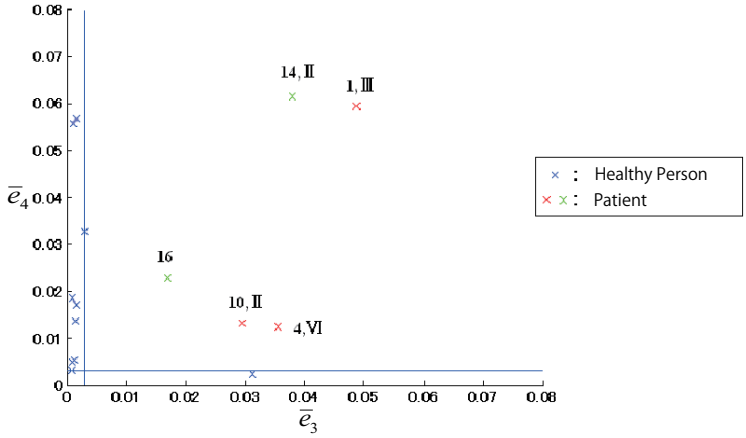

Fig. 15. Distribution charts of quantitative evaluation scores (Moved distance: 20[cm])

The Roman number on the right is the stage number of Brunnstrom stage. The red and green marks denote the results of the patients measured on 5 June, 2007 and 7 November, 2007, respectively. Patient 6 and patient 11 are the same person. The Br.stage of Patient 6 increases from 1 to 2 after performing the sanding training for 5 months. It is seen from Figs. 14 and 15 that the marks of all the patients are out of the region of healthy persons. This implies that the movement of all the patients is different from that of a healthy person. It is seen from Fig. 14 that the marks of the patients 8, 13 and 15 are close to the region of healthy persons. This implies that the movement of the patients 8, 13 and 15 is similar to that of a healthy person.
The relationship between the quantitative evaluation scores $\bar{e}_1$ through $\bar{e}_4$ and Br.stages is examined. The marks of the patients of Br.stage I are close to the region of healthy persons in Fig. 14, because muscle contraction and involuntary motion do not occur on the paralyzed arm, and only the healthy arm can move the sanding tool smoothly. The marks of the patients of Br.stages II and III are far from the region of healthy persons in Fig. 14 or are plotted in Fig. 15, because involuntary motion due to associated movement and stereotyped of motor synergy occur on the paralyzed arm, and the patient can not move the sanding tool smoothly. The marks of the patients of Br.stages IV, V and VI are plotted in Fig. 14. Some of them are close to the region of healthy persons.
Consequently the followings are suggested. By observing the mark for its change with time in the distribution chart, the effect of training can be found. The patients need to do rehabilitation training so that the personal mark approaches the region of healthy persons. Moreover, the proposed evaluation method can be used to evaluate recovery.

4. Conclusions

In order to evaluate the therapeutic effects of sanding training, we proposed three quantitative evaluation methods for the achievement level, the cooperative movement of the healthy and paralyzed arms and the cooperative movement of the upper arm and forearm. The validities of the proposed methods are confirmed by applying the patients' data to them. Moreover, the relationships between the evaluation results and the Brunnstrom stage were examined. It

is suggested that the proposed evaluation methods can be used to evaluate recovery in the sanding training.
The future works are to install the proposed evaluation methods to the rehabilitation training support robot(8), and to perform the clinical demonstrations using the proposed system in cooperation with medical facilities.

Acknowledgments

This clinical measurement was supported by the physical therapists in the department of rehabilitation at Kunitomi Gastrointestinal Hospital in Japan.

5. References

[1] Krebs, H. I.; Hogan, N., Aisen, M. L. & Volpe, B. T. (1998). Robot-Aided Neurorehabilitation, *IEEE Trans. on Rehabilitation Engineering*, Vol.6, No.1, pp.75-87

[2] Furusho, J.; Koyanagi, K., Imada, Y., Fujii, Y., Nakanishi, K., Domen, K., Miyakoshi, K., Ryu, U., Takenaka, S. & Inoue, A. (2005). A 3-D Rehabilitation System for Upper Limbs Developed in a 5-year NEDO Project and Its Clinical Testing *Procs of the 2005 IEEE 9th Int. Conf. on Rehabilitation Robotics (ICORR2005)*, pp.53-56

[3] Furusho, J.; Kikuchi, T., Oda, K., Ohyama, Y., Morita, T., Shichi, N., Jin, Y. & Inoue, A. (2007). A 6-DOF Rehabilitation Support System for Upper Limbs including Wrists "Robotherapist" with Physical Therapy", *Procs of the 2007 IEEE 10th Int. Conf. on Rehabilitation Robotics (ICORR2007)*, pp.304-309

[4] Kikuchi, T.; Xinghao, H., Fukushima, K., Oda, K., Furusho J. & Inoue, A. (2007). Quasi-3-DOF Rehabilitation System for Upper Limbs: Its Force-Feedback Mechanism and Software for Rehabilitation, *Procs of the 2007 IEEE 10th Int. Conf. on Rehabilitation Robotics (ICORR2007)*, pp.24-27

[5] Colombo, R.; Pisano, F., Micera, S., Mazzone, A., Delconte, C., Carrozza, M. C., Dario P. & Minuco, G. (2005). Upper Limb Rehabilitation and Evaluation of Stroke Patients Using Robot-Aided Techniques, *Procs of the 2005 IEEE 9th Int. Conf. on Rehabilitation Robotics (ICORR2005)*, pp.515-518

[6] Beer, R. F.; Naujokas, C., Bachrach, B. & Mayhew, D. (2008). Development and Evaluation of a Gravity Compensated Training Environment for Robotic Rehabilitation of Post-Stroke Reaching, *Proc. of the second IEEE/RAS-EMBS International Conference on Biomedical Robotics and Biomechatronics (BioRob 2008)*, pp.205-210

[7] Morita, Y.; Kakami, H., Ukai, H. & Kando, H. (2006). Discrimination of Old/Young Persons from Acceleration Data during Walking based on Neural Networks, *Systems and Computers in Japan*, Vol.37, No.4, pp.1-10

[8] Morita, Y.; Hirose, A., Uno, T., Uchida, M., Ukai, H. & Matsui, N. (2007a). Development of Rehabilitation Training Support System using 3D Force Display Robot, *Robot Motion and Control 2007 (Lecture Notes in Control and Information Sciences, Vol. 360)*, Krzysztof Kozlowski(Ed.), pp. 303-310, Springer, ISBN: 9781846289736, Europe

[9] Morita, Y.; Yamamoto, T., Tanioku, R., Uchida, M., Ukai, H. & Matsui, N. (2007b). Analysis and Modeling of Upper Limb Motion during Sanding Training, *Procs. of Int. Conf. on Control, Automation and Systems 2007 (ICCAS2007)*, pp.1585–1590

[10] Morita, Y., Tanioku, R., Horie, T., Uchida, M., Ukai, H. & Matsui, N. (2008b). Study on Quantitative Evaluation Methods of Therapeutic Effects of Sanding Training, *Procs. of Int. Conf. on Control, Automation and Systems 2008 (ICCAS2008)*, pp.913–918

[11] Morita, Y., Tanioku, R., Horie, T., Uchida, M., Ukai, H. & Matsui, N. (2008). Study on Quantitative Evaluation Methods of Therapeutic Effects of Sanding Training, *Procs. of Int. Conf. on Control, Automation and Systems 2008 (ICCAS2008)*, pp.913–918

[12] Morita, Y., Nagasaki, M., Ukai, H., Matsui, N. & Uchida, M. (2009). Development of rehabilitation training support system of upper limb motor function for personalized rehabilitation, *Procs. of the 2008 IEEE Int. Conf. on Robotics and Biomimetics (ROBIO2008)*, pp.300–305

[13] Reinkensmeyer, J.D.; Takahashi, D.C., Timoszyk, K.W., Reinkensmeyer, N.A. & Kahn, E.L. (2000). Desigan of robot assistance for arm movement therapy following stroke, *Advanced robotics : the international journal of the Robotics Society of Japan*, Vo.14, No.7, pp.625-637

[14] Jezernik, S.; Colombo, G., Keller, T., Frueh, H. & Morari, M. (2003). Robotic Orthosis Lokomat: A rehabilitation and Research tool, *Neuromodulation*, Vol.6, Issue 2, pp.108-115, Published Online

12

Quasi-3 DOF Rehabilitation System for Upper Limbs, "PLEMO"

Takehito Kikuchi and Junji Furusho
Osaka University
Japan

1. Introduction

The increasing numbers of the aged people and their physical deteriorations have become one of the most serious problems in many countries. Many stroke patients suffer from disabilities which restrict normal motions, e.g., locomotion, reaching, pointing and so on. Therefore, sufficient rehabilitative training is necessary for such patients. In general, therapists make rehabilitation programs based on their inspections and measurements of each patient. However, it is difficult to adopt appropriate rehabilitative programs for all patients, because the evaluation method is based on experiences of each therapist.

Nowadays, Evidence Based Medicine (EBM) is strongly required in the field of rehabilitation (Miyai et al, 2002). Therefore, rehabilitation systems using robotics technologies are expected for; 1) quantification of the effect of the rehabilitative training; 2) enhancement of the motivation for patients with creating new training methods (many patients are giving up rehabilitative training because of its boredom); 3) improvement of the efficiency of physical therapist's works.

Many robot systems for upper limbs rehabilitation have been suggested by researchers all over the world (Krebs et al., 2000; Loureiro & Harwin, 2007, Lum et al., 2004; Zhang et al., 2007; Perry et al., 2007; Wolbracht et al., 2006; Nef et al., 2007), and clinical tests have been conducted. Krebs et al. (Krebs et al., 2000) developed MANUS system, which has two degrees of freedom (DOF) for active control of force-feedback, and conducted clinical tests of exercises for shoulders and elbows. Many movements in daily activities, however, need to move arms in a vertical direction. Therefore, a system which enables exercise in three dimensions is effective for upper limbs training. Actually, in a sanding-training (woodworking as sanding long boards shown in Fig.1) (Trombly, 1982), which is one of the clinical training in the occupational therapy, the inclination of the sanding board can be adjusted. Patients tries to push up the sander higher and higher which provide some stretch to extensor muscles of the arm. Because the range of motion or muscles used in the training are different depending on the inclination, the therapists can gradually change the inclination as the patient improves.

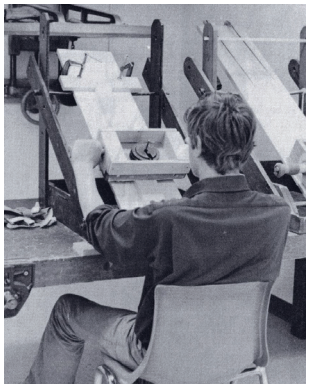

Fig. 1. Sanding on an inclined plane (Trombly, 1982)

Although the MIME system (Lum et al., 2004) using PUMA-560 by VA and Stanford Univ. can perform three-dimensional training, the PUMA-560 is the robot originally developed for industrial use and not safe for human-interactive use.
In a current research, we developed 3-DOF rehabilitation system for upper limb "EMUL" (Furusho et al., 2005) and conducted clinical tests with several kinds of video game (Furusho & Kikuchi, 2007). "EMUL" adopted to use ER actuators (Furusho & Sakaguchi, 1999) and clutch mechanism as its actuation part. This mechanism makes EMUL so safe and back-drivable. However, EMUL has disadvantages in cost or ease of maintenance, because this system was enlarged to realize force-feedback in large 3-D space. Practical systems should be required to be more compact and better for maintenance.
To meet these demands above, we developed a new haptic device which has 2-DOF force-feedback function in working plane but its inclined angle of the working plane can be adjusted. We named this system "Quasi-3-DOF Rehabilitation System for Upper Limbs" or "PLEMO". PLEMO was developed to realize quantitative evaluation of rehabilitation training for hemiplegic patients or elderly persons. In this chapter, history, basic structure, properties, experimental results of clinical test and future works on PLEMO are presented.

2. History

In the Virtual Reality 2001 Conference, Sakaguchi et al. (Sakaguchi et al., 2001) presented a passive force display using ER brakes. By using ER brakes, which have quick response, low moment of inertia and good controllability of brake torque, the developed 2 DOF haptic device (Fig.2) has good properties as haptic devices. Passive force displays is inherently safe because it doesn't move actively.
By utilizing these good properties, i.e. safety and good controllability, we designed first prototype of passive force display for upper limbs rehabilitation with the quasi-3DOF configuration (Fig.3). This machine has two controllable DOFs in a working plane (working table) and one adjustable DOF for the inclined angle of the working plane. Haptic control is based on the passive haptic control with ER brakes. We can adjust the angle of the table depending on the training direction for patients. This configuration becomes a basic of the PLEMO mentioned following section.

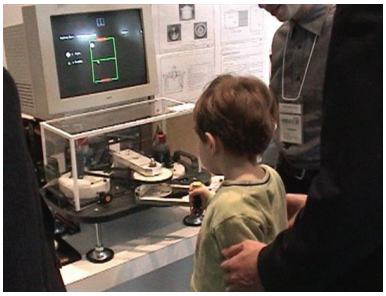

Fig. 2. Passive force display using ER brakes [14]

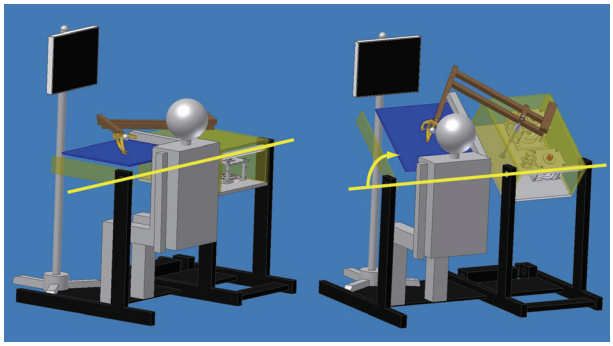

Fig. 3. Quasi-3-DOF configuration: Horizontal state (left) and inclined state (right)

3. Core technology

3.1 ER Fluid

ER fluid is a fluid whose rheological properties can be changed by applying an electrical field (Winslow, 1949). By using the ER fluid as a working fluid, we can construct electrically controllable brake (ER brake) with high-performance (quick response and good repeatability of brake torque) (Kikuchi et al., 2003). We used this brake for force generators of a new rehabilitation system (force-feedback system).

3.2 ER Brake

Figure 4 shows a basic structure of a cylindrical-type ER brake. It consists of fixed cylinders and rotating cylinders with the ER fluid between them. These two cylinders also play the role of a pair of electrodes. The rotating cylinder is fixed to the output shaft and driven by external forces through this shaft. When a voltage is applied between the pair of cylinders, the electric field is generated within the ER fluid, and then the viscosity of the fluid increases. This increase of viscosity generates the braking torque and reduces the rotational speed.

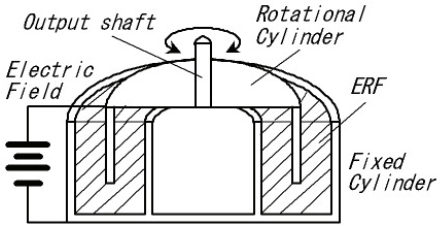

Fig. 4. Basic structure of ER Brake

Figure 5 shows a sectional view and an appearance of the ER brake used in this chapter. As shown in the left hand of Fig.5, this brake consists of multi-layered disks. ER fluid is filled between these rotor-disks and stator-disks. As a result, six layers of ER fluid generate the brake torque with change of the fluid. Piston mechanism in this structure works for the prevention of liquid leakage depending on expansion of the fluid.

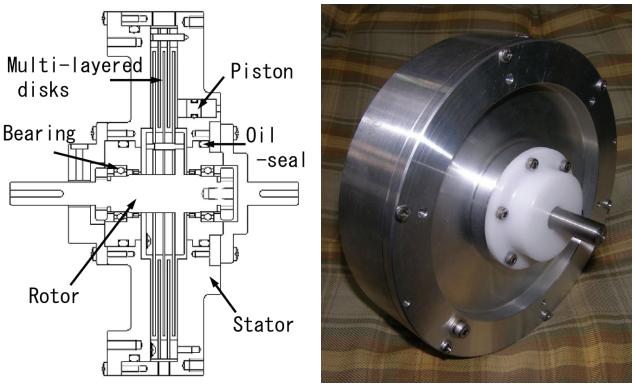

Fig. 5. ER Brake: Sectional view (left) and picture (right)

Table 1 shows basic characteristics of the ER brake. We can control the brake torque from 0.1 Nm to 4.0 Nm with the electric field from 0.0 kV/mm to 3.0 kV/mm, respectively.

Total weight	2.3 kg
Diameter	15cm
Height	4cm
Maximum brake torque	4.0Nm (at 3.0kV/mm applied)
Idling torque	0.1Nm (at 0.0kV/mm applied)
Num. of rotor disks	3
Disk gap	1mm
Time constant of response	2~3 msec

Table 1. Basic characteristics of ER brake

Left hand of the Fig.6 shows a step response of the ER brake. In this figure, a solid line is the torque response of the ER brake, and a dashed line is input signal of electric fields. As shown in this figure, time constant of the response is 2~3 ms (Kikuchi et al., 2003). Thanks to this rapidity, a haptic device using this ER brakes can realize a high frequency response (e.g. it can generates an impact force of virtual hockey clearly. Refer to Fig. 12.)
Right figure of Fig.6 shows static brake torques vs. the electric field applied to it. The static torque has good repeatability and we can formulate this relation as follows in this case;

$$T = 0.39\,E^2 + 0.12\,E + 0.10 \quad (1)$$

where, "T" represents the brake torque [Nm] and "E" represents the electric field [kV/mm].

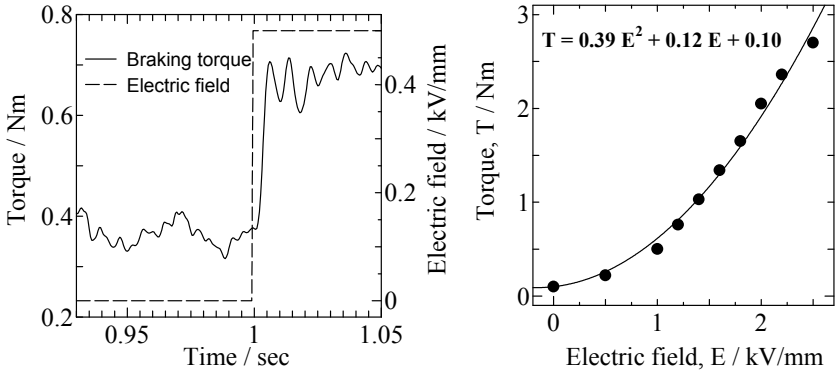

Fig. 6. Basic characteristics of the ER brake: Step response (left) (Kikuchi et al., 2003) and braking torque vs. electric field (right)

4. Basic structure and property of PLEMO-P1

We developed a new haptic device with two ER brakes shown in Fig. 7. This is a passive-type force display which can perform several kinds of virtual force, for example resistance, viscosity, vibration etc.
This machine has two controllable DOF in a working plane (working table) and one adjustable DOF for the inclined angle of the working plane. We named this system "Quasi-3-DOF Rehabilitation System," or "PLEMO-P1". "PLEMO" is a combination of "PLEasant" and "MOtivation". This name came from our hope that this system gives patents a pleasant experience of recovery and motivation for rehabilitation trainings. "P1" means first prototype with passive force feedback mechanism. This system is safe for human because it does not use any actuator.

Fig. 7. PLEMO-P1

Two ER brakes are included in a force control unit and the brake torque generates output-force on a handle through a parallel linkage. Figure 8 shows parallel linkage of this system. In this figure, T1 or brake torque of brake1 generates force F1 and similarly torque T2 generates force F2. If the movement of the handle is vertical direction like this figure and then this system generates force F1 and F2, the user feel resistance against his movement direction. If these forces are constant, users feel constant resistance. In other case, if these forces are proportional to velocity of the movement, the users feel viscous force. Necessary torques T1 and T2 are calculated from required forces F1 and F2 based on the inverse kinematics. Lengths of the link 1 and the link 2 are 450mm. This value is designed on the basis of the manipulability-analysis.

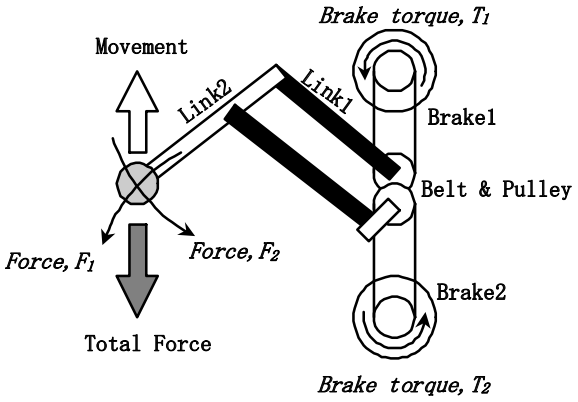

Fig. 8. Parallel linkage of PLEMO-P1

Figure 9 is a structure and a signal flow of this system. Absolute encoders (FA Coder, TS566N320, Tamagawa Seiki Inc., Japan, resolution: 17bits) measure the rotational angle of brakes. We can calculate the position and the velocity of the handle depending on each angle of brakes. Digital Input/ Output (DIO) board (PCI-2154C, Interface Inc., Japan) loads this information to a controller (personal computer). Operating handle includes a force sensor (IFS-70M35A, Nitta Inc., Japan), and operating force is measured by this sensor. A potentiometer (CP-2F, Midori Precision Inc., Japan) measures the inclination of the worktable and the angle is loaded by Analog/Digital converter (A/D) board (PCI-3165, Interface Inc., Japan, resolution: 16bits). The brake torque of the ER brake is controlled by applied voltage from high voltage amplifiers (HEOP-3P10-LS, Matsusada Precision Inc., Japan). Digital/Analog converter (D/A) board (PCI-3338, Interface Inc., Japan, resolution: 12bits) outputs the reference signal to the amplifiers.

A controller of PLEMO-P1 is a personal computer (DOS/V), and an operating system (OS) is Vine Linux 2.6 and ART-Linux (kernel 2.4.20), that is real-time OS made in Japan. Open-GL and Glut3.7 are used for the graphic library. Graphic process and control process are executed by one PC. Multi-process programming is used to realize it. The control process is repeated every 3 ms exactly.

Depending on the above specifications of the components, specifications of the PLEMO system are as follows;

1. Resolution of the angle is 4.8×10^{-5} rad and resolution of the displacement is 0.02 mm for each DOF.
2. Resolution of the braking torque is 6.5×10^{-3} Nm and resolution of the force at the end-effecter is 1.4×10^{-2} N for each DOF.
3. Working area is 600 mm (W) x 500 mm (D).
4. Adjustable angle of the inclination is from -30 to 90 degree.

PLEMO-P1 realizes from vertical training to horizontal training by only one system. Total size of the system is 1000 mm (W) x 600 mm (D) x 700 mm (H), except for the display. This is similar to the size of an office desk. This passive system is more compact, simple, and reasonable for the cost than conventional actuator-type systems.

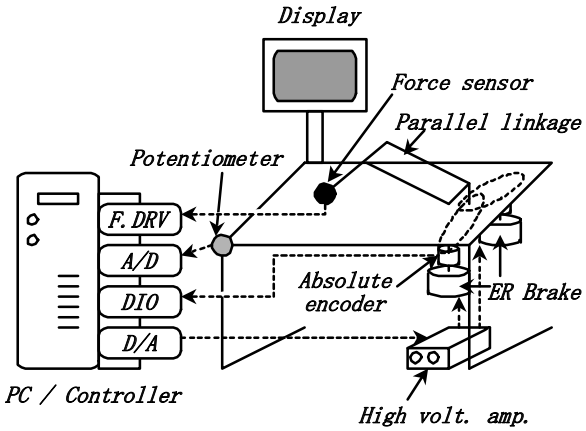

Fig. 9. Structure and signal flow of PLEMO-P1

5. SOFTWARE OF PLEMO-P1

We developed several kinds of rehabilitation and virtual haptic software as shown in figure 10, 12~14. Figure 10 shows a view of tracking test program. An operator grips the handle and moves it with tracking a target trajectory and a target ball. A position of the operating handle is displayed as a red sphere. The target ball is moving along the target trajectory. White zones in this figure mean smooth area without any force-feedback. Blue zones mean sticky area; operator feels virtual force like moving his hand in a viscous fluid. It is easy to change kinds of the virtual forces and its location.

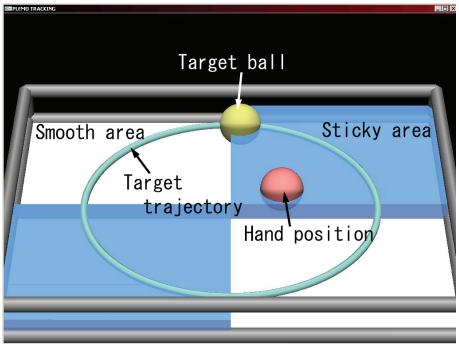

Fig. 10. Tracking test of PLEMO-P1

We also developed evaluation tools as shown in Fig. 11. Data of position, velocity and operating force are saved in a host computer, and test results can be shown graphically and automatically whenever you want to see. We can assess the motion abilities of the patients with accuracy of poison and velocity, range of motion, cognitive faculty and so on. In the Fig.11, position data of tracking test (circular trajectory) is shown as an example.

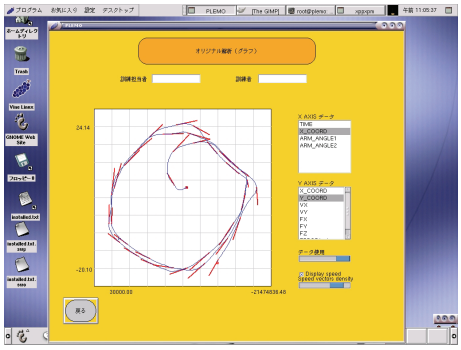

Fig. 11. Evaluation tools of PLEMO-P1

Figure 12 shows a view of virtual hockey game. We develop this software as an amusement use. Users operate the handle and manipulate the racket. When the racket hits the puck, impulse force is generated on the handle and the users feel like impact from a real puck thanks to the quick response of the ER brake.

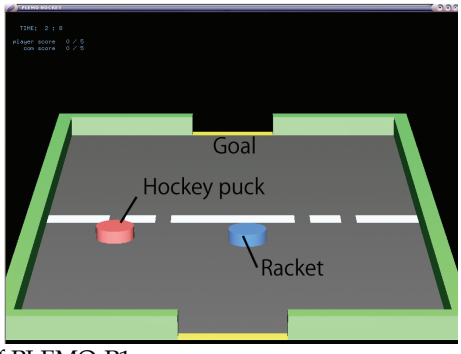

Fig. 12. Virtual hockey of PLEMO-P1

Figure 13 shows a view of window cleaning. At first, a semitransparent mask covers the all area of a picture. The goal is to erase this musk with an eraser that can be manipulated with the handle of PLEMO. When the eraser erases the musk, ER brakes generates preset resistance. For example, when 80 percent of the mask is erased, this picture vanishes and then the next new picture appears. The pictures are changed one after another. This software is effective to improve dexterity of reaching and movable range of motion.

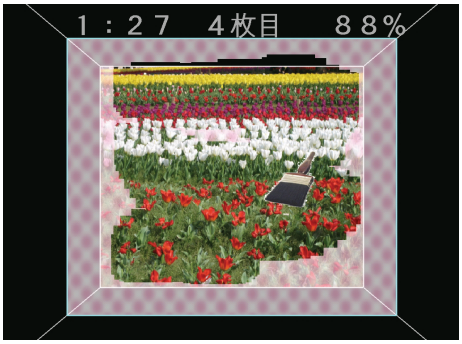

Fig. 13. Window cleaning of PLEMO-P1

We suggested application software "Virtual Sanding" for reaching trainings shown in Fig.14. This software was developed on the basis of conventional sanding training in the occupational therapy. In "real sanding", the patient is instructed to actively push up the sander higher and higher which provide resistance against the extensors. This resistance activates patient's intention to move their own arm. Actually, in physical therapy and occupational therapy, reaching training is done without pulling patient's hand in the correct direction, but with giving resistance against correct direction. The inclination of the sanding board is adjusted depending on the recovery level of the patients. So therapists gradually change the inclination depending on recovery level of their motor functions.
On the other hand, in the "Virtual Sanding", patients are instructed to actively push the rectangle with extending their arm toward front direction like a real sanding. The position of the hand is feed backed visually, so patients can check physical relationship between the object (a rectangle box) and their own hand (a sphere). In the only case that the patients push the box to the proper direction (straight front), the box move to the front and resistive force was generated on the end-effecter. Moreover, if the system detects their abnormal movements, the system stops presenting the force. Following the hand position, velocity and operating force, this system can judge the patient's movements. Objective of this training is to help the patients recognize a correct movement and to restructure their motion control function which they lost following stroke (Post stroke patients basically lose independent control of individual joints and coordination among the joints. Especially, it is difficult for them to control movements toward extension). The width of the box can be adjusted depending on the recovery level of the patients.

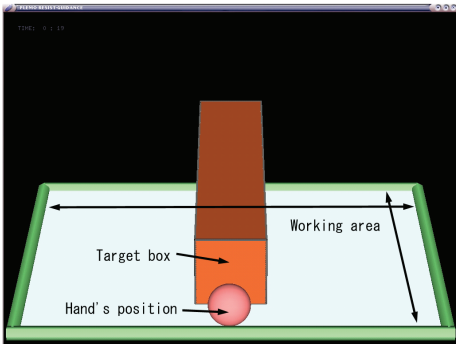

Fig. 14. Virtual Sanding of PLEMO-P1

Figure 15 shows an experimental result of the Virtual Sanding. An “Allowable area” means the width of the box. The solid line is a trajectory of the hand and white circles represent hand’s position under the proper training. As shown in this figure, the hand departed from the allowable area at the point A. Once the operator departed from this area, he recognized disappearance of the resistive force (point B), modified his trajectory to the allowable area and restarted the proper reaching (point C).

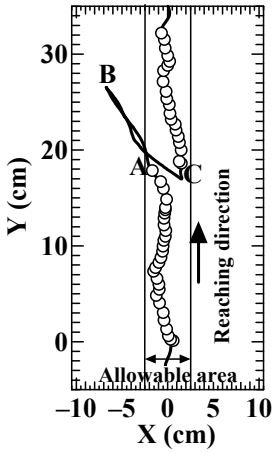

Fig. 15. Experimental result of virtual sanding

6. PLEMO-P2 & its clinical tests

6.1 PLEMO-P2

In order to conduct clinical tests in a hospital, we improved the torque generation unit and appearance of the PLEMO-P1. By utilizing a double-output ER brake (Kikuchi et al., 2008)[18], basic structure of the brake unit was simplified. We named the newly developed machine PLEMO-P2. Figure 16 shows appearance of the PLEMO-P2. Quasi-3DOF structure mentioned above was also utilized to the PLEMO-P2. Table angle can be adjusted by linear actuators with Up-Down switches in front of users.

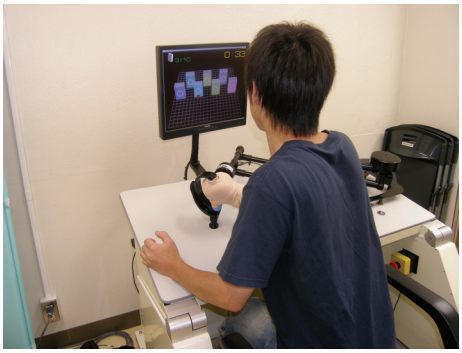

Fig. 16. PLEMO-P2 and post-stroke patient

6.2 Clinical tests

PLEMO-P2 is now under clinical tests in Hyogo College of Medicine. Until now, 8 chronic stroke patients with Brunnstrom stage 4~5 have examined clinical tests. All tests were safely executed. Experimental results will be reported from research team of the Hyogo College of Medicine soon.

Figure 17~19 show views of training software used in the clinical tests with PLEMO-P2. Figure 17 shows a view of wall pushing. 7 target walls are located in specific position on the plane, and operator is required to push each wall toward proper direction. If the operator pushes a wall with proper direction, proper force and proper time, the wall disappears. The operator can lean proper reaching motion with this training.

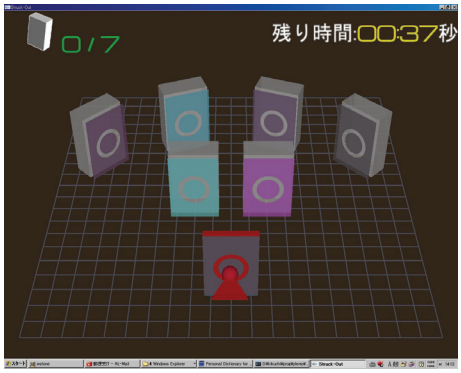

Fig. 17. Wall pushing of PLEMO-P2

Figure 18 shows a view of tracking test of PLEMO-P2. Basic function of this program is same as the tracking test of the PLEMO-P1. In the clinical tests, PLEMO-P2 did not perform resistance force; all of area was under free force.

Figure 19 shows a view of Whack-a-mole game of PLEMO-P2. This game was utilized to get patients relaxed between formal tests.

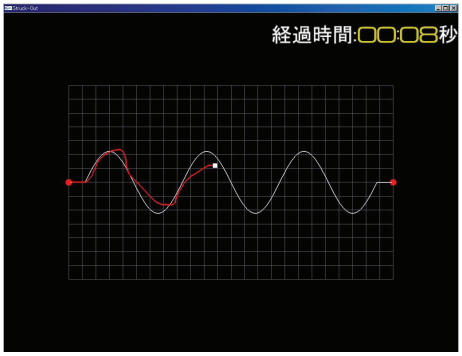

Fig. 18. Tracking test of PLEMO-P2

Fig. 19. Whack-a-mole of PLEMO-P2

6.3 Problems

In the clinical tests conducted in the hospital, we realized several problems. In the previous PLEMO system, we could not detect symptoms of abnormal movement of patients, for example synergy patterns of hemiplegic patients, because of a lack of sensors.

Fig. 20. Abnormal palmar flexion of wrist

Furthermore, in reaching tests with the previous system, we realized unfavorable movements of stroke patients as follows;
1. Excessive reaction force against the table,
2. Excessive gripping force,
3. Abnormal flexion of the wrist (Fig.20).
The synergy movements of hemiplegic patients must have caused such symptoms. In other words, if we can measure such information, we have a chance to detect their synergy movements and give patients a warning for their abnormality. It becomes great help for their effective recovery.

7. Future works

Figure 21 shows mechanisms of our former and current handle. The former handle mechanism is shown in Fig. 21(A): it is gimbal mechanism with no sensors. On the other hand, the current handle (Sensor grip device) consists of three kinds of sensors (shown in Fig. 21(B), (D)): four grip force sensors for grasping; a potentiometer for yaw rotation of patient's wrist; one axis force sensor for detecting the reaction force against the table.
We are now trying to detect abnormal movements or forces during patients' reaching with the sensor grip devices (Fig.22). In the future, the results will be reported.

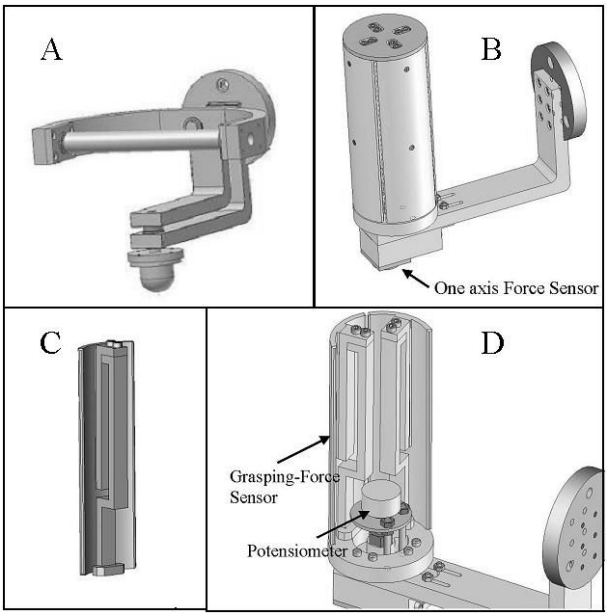

Fig. 21. Sensor grip device to detect abnormal movement

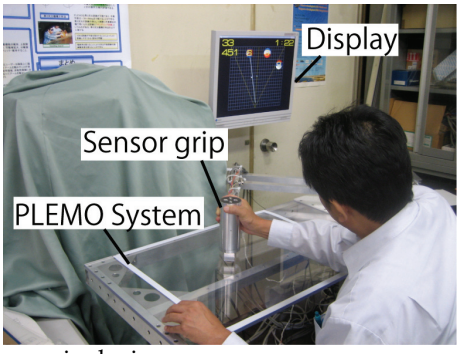

Fig. 22. PLEMO with sensor grip device

8. Conclusion

In this chapter, we presented the development of “Quasi-3DOF Rehabilitation System for Upper Limb”; PLEMO-P1 & PLEMO-P2 and its software. PLEMO-P1 has two controllable DOF on a working plane and one adjustable DOF for the inclination of the working plane. Using the ER brake, PLEMO-P1 has a good performance for its force feedback and guarantees the safety for humane by prevention of the attack from external force because PLEMO-P1 is passive haptic device; it does not have any actuators and it cannot move automatically. PLEMO-P2 was developed based on the PLEMO-P1 for clinical tests. PLEMO-P2 and PLEMO-P1 with sensor grip device were now under clinical tests. The results will be reported soon.

9. Acknowledgments

This work was financially supported by a JAPAN Grant-in-Aid for Scientific Research. We thank Dr. Akio Inoue, who is the president of ER tec Co. Ltd. and contributed to the developments of all ER fluid devices.

10. References

Furusho J. & Kikuchi T. (2007). A 3-D Rehabilitation System for Upper Limbs "EMUL", and a 6-DOF Rehabilitation System "Robotherapist", and Other Rehabilitation System with High Safety, *Rehabilitation Robotics* (Edited by Sashi S Kommu), Chapter 8, I-Tech Education and Publishing, pp.115-136

Furusho J., Koyanagi K., et al. (2005). Development of a 3-D Rehabilitation System for Upper Limbs Using ER Actuators in a NEDO Project, International Journal of Modern Physics B, Vol. 19, No. 7-9, pp.1591-1597

Furusho J. & Sakaguchi M. (1999). New actuators using ER fluid and their applications to force display devices in virtual reality and medical treatments, *International journal of Modern Physics B*, vol.13, no.14, 15 & 16, pp.2151-2159

Kikuchi T., Furusho J. & Oda K. (2003). Development of Isokinetic Exercise Machine Using ER Brake, *Proceedings of 2003 IEEE International Conference on Robotics and Automation*, pp214-219

Kikuchi T., Jin Y., Fukushima K., Akai H. & Furusho J. (2008). "Hybrid-PLEMO", Rehabilitation system for upper limbs with Active / Passive Force Feedback mode, *Proceedings of the 30th Annual International Conference of the IEEE Engineering in Medicine and Biology Society*, pp.1973-1976

Krebs H.I., Volpe B.T., et al. (2000). Increasing productivity and quality of care: Robot-aided neuron rehabilitation, *Journal of Rehabilitation Research and Development*, Vol.37, No.6, pp.639-652

Loureiro R.C.V. & Harwin W.S. (2007). Reach & Grasp Therapy: Design and Control of a 9-DOF Robotic Neuro-rehabilitation System, *Proceedigs on the IEEE 10th International Conference on Rehabilitation Robotics*, pp. 757-763

Lum P.S., Burgar C.G. & Shor P.C. (2004). Evidence for improved muscle activation patterns after retraining of reaching movements with the MIME robotic system in subjects with post-stroke hemiparesis, *Proceedings on the IEEE Transactions on Neural Systems and Rehabilitation Engineering*, Vol.12, pp.184-194

Miyai I., Yagura H., et al. (2002). Premotor Cortex Is Involved in Restoration of Gait in Stroke, *Annals of Neurology*, Vol.52, No.2, pp.188-194

Nef T., Mihelj M., Kiefer G., Perndl C., Muller R. & Reiner R. (2007). ARMin - Exoskeleton for arm therapy in stroke patients, *Proceedings on the IEEE 10th International Conference on Rehabilitation Robotics*, pp. 68-74

Perry J.C., Rosen J. & Burns S. (2007). Upper-Limb Powered Exoskeleton Design, *IEEE Transactions on Mechatronics*, vol.12, pp.408-417

Sakaguchi M., Furusho J. & Takesue N. (2001). Passive Force Display Using ER Brakes and its Control Experiments, *Proceedings of the 2001 IEEE Virtual Reality Conference*, pp.7-12

Trombly C.A. (1982). *Occupational Therapy for Physical Dysfunction*, Second Edition, Williams & Wilkins, pp.230-241

Winslow, W.M. (1949). Journal of Applied Physics, Vol.20, pp.1137-1140

Wolbrecht E.T., Leavitt J., Reinkensmeyer D.J. & Bobrow J.E. (2006). Control of a pneumatic orthosis for upper extremity stroke rahabilitation, *Proceedings on the IEEE Engineering in Medicine and Biology Conference*, pp. 2687-2693

Zhang L.Q., Park H.S. & Ren Y. (2007). Developing An Intelligent Robotic Arm for Stroke Rehabilitation, *Proceedings of the IEEE 10th International Conference on Rehabilitation Robotics*, pp. 984-994

13

Wearable Robots in Rehabilitation Engineering Tremor Suppression

E. Rocon, J.C. Moreno, J.A. Gallego and J.L. Pons
Bioengineering group, CSIC
Spain

1. Introduction

Wearable robots (Soft robots) are person-oriented robots. They can be defined as those worn by human operators, whether to supplement the function of a limb or to replace it completely. Wearable robots may operate alongside human limbs, as in the case of orthotic robots or exoskeletons, or they may substitute for missing limbs, for instance following an amputation. Wearable Robots have been proposed in the context of rehabilitation, but practical implementation of these rehabilitation robots is strongly limited by available actuator and sensor technologies. In most instances technologies are the limiting factor in developing novel robots. This is also true of wearable robots. Wearable robots are in many cases related to portable and ambulatory applications; however, only a few examples of fully portable wearable robots can be found in the literature, one reason being a lack of enabling technologies.

Ambulatory scenarios require compact, miniaturized, energetically efficient technologies, e.g. control, sensors, actuators. All technologies involved in robotics need further development, but actuators and power sources are the ones that probably most limit wearability and portability at the present time while sensors are the ones most limiting efficient implementation of cHRI (Pons, 2005).

Portability is one important aspect of wearable robotics, but the distinctive characteristic of wearable robots is dual cognitive and physical interaction with the human wearer. This immediately raises dependability and safety issues in robotics. Dependability and safety ultimately have a close bearing on control, sensor and actuator technologies. In the area of Rehabilitation WRs, the key idea is empowering a weak musculo-skeletal system or a person with deficient motor control.

It is clear that the design of wearable robots can benefit from biological models in a number of aspects like control, sensing and actuation. Likewise, wearable robots can be used to understand and formalize models of biological motor control in humans.

This book chapter aims to analyse these issues in the framework of tremor suppression. First, the chapter will introduce the work performed by authors in the development and validation of an upper limb exoskeleton for tremor suppression called WOTAS (wearable orthosis for tremor assessment and suppression). It will describe in detail the general concept for WOTAS, outlining the special features of the design and selection of system

components. A control strategy developed for tremor suppression based on the exoskeletons will be described. Results from experiments using these two strategies on patients with tremor will be summarized. Finally, results from clinical trials will be presented. Results indicate that the exoskeleton is able to attain a reduction ratio in the order of 80% tremor power in specific joints of patients with severe tremor. Robotics based solutions have shown clinical evidence of the approach based on human limb impedance control. However it results in bulky and non-cosmetic solutions for which patients are especially reluctant, (Rocon et al., 2007).
At the end, the chapter will describe the work being performed in the framework of TREMOR project that tries to overcome these limitations by exploring the so-called enabling technologies. TREMOR project is focused on the development of a new methodology for Functional Electrical Stimulation, FES, based on addressable arrays of electrodes, which overcome the limitations of actual electrodes for functional stimulation, therefore FES is proposed as an alternative actuation technology for this sort of robots. Moreover, the chapter will evaluate the application of inertial sensors (Inertial Measurement Units, IMU) as sensing technologies in controlled wearable/soft robots.

2. Tremor suppression by means of an upper limb exoskeleton

Tremor is defined as a rhythmic oscillatory activity of body parts (Findley and Koller 1995). The oscillatory activities are related to various combinations of four basic mechanisms: (a) mechanically-induced oscillations, (b) oscillations due to reflexes, (c) oscillations generated by neuronal generators in the central nervous system, (d) oscillations resulting from impaired feedforward and feedback loops (Deuschl et al. 2001). Tremor amplitude tends to increase and progress more medially (from distal to proximal joints) over time, while tremor frequency tends to be inversely related to age (Rajput et al. 2004). More than 90 % of patients who come to medical attention report disability (Louis 2005). For instance, Essential Tremor (ET) affects approximately 4 % of the population above 65 years of age, representing the most common movement disorder in the elderly (Benito-Leon et al. 2003; Louis et al. 2005; Thanvi et al. 2006).
Current strategies in the treatment of tremor are based on drugs (mainly the front-line agents primidone and propranolol), and surgery (thalamotomy and deep brain stimulation) in those patients being refractory to drugs (Louis 2005; Ushe et al. 2004). Gamma knife thalamotomy could represent an option for difficult cases (Niranjan et al. 2000; Young et al. 2000). However, (a) tremor is not managed effectively or sufficiently in about 25 % of patients, (b) the drugs used often induce side effects, may be contra-indicated or do present potential side effects or contra-indications which make their use more difficult, and (c) surgery is associated with a risk of hemorrhage and psychiatric manifestations (Binder et al. 2003). Moreover, a high rate of suicide (4.3 %) has been found recently in patients treated with deep brain stimulation (Burkhard et al. 2004). Therefore, further research and new therapeutic options are required to manage tremor most effectively.

2.1 Wearable orthosis for tremor assessment and suppression

The effects of load and force on tremor have received considerable attention by the research community. Amongst others, Adelstein (Adeltein 1981), has conducted a thorough analysis of the effect of viscous loading as a means for active reduction of intention tremor. As a

result, Adelstein reports that significant and steady reductions of tremor amplitude are observed as the viscous loading increase. This phenomenon gives rise to the possibility of an orthotic management of tremor. An orthosis is defined as a medical device that acts in parallel to a segment of the body in order to compensate some dysfunction. In the case of tremor management, the orthosis must apply a damping or inertial load to a selected set of limb articulations. As a wearable device, it must exhibit a number of aesthetics, cosmetic as well as functional characteristics. Aesthetics and cosmetics are more directly related to size, weight and appearance of the orthosis. Functionality is more related to the trade-off required in terms of required torque and velocity and to the robustness of operation.
This section presents the active orthosis (exoskeleton) WOTAS, which is able to apply effective viscosity and/or inertia attached to the upper limb of the patient (Figure 1). This active orthosis is designed after the shape and function of the human upper limb, segments and joints correspond to some extent to these of the human body while the system is externally coupled to the person. The exoskeleton activates the elbow and wrist joints, being able to measure and apply forces on three movements of the upper limb: elbow flexion-extension, forearm pronation-supination and wrist flexion-extension. WOTAS is activated by a set of rotary flat DC motors (EC 45 Flat Brushless DC motor, Maxon Inc.) and harmonic pancake transmissions (Rocon et al., 2007). This solution was selected based on a comparison of available technologies for actuation and represent a compact and light solution suitable for wearable devices.

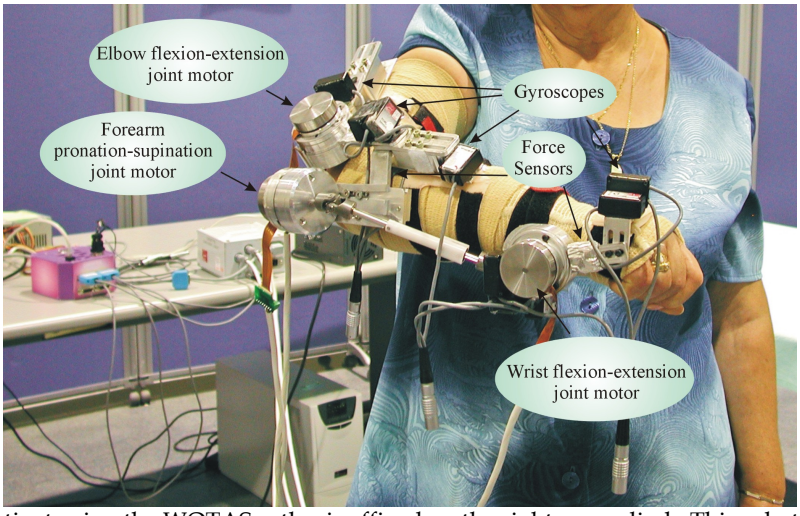

Fig. 1. Patient using the WOTAS orthosis affixed on the right upper limb. This robotic device spans the elbow and wrist joints, being able to apply independent tremor suppression strategies to elbow flexo-extension, wrist flexo-extension and wrist prono-supination.

The mechanical design of the exoskeleton elbow joint is based on a hinge joint with the axis of rotation placed in the line between the two epycondyles. The actuator solution adopted is attached to the structure with its rotary axis aligned with the elbow joint of the exoskeleton. The wrist joint adopted the same solution but with the axis of rotation placed in the line between the capitate and lunate bones of the carpus. The solution developed for the control

of pronation-supination movement is novel and based on controlling the rotation of a bar placed parallel to the forearm, see Figure 1. The total weight of the final system is roughly 850 gr.

The active orthosis developed aims at allowing both monitoring of upper limb movements and implementation of tremor suppression strategies. Therefore, it is equipped with kinematics (angular velocity) and kinetic (interaction force between limb and orthosis) sensors. The rate of rotation of each activated joint is detected by sensor system based on a combination of two independent chip gyroscopes (ENC-03J manufactured by Murata Inc.), placed distally and proximally to each activated joint. Angular position and acceleration information are obtained through mathematical operations. The interaction force between the exoskeleton and the user is measured by a force sensor based on strain gauges (Rocon et al., 2007).

Other important aspect of the design of active orthoses that will apply dynamic force between segments of the human limbs is the transmission of load through the soft tissues to the human skeleton. In order to minimize this difficulty, the WOTAS orthosis is adaptable to each configuration of the joint among different patients owing to the use of thermoplastics, see Figure 1. In addition, a textile substrate was used to compress the soft tissues and enhance performance of the fixation supports.

The active orthosis is controlled by a computer with a dedicated software application that implements an algorithm able to distinguish in real time tremorous from voluntary movement at joint level, and to calculate the force to be applied by the active orthosis on the upper limb in order to change its biomechanical characteristics and, consequently, suppress tremor. In summary, the control system works as follow:

1. the sensors coupled to the limb measure its motion,
2. an error cancelling algorithm performs a real-time discrimination of the undesired component of motion,
3. tremor information is sent as the input to the controller in order to generate the desired exoskeleton actuation to suppress the tremor (see Figure 2a).

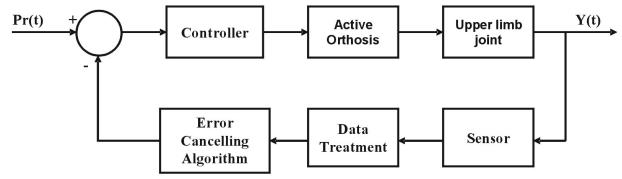

a)

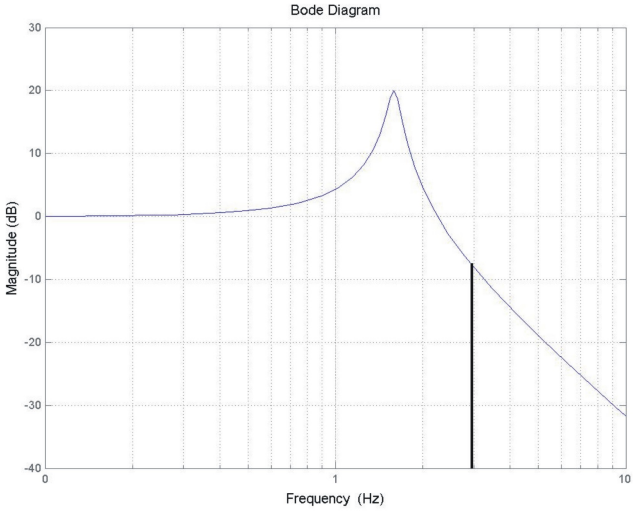

b)

Fig. 2. a) Tremor suppression control system. The movement of each upper limb joint is detected by gyroscopes. An error cancelling algorithm performs a real-time discrimination of the tremorous (undesired) component of motion. The angular velocity information from the estimated tremorous component is used to calculate the reference mass and damping characteristics of the upper limb. This process estimates the actual impedance force of the system, defining the apparent impedance of the upper limb and consequently reducing the tremor. b) The musculo-skeletal system is modelled as a second order biomechanical system. The active orthosis is used to modify the apparent biomechanical characteristics of the upper limb so that the cut-off frequency, fc, lies between the frequency range of voluntary and tremor motion.

In this approach, the musculo-skeletal system (each upper-limb joint contributing to tremor) is modelled as a second order biomechanical system exhibiting a low-pass filtering behaviour. The cut-off frequency of this second order system is directly related to the biomechanical parameters of the second order system, i.e. inertia, damping and stiffness. Our approach consists in selecting the appropriate modified values of inertia and damping of the musculo-skeletal system, so that the cut-off frequency lies immediately above the maximum frequency of the voluntary motion and well below the tremor frequency, see Figure 2b.

For a successful active tremor absorption mechanism, a means for intelligent detection of tremor vs. voluntary motion is required. To this end, a model of the tremor motion is

proposed. The algorithm developed is based on a two-stage method that estimates voluntary and tremorous motion with a small phase lag (Rocon et al., 2007). It is based on the fact that the the voluntary motion of activities of daily living, ADL, occurs at frequencies lower than the tremorous movements (Riviere, 1995). Based on this, in the first stage of the algorithm, the voluntary motion is estimated using a Benedict-Bordner filter tuned to estimate low frequency movements. In the second stage, the estimated voluntary motion is removed from the overall motion and it is assumed that the remaining movement is tremor. Next, an adaptive algorithm estimates tremor using a sinusoidal model, estimating its time-varying frequency, amplitude and phase (Riviere, 1995). This algorithm was evaluated with 33 subjects presenting different tremor diseases. Results demonstrated the correct operation of the algorithm, being able to estimate with a small phase lag (roughly 1 ms of time delay introduced) the voluntary and tremor components from the overall movement.

2.2 Experimental protocol

The performance of the WOTAS active orthosis was evaluated in an experimental phase involving six patient suffering from Essential tremor (3 female; 3 male; mean age 72,3 +/- 4.3 years). These patients were exhibiting a bilateral postural/kinetic tremor in upper limbs at intensities of 2/4 to 4/4 despite regular intake of medication (primidone up to/day 500 mg, propranolol up to 160 mg/day, or a combination of both), in agreement with the criteria of ET (consensus statement of the MDS). Regular anti-tremor medications were maintained stable during the week preceding the assessment. The investigation was approved by the ethical committee and patients gave their written informed consent.

The effects of biomechanical loading were investigated for the upper limb on one side during the execution of the different clinical tasks (keep the upper limbs outstretched in a horizontal position, point the nose with the index starting from the thigh, and keep the arm in a rest position over the thigh). These tasks have been previously used to characterise tremor movement (Belda-Lois et al., 2004).

During the experiments, WOTAS operated basically in two different control modes:

1. Monitoring mode: WOTAS operates in free mode (no force is applied on the upper limb) and monitor tremor parameters of the patients.
2. Suppression mode: WOTAS is able to change biomechanical characteristics of upper limb, such as viscosity or inertia, in order to suppress tremor.

The order in which the modes have been applied has been alternated, as well as the order in which the patients have executed the tasks. This approach was adopted in order to avoid interactions in the analysis, as well as learning effects (Belda et al., 2004). During the experiments the patient did not know when the system were applying a suppressing strategy or when it was operating in monitoring mode. Just the computer operator knew when the systems were applying the suppression strategy. For formal purposes, we consider this arrangement equivalent to a double-blind trial in order to reduce the placebo effects in the experimentation phase (Belda et al., 2004).

The figure of merit adopted to quantify the reduction achieved by the active orthosis is the ratio between the signal analysed in monitoring mode, and the signal analysed in suppression mode. Therefore, the reduction of tremor was measured with the patients under the same conditions: with the orthosis placed on the upper limb.

2.3 Results

The effects of adding effective biomechanical loading were investigated for the upper limb during the execution of the different clinical tasks. During the trials, some patients were able to identify when the system was operating in suppression mode, relating to the clinician either 'now the system is suppressing my tremor' or 'now it is not'.

According to the results, the efficiency of the active orthosis increases as tremor power increases. A statistical analysis has been made to characterize the tremor suppression. The statistical analysis has been made using R. A second order polynomial fit has been made with the natural logarithms of power spectra in free and suppression mode. This method allows us to identify a lower limit for efficient tremor suppression; this limit is roughly 0.15 rad^2/s^3. It is mainly related to the interface of the orthosis with the uppper limb since stiffness between the orthotic device and the body is a key factor to control a dynamic process such as tremor. Therefore the characteristics of the transmissions through the soft tissues play an important role in the efficiency of tremor suppression.

Figures 3a and 3b illustrate the effects of WOTAS in the tremorous movement when operating in suppression mode in one patient with a severe tremor. Figure 3a shows the time series corresponding to the tremorous movement of the wrist joint during the arm-outstretched task of one patient exhibiting a severe essential tremor. The top part of the figure shows the time signal with WOTAS in the monitoring mode (left) and in the damping mode (right). Notice that the amplitude of tremor is clearly lower in the damping condition as compared to the monitoring mode. Bottom panels illustrate the same reduction in the frequency domain. The Power Spectrum Density (PSD) has been obtained from the part of the signal with detectable tremor. A clear peak of tremor activity close to 6 Hz is identified. The peak of energy corresponding to the tremorous activity when WOTAS is operating in suppression mode presents a clear reduction. The reduction of the power spectral density (PSD) was 80.4 % in this patient. Notice that the dominant tremor frequency is stable despite of the reduction in its amplitude. Figure 3b illustrates a similar phenomenon for the elbow. Figures 3c and 3d show the effects of the active orthosis on the kinetic tremor associated with finger-to-nose test. A strong reduction in tremor was also observed.

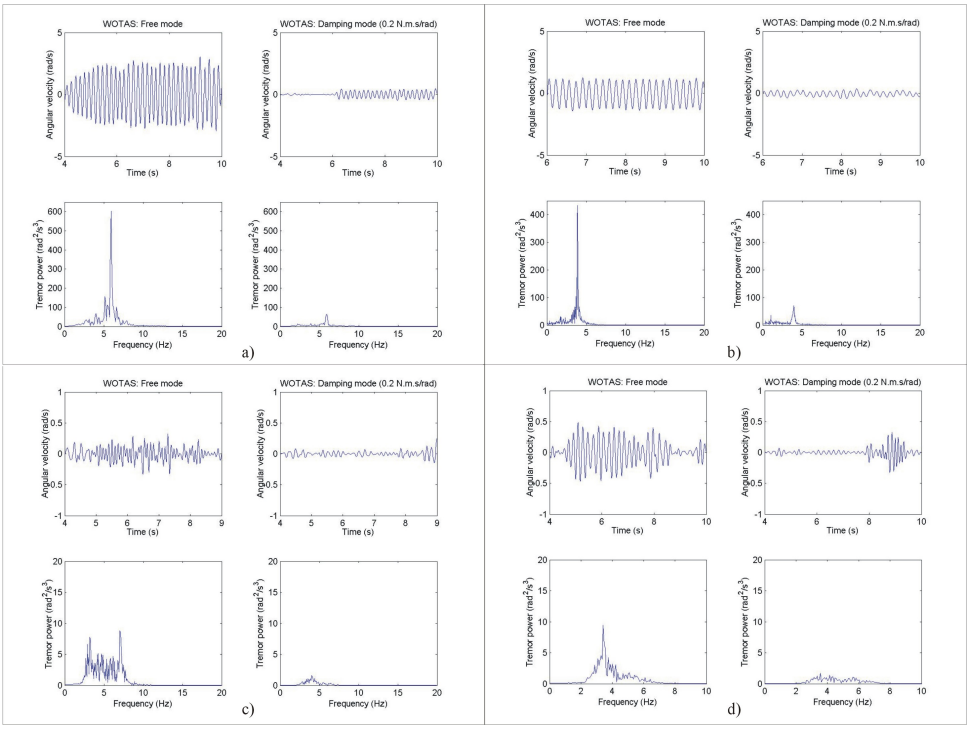

Fig. 3. This figure illustrates the oscillations of the wrist with the associated power spectral density (PSD) of tremor with the motor in a free mode (left panels) and providing viscosity of 0.2 Nms/rad (right panels) in one of the patients. Note the strong reduction in the PSD when viscosity is applied. Oscillations are expressed in rad/sec and PSD is expressed in rad²/s3. a) Reduction of postural tremor of the wrist with WOTAS, b) Reduction of postural tremor of the elbow with WOTAS, c) Reduction of kinetic ("intention") tremor at the elbow with WOTAS, d) Reduction of tremor at elbow level in a patient performing a finger-to-nose task.

Results indicated that the device could achieve a consistent tremor power reduction of 40 % for all patients, being able to reach a reduction ratio in the order of 80% tremor power in determined joints of patients with the most severe tremor. In one patient, the reduction of tremor in the wrist and elbow was associated with a possible rise in tremor intensity at the shoulder level. However, in the majority of patients there was no visible displacement of tremor movement from distal to proximal joints. We call this phenomenon DPTS (distal to proximal tremor shift). The authors believe that it is important to investigate and define the profile of the users who might be affected by this new phenomenon.

There are hints that the mechanical suppression of tremor could produce a "positive" feedback to essential tremor patients. Patients reported that when they realized that the orthosis was suppressing tremor they felt more and more confident to accomplish the task. This behaviour has been detected in patients with severe tremor and requires further research to be confirmed and investigated in-depth.

Overall, patient tolerance was good. No lesions were observed on their skin, expect for a moderate and transient change in skin aspect due to the orthosis. A slight discomfort was reported by some patients. These results suggest this new technique as a possible therapy for tremor suppression in human disorders characterized by postural/kinetic tremor in upper limbs. It opens possible perspectives for disabling forms of tremor, such as tremor encountered in cerebellar and/or brainstem disorders.

3. Enabling technologies

The history of robotics is one of ever closer interaction with the human actor. Originally, robots were only intended for use in industrial environments to replace humans in tedious and repetitive tasks or in those requiring high force and precision, but the current scenario is one of transition towards increasing interaction with the human operator. This means that interaction with humans is expanding from a mere exchange of information (in teleoperation tasks) and service robotics to a close interaction involving physical and cognitive modalities.

It is in this context that the concept of Wearable Robots (WRs) has emerged, (Pons, 2008). Wearable robots are person-oriented robots. They can be defined as those worn by human operators, whether to supplement the function of a limb or to replace it completely. Wearable robots may operate alongside human limbs, as in the case of orthotic robots or exoskeletons, or they may substitute for missing limbs, for instance following an amputation. Wearability does not necessarily imply that the robot is ambulatory, portable or autonomous. Where wearable robots are nonambulatory, this is in most instances a consequence of the lack of enabling technologies, in particular actuators and energy sources. Of the different wearable robots, exoskeletons are the ones in which the cognitive (information) and physical (power) interactions with the human operator are most intense.

In most instances technologies are the limiting factor in developing novel robots. This is also true of wearable robots. Wearable robots are in many cases related to portable and ambulatory applications; however, only a few examples of fully portable wearable robots can be found in the literature, one reason being a lack of enabling technologies.

Ambulatory scenarios require compact, miniaturized, energetically efficient technologies, e.g. control, sensors and actuators. All technologies involved in robotics need further development, but actuators and power sources are the ones that probably most limit wearability and portability at the present time while sensors are the ones most limiting efficient implementation of cHRI, as described in previous section with WOTAS exoskeleton.

In the area of rehabilitation wearable robots, the key idea is empowering a weak musculo-skeletal system or a person with deficient motor control. Functional Electrical Stimulation (FES) becomes an ideal actuation alternative as it uses the muscular system of the user as actuator.

In this context, the authors are collaborating with the European project TREMOR, that tries to overcome the limitations of WRs by exploring the concept of controlling human upper limb muscles as actuators of a Brain computer interface BCI-based system for selective tremor suppression. The final result of the project will take the form of an active garment usable in activities of daily living (ADL). The next sections introduce the main technologies identified by the authors as the ones that will enable the constructions of the next generation

of Wearable robot for rehabilitation. First, the use of human muscles as actuators in the pHRI is discussed. Afterwards, exploitation of biological information for the cHRI is presented. This considers both central and peripheral nervous activity, and the resultant motion.

3.1 FES techniques

FES consists in directly activating muscles by stimulating motoneurons and/or triggering reflexes by stimulating sensory nerve fibres. The regulation of the strength of a motor response is controlled by current rate and charge delivered to the sensory-motor systems, (Popovic et al., 2000). FES has been implemented in a wide range of applications: development of neuroprostheses (e.g. for gait restoration, shoulder rehabilitation) paraplegic standing-up (Riener et al. 1998) and walking, correction of drop foot, control of arm movements, or restoring hand grasp function are some examples of FES research.

The already existing FES systems also have some important drawbacks that TREMOR project expects to overcome, namely, muscular fatigue and both discomfort and painful sensations while muscles are being stimulated. Furthermore, the control of the stimulators is not intelligent enough to achieve integration into the natural motor regulation.

TREMOR concept proposes a new methodology for FES, based on arrays of electrodes which overcome the limitations of current electrodes for functional stimulation. In addition it will allow a more selective stimulation of muscles. To achieve this, an innovative addressable electrode array system will be implemented as a new approach to diminish fatigue, (Popovic-Bijelic et al., 2005). Moreover, this FES array is expected to improve comfort and reduce pain due to current distribution. This would be an important advance for FES in general and would go in the direction of minimizing the electrodes to locate on the subject, in order to enhance the wearability of the system. A feasible model of the upper limb musculoskeletal system, allowing to establish dynamic configurations of muscle recruitments that (theoretically) generate the expected compensatory output, would be beneficial for the real-time application of selective artificial muscle activation.

Moreover, our methodology is expected to establish the basis for the development of so-called Soft Robots (SRs). Soft Robots are wearable robots that rely on biological information to interpret both state and intention of the user, and take advantage of his muscles as actuators. There are some challenging issues related to this approach. Regarding at the physical interaction, selective stimulation and control of force must be assured in order to create performing rehabilitation garments.

Impedance Control has been extensively used within the rehabilitation robotics field. TREMOR project aims at creating an easy-to-test platform to validate upper limb impedance control strategies implemented with FES techniques. Consequently, inverse dynamic musculo-skeletal upper limb models will be provided. Regarding at the state of the art, several inverse dynamic models for the generation of motor commands relying on attested muscle models such as Hill's, have been proposed (Riener et al., 1998, Makssoud et al., 2004).

Figure 4 summarizes a preliminary model of elbow control based on activation of the two antagonist muscle groups acting on it, namely biceps brachi and triceps brachi. Real data of a Parkinsonian patient is employed. The proposed model considers the biomechanical characteristics of the upper limb and the current orientation of the arm, and takes as input

the EMG activity of both muscles. The EMG-driven Hill muscle model consists of a series elastic element, a contractile element, which is capable of contracting when stimulated either naturally or by means of FES, and a passive spring in parallel to them, and is based on (Zajac, 1989, Lloyd et al., 2003). Muscle lengths and their ratio of variation, which define force-length and force-velocity contributions of each muscle, are obtained with a regressive model that relates normalised muscle lengths with joint flexion angles, (Hawkins et al., 1990). Satisfying results are obtained.

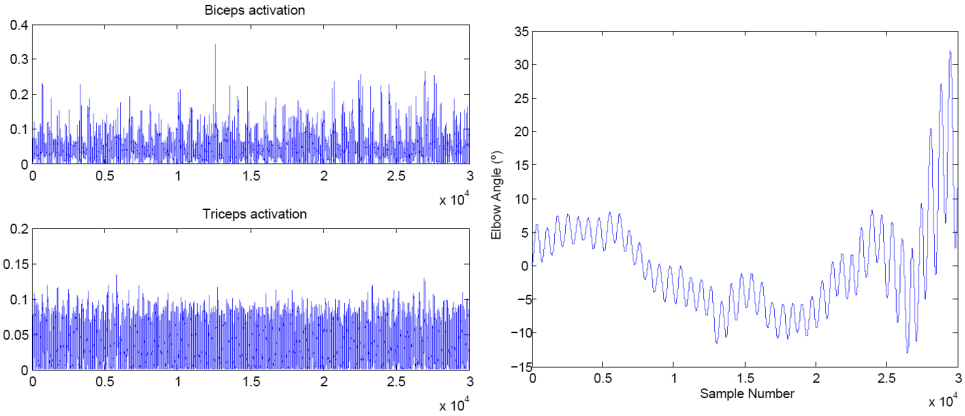

Fig. 4. This figure shows the resultant elbow angle (right) based on rectified biceps and triceps EMG activity (right). EMG signals were acquired at 3008 Hz. A 90º angle between the arm and forearm is considered as reference (0º). Forearm motion has the same frequency than the one measured by piezoelectric accelerometers attached at the distal part of the forearm, and shows an increase in tremor amplitude due to a posture change.

This model sets the basis for the development of inverse models for a 3D scenario that envisage the presence of non-predictable external forces. These will be one of the contributions of the TREMOR project: controllable (i.e. real-time feasible), three-dimensional, upper limb joint models. They will account of non planar movements and will strengthen the physiological congruity in the FES field by including fatigue in the dynamic representation.

3.2 Inertial sensing technology

MEMS inertial sensors are suitable for tracking changes in velocity, position and orientation. In the past, accelerometers have been built with large mechanical masses and gyroscopes with multiple mechanical gimbals and bearings. Recent advances in microelectromechanical system (MEMS) technologies have made miniaturized inertial sensors possible. These devices are currently an exciting alternative to motion capture in wearable applications. In particular, accelerometers have been judged suitable for compensation of user motion, e.g. in closed loop configurations for wearable vision platforms, (Mayol et. al., 2000), or tremor compensation in instruments for microsurgery, (Riviere et al., 1995). Examples of applications of rate gyroscopes include active compensation of upper limb tremor by means

of motorized exoskeletons, (Rocon et al., 2007), control and monitoring of leg orthoses, (Moreno et al., 2006), and others.
In the framework of TREMOR project recording of upper limb movement with IMU sensors aims at two goals. First, IMU sensors will provide the orientation of each segment based on a sensor fusion approach that merges accelerometer and gyroscope information using a Kalman filter. This will serve as an input for the calculation of the current muscle length and velocity, which are required by the inverse musculo-skeletal models. Second, two IMUs placed at the distal and proximal segments of a joint will provide directly its angular velocity, (Rocon et al., 2006). On the basis of this, a two-stage algorithm for estimation of instantaneous tremor frequency and amplitude has been developed as described below.

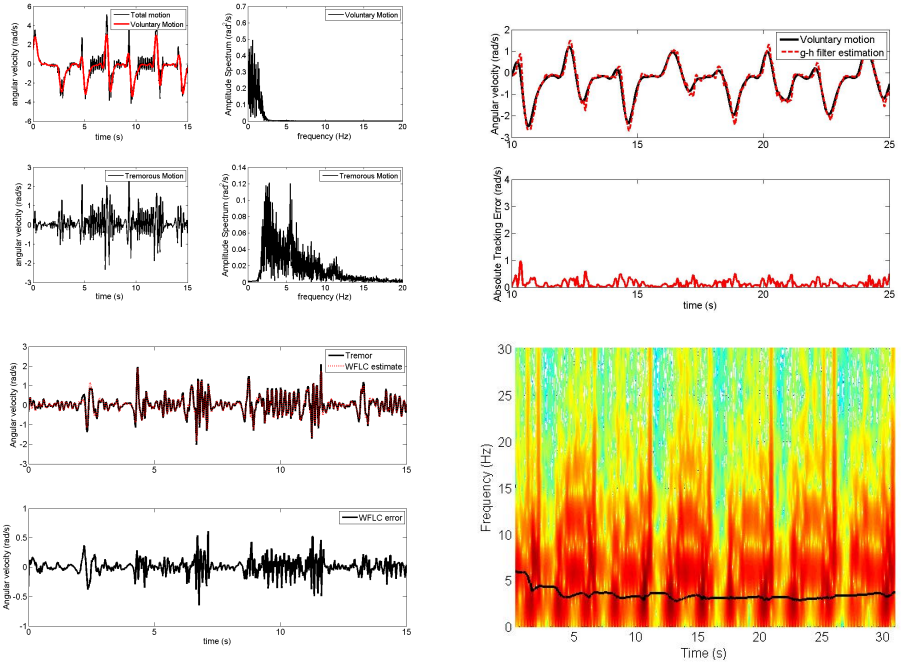

Fig. 5. Top left: Example of application of the two stage algorithm: Voluntary and tremorous motions are estimated based on their different frequency content. Top right: Voluntary motion estimation for the wrist recording of a tremor patient by means of a critically dampened filter and its estimation error. Bottom left: tremor estimation for the wrist joint obtained with the WFLC and estimation error. Bottom right: amplitude spectrum of the tremor recording and WFLC tremor frequency estimation.

It has been demonstrated that tremor happens at higher frequency than voluntary motion (Mann et al., 1989), and that affects it in an additive manner, (Riley et al., 1982). Therefore, voluntary motion estimation can be thought of as a tracking problem where tracking of slow dynamics of total movement is desired. Subtracting an accurate estimation of voluntary motion to the overall recorded movement provides directly the "isolated" tremor signal, Fig.

5 (top left). This tremor estimation is fed into an adaptive algorithm, which calculates its amplitude and frequency.
Voluntary motion tracking based on g-h filters and a Kalman filter is evaluated. Based on data from a group of patients suffering the major tremor disorders, it is concluded that the critically dampened filter (Brookner, 1998), a special type of g-h filter, provides the best performance, Fig. 5 (top right). Once this voluntary motion estimation is subtracted from the overall movement, a tremor estimate is directly generated. Instantaneous tremor amplitude and frequency are obtained with the Weighted Frequency Fourier Linear Combiner (WFLC), which continuously adapts a time-varying Fourier series to the input signal (Rivere, 1995). The WFLC is based on the Least Mean Square method, a gradient descent-like approach, (Widrow et al., 1985). Figure 5 (bottom left and right) demonstrate the performance of the WFLC as both amplitude and frequency tracker for a recorded wrist tremor signal.

3.3 BCI and the context of tremor identification, characterization and tracking

BCIs can be considered as any means that makes it possible to create a direct communication pathway between the human nervous system and any external device. This definition encompasses a broader term than that generally considered as coming from the original acronym, which is Brain Computer Interface: as a matter of fact, BCI has been recently re-phrased as the acronym for Brain Controlled Interface, (Schwartz et al., 2006), thus enclosing any kind of device which might be controlled by the brain, such as a speech synthesizer, any assistive appliance, and neural prostheses, (Mason & Birch, 2003).
Results obtained in the last years in this context enlightened the possibility of using interfaces that can non-invasively provide non-muscular communication and control for people with severe motor disabilities, including ALS patients, (Sellers & Donchin, 2006), stroke survivors, (Dobkin, 2007), and SCI subjects, (Boord et al., 2004). In fact, despite the increasing number of experiments in the context of BCI denounces the interest in the area of assistive technology, results in controlled environments are still somewhat contradictory, and render the applicability of the techniques devised up to now still unpopular.
One of the reasons that may justify this has been recently singled out by considering the physiological principle of combination and distribution of roles in the planning and execution of movements in humans, (Wolpaw, 2003): motor outputs are obtained by a blend of activities of different areas including not only the relevant CNS areas. By adopting a "goal selection" strategy, and then limiting the BCI to give reliable information on user's goal, and let another structure to work on the lower aspects, the variability in performance of BCI-based systems can be reduced. Following this perspective, BCI-based systems need to be complemented with several kinds of information ranging from central to peripheral motor structures.
The second limitation resides in the intrinsic difficulty of classifying different intended movements or actions by using a limited number of EEG electrodes. This at present limits the reconstructed flow of information at around 25 bits/min (i.e. resolving 25 binary answers every minute), (Wolpaw et al., 2002). As a matter of fact, if in controlled environments and with trained subjects it is at present possible to reveal the intention to move, and discriminate between e.g. four directions to drive a cursor or a wheelchair, (del Millán, 2003), having an interface solve complex and functional tasks such as grasping a glass, or handling a fork is still a challenge.

Moreover, the development of interfaces based on EEG electrodes raises functional operational issues:

1. Placement of the acquisition system on the user requires the assistance of a trained carer.
2. The process requires a time consuming and costly training process for EEG classifiers.
3. The robustness is still low due to quality and variability of the EEG signal. Some of the factors influencing negatively robustness are: noise and artifacts, long-term interface stability (long-term stability here meaning a matter of hours), drying of the electrolytic contact gel, fatigue, hormone levels, the time of day, the environment itself, etc. These factors can influence the signal negatively, resulting in patterns that the interface algorithms have difficulty in recognizing.

But if the challenge coming from the complexity of functional movements hasn't been solved yet, the possibility to combine EEG signals and other source of data to minimize perturbations (e.g. essential tremor, dyskinesia) to the desired movements is a more manageable effort. In this context, some new findings have been reported: it has been indeed verified that, for instance, muscular tremor is proxied and predicted at the cortical level of the contra-lateral side, (Hellwig et al., 2001), with time delays of some tens of ms, (Raethjen et al., 2000), (this has been quantified by using isocoherence maps between EEG and EMG). This sets the basis for the possibility of adding reliable and timing information on the onset of tremor at the peripheral level, by acquiring EEG data in combination with signals acquired at the peripheral level.

The detection of tremor contribution on EEG signals together with the one of voluntary movement, which is typical of all the classical BCI studies and is gathered by the depression of μ and β bands, can be used as a further input for algorithms dealing with the tremor detection. In this case, the multimodal BCI would rely on EEG, EMG, and IMU data to be combined together to 1) determine movement intent and initiation, 2) predict and reveal the presence of tremor, and 3) provide a real-time estimation of time-varying characteristics (amplitude and frequency) of this tremorous movement.

Over the last years, many research efforts have been focused on the fusion of the information from several different sensors technologies, e.g. EEG, EMG and inertial (gyroscopes and accelerometers). The main focus of this research is on the study of: synchronisation between muscle and the motor cortex activity, coupling in muscles and detection of oscillators, (Manto et al., 2003). EMG contains rich information that can be used to recognise neuromuscular activity in a non-invasive manner. Under normal conditions, muscle contraction is activated by the motor cortex. The control signals flow from the CNS to the PNS, finally reaching the muscle tissue. Electromyography is the study of the potentials generated during muscle contractions. The acquired EMG signal is usually considered to be random. Extracting information from EMG signals is not trivial. Many models have been proposed for surface EMG (sEMG), e.g. the Anvolcon model, (Blok et al., 1999), the EMGsim model, (Farina et al., 2001), the RRDsim model, the SiMyo model, (Duchene & Hogrel, 2000), and the Fuglevand model. However, these models do not include all the factors that affect EMG signals, such as electrode configuration and location, fibre type, blood flow, subcutaneous tissue, skin preparation, signal conditioning electronics, processing techniques and others. In the sEMG for Non-Invasive Assessment of Muscles

(SENIAM) project, most of the above-cited models were analysed and the limitations of each model discussed, (Hermens et al., 1999).
The EMG sensors not only measure mechanical limb tremor. The signals contain a broader spectrum of the muscle excitation patterns. This is an advantage of EMG as compared to inertial sensors. However, most of the methods applied to process EMG signals require certain assumptions like stationarity of the involved process. Sudden oscillators causing tremor can appear under certain conditions violating the stationarity principle. Fatigue-induced tremor is an example of time dependent tremor, (Brunetti et al., 2007).
Many research projects have used EMG to enable Human Machine Interfaces, (Ferris et al., 2006). As in EEG, the development of interfaces for wearable devices based on EMG electrodes raises operational issues, (Pons, 2008):

1. The measurement of the muscle activity is sensitive to the placement of the electrodes on the user.
2. The selectivity of the measurement is low since the acquired signal is usually considered to be random. The extraction of features from the signal requires complex models.
3. EMG-based systems usually require a learning and training process from the user.
4. The measurement of an EMG sensor could be influenced by FES electrodes.

TREMOR project aims at implementing a BCI-based detection, identification, characterization and tracking system to provide information on tremorous and voluntary motion and will allow us to be selective in the application of FES forces on only tremorous motion.

4. Discussion and conclusions

Wearable Robots (WR) may set the basis for new rehabilitation techniques. All technologies involved in robotics need further development, but actuators are the one that probably most limit wearability and portability at the present time while sensors are the most limiting efficient implementation of cHRI and pHRI.
This paper introduces WOTAS, a wearable exoskeleton able to attain a reduction ratio in the order of 80 % tremor power in specific joints of patients with severe tremor. The work presented validated the concept of tremor suppression by means of biomechanical loading. Nevertheless, the approach to mechanical suppression of tremor by means of orthotic devices presents limitations mainly due to the physical interaction between the exoskeleton and the human limb:

1. The transmission of forces through soft tissues plays an important role in the efficiency of tremor suppression. There is a physical limitation for tremor suppression through wearable devices due to force generation (size and power consumption of the actuators) and transmission through soft tissues.
2. Despite the success of the approach, there is no suitable actuator technology in terms of cosmetic and aesthetic (low weight, compact to be worn beneath the clothes) as well as functional requirements (torque, bandwidth).
3. Patients related that these bulky exoskeletons could not be considered as a solution to their problem since it is considered that the use of such device should cause social exclusion.

In summary, robotics based solutions have shown clinical evidence of the approach based on human limb impedance control. However it results in bulky and non cosmetic solutions for which patients are especially reluctant. Based on these results, authors of this book chapter identified the main limitations of the current technology used on wearable robots. In section 3, authors identify the technologies that will pave the way for the next generation of wearable robots. The use of the identified techniques is presented in the framework of the European project TREMOR.

Human muscles can be set as actuators of a wearable robotic systems. The integration of FES systems within WRs techniques over a textile sustrate will allow the creation of Soft Robots. Soft Robots are wearable robots that rely on biological information to interpret both state and intention of the user, and take advantage of his muscles as actuators. In this context, TREMOR project aims at the development of biomechanical models of human muscles under FES, in order to obtain optimal (in the senses of fatigue minimization and improvement of confortcomfort) stimulation patterns. Also an individually addressable, multielectrode FES array will be developed in order to obtain dependable and safe actuation at the pHRI.

The BCI in the context of tremor suppression must identify high-level mental states that reflect a user's desire to convey information. For this, the BCI device is defined to translate direct measures of brain activity into messages or commands to the soft robot and provide the user with real-time feedback. This BCI can also include systems that rely on passive monitoring, information derived from the peripheral nervous system and indirect measures of neural activity, such as EMG

Acquisition of bioelectrical information can be complemented with recording of actual motion by means of IMU sensors. IMU sensors provide an ambulatory, wearable means of recording limb kinematics, and, in the case of TREMOR project, serve to estimate the state of the musculo-skeletal system and to characterize tremor at joint level.

5. Acknowledgments

The work presented in this paper has been carried out with the financial support from the Commission of the European Union, within Framework 7, specific IST programme "Accessible and Inclusive ICT", Target outcome 7.2 "Advanced self-adaptive ICT-enabled assistive systems based on non-invasive Brain to Computer Interaction (BCI) ", under Grant Agreement number ICT-2007-224051, "TREMOR. An ambulatory BCI-driven tremor suppression system based on functional electrical stimulation."

6. References

Adelstein B.D., Peripheral mechanical loading and the mechanism of abnormal intention tremor, Masther thesis, MIT, 1981.

Belda-Lois J, M. Vivas, A. Castillo, F. Peydro, J. Garrido, J. Sanchez- Lacuesta, R. B. R, R. Poveda, and J. Prat, Functional assessment of tremor in the upper-limb, in *Proceedings of the 8th Congress of European Federation for Research in Rehabilitation*, 2004, p. MP30.

Benito-Leon J, Bermejo-Pareja F, Morales JM, Vega S, Molina JA. Prevalence of essential tremor in three elderly populations of central Spain. Mov Disord 2003 ;128 :389-394.

Binder DK, Rau G, Starr PA. Hemorrhagic complications of microelectrode-guided deep brain stimulation. Stereotact Funct Neurosurg 2003 ;80 :28-31.

Blok J., D. Stegeman, B. Freriks and H. Hermens, "The SENIAM Model for Surface Electromyography". 1, 71-80, 1999.

Boord P., A. Barriskill, A. Craig and H. Nguyen, "Brain-Computer Interface – FES Integration: Towards a Hand-Free Neuroprothesis Command System", J. of Neuromodulation, 7(4), 267-276, 2004.

Brookner E., *Tracking and Kalman filtering made easy*, John Wiley & Sons, Ltd., 504 pp., ISBN 0-471-18407-1.Brunetti F., M. Manto and J.L. Pons, "On the Use of a Wearable Electromyographic Tool for Neuromotor Research", 4th IEEE-EMBS Int.l Summer School and Symp on Medl Dev and Biosensors (ISSS-MDBS 2007), 98-101, 2007.

Burkhard PR, Vingerhoets FJ, Berney A, Bogousslavsky J, Villemure JG, Ghika J. Suicide after successful deep brain stimulation for movement disorders. Neurology 2004;63:2170-2172.

del Millán J.J., "Asynchronous BCI and Local Neural Clasifiers: An Overview of the Adaptive Brain Interface Project", IEEE Trans Neural Syst Rehabil Eng. 11(2), 159-161, 2003.

Deuschl G, Raethjen J, Lindemann M, Krack P. *The pathophysiology of tremor. Muscle Nerve* 2001 Jun;24(6):716-735.

Dobkin B.H., "Brain-Computer Interface Technology as a Tool to Augment Plasticity and Outcomes for Neurological Rehabilitation". J. Physiol., 579(3): 637-642, 2007.

Duchene J. and J. Hogrel, "A Model of EMG Generation". IEEE Trans on Biomed Eng, 47(2), 192-201, 2000.

Farina D., A. Crosetti and R. Merletti, "A Model For The Generation of Synthetic Intramuscular EMG Signals to Test Decomposition Algorithms". IEEE Trans on Biomed Eng, 48(1), 66-77, 2001.

Ferris D.P., K.E. Gordon, G.S. Sawicki and A. Peethambaran, "An Improved Powered Anklefoot Orthosis Using Proportional Myoelectric Control", Gait & Posture, 23, 425-28, 2006.

Findley LJ, Koller WC. Definitions and behavioral classifications. In: *Handbook of tremor disorders*. Findley LJ, Koller WC (eds). Marcel Dekker, New York, 1995, pp 1-5.

Hawkings D. and Hull M., "A Method for Determining Lower Extremity Muscle-Tendon Lengths during Flexion/Extension Movements", *Journal of Biomechanics*, 23, 487-494, 1990.

Hellwig B., S. Haussler, B. Schelter, M. Lauk, B. Guschlbauer, J. Timmer and C.H. Lucking, "Tremor-Correlated Cortical Activity in Essential Tremor". Lancet, 357(9255), 519-523, 2001.

Hermens H., B. Freirks, R. Merletti, D. Stegeman, J. Blok, G. Rau, C. Disselhorst-Klug and G. H'agg, "European Recommendations for Surface Electromyography". Roessingh Research and Development, 8, 1999.

Lloyd D.G. and Besier T.F., "An EMG-Driven Musculoskeletal Model to Estimate Muscle Forces and Knee Joint Moments in Vivo", *Journal of Biomechanics*, 36, 765-776, 2003.

Louis ED. Essential tremor. Lancet Neurol 2005; 4 :100-110.

Louis ED, Honig LS, Vonsattel JP, Maraganore DM, Borden S, Moskowitz CB. Essential tremor associated with focal nonnigral Lewy bodies: a clinicopathologic study. Arch Neurol 2005;62:1004-1007.

Mann K.A., Werner F.W., Palmer A.K., "Frequency spectrum analysis of wrist motion for activities of daily living. Journal of Orthopedic Research", 7, 304-306, 1989.

Makssoud H.E., Guiraud D. and Poignet P., Mathematical muscle model for functional electrical stimulation control strategies », *International Conference on Robotics and Automation*, 2, 1282-1287, 2004.

Manto M., M. Topping, M. Soede, J.Sanchez-Lacuesta, W. Harwin, J.L. Pons, J. Williams, S. Skaarup and L. Normie, "Dynamically Responsive Intervention for Tremor Suppression", IEEE Eng. in Med. and Biol., 22(3), 120-132, 2003.

Mason S.G., and G.E. Birch, "A General Framework for Brain-Computer Interface", IEEE Trans Neural Syst Rehabil Eng, 2003. 11(1), 70-85, 2003.

Mayol WW, Tordoff B, Murray DW, 2004. Towards wearable active vision platforms. In Systems, Man, and Cybernetics, 2000. *Conference Proceedings. 2004 IEEE International Conference on*, 3, pp. 1627–1632.

Moreno JC, Rocon E, Ruiz A, Brunetti F, Pons JL 2006 Design and implementation of an inertial measurement unit for control of artificial limbs: application on leg orthoses. *Sensors and Actuators B* 118, pp. 333–337.

Niranjan A, Kondziolka D, Baser S, Heyman R, Lunsford LD. Functional outcomes after gamma knife thalamotomy for essential tremor and MS-related tremor. Neurology 2000;55:443-446

Pons, J.L., 2005, *Emerging Actuator Technologies. A Micromechatronic Approach*, John Wiley & Sons, Ltd., 278 pp., ISBN 0-470-09197-5.

Pons, J.L. (ed.), 2008, *Wearable Robots: Biomechatronic Exoskeletons*, John Wiley & Sons, Ltd., 360 pp., ISBN 978-0-470-51294-4.

Popovic, D.B., Sinkjaer, T., 2000, Control of the movement of the physically disabled, Springer Verlag, 481 pp., ISBN 978-1-852-3-32279-4.

Popovic-Bijelic, A., Bijelic, G., Jorgovanovic, N., Bojanic, D., Popovic, M.B., Popovic, D.B., 2005, 'Multi-filed surface electrode for selective electrical stimulation', Artificial Organs, 29(6):448-452.

Raethjen J., R.B. Govindan, F. Kopper, M. Muthuraman and G. Deuschl, "Cortical Involvement in the Generation of Essential Tremor", J. Neurophysiol., 97(5), 3219-3228, 2000.

Rajput A, Robinson C, Rajput AH. *Essential tremor course and disability: a clinicopathologic study of 20 cases*. Neurology 2004; 62: 932-936.

Riener, R., Fuhr, T., 1998, 'Patient-driven control of FES-supported standing up: a simulation study', *IEEE Transactions on Rehabilitation Rehabilitation Engineering*, 6(2):113-124.

Riley P.O., Rosen M.J., "Evaluating manual control devices for those with tremor disability", *Journal of Rehabilitation Research and Development*, 24, 99-110, 1982.

Riviere C. *Adaptive suppression of tremor for improved human-machine control*, Ph.D. thesis, Johns Hopkins University, 1995.

Rocon E., Andrade A.O., Pons J.L., Kyberd P. and Nasuto S.J.. "Empirical mode Decomposition: a Novel Technique for the Study of Tremor Time Series", *Medical and Biological Engineering and Computing*, 44(7), 2006.

Rocon E., Belda-Lois, J.M., Ruiz, A.F., Manto, M., Moreno, J.C., Pons, J.L, 2007, Design and validation of a rehabilitation robotic exoskeleton for tremor assessment and suppression', *IEEE Transactions on Neural Systems and Rehabilitation Engineering*, 15(3):367-378.

Schwartz A.B., X. Cui, D. Weber and D. Moran, Brain-controlled interfaces: movement restoration with neural prosthetics, *Neuron*, 52(1), 205-220, 2006.

Sellers E.W., and E. Donchin, "A P300 Based Brain-Computer Interface: Initial Tests by ALS Patients", Clin Neurophysiol, 117(3), 538-548, 2006.

Thanvi B, Lo N, Robinson T. Essential tremor – the most common movement disorder in older people. Age Ageing 2006;35:344-349.

Ushe M, Mink JW, Revilla FJ, Wernle A, Schneider Gibson P, McGee-Minnich L, Hong M, Rich KM, Lyons KE, Pahwa R, Perlmutter JS. Effect of stimulation frequency on tremor suppression in essential tremor. Mov Disord 2004;19:1163-1168.

Widrow B. and Stearns S.D., *Adaptive signal processing*, Prentice Hall, 528 pp, ISBN 0-130-04029-0. Wolpaw J.R., N. Birbaumer, D. McFarland, G. Pfurtscheller and T. Vaughan, "Brain-Computer Interces for Communication and Control", Clin Neurophysiol., 113, 767-791, 2002.

Wolpaw J.R., "Brain-Computer Interfaces as a New Brain Output Pathways". J. Physiol, 579(3), 613-619, 2003.

Young RF, Jacques K, Mark R, et al. Gamma knife thalamotomy for treatment of tremor: long-term results. J Neurosurg 2000;93:128-135.

Zajac, F.E., "Muscle and Tendon: Properties, Models, Scaling and Application to Biomechanics and Motor Control", *Critical Reviews in biomedical Engineering*, 17(4), 359-411, 1989.

14

Processing surface electromyographical signals for myoelectric control

Sorin Herle and Sergiu Man
Technical University of Cluj Napoca
Romania

1. Introduction

Myoelectric control is the most widely used approach for the control of upper limb prostheses (Ping et al., 2006); (Light et al., 2002); (Chan & Englehart, 2005). When used as control input, the myoelectric signal has dominated because it has several advantages over other input types. Among these advantages are the detection of the signal on the skin surface without any injury for the patient, the small magnitude of the muscle activity required to provide control signals, which resemble the effort required of an intact limb, and the possibility to use the signal for proportional control with relative ease (Parker et al., 2006).

The functionality requirement of the prosthesis increases with the level of amputation, and this demands more effort to control the device. To compensate for the burden, the challenge is to develop control systems that are able to assist the patient in using the prosthesis. As the myoelectric prostheses use biological signals to control their movements, it is expected that they should be much easier to be used by a patient. Contrary to this idea, as Soares et al. (2003) mention, the prosthesis control is very unnatural and requires a great mental effort, especially during the first months after fitting.

Various factors such as the anatomical and physiological properties of muscles, the characteristics of the instrumentation used for detection and processing, the position were the sensor is applied, the surface of the skin and the tissues between de skin and the muscle (Soares et al., 2003) determine the complexity of the surface electromyographical (SEMG) signal. Therefore, a precise detection of the SEMG signal is an important issue. Due to the small amplitude of the SEMG signal, the accuracy of the acquired signal is affected by noise.

Several methods have been developed to process the surface electromyographical signals used in myoelectric control. In this chapter few of them will be described and some results will be presented. The remainder of this chapter is organized as follows. Section 2 is dedicated to pattern-recognition based methods, different approaches are presented and two examples are given. Section 3, reviews few non-pattern recognition based methods. The chapter concludes with a comparison of the methods presented and with an outline of promising directions for future research.

2. Processing of surface electromiographical signal based on pattern recognition

2.1 Short description

The surface myoelectric signals provide rich information about the neuromuscular activity from which they originate and, as a consequence, about the intention to achieve a certain movement. The analysis of myoelectric signals has generated useful information used in clinical diagnosis, as well as in control systems for assistive devices.

The objective of SEMG analysis is to extract meaningful features from the SEMG signals, which can find their use in myoelectric control systems for rehabilitation devices or assistive robots.

The first investigator to study electromyographical (EMG) signals is considered H. Piper using a string galvanometer. The EMG signal began to be used in clinical diagnosis since 1928 and it was in the 1960s when a team of experts presented the first myoelectric prosthesis. Myoelectric control has seen an incremental evolution since then. Still, the complexity of the EMG signal represents the greatest challenge in its application.

There are two different classes of myoelectric control systems: pattern recognition based and non-pattern recognition based. In the former, classifiers are used for discriminating the desired classes from signal patterns. Non-pattern recognition based controllers are mainly constructed on finite state machines or threshold control. Over the last years, as classification algorithms have become more and more complex, the greatest success in myoelectric control has been realized by pattern recognition based control systems. The idea is to associate the different patterns found repeatedly in the EMG signal with the corresponding member movements.

2.2 Segmentation of data

As myoelectric based control systems must meet certain real-time requirements, segments are usually used in EMG analysis. A segment is a time section considered for analysis and feature extraction. Various windowing techniques can be used for these tasks, but all should respect the assumption that, considering real-time constraints, the response time of the control system should be equal or less than 300 ms (Oskoei & Hu, 2007)

There are two basic major windowing techniques used in data segmentation, the adjacent windowing and the overlapped windowing. The adjacent windowing technique uses custom length adjacent segments for analysis and feature extraction, as shown in Fig. 1.

Because of high-speed processors, usually, the processing time is less than the duration of each time segment, so, for each segment, there remains a certain amount of idle time. In the overlapping windowing technique, this idle time of the processor is used for acquiring more data to be processed. The technique is making full use of the processor, and each time segment slides over the one before, as Fig. 2 illustrates. The technique, applied by Englehart and Hudgins (2003) achieves the best performance using continuous segmentation and a segment length of 32 ms. Majority voting was also used as a post-processing method. For a given point majority voting includes a number of k last and next decisions to generate a new one based on the greatest number of occurrences. The computing time for making each decision should not be greater than the acceptable delay of the system.

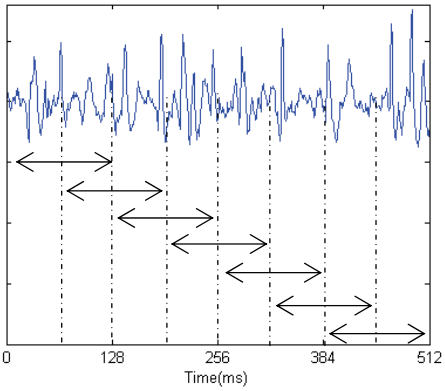

Fig. 1. Adjacent windowing technique

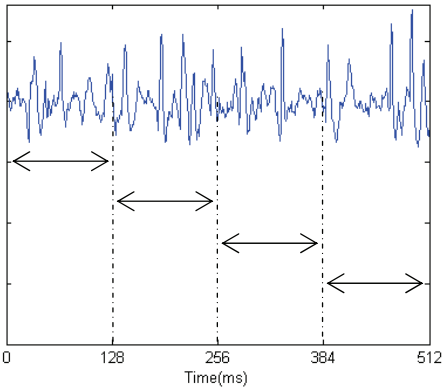

Fig. 2. Overlapped windowing technique

2.3 Feature extraction

The use of row myoelectric signal in a control system is impractical, especially due to the large number of inputs. Noise, randomness of the signal, and the large dimension of the input vector all become real problems in an EMG control system, especially when using embedded systems with limited resources. Moreover, if the final goal is to use this signal to control a prosthetic device, it is absolutely mandatory to reduce as much as possible the length of the input vector. That is because their controllers must meet very strict real time constraints and the classifiers they implement perform much faster when handling small input vectors. Transformation of the initial input space into a more adequate one, by mapping each input vector into a smaller dimension feature vector, is called *feature extraction*. Over the years, feature extraction has been used in pattern recognition and image processing. Oskoei and Hu (2007) review various feature extraction methods used over the time in myoelectric control systems. Based on their classification time domain, frequency domain and time-scale domain features will be analyzed and compared in next section, with focus on using the results for creating a robust control scheme for myoelectric control.

2.3.1 Time domain features

The accessibility and the computational simplicity make time domain features the most popular tools for generating outputs for the myoelectric control system. They are based on time-amplitude representation of the signal, and can indicate measures like signal energy force and duration. Hudgins et al. (1993) and Herle et al. (2008) studied a set of five features and used the results for generating inputs for an neural network based classifier, to achieve a classification rate between 90 and 96.67%. The set they used contains five representative features for time domain representation:

MAV represents the mean absolute value of the segment analyzed. Eq. 1 is used to compute this value:

$$\overline{x_i} = \frac{1}{S} \sum_{m=1}^{S} \left| x_m \right| \tag{1}$$

where: $i = 1 \ldots I$ is the segment number; S is the number of samples for a segment and x_m is the m^{th} sample in the segment i. MAV usually provides a maximum estimation of amplitude when the signal is modeled as a Laplacian process, the alternative being Root Mean Square (RMS) (witch better estimates Gaussian processes). Farina and Merletti (2000) provided a comparative review of the two.

The Mean Absolute Value Slope is the difference between the Mean Absolute Values computed for two adjacent segments:

$$\overline{\Delta x_i} = \overline{x}_{i+1} - \overline{x}_i \tag{2}$$

where i and $i+1$ are two adjacent segments and $i = 1 \ldots I-1$.

Zero Crossings is a measure of frequency which can be obtained by counting the number of times the waveform crosses zero. A threshold was included in order to reduce the noise-induced zero crossings. The zero crossing counter is incremented if the condition described by Eq. 3 is satisfied for two consecutive samples x_m and x_{m+1}.

$$\begin{aligned} &\{x_m > 0 \ and \ x_{m+1} < 0\} \ or \ \{x_m < 0 \ and \ x_{m+1} > 0\} \\ &and \ \left| x_m - x_{m+1} \right| \geq \varepsilon \end{aligned} \tag{3}$$

The Slope Sign Changes counts the number of times the slope changes sign. The same threshold as for the zero crossings was used. The SSC counter is incremented if the condition (4) is true for three consecutive samples, x_{m-1}, x_m, x_{m+1}:

$$\begin{aligned} &\{x_m > x_{m-1} \ and \ x_m > x_{m+1}\} \ or \\ &\{x_m < x_{m-1} \ and \ x_m < x_{m+1}\} \ and \\ &\left| x_m - x_{m+1} \right| \geq \varepsilon \ or \ \left| x_m - x_{m-1} \right| \geq \varepsilon \end{aligned} \tag{4}$$

Eq. 5 indicates a measure of the waveform amplitude, frequency and duration in a single parameter called waveform length:

$$l = \sum_{m=1}^{S} \left| \Delta x_m \right| \tag{5}$$

where:

$$\Delta x_m = x_m - x_{m-1} \tag{6}$$

Time domain features are also used in combination with other techniques to produce a high classification rate. Chan and Englehart (2005) used the combination of autoregressive coefficients and RMS and obtained a classification rate about 94.6 %.

2.3.2 Frequency domain features

Up until now, we have discussed features extracted from time domain representation of signal. Another class of features, mostly used in fatigue study, are frequency domain features. The power spectrum of a signal represents the contribution of every frequency of the spectrum to the power of the overall signal. It is useful because many signal processing applications, such as noise cancellation and system identification, are based on frequency-specific modifications of signals. The frequency content of a stationary signal is derived from the Fourier transform of the signal, defined by

$$FT_x(f) = \int x(t)e^{-2\pi jft}dt \tag{7}$$

$$X(t) = \int FT(f)e^{2\pi jft}df \tag{8}$$

Spectral analysis is the process of identifying component frequencies in data. Power spectral density (PSD) is a positive real function of a frequency variable associated with a stationary stochastic process, or a deterministic function of time and plays a major role in spectral analysis. PSD describes how the power of a signal or time series is distributed with frequency and is defined as the Fourier transform of the autocorrelation function of a signal. The mean frequency and the median frequency are characteristic variables of PSD intensively used in EMG signal analysis, especially in fatigue, force and angle or torque studies (Gerdle & Karlsson, 1994). Peak frequency, mean power and total power are also spectral parameters used in EMG analysis. PSD estimation techniques can involve parametric or non-parametric approaches, and may be based on time-domain or frequency-domain analysis. For example, a common parametric technique involves fitting the observations to an autoregressive model. A common non-parametric technique is the periodogram. In the autoregressive method, the main problem is the determination of the model order. With the periodogram, other problems, such as large estimation variance and small frequency resolution, still remain a challenge. Also, with all PDS estimation methods we lose the information regarding the time at which each event took place.

2.3.3 Time-frequency features

The coefficients X(f) from the Fourier Transform denote the frequency domain distribution of a signal with no temporal resolution and, as a consequence, they do not reflect the transient proprieties of a signal. Time frequency representations (TFR) preserve information regarding both the time structure and frequency structure of a signal. They combine the above-mentioned methods of analysis to yield a clearer picture of a signal's spectral characteristics at very precise temporal localizations. Image processing, speech recognition or geo-acoustic applications, all found the utility of TFR representations. TFR are divided in two groups: linear TFRs (Fourier and wavelet transform) and quadratic TFRs (Wigner-Ville distribution). As the extracted features are usually used in real time applications and the

quadratic methods are based on complex, time consuming algorithms, in the next section we will concentrate on the former. The central concept of linear methods is that of decomposing a signal into time frequency atoms (Eq. 9):

$$x(t) = \sum_{i=1}^{N} c_i \beta_i(t) \tag{9}$$

where $\beta_i(t)$ are the so called basis functions and c_i the corresponding coefficients. The basis function must offer good time frequency localization and also, be computationally efficient. In the following section we will discuss three TFRs: the short time Fourier transform, the wavelet transform and the wavelet packet transform.

2.3.3.1 The Short Time Fourier Transform

The short time Fourier transform (STFT) is a two dimensional function of time and frequency. The central idea of STFT is to partition the time axis through a limited window, and assume that the signal is stationary over short periods of time. If $w(\tau-t)$ is the windowing function, the STFT equation is:

$$STFT(t, f) = \int x(\tau) w^*(\tau - t) e^{-2\pi j f \tau} d\tau \tag{10}$$

It is important to observe that the information provided by STFT is limited by the size of the analysis window. The choice of $w(t)$ is the main factor on which the time frequency resolution depends. It is important to know that the product between time and frequency resolution must be lower bounded by $1/4\pi$ according to the time-bandwidth uncertainty principle.

2.3.3.2 The Wavelet Transform

Wavelet theory was first described in the early 20th century. It occurred as the next logical step: a windowing technique with variable-sized regions. Wavelet analysis allows the use of long time intervals where we want more precise low-frequency information, and shorter regions where we want high-frequency information. Wavelet analysis reveal particularities of data that other signal analysis techniques miss, like discontinuities in higher derivatives, trends and breakdown points. Wavelet analysis can also compress or de-noise a signal without appreciable degradation.

The continuous wavelet transformation (WT) can be defined as:

$$CVT(a, t) = \frac{1}{\sqrt{a}} \int x(\tau) \psi^*\left(\frac{\tau - t}{a}\right) d\tau \tag{11}$$

and determines the correlation of the signal with a shifted and scaled mother wavelet. The term scale is preferred to the term frequency when using WT because time-scale view is a very natural way to view data deriving from a great number of natural phenomena. A high scale shows slowly changing features, with low frequency, and a low scale illustrates the high frequency details of a signal.

2.3.3.3 The Wavelet Packet Transform

The wavelet packet transformation (WPT) is a generalization of wavelet decomposition that offers a richer range of possibilities for adapted signal analysis. It uses a configurable tiling of the time-frequency space, so the partitioning of the axis may take many forms to suit the application. The main difference between STFT, WT and WPT is the manner in which they partition the time frequency or the time scale plane. A STFT use a plane composed of cells with identical aspect ratio in time and in frequency. A WT offers a variable tiling of time scale plane, as frequency resolution is proportional with the center frequency, allowing greater frequency resolution at lower frequencies and better time resolution at high frequencies.

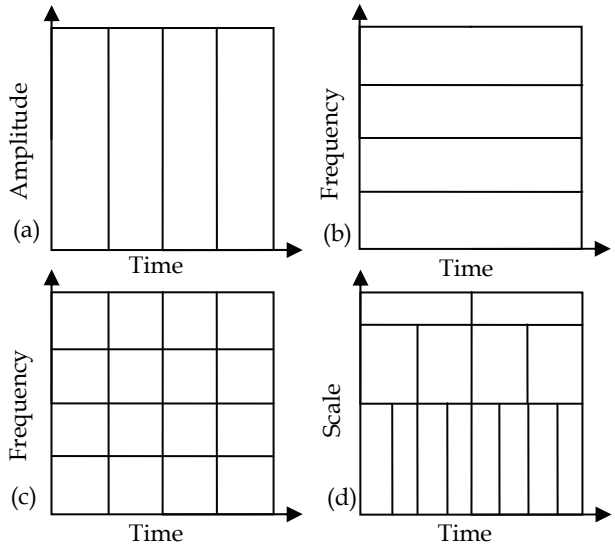

Fig. 3. Four partition methods: (a) Time domain (Shannon), (b) Frequency, Domain (Fourier), (c) STFT (Gabor), (d) Wavelet analysis

The arbitrary segmentation of the frequency axis is provided by WPT. This allows a selection procedure for providing the best set partition for a specific application.
Fig. 3 illustrates the way each technique partitions the corresponding representation plane.

2.3.4 Dimensionality reduction

The methods mentioned above transform the initial input space in a more adequate one, but not necessary in a smaller dimension. The dimensionality reduction's role is to retain the most important information for class discrimination and discard what is irrelevant for the purpose of classification. It is easier to analyze and build a classifier with fewer inputs. This information selection can be achieved by selecting an optimal feature set. Feature selection and feature projection are two fundamentally different approaches to determining the beast feature set.

Feature selection, also known as variable subset selection, is the technique of selecting a subset of relevant features according to some criterion. It requires a search strategy such as sequential forward or backward selection, simulated annealing or Genetic algorithms.
Feature projection methods try to achieve minimal loss of information while describing the data as concisely as possible. Principal component analysis (PCA) and linear discriminate analysis techniques are two of the mapping functions used for feature projection. For instance, PCA will generate components ranked according to the information they contribute to the data, in a mean square error sense. Different feature projection techniques can also be used together for obtaining better results. K. Englehart et al. (1999), investigated feature projection techniques in time-frequency features and achieved the highest classification rate using the WTP/PCA/LDA combination. Also a self-organizing feature map was used in addition to PCA by Chu et al. (2005), leading to significant improvements.

2.4 Classification

As Fig. 4 illustrates, the classification of EMG signal is a multi stage process, and the actual classification algorithm is only the last of the stages. As already seen, signal representation, achieved by feature extraction, and dimensionality reduction, are vital for obtaining meaningful information for classification. The classifier's role is to use this information and generate distinctive classes corresponding to the desired motions.

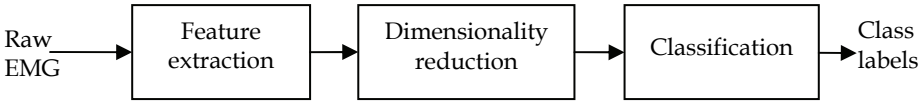

Fig. 4. The stages of the classification problem

The recognition of the signal characteristics has been performed using a number of soft-computing approaches, such as neural networks (NN), fuzzy logic or neuro-fuzzy.

2.4.1 Neural networks based classifiers

Neural networks are structures composed of elements inspired by biological nervous systems. As in nature, the connections between elements largely determine the network function. In the last decade, NNs have been intensively used for modelling linear and non linear relationships from a finite number of samples. Once the model is obtained from the training data, it can be used to predict the output values corresponding to the input vector. One of the main advantages in using NNs is that they require no a prior information about the process, and still yield high classification rates.
For example, Soares et al. (2003), have used a multi-layer perceptron (MLP) in combination with an AR technique for feature extraction, and have obtained a very high rate of success. Kuruganti et al. (1995) used two channels with five time domain features per channel to classify four functions with an NN classifier and 90% classification. Chaiyaratana et al. (1996) have used two different types of radial basis function NN. Also, Englehart et al. (1999) used a combination of time scale features, principal component analysis and a MLP classifier to obtain a high rate of success (over 90%). Also time-delayed artificial neural network had been used by Au and Kirsch (2000) in combination with time domain features.

2.4.1.1 Multi-layer perceptron

Multi-layer perceptron is the most commonly used NN architecture for pattern classification.

MLP is composed of neurons or nodes, which usually employ a sigmoid nonlinearity or a linear function. Fig. 5 illustrates the architecture of a typical MLP network:

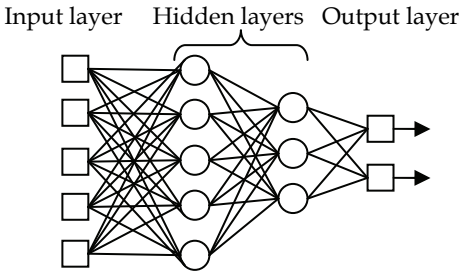

Fig. 5. MLP network architecture

Its fundamental computational unit is the perceptron. Its role is to form a weighted sum of the components of the input vector and to add a bias value. The result is then passed through nonlinearity as *logistic sigmoid* or *hyperbolic tangent sigmoid.*

In the training process, the network weights are adapted so as to provide suitable mapping of input vectors in a set of desired responses. The most used training algorithm for MLP is the backpropagation algorithm. It is a stochastic approximation of the steepest descent algorithm, in which the network weights are moved along the negative of the gradient of the performance function. The process of computing the gradient and adjusting the weights is usually stopped when a certain stopping criteria is achieved. A minimum value of the magnitude of the gradient, or of the sum squared error is common stopping criterions.

The input vector feeds into the first layer and each node of the output layer corresponds to a class in a pattern recognition problem The MLP architecture may contain multiple hidden layers, but according to Haykin (1998), given sufficient neurons, a single hidden layer is enough to approximate arbitrary functions.

Karlik et al. (1994), Ito et al. (1991) and Kelly et al. (1990) published early studies on using MLP as a myoelectric classifier. Recently, Zhao et al. obtained an accuracy of 95% by applying MLP to recognize six motion patterns.

2.4.2 Fuzzy classifiers

Fuzzy logic approaches exploit the partial truth and uncertainty, which make them popular in bio-signal classification and processing. Fuzzy logic systems can discover patterns difficult to detect, and can tolerate contradictions in data. One can also create a fuzzy system to match any set of input-output data. The values detected by the EMG sensors are transformed by the fuzzyfier into linguistic variables, that is, variables whose values are words rather than numbers.

In (Micera et al., 2000) authors evaluated the performance of a variety of neural and fuzzy classifiers: self-organizing maps (SOM), fuzzy c-means (FCM), multi-layer perceptrons (MLP), and Abe-Lan fuzzy network (ALFN) using small-sized training sets. The reported

results were: 50% for SOM, 53.33% for FCM, 86.66% for MLP, and 93.33% for ALFN. Also, in (Leowinata et al.,1998) a fuzzy logic classifier was used on data collected from an array of electrodes, and in (Weir et al., 2003), authors also proposed a fuzzy logic based prosthesis controller.

2.4.3 Neuro-fuzzy classifiers

Neuro-fuzzy is a way to exploit the advantages of both techniques by combining fuzzy logic and neural networks. Neuro-fuzzy techniques have been widely used for data analysis and decision-making (Nauck & Kruse, 1997). A neuro-fuzzy system can be viewed as a feed forward neural network where the first layer represents input variables, the middle (hidden) layer represents fuzzy rules and the third layer represents output variables (Nauck et al., 1997). Neuro-adaptive learning techniques provide a method for the fuzzy modeling procedure to learn information about a data set. Fig. 6 presents a typical structure of a neuro-fuzzy system.

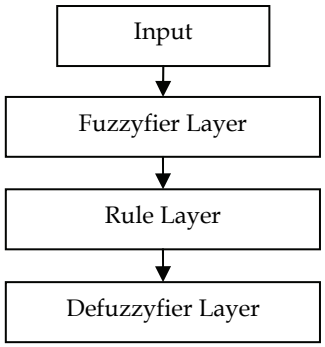

Fig. 6. Structure of a neuro-fuzzy system

(Hussein & Granat., 2002) uses a neuro-fuzzy inference system (ANFIS) on atoms obtained with the Gabor matching pursuit algorithm. He used a generalized bell function (Eq. 12) as the membership function for the Sugeno type fuzzy classifier and the least-squares error Eq. 13 as a cost function for adjusting the coefficients.

$$\mu(x) = \frac{1}{1 + \left| \frac{x - c}{a} \right|^{2b}} \tag{12}$$

$$\varepsilon(n) = \frac{1}{2} \sum_{i=1}^{N} e_i(n)^2, e_i(n) = d_i(n) - y_i(n) \tag{13}$$

Where $d_i(n)$ is the desired output and $y_i(n)$ is the actual output of the network. He obtained a 95% rate of classification.

In (Karlik et al., 2003), authors presented a comparative study of the classification accuracy of myoelectric signals using three classifiers: MLP NN, conic section function NN and fuzzy clustering NN. They obtained the highest classification rate (98.3%) with the fuzzy

clustering NN. A 6 class motion recognition system was proposed in (Kiguchi et al., 2003), applied on time features extracted from 11 channels data, based on a neuro-fuzzy classifier.

2.5 Examples

The next section will present the development of two multifunction myoelectric classifiers. Different types of features and different classifier schemes will be used.

2.5.1 Example 1

The first example will describe a myoelectric classifier based on a multi-layer perceptron. The inputs provided to the network are the autoregressive coefficients. The classification performance of the feature sets was investigated for four classes of movement. The system architecture is presented in Fig. 7.

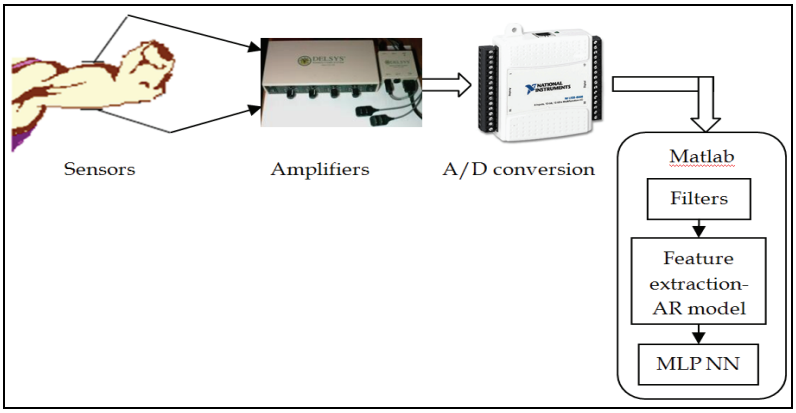

Fig. 7. System architecture based on neural network classifier

Bagnoli 4 system from Delsys Inc. was used for data acquisition, in combination with NI USB-6009 AD card from NATIONAL INSTRUMENTS, The system offers a gain factor between 0 and 10000 and a bandwidth of 20-450 Hz ±10%.
The signals were acquired from the biceps ant the triceps muscles using two differential sensors and a amplification of 1000. Adjacent segments with lengths of 256 samples each were processed. The forearm movements were detected using a goniometer, like the one in Fig. 8 and each class of movement have been associated with a correspondent segment of the myoelectric signal.

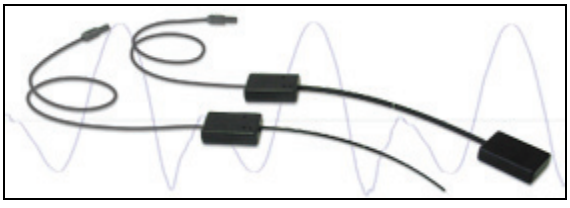

Fig. 8. The goniometer

As the power spectrum of the signal is concentrated in the 20-500Hz range (Soares et al. 2003), first step in signal processing is applying a Butterworth band-pass filter with cut-off frequencies of 20 Hz (low) and 450 Hz (high).

Soares et al. (2003) had shown the fact that AR modeling of the EMG signal offers very good performance in MES classification. It also leads to a small dimension feature vector and therefore to a reduced processing time.

Autoregressive model is commonly used to parameterize linear systems. AR model attempt to predict an output $\overline{x(n)}$ of a system based on the previous outputs (*x(n-1), x(n-2),…)*. AR model is based on the Eq. 14:

$$\overline{x(n)} = \sum_{i=1}^{M} a_i x(n-i) + e(n), n = 0..N-1 \tag{14}$$

where a_i are the AR coefficients, M is the model order and N, the size of the segment considered for analysis, $x(n)$ are the samples of the actual signal and $\overline{x(n)}$, the samples of the modeled signal. AR methods are widely used for spectral estimation, as they are determined by considering x(n) as the output of a system characterized by the transfer function Eq. 15:

$$G(f) = \frac{1}{1 + \sum_{i=1}^{N} a_i e^{-2\pi jft}} \tag{15}$$

with Gaussian noise used as input.

The power spectral density of $x(n)$ can, therefore, be expressed as Eq. 16 illustrates. The estimation of power spectrum consists of the AR parameters determination according to a proper algorithm.

$$P_{xx} = \sigma_w{}^2 G(f)^2 \tag{16}$$

Studies have shown that an AR model of a sufficiently large, but finite order M, might approximate, with a specified degree of accuracy, any model (Hefftner et al., 1988). In calculating the AR coefficients we followed the steps suggested in (Akay, 1996) :

- initialize the filter coefficients.
- calculate the predicted value of the input signal

$$\overline{x(n)} = \sum_{i=1}^{M} a_i x(n-i) \tag{17}$$

estimate the prediction error

$$e(n) = x(n) - \overline{x(n)} \tag{18}$$

update the AR-coefficients using the constant of convergence μ

$$a_i(n+1) = a_i(n) - 2\mu e(n) x(n-i) \tag{19}$$

An ideal value for the constant of convergence cannot be found, and it is not practical to look for a specific value of μ for every single EMG signal to be processed. Based on multiple tries, we used μ=0.01, as it provided the best approximation for most of the signals used.
Farina and Merletti (2000) showed that a model of order 10 works appropriately for any segment length. Soares et al. (2003), concluded that a fourth order model can adequately represent the EMG signal. We searched a best approximation in models with orders between 4 and 10. As the results didn't show improvements when using a higher model order, order 4 was the choice for calculating the AR coefficients.
A three-layered feed-forward neural network was used in the next step for classifying the obtained AR coefficients into the four classes of motion.
There were recorded a set of 200 patterns for each of four classes of motion for training the network. Also, typically, the backpropagation algorithm had been used in the training process. The number of epochs set for the training stage was 200. This value had been chosen considering the use of Levenberg-Marquardt method for backpropagation algorithm, which appears to be the fastest method for training moderate-sized feed-forward neural networks.
After trained, the neural network was presented with a new set of EMG pattern. The test set was represented by 200 patterns for each of four classes of motions. A 91.50% classification rate was achieved. The recognition rates varied between 90% and 92.50% as follows: 90% for flexion, 92.50 for extension, 92% for pronation and 91.50 for supination.

2.5.2 Example 2

Herle et al. (2008) presented the architecture of a rehabilitation system able to assist the patient. They used a neural network classifier to classify time domain features. Four motions of the forearm: extension, flexion, pronation and supination were controlled using a feed-forward neural network (FFNN) based classifier.
Feeding the SEMG signal as a time sequence, directly into the classifier, is not a feasible approach, because of the complexity of SEMG signal, the large number of inputs and randomness of the signal. Moreover, if the final goal is to use this signal to control a prosthetic device, it is absolutely mandatory to reduce as much as possible the length of the input in order to reduce the delay between signal detection moment and the effective actuation of the device. One solution is to map the initial sequence into a smaller dimension vector, called the feature vector.
Over the years many features were suggested for myoelectric classification. The amplitude of a SEMG signal and its related features are often investigated in time-domain analysis. Time-domain features are the most popular in myoelectric classification due to their computational simplicity.
Features were extracted from a window of two hundred samples (200 ms) of the SEMG signal, even if the length of the recorded signal was one second. The 200 ms window was empirically selected. It is better to use, however, first 200 ms after onset moment. The two hundred samples were divided into five segments, each one having a length of 40, as Figure 9 show. For each segment five features have been computed: Mean Absolute Value (MAV), Mean Absolute Value Slope (MAVS), Zero Crossing (ZC), Slope Sign Changes (SSC), and Waveform Length (WL) (Hudgins et al., 1993).

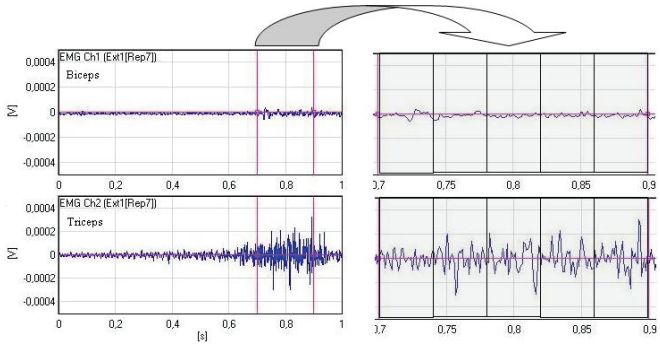

a) b)

Fig. 9. Waveform segmentation. a) The SEMG signal from biceps (up) and triceps (down) during 1 second. b) Five segments of 40 ms used for feature extraction (Herle et al., 2008)

Subasi et al. (2006) used an extra segment beside the five segments. The features for the sixth segment were calculated as the arithmetic mean of the values computed for the first five segments.

A set of 60 features (5 features/segment x 6 segments x 2 channels) were computed for each movement (Herle et al., 2008). Using the 60 features as inputs for the neural network classifier conducted to a rate of discrimination around 90%. Previous studies showed that by reducing the set of features and choosing the best features according to some criteria, the classifier performance can be improved. The classifier architecture was modified using a neural network with ten neurons on the input layer, two hidden layers each one having ten neurons, and one output layer with four neurons. The transfer function of the hidden layers was a sigmoid and that of the output layer was linear. After the training session, the classifier was tested with features extracted from signals that never been used. The meaning of the outputs' values, used to discriminate among the four motions is presented in Table 1. Figure 10 illustrate the classifier performances.

Network's outputs	Forearm movements			
	Extension	Flexion	Pronation	Supinatio
1	1	0	0	0
2	0	1	0	0
3	0	0	1	0
4	0	0	0	1

Table 1. Codification of the four movements

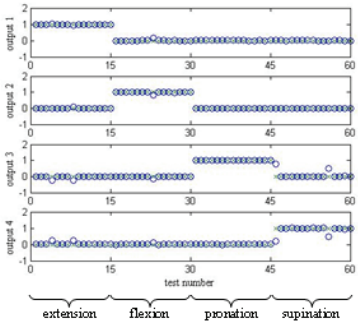

Fig. 10. Classifier responses to 60 test movements (Herle et al., 2008)

The rate of recognition increased from about 90%, when 60 inputs were used, to 96.67% when 10 inputs were used.
This example show that a satisfactory rate of discrimination can be achieved using an easy to implement classifier. The main disadvantage of this approach is the computational time required by the classifier.
Actually there is a trade between the computational time and the performance of the classifier.

3. Processing of surface electromyographical signals using non-pattern recognition based methods

Non-pattern recognition-based methods can be applied in myoelectric control. These methods are used in rehabilitation field for specific applications like wheelchair control (Moon et al., 2005); (Felzer & Freisleben, 2002), upper and lower limb prosthesis control, etc. Different types of control systems can be implemented based on these methods. Thus proportional control, threshold control, onset analysis and finite state machines are approaches included in the category of non-pattern recognition based methods. These approaches will be presented in the remaining of this section. The main drawback of these methods is the limited number of functions that can be implemented, comparing with the pattern-recognition based methods. In some cases non-pattern recognition based methods are combined with pattern-recognition based methods, resulting in a more efficient method in terms of computational power and time required.

3.1 Proportional control

In proportional control, the level of contraction of a muscle is used to control the speed or force of a prosthetic limb. Due to the complexity of SEMG signal it is mandatory to preprocess the signal acquired by sensors before using it as input for the proportional controller. Proportional control is usually used in conjunction with other non-pattern recognition-based method or pattern recognition-based method. This combination will increase the accuracy of positioning and force level.

3.2 Threshold control

Like proportional control, threshold control can be used in conjunction with other pattern recognition-based methods. In threshold control a signal level is used to discriminate between two states. For example if the amplitude of the EMG signal is over a threshold, a given action will take place, based on the command generated. Figure 11 illustrates this mechanism. This type of control is suitable only for discrete actions like "*open hand*" or "*close hand*".

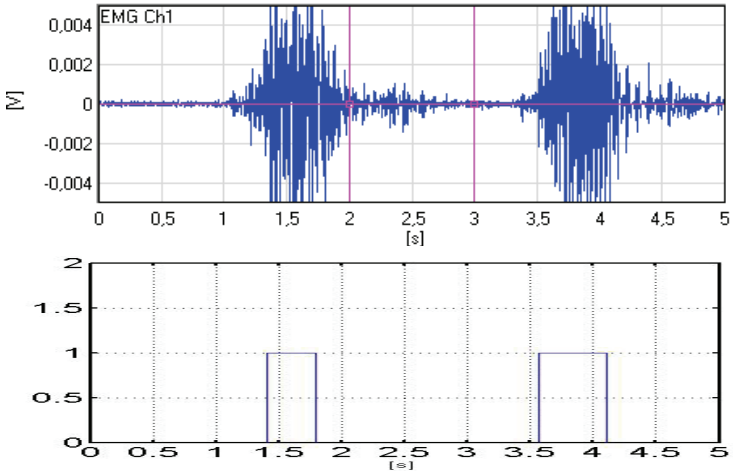

Fig. 11. Threshold control command generated

3.3 Onset analysis

Due to the complexity of the SEMG signal, it is better to use some characteristics of it. Using temporal characteristics like *onset time* and *offset time*, muscle activation and deactivation can be detected. A controller structure based on onset analysis is illustrated in Figure 12. Onset detection can be obtained using different methods. The performance of these methods is evaluated in terms of bias and variance of estimated onset time. Also, the sensitivity to the signal-to-noise ratio (SNR) is a measure of detection quality.

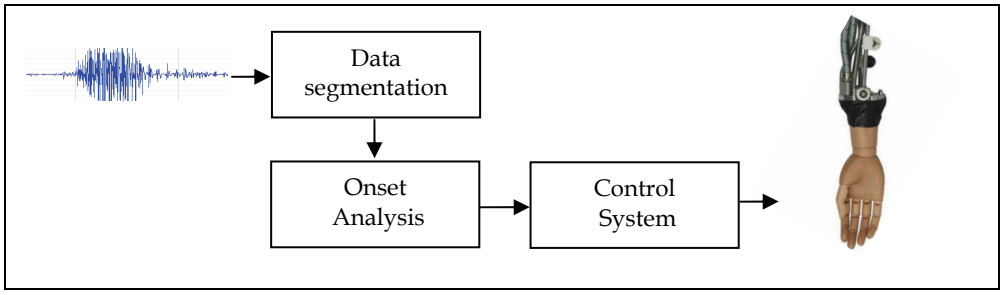

Fig. 12. Onset analysis based myoelectric control system

Single-threshold and double-threshold are the most used methods. In single-threshold method rectified raw signals are compared with some thresholds. These thresholds are obtained based on the mean power of background noise. This method is simple and very fast, but its main drawback is related to the excessive sensitivity to the SNR. In order to overcome this disadvantage the following improvement is possible.
Instead of using instant values of the SEMG signal, a time enveloped signal is used. This improved single-threshold method can be implemented using the Marpel-Hovart and Gilbey algorithm (Sun et al., 2005). In this algorithm two adjacent windows called leading and trailing windows are used to slide over a sequence of data. The lengths of the two windows are the same. For the leading window, the mean absolute value of the signal is computed and compared with the signal in the trial window. Accordingly with the hypothesis that the maximum differences of the two mean absolute value, computed for leading and trailing window, occur when one window contains a muscle contraction and the other doesn't, onset and offset time can be determined.
Another approach was presented by Sun et al. (2005). They use a maximum value detection algorithm, assuming that a muscle is in contraction if the signal acquired show a peak value greater than a given threshold, within a segment of acquired signal. The segment length depends on the EMG sensors and on the tissue. Even this improved method has some disadvantages. It is possible that noise signals to be interpreted as correct signals.
Bonato et al. (1998) reported an improved method used for gait analysis. The double-threshold method based detector operates directly on the raw myoelectric signal. Its performances are fixed by the values of 3 parameters, namely, false-alarm probability, detection probability, and time resolution. The false alarm probability represents the probability that a noise sample to be wrong interpreted as a signal. The detection probability represents the probability that a noises affected signals to be correctly recognized. The time resolution parameter characterizes the length of the observation window. The improvement of this double-threshold method is represented by the possibility to independently adjust the three above parameters.
Another way to improve onset time detection is to use sensor fusion as in section 2 was presented. We used a goniometer mounted at the elbow joint and synchronized the signal detected by this with the signal detected by the EMG sensors mounted on the biceps and triceps in a flexion extension movement. Thus onset time can be detected with very little computation and very fast.

3.4 Finite state machine based control

In finite state machine based control, finite number of states, transition between them, and commands describe the control. The states, state transition roles and the output commands have to be defined. In the case of upper limb prosthesis, the states often represent predefined motion commands like *open, close, rotate inside, and rotate outside.* Transition roles are usually associated with the signal features. The block diagram of a myoelectric controller based on finite state machines is shown in Figure 13.

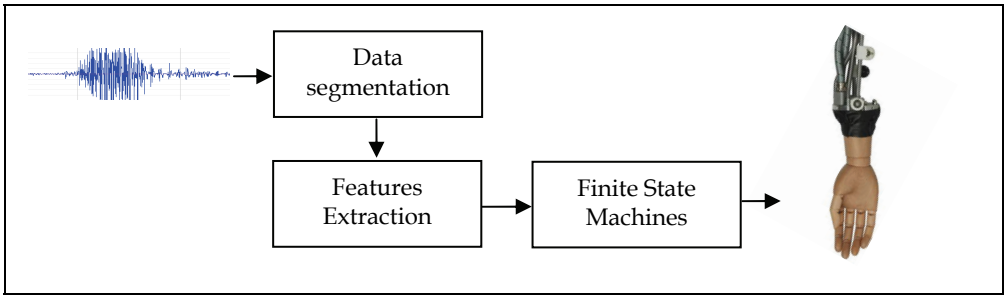

Fig. 13. Finite state machine based control architecture

Finite state machine based myoelectric control was applied by many researchers to drive rehabilitation devices like wheelchair (Felzer & Freisleben, 2002); (Moon et al., 2005), upper and lower limb prosthesis, assistance robots (Zhang et al., 2008), etc. The results reported by Felzer and Freisleben (2002), Moon et al. (2005) show that this method is still limited for wheelchair control. They reported an increase of necessary time to control the wheelchair by 50%, comparing with the case when a joystick was used to drive.

Based on the idea proposed by Moon et al., we developed a myoelectrical control system used to control for motions of a prosthetic hand. The motions controlled are: *open hand, close hand, rotate inside,* and *rotate outside*. Two EMG sensors, placed over the biceps and triceps are used to detect the intention of movement. The biceps sensor commands two motions *close hand* and *rotate inside*, and the triceps sensor commands *open hand* and *rotate outside* motions. Because each sensor commands two movements, it is necessary to discriminate between these movements. Therefore two modes are used. In mode 1 *open* and *close* motion are executed. In mode 2, *rotate inside* and *rotate outside* motions are executed. In order to switch between the two modes, both sensors have to be activated simultaneously, which correspond to a simultaneous contraction of biceps and triceps.

Figure 14 illustrate the state transition diagram that describes the controller functions, where *b* stands for biceps and *t* for triceps.

The indicator *1* codes the presence of a contraction, and *0* its absence.

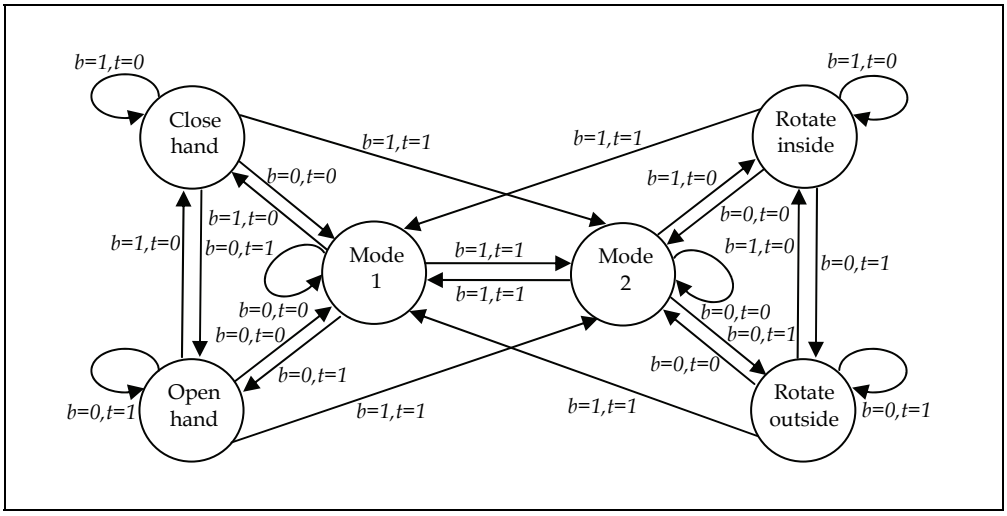

Fig. 14. Finite state machine control architecture for a prosthetic hand

4. Conclusions

As has been mentioned SEMG signals can not be used directly as inputs for a controller. Therefore pre-processing techniques are required to extract meaningful information from the raw signal. This information is used by the classifiers that provide input signals to the controller. The performance of the control system is highly dependent on the processing methods used. Unfortunately there is always a trade-off between the performance of the classifier, as interface between the EMG sensors and the controller, and the computational power required. Better results can be obtained if proper features extraction methods and suitable classifiers are used. For example, time-frequency features yield better results when using a linear discriminant analysis classifier, and time-domain features lead to better results when using neural network based classifiers.

Even a lot of work has been done on this challenging field, still remains problems that must be overcome.

One drawback of myoelectric control is related to its open loop architecture. It is known that open-loop control systems are not so reliable, comparing with close-loop ones. More over open loop myoelectrical control systems requires a great mental effort, especially during the first months after fitting.

In order to reduce this effort hybrid controllers are more suitable. These types of controllers combine myoelectrical control with classical closed loop control. In this case, the wearer's effort is reduced because he should only initiate the action which is finalized by the controller using information from sensors mounted into the prosthesis. Combining information from different type of sensors like SEMG sensors, force sensors, goniometers, pressure sensors, or other feedback elements, better closed loop controllers could be implemented.

5. References

Akay, M. (1996). *Detection and Estimation Methods for Biomedical Signals*, Academic Press, Inc., ISBN: 0120471434, Orlando, FL, USA.

Bonato, P.; D'Alessio, T. & Knaflitz, M. (1998). A statistical method for the measurement of muscle activation intervals from surface myoelectric signal during gait. *IEEE Transaction on Biomedical Engineering,* Vol. 45, No. 3, (March, 1998) page numbers (287-299), ISSN 0018-9294

Chan, A.D.C. & Englehart, K.B. (2005). Continuous myoelectric control for powered prostheses using hidden Markov models, *IEEE Transaction on Biomedical Engineering*, Vol. 52, No. 1, (January 2005), page numbers (121 - 124), ISSN: 0018-9294

Chaiyaratana, N.; Zalzala, A.M. & Datta, D. (1996). Myoelectric signal pattern recognition for functional operation of upper-limb prosthesis, *Proceedings of International Conference on Disability, Virtual Reality and Associated Technologies*, pp. 151-160, ISBN: 1-58113-911-X, Maidenhead, U.K, July 1996

Chu, J.; Moon, I.; Kim, S.; Mun, M. (2005). Control of multifunction myoelectric hand using a realtime EMG pattern recognition, *Proceedings of the IEEE/RSJ International Conference on Intelligent Robots and Systems*, ISBN: 0-7803-8913-1, pp. 3511-3516, Edmonton, Canada, 2005, IEEE

Englehart, K.; Hudgins, B.; Parker P.; Stevenson M. (1999). Classification of the myoelectric signal using time-frequency based representations. *Medical Engineering & Physics*, Vol. 21, No. 6-7, (July - September 1993), page numbers (431–438), ISSN: 1350-4533

Englehart, K.; Hudgins, B.. (2003). A robust, real-time control scheme for multifunction myoelectric control. *IEEE Transaction on Biomedical Engineering*, Vol. 50, No. 7, (January 1993), page numbers (848-854), ISSN: 0018-9294

Farina, D.; Merletti, R. (2000).Comparison of algorithms for estimation of EMG variables during voluntary isometric contractions. *Journal of Electromyography and Kinesiology,* Vol. 10, No. 5, (October 2000) page numbers (337-349), ISSN: 1050-6411

Felzer,T. & Freisleben, B. (2002). HaWCoS: the hands-free wheelchair control system, *Proceedings of the ACM SIGCAPH Conference on Assistive Technologies*, pp. 127-134, ISBN: 1-58113-469-9, Edinburgh, Scotland, 2002, ACM Press, New York

Gerdle, B. & Karlsson, S. (1994). The mean frequency of the EMG of the knee extensors is torque dependent both in the unfatigued and the fatigued states. *Journal of Clinical Physiology and Functional Imaging,* Vol. 14, No. 4, (July 1994) page numbers (419-432), ISSN: 1475-0961

Haykin, S. (1998). *Neural Networks: A Comprehensive Foundation*, Prentice Hall, ISBN: 9780132733502.

Hefftner, G.; Zucchini, W.; Jaros, G.G. (1988). The electromyogram (EMG) as a control signal for functional neuromuscular stimulation. I. Autoregressive modeling as a means of EMG signature discrimination. *IEEE Transaction on Biomedical Engineering*, Vol. 35, No. 4, (April 1988), page numbers (230 - 237), ISSN: 0018-9294

Herle, S.; Raica, P.; Lazea, Gh.; Robotin R.; Marcu C.; Tamas L. (2008). Classification of surface electromyographic signals for control of upper limb virtual prosthesis. *Proceedings of 2008 IEEE International Conference on Automation, Quality and Testing, Robotics*, pp. 160-165, ISBN: 978-1-4244-2576-1,Cluj-Napoca , May 2008, IEEE, inc.

Hudgins, B.; Parker, P. & Scott, R.N. (1993). A new strategy for multifunction myoelectric control. *IEEE Transaction on Biomedical Engineering*, Vol. 40, No. 1, (January 1993), page numbers (82 - 94), ISSN: 0018-9294

Hussein, S.E.; Granat, M.H. (2002). Intention detection using a neuro-fuzzy EMG classifier. *IEEE Engineering in Medicine and Biology Magazine*, Vol. 21, No. 6, (November - December 2002), page numbers (122 - 129), ISSN: 0739-5175

Ito, K.; Tsuji, T.; Kato, A. & Ito, M. (1991). Limb-function discrimination using EMG signals by neural network and application to prosthetic forearm control, *Proceedings of IEEE International Joint Conference on Neural Networks*, pp. 1214-1219, ISBN: 0-7803-7046-5, Singapore, November 1991, IEEE inc..

Karlik, B.; Osman Tokhi, M. & Alci, M. (2003). A fuzzy clustering neural network architecture for multifunction upper-limb prosthesis. *IEEE Transactions on Biomedical Engineering*, Vol. 50, No. 11, (November 2003) page numbers (1255-1261), ISSN: 0018-9294

Karlik, B.; Pastaci, H. & Korurek, M. (1994). Myoelectric neural networks signal analysis, *Proceedings of 7th Mediterranean Electrotechnical Conference,* pp. 262-264, ISBN: 0-7803-1772-6, Antalya, July 1994, IEEE.

Kelly, M.; Parker, P.A. & Scott, R.N. (1990). The application of neural networks to myoelectric signal analysis: A preliminary study. *IEEE Transactions on Biomedical Engineering*, Vol. 37, No. 3 (March 1990) page numbers 221-230, ISSN: 0018-9294

Kiguchi, K.; Esaki, R.; Tsuruta, T.; Watanabe, K.; Fukuda, T. (2003). An exoskeleton system for elbow joint motion rehabilitation, *Proceedings of IEEE/ASME International Conference on Advanced Intelligent Mechatronics*, pp. 1228 - 1233, ISBN 0-7803-7759-1, Japan, July 2003, IEEE.

Kuruganti, U.; Hudgins, B. & Scott, R.N. (1995). Two-channel enhancement of a multifunction control system. *IEEE Transactions on Biomedical Engineering*, Vol. 42, No. 1, (January 1995) page numbers (109-111), ISSN: 0018-9294

Leowinata, S.; Hudgins, B. & Parker, P.A. (1998). A multifunction myoelectric control strategy using an array of electrodes. *The 16th Annual Congress of the International Society Electrophysiology and Kinesiology*, Montreal, Canada, 1998.

Light, C.M.; Chappell, P.H.; Hudgins, B. & Engelhart, K. (2002). Intelligent multifunction myoelectric control of hand prosthesis. *Journal of Medical Engineering* and *Technology,* Vol.26, No. 4, (July 2002) page numbers (139-146), ISSN: 0309-1902

Micera, S.; Sabatini, A. M. & Dario, P. (2000). On automatic identification of upper-limb movements using small-sized training sets of EMG signals. *Journal of Medical Engineering and Physics*, Vol. 22, No. 8, (October 2000) page numbers 527-533, ISSN: 1350-4533

Moon, I.; Lee, M.; Chu, J. & Mun, M. (2005). Wearable EMH-based HCI for electric-powered wheelchair users with motor disabilities, *Proceedings of the IEEE International Conference on Robotics and Automation,* pp. 2660-2665, Barcelona, Spain, April 2005

Nauck, D. & Kruse, R. (1997). A neuro-fuzzy method to learn fuzzy classification rules from data. *Journal of Fuzzy Sets and Systems*, Vol. 89, No. 3, (August 1997) page numbers (277-288), ISSN: 0165-0114

Nauck, D.; Klawonn, F. & Kruse, R. (1997). *Foundations of Neuro-Fuzzy systems*, John Wiley & Sons Inc, ISBN: 978-0471971511 Chichester.

Oskoei, M.; Hu, H. (2007). Myoelectric control systems – A survey. *Biomedical Signal Processing and Control,* Vol. 2, No. 4, (October 2007) page numbers (275-294), ISSN: 1746-8094

Parker, P.; Englehart, K. & Hudgins, B. (2006). Myoelectric signal processing for control of powered limb prostheses. *Journal of Electromyography and Kinesiology,* Vol. 16, No. 6, (December 2006) page numbers (541-548), ISSN: 1050-6411

Ping, Z.; Lowery, M.M.; Dewald, J.P.A. & Kuiken, T.A. (2006). Towards Improved Myoelectric Prosthesis Control: High Density Surface EMG Recording After Targeted Muscle Reinnervation, *27th Annual International Conference of the Engineering in Medicine and Biology Society*, pp. 4064-4067, ISBN: 0-7803-8741-4, Shanghai, January 2006.

Soares, A.; Andrade, A.; Lamounier, E. & Carrijo, R. (2003). The Development of a Virtual Myoelectric Prosthesis Controlled by an EMG Pattern Recognition System Based on Neural Networks. *Journal of Intelligent Information Systems,* Vol. 21, No. 2, (September 2003) page numbers (127-141), ISSN: 0925-9902

Subasi, A.; Yilmaz, M. & Ozcalik, H.R. (2006). Classification of EMG signals using wavelet neural network. *Journal of Neuroscience Methods*, Vol. 156, No. 1-2, (September 2006), page numbers (360-367), ISSN: 0165-0270

Sun, Q.; Sun, Y. ; Ding, X. & Ma, Z. (2005). Onset determination of muscle contraction in surface electromyography signals analysis, *Proceedings of IEEE International Conference on Information Acquisition*, pp. 384-387, Hong Kong, China, June–July 2005

Weir, R.F. & Ajiboye, A.B. (2003). A multifunction prosthesis controller based on fuzzy logic techniques, *Proceedings of the 25th Silver Anniversary International Conference of the IEEE Engineering in Medicine and Biology Society,* Cancun, Mexico, September 2003, IEEE

Zhang, X.; Wang, X.; Wang, B.; Sugi, T. & Nakamura, M. (2009). Finite State Machine with Adaptive Electromyogram (EMG) Feature Extraction to Drive Meal Assistance Robot, *IEEJ Transactions on Electronics, Information and Systems,* Vol. 129, No. 2, (2009), page numbers (308-313), ISSN: 0385-4221

A 6-DOF Rehabilitation System for Upper Limbs "Robotherapist"and Other Rehabilitation Systems with High Safety

Junji Furusho and Ying Jin
Osaka University Japan

1. Introduction

The percentage of aged persons in society and their number are increasing, and their physical deterioration has become a social problem in many countries. Early detection of function deterioration and sufficient rehabilitation training are necessary, not only to decrease the numbers of aged who are bedridden or need nursing care, but also to enable the aged to take an active part in society. Movements of the upper limbs, such as eating and operating appliances are complicated, various and indispensable for daily activities. It therefore is important for the aged to exercise to keep their upper limb function. Moreover, there are many patients of paralysis caused by stroke. For example, in Japan more than two hundred and fifty thousand people have stroke every year, and many of them are paralyzed. The human brain is capable of an extraordinary degree of plasticity (selforganization), enabling learning, and leaving open the possibility for motor recovery (Janet & Shepherd, 1998). Therefore, neuro-rehabilitation for stroke-patients is effective. Using apparatus that applies robotic technology and virtual reality makes new training methods and exercises in rehabilitation possible (Krebs, Volpe et al., 2000), (Burgar, Lum et al., 2000),(Charles, Krebs et al., 2005).

Feeding back the quantitative evaluations to the training by a computer can enhance the qualitative effect of training. Therefore, some rehabilitation systems using these technologies for upper limbs have been developed. However, most of them apply training within a two-dimensional horizontal plane. Many movements, however, in daily activities need to move arms in a vertical direction. A system therefore that enables exercise in three-dimensions would seem to be more effective for such training. Although the MIME system (Burgar, Lum et al., 2000) using PUMA-560 by VA and Stanford Univ. can give training in three-dimensions, the PUMA-560 is a robot originally developed for industrial use and may not be sufficiently safe to train the aged and/or disabled.

Furusho Laboratory of Osaka University have developed innovative rehabilitation supporting robots "Robotherapist", which is a 6-dofrehabilitation system for upper limbs including wrists in the 2-year NEDO Project (2004-2005). This system enables efficient rehabilitation trainings, which focuses on the harmonic movement of the whole upper limb. and Robotherapist was exhibited at the Prototype Robot Festival at the 2005 International

Exposition held in Aichi Prefecture, Japan. "Robotherapist" Furusho Laboratory of Osaka Univ. and Osaka Electro-Communication Univ. are developing the rehabilitation software based on a physical therapy technique PNF using Robotherapist. In PNF, a therapist gives opposite force to patient in order to guide patient's hand in the desired direction. Then the patient resists the force from the therapist and knows which the desired direction is. We name this technique "Guidance Utilizing Reaction". In this chapter, we describe mechanism and software of Robotherapist and other rehabilitation systems using functional fluids with high safety.

Furusho Laboratory of Osaka University developed 2-D rehabilitation system for upper limbs "NIOH-1" using ER fluid actuators in 1997 (Furusho & Sakaguchi, 1999). Robotherapist were developed on the basis of the technology of NIOH. Furusho Laboratory also developed 3-D rehabilitation system "EMUL". EMUL was developed through robotic and virtual reality technology in a 5-year NEDO (New-Energy and Industrial Technology Development Organization of Japanese Government) project and has performed well in clinical studies. Recently we have developed a upper-limb-rehabilitation system "PLEMO-P" using ER fluid brakes which could be used in facilities for elderly people and so on. Furusho Laboratory developed the passive-type force display system with two redundant brakes and a novel method is presented on the performance evaluation of the passive-type force display system with redundant brakes. We also have developed highly safe isokinetic exercise systems using only brakes with functional fluids (ER fluid or MR fluid). Because of rapid response of these fluids, such a machine has good responsibility and controllability. Meanwhile, Furusho Laboratory studied biped locomotion robots during the 1980s and the beginning of 1990s, and realized the human-like biped locomotion with kick action [Furusho & Masubuchi, 1987], [Furusho & Sano 1990]. On the basis of this biped locomotion technology and the technology about functional fluids, we developed the first intelligent prosthetic ankle. Moreover we are developing intelligent ankle-foot orthoses using MR (Magnetorheological) fluid in a 3-year NEDO project. Furusho Laboratory has developed the intelligently controllable AFO (I-AFO) which can control its ankle torque by using compact Magneto-rheological fluid (MRF) brakes. These systems are also introduced in this chapter.

2. 2-D Rehabilitation System "NIOH" 2.1 ER Actuaor

2.1 ER Actuaor

ER fluid is a fluid whose rheological properties can be changed by applying an electrical field (Bossis, 2002). Fig. 1 shows the conceptual illustration of an ER fluid actuator. The ER actuator is composed of an ER clutch and its drive mechanism consisting of a motor and a reduction-gear-unit. The rotational speed of the motor is kept constant. The output torque of ER actuator is controlled by the applied electric field (Furusho, 2001), (Furusho & Kikuchi, 2006). The input torque is transferred to the rotating cylindrical section of the output axis via the particle-type ER fluid filled in the rotating cylinder. Both the input axis cylinders and the output axis cylinder serve as electrodes, and output torque is controlled by the electric field applied between the electrodes. The output cylinder is made of aluminum alloy in order to reduce the moment of inertia of the output axis. An actuator using ER fluid is effective for human-coexistent mechatronics systems like rehabilitation systems for upper limbs. Fig. 2 shows a conceptual illustration of Human-Machine-Coexistent-Mechatronics (HMCM)

System using ER Actuators. Merits of ER actuators in applications to HMCM system are as follows:

A: From the Viewpoints of the Characteristics of Operation

(1) Since ER actuators have good back-drivability, the operator can easily operate HMCM system from its end-effector.

(2) When HMCM system is driven by the operator from its end-effector, HMCM system can be moved quickly over the rotational speed of the input cylinder of the ER clutch.

B: From the Viewpoints of Performances in Force Display System

(1) Quick force response property originated from the low inertia property of ER actuator and the rapid response of ER fluid make the force presentation with high fidelity possible.

(2) Force display systems with large-force presentation ability can be realized safely.

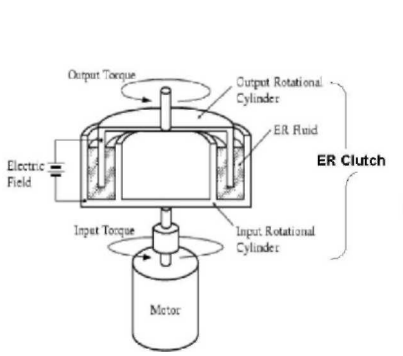

Fig. 1. Conceptual illustration of ER actuator

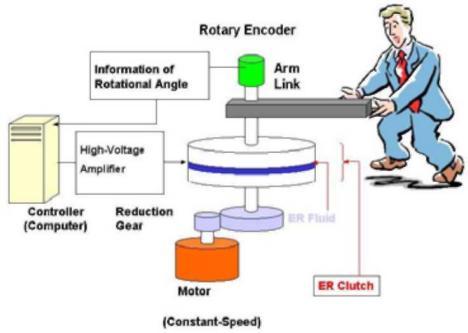

Fig. 2. Conceptual illustration of Human-Machine-Coexistent-Mechatronics (HMCM) Systems using ER actuators.

2.2 Consideration about Safety

A rehabilitation system for upper limbs which has large working area can be regarded as a kind of robots. In such a human-coexistent robot system where an operator must be in contact with or close to the robot, the safety-securing system is necessary in order that an operator can use the robot safely (ISO10218). In industrial robots, an operator cannot access a robot except for teaching in order to avoid hazardous conditions. Fig. 3 shows the structure of safety in human-coexistent robots.

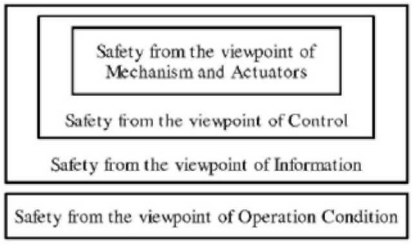

Fig. 3. Structure for securing safety in Human-Coexistent Robots.

ER actuators have the following merits from the viewpoint of safety.

(1) The maximum driving speed of the output shaft of the ER actuator is restricted by the rotational speed of the input shaft of the ER clutch. Therefore, when the rotational speed of the input shaft is set slow, HMCM systems using ER actuators are safe for operators.

(2) The inertia of the output part can be made very small. So, in the case of unexpected accidents, the impact force caused by the inertia of the actuator can be reduced.

Since International Safety Standards for human-coexistent robots have not been established yet, we have no other choice but to use the ISO and domestic standards for machines working close to human beings (see Table 1). The developed rehabilitation system can assure these standards of Table 1 by the usage of ER actuators and the mechanical design as follows:

(1) The items (a) and (b) of Table 1 are satisfied by setting the rotational speed of the input cylinder slow.

(2) The item (c) is satisfied by using a 60-watt motor for the drive of the input rotational cylinder.

(3) Risk Reduction by Design (item (d)) is realized by mechanical limitation of each joint, mechanical gravity-compensation and the usage of ER actuators.

(a) End-effector Speed is less than 0.25 [m/s]	ISO10218: Manipulating industrial robots--Safety
(b) Low Energy Property	ISO14121: Safety of machinery— Principles of risk assessment
(c) Actuator Power is less than 80 [W]	JAPAN, JIS B 8433, 1983: General Code for Safety of Industrial Robots
(d) Risk Reduction by Design	ISO12100: Safety of machinery—Basic concepts, general principles for design

Table 1. International and domestic safety standards.

2.3 Rehabilitation and Force Display Systems Using ER Fluids

Furusho Lab. of Osaka University has been developing rehabilitation systems and force display systems using ER fluids since 1993 (Furusho, Wei et al., 1995).

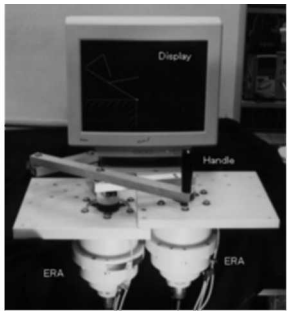

Fig. 4. Rehabilitation system "NIOH-1".

Fig. 5. Rehabilitation system "NIOH-2".

Fig. 4 shows the 2-DOF rehabilitation systems "NIHO-1" using ER actuators (Furusho & Sakaguchi, 1999). The rehabilitation training system was installed in a hospital for testing purpose. 13 patients volunteered to participate in several experiments for evaluation of upper limb's physical capability and for rehabilitation training (Sakaguchi, Furusho et al., 1999). The patients suffered from arm paralysis due to a damaged spinal cord or clogged brain artery. Fig. 5 shows the 2-DOF rehabilitation system "NIHO-2" using ER actuators (Ishikawa, 2000).

3. 6-DOF Rehabilitation System for Upper Limbs including Wrists "Robotherapist"

3.1 Introduction

We have developed Robotherapist, which is a 6-DOF force display system for upper limbs including wrists (Furusho, Hu et al., 2006). The system can measure positions and postures of an operator's hand, and generate a large force sense including the wrist torque to the operator. This system enables efficient rehabilitation trainings, which focus on the harmonic movement of the whole upper limb. Robotherapist was exhibited at "The Prototype Robot Festival at the 2005 International Exposition held in Aichi Prefecture, Japan" (shown in Fig. 6).

Fig. 6. Rehabilitation system "Robotherapist".

3.2 Mechanism of Robotherapist

A structure of Robotherapist can be divided into two mechanism groups: one is for positioning of an operating part (3-DOF) and another is for posturing of it (3-DOF). ER actuators drive all of 6-DOF.

A: Mechanism for positioning of an operating part

Fig. 7 shows the mechanism for the positioning. As seen from this figure, Robotherapist has 2-DOF for a horizontal rotation and 1-DOF for a vertical movement in arm parts. Actuators for arm motions are set on a base in order to reduce the inertia of the moving parts. Link2 is a parallel link mechanism. A counter-balance weight compensates a gravity-effect of these links in all posture.

B: Mechanism for posturing of an operating part

The mechanism for posturing has 3-DOF; that is, roll, pitch and yaw rotation. Generally, a heavy weight of an end-effecter impairs smooth acceleration of operation. Additionally,

such a weight is very risky when the end-effecter collides with the operator. Therefore, the operating part was designed as light as possible. Actuators for the operating part are placed near Link1, and a torque of each actuator is transmitted to it by driving shafts and wire-pulleys systems.

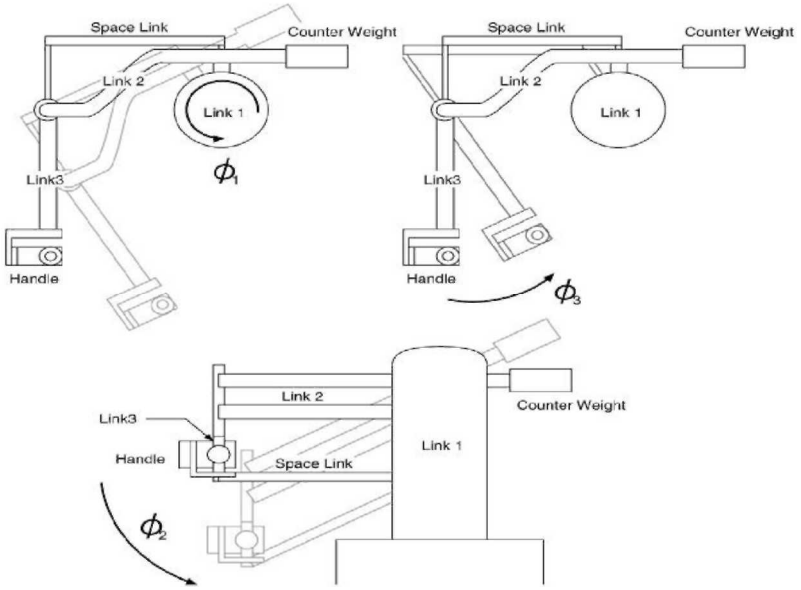

Fig. 7. Configuration of Robotherapist.

3.3 Application Software of Robotherapist

We have also developed application software of Robotherapist for upper limb rehabilitation that includes upper limb's harmonic movements. Important viewpoints for the rehabilitation training software are as follows:

(1) Many movements using the shoulder, the elbow, and the wrist harmonically are included.
(2) The sense of amusement is needed for long-term training.
(3) The recovery degree of upper limbs function can be evaluated properly.

The developed applications are the following four kinds.

A: Water Supply (Shown in Fig. 8)

The operator grasps a handgrip of a watering pod and gives water to the ground. The amount of the water, which comes out of the pod is calculated according as a tilt of the pod, and flower blooms gradually grow up according to the quantity of the given water. The goal of this game is making flower blooms on the whole ground. The system gives the operator a force depending on the tilt and the weight of residual water in the pod. The operator has to cooperate his shoulder, elbow, and wrist, in order to control the position and the tilt of the pod.

B: Window Sweep (Shown in Fig. 9)

At first whole area of the window is masked in white. The operator grasps a wiper and removes the white mask. If the mask is removed, a picture appears in the window. When

the wiper is pressed on the window, the reaction force from the window is given to the operator. In order to remove the white mask efficiently, it is necessary to control not only the position but also the posture of the wiper. Therefore, the operator should move his shoulder, elbow, and wrist harmonically.

Fig. 8. Water supply.

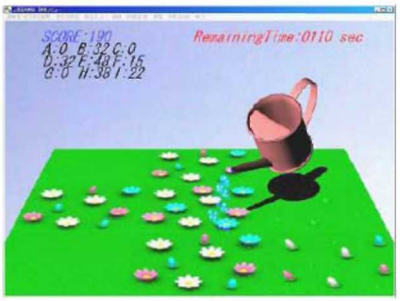

Fig. 9. Window sweep.

3.4 Application Software of Robotherapist Based on PNF Techniques

Furusho Laboratory of Osaka Univ. and Prof. Kunihiko Oda of Osaka Electro-Communication Univ., Dept. of Physical Therapy are developing the evaluating software developed for the rehabilitation of patients suffered from cerebellum malfunction based on Proprioceptive Neuromuscular Facilitation (PNF) techniques (Furusho, Kikuchi, Oda et al., ICORR 2007).

A: Rhythmic Stabilization

Fig. 10 shows the image of Rhythmic Stabilization, and Fig. 11 shows the graphics of Rhythmic Stabilization. As shown in Fig. 10 and Fig. 11, a therapist gives each force from random directions quickly to the hand of a patient. And then the patient is instructed to maintain the position of his/her hand. In Rhythmic Stabilization, therapist want to know whether a patient can maintain the position of his/her hand, and how strong the force is, and which direction he is weak in.

B: Finger Nose Finger (FNF)

As shown in Fig. 12 and Fig. 13, a patient repeats the movement between therapist's finger and his/her nose under the expected orbit. In FNF, therapist would judge recovery degree of patient by his/her movement.

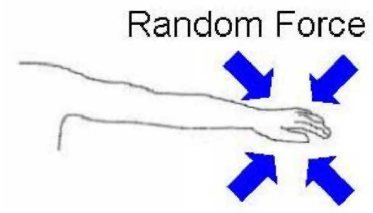

Fig. 10. Image of rhythmic stabilization.

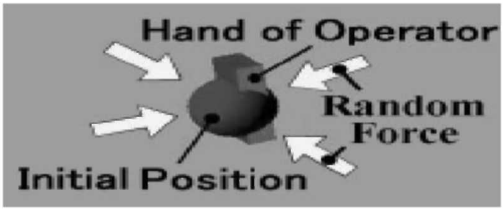

Fig. 11. Display of rhythmic stabilization.

Fig. 12. Image of FNF.

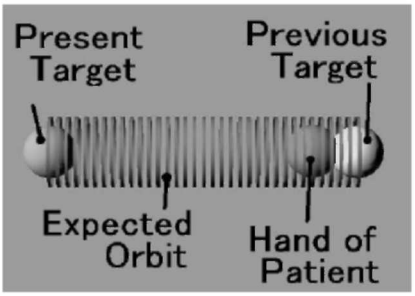

Fig. 13. Display of finger nose finger.

C: Arc Exercise with GUR

In PNF, a therapist gives opposite force to patient in order to guide patient's hand in the desired direction. Then the patient resists the force from the therapist and knows which the desired direction is. We name this technique "Guidance Utilizing Reaction". As shown in Fig. 14, a patient extends his/her arm and moves his/her handle just on the arc orbit. When he moves it along the orbit, there is no force. Otherwise when the handle is away from the given orbit, the patient can sense force to his/her body.

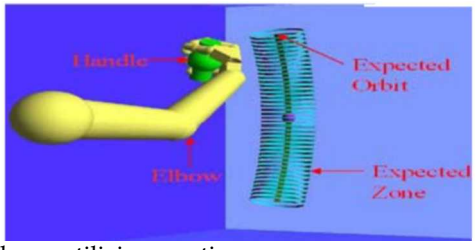

Fig. 14. Display of guidance utilizing reaction.

3.5 Measurement of Reaching Movement with "Robotherapist"

A: Stroke Rehabilitation

The central paralysis is represented by hemiplegia of stroke. A qualitative abnormal exercise called synergy pattern in a recovery process appears to stroke survivors. If recovery progresses, stroke survivors return to a normal state. Synergy pattern is the movement which can move plural joints only along a certain constant pattern like flexor synergy or extensor synergy (Fig. 15 and Fig. 16). Therefore, when we evaluate a recovery state of upper limbs of stroke survivors, it is important to measure a movement pattern of the whole arm and to evaluate presence and degree of synergy pattern.

Fig. 15. Flexor synergy.

Fig. 16. Extensor synergy.

Many patients cannot move their hands actively as they like. Though they know a desired direction, they do not know how to move their hands in that direction. However, they can resist the force passively as they like. Therefore, we introduce physical therapy into application software.

We adopt techniques of Proprioceptive Neuromuscular Facilitation (PNF) in physical therapy. Techniques of PNF are used to place specific demands in order to secure a desired response (D.E.Voss, M.K.Ionta et al.). One of the techniques of PNF is the following: in order to guide a hand of a patient in one direction, a therapist adds force to the patient in the opposite direction, and the patient resists it (Fig. 17). Then his/her brain and body know how to move his/her hand in the correct direction. The force that the therapist adds depends on the maxim power of the patient. Utilizing the reaction against the force toward the opposite direction, the patient can tell correct movements to his/her brain and body. By repeating training with this technique, their brain learns the correct pattern of movements. We name this technique "Guidance Utilizing Reaction (GUR)". Then we introduce GUR technique to a rehabilitation robot system "Robotherapist" and its software.

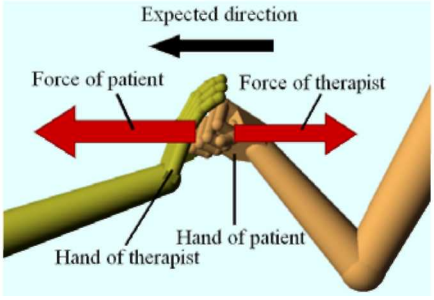

Fig. 17. Guidance Utilizing Reaction (GUR).

B: Measurement Experiment of Reaching Movement

We experimented on a measurement of reaching movement with Robotherapist. Additionally, we made a model of movement peculiar to stroke survivors and a model of movement of healthy people.

(1) Way of Experiment

Subjects are eight students who are healthy people and one therapist. Eight students did natural reaching movement of the right hand, and one therapist did reaching movement of the right hand which simulated stroke survivors. An appearance in an experiment is shown

in Fig. 18. A screen such as Fig. 19 was displayed in the experiment. Subjects moved the handle to front and back along the aim orbit. We measured and recorded the position and posture of the handle and the wrist angle and estimated the elbow position.

Fig. 18. Appearance in experiment.

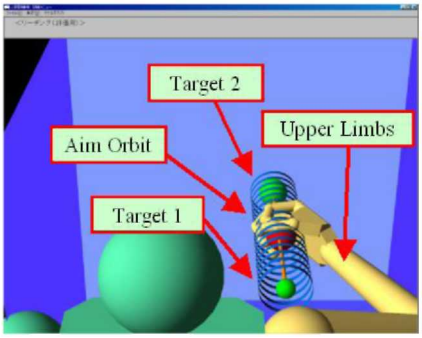

Fig. 19. Screen in experiment.

C:Application Software for Reaching Training

In this section, we describe application software for reaching training that we developed. A trainer operates Robotherapist while looking at a screen. As a reaching training menu, there are two modes to guide the position of the handle part and to improve the posture of the handle part.

(1) Guide Mode of Handle Part

Based on the method of GUR, Robotherapist presents force sense of the opposite direction to the expected direction to a trainer. The expected direction is the direction to the target. When the position of the handle part leaves aim orbit more than a certain distance, a message is displayed on the screen and he is warned by a sound. Simultaneously, the expected direction changes to a direction returning to the aim orbit.

(2) Improvement Mode of Upper Limbs

We intend for a patient who can extend his arm along the aim orbit. In this mode, Robotherapist doesn't present force sense to guide the position of the handle part. When he extends his arm, a wrist angle, a direction of palm and a position of an elbow are measured. If reaching movement is abnormal, he is warned by a message and a sound. We use the model of stroke survivors and that of healthy people in a foregoing section for abnormal search. When his reaching movement approaches in the model of stroke survivors, we judge that it is abnormal. If his reaching movement is judged abnormal about dorsal flexion, palmar flexion, supination and pronation, Robotherapist presents force sense.

4. A 3-D Rehabilitation System for Upper Limbs Developed in a 5-year NEDO Project "EMUL"

4.1 Introduction

The percentage of aged persons in society and their number are increasing, and their physical deterioration has become a social problem in many countries. Early detection of function deterioration and sufficient rehabilitation training are necessary, not only to decrease the numbers of aged who are bedridden or need nursing care, but also to enable the aged to take an active part in society. This research has been conducted as a part of the NEDO (New Energy and Industrial Technology Development Organization) 5-year Project, "Rehabilitation System for the Upper Limbs and Lower Limbs" since 1999. Furusho Laboratory of Osaka University and Asahi-kasei Group developed a 3-D rehabilitation system for upper limbs "EMUL". Hyogo Medical College took part in the project in the final year.

4.2 3-DOF Rehabilitation Training System

We have developed a 3-D rehabilitation system that has a performance suitable for rehabilitation for upper limbs and can display force senses in three-dimensional space (Furusho, Koyanagi, Imada et al., 2005), (Furusho, Koyanagi, Kataoka et al., 2005).
Fig. 20 shows the whole rehabilitation system. The maximum output torque of the ER actuator is about 3.0 [Nm]. As shown in Fig. 20, exercise machine. The major targets in this study are hemiplegic patients who were paralyzed by stroke. The training in general includes physical therapeutic exercises, such as passive and active exercises, and occupational therapeutic exercise like eating movement. EMUL has the following specifications.

(1) EMUL has 2 DOF for horizontal rotation and 1 DOF for vertical rotation.
(2) The length of each link is 0.45 [m] and the height of the whole machine is about 1 [m].
(3) All the actuators are set on the base of EMUL.
(4) The vertical rotation part adopts a parallel link mechanism. This makes the gravity-effect compensation by counterbalance-weight in all posture possible.
(5) The 3rd link is driven by spatial parallel link mechanism instead of belt-pulley and gear transmission system.
(6) The motion range is about 0.90[m] (W) * 0.54[m] (D) * 0.50[m] (H).
(7) The generative force at the end-effector is about 23 [N] in the horizontal plane and about 60 [N] in the vertical direction.

4.3 Software for Training

We show several examples of the training software.

A: Picture-Mask Erasing

As shown in Fig. 21, a semitransparent mask of a picture of 0.40 [m] * 0.40 [m] is erased by a virtual eraser which is operated by a patient. The patient can sense a reaction force from the picture surface through the gripper of 3-D rehabilitation system. This software has the effect of improvement about the dexterity and the movable range of limbs.

B: Virtual Maze & Virtual Hockey

Fig. 22 shows a virtual maze of 0.40 [m] * 0.30 [m]. This software has the effect of improvement about the dexterity and the movable range of limbs. Fig. 23 shows a virtual

hockey game with impact-force-sense. Virtual hockey has the training effect about dexterity and agility.

Fig. 20. Rehabilitation system "EMUL".

Fig. 21. Picture-mask erasing.

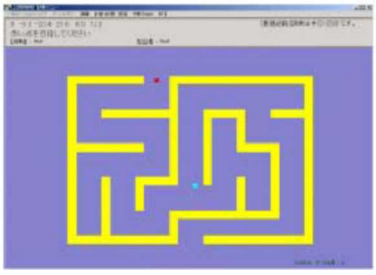

Fig. 22. Virtual maze.

Fig. 23. Virtual hockey.

4.4 Clinical Evaluation of EMUL

We conducted clinical testing for six stroke patients shown in Table 2. Each patient underwent 40 minutes of robotic therapy three times a week for six weeks. No patient showed severe cognitive impairment. None of the subjects was engaged in conventional occupational or physical therapy. Fig. 24 shows the shape of movable range in Picture-Mask-Erasing training of the female patient of 60 years old. As seen from this figure, the movable volume is expanded by the training.

Age	Gender	Location of Cereberal Vascular Accident (CVA)	Months since CVA
60	Female	Right thalamus・Infract	45 months
67	Male	Right corona radiata・Infract	18 months
20	Male	Left parietal cortex・hemorrhage	39 months
62	Female	Left frontal cortex・Infract	94 months
67	Female	Right corona radiata・Infract	110 months
57	Female	Left frontal cortex・Infract	40 months

Table 2. Cases

Professor Kazuhisa Domen's group of Hyogo Medical College and professor Junji Furusho's

group of Osaka University reported the clinical evaluation results shown in Table 3 in the Japanese Journal of Rehabilitation Medicine (Miyakoshi, Domen et al., 2006). As seen from these tables, the training using EMUL improves the motion ability of the patients.

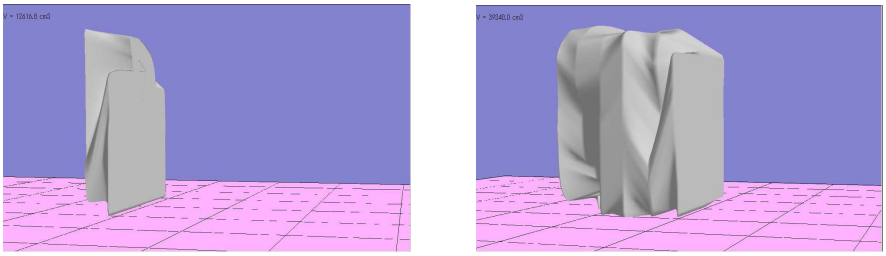

(a) Result of the first training (b) Result of the final training.

Fig. 24. Picture-mask erasing

Methods of Assessment (Range of Points)	Pre-treatment mean± SD	Post-treatment mean± SD	p
FMA* ; total (0 ~ 66)	45.2± 11.3	51.2±11.7	0.0273
FMA ; shoulder/elbow/forearm (0 ~ 36)	25.8±7.5	28.3±6.1	0.0412
FMA ; wrist (0 ~ 10)	5.2±2.6	6.2± 4.2	0.2356
FMA ; finger (0 ~ 14)	11.2±3.1	12.7±1.2	0.2763
FMA ; speed/coordination(0 ~6)	3.0±1.9	4.0± 1.5	0.0633
Motricity index (0 ~ 100)	77.7±7.6	85.8± 10.0	0.0679
Grasping Power [N]	78.4± 35.3	105.8± 38.2	0.0782
12-Stages -Grade by Ueda** (0 ~ 12)	6.2± 1.8	7.7± 2.3	0.0412

*FMA: Fugl-Meyer Assessment (Fugl-Meyer . et al., 1975)
**Ueda Grade: 0 (Brunnstrom Stage I); 1,2(Brunnstrom Stage II); 3-6(Brunnstrom Stage III); 7,8(Brunnstrom Stage IV); 9-11(Brunnstrom Stage V); 12(Brunnstrom Stage VI)

Table 3. Results of Assessment at Pre-treatment and Post-treatment (n=6) (This table is a revised version of the reference paer by Miyakoshi, Domen et al., 2006.)

4.5 Development of Evaluation System of the Motor Function for Upper Limbs using 3-D Rehabilitation Robot "EMUL" and Brain Function Imaging Method "NIRS"

In recent years, the rehabilitation system using robot and virtual reality is expected to quantify the effect of rehabilitative training. In this section, we describe about the development of evaluation system of motor function for upper limbs using 3D rehabilitation Robot "EMUL" and brain function imaging method "NIRS". This makes the evaluation system more quantitative. This work is joint research between Osaka University and Morinomiya Hospital.

A: NIRS

NIRS is a method of the brain function mapping utilizing the near-infrared lay (wavelength from 700 nm to 2500 nm), which has high transmission to body issues. By irradiating the near-infrared lays to the body issues and observing that transmitted lay, cerebral cortical changes in hemoglobin can be detected. NIRS has the advantage that it can observe the

cortical activities during dynamic movements against the other brain mapping methods: fMRI, PET, MEG and so on.

B: Clinical Evaluation

In order to evaluate the relationship between training using EMUL and cortical activation during operation the robot, we prepare "Eight Vertex Reaching Program" (shown in Fig. 25) as training / evaluation software of EMUL. Fig. 26 shows the software of "Eight Vertex Reaching Program". In this program, subjects reach each vertex of virtual cube on the display of EMUL. subject's hand is guided to a starting vertex by the robot arm of EMUL. During these training, the motion data of subject's hand are observed with EMUL and the cortical activation data are observed with NIRS.The subjects participating in this experiment are 7 healthy adults. They have not excised with rehabilitation robots before. This measurement experimentation are performed at the Morinomiya hospital. Fig. 27 shows the experimental scene.

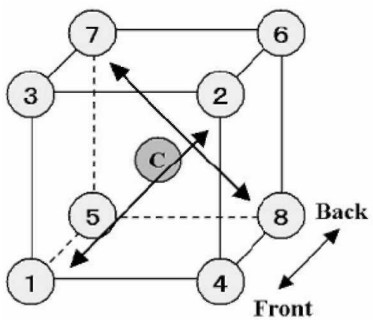

Fig. 25. Eight vertex reaching program

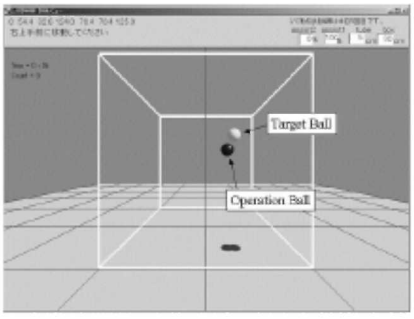

Fig. 26. Eight vertex reaching program (software)

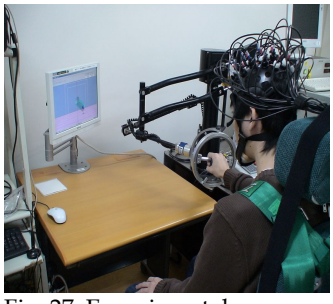

Fig. 27. Experimental scene using EMUL & NIRS.

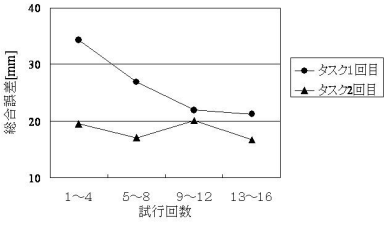

Fig. 28. Total Error

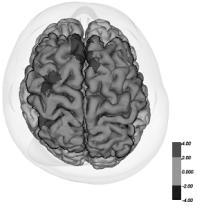

Fig. 29. Cortical activation data.

One of the motion data , for example, "Total Error", which is the distance between the target ball and the operation ball, is shown in Fig. 28. This index means the accuracy of tracking. Fig. 29 shows one of the cortical activation data of NIRS. The data are the average of all subjects' Oxygenated-Hemoglobin changes from 0 [sec] to 12 [sec] after beginning of the program. The area becomes the more red, it shows that area are more activated comparing with the condition during the rest time. The prefrontal cortex area and the premotor cortex

area had activated in the task-Al, however, that performance had calmed down after task-B. When comparing the data of task- Al and task-A2, there are significant differences at the left premotor cortex area and the medial prefrontal cortex area.

5. Quasi-3-DOF rehabilitation System "PLEMO"

5.1 Introduction

In general, therapists make the rehabilitation program based on an inspection and a measurement of each patient. However, it is difficult to adopt appropriate rehabilitation programs for all patients, because the evaluation method is based on experiences of each therapist. Recently, Evidence Based Medicine (EBM) is required strongly in the field of rehabilitation. Therefore robot-aided rehabilitation is expected to quantify the effect of rehabilitative activities. We developed 3-D rehabilitation system for upper limb "EMUL" and 6-DOF rehabilitation system "Robotherapist", and conducted clinical test with several kinds of video game. EMUL and Robotherapist adopted to use ER actuators and clutch mechanism for its actuation part. This mechanism makes these systems so safe and back-drivable. However, they have disadvantages in cost or ease of maintenance, because this system became enlarged to realize the force-feedback in large 3-D space. A system which is more compact and better for maintenance should be required for practical use. To meet the demands above, we developed new haptic device which has 2-DOF force-feedback function in working plane but its working plane can be adjusted the inclination. We named this system "Quasi-3-DOF Rehabilitation System for Upper Limbs" or "PLEMO" (shown in Fig. 30) (Kikuchi, Furusho, Jin et al., CME2007). PLEMO was developed to realize quantitative evaluation of the rehabilitation training for patients with spasticity after stroke. In this section, we describe the mechanism of PLEMO and its software for upper limb rehabilitation.

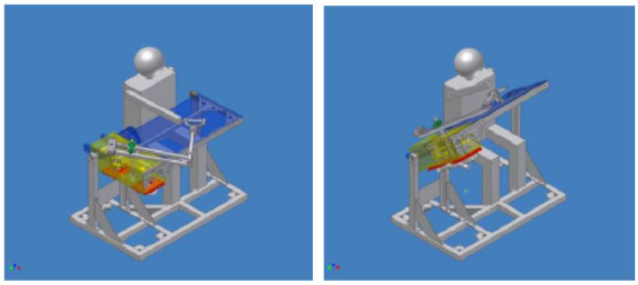

(a) Horizontal state (b) Slanted state

Fig. 30. Quasi-3-DOF rehabilitation system "PLEMO".

5.2 ER Brake

Using ER fluid as working fluid, we construct electrically controllable brake (ER brake) with high-performance (good rapidity and repeatability of brake torque) (Kikuchi, Furusho et al., 2003). We use this brake for the force generators of new rehabilitation system (forcefeedback system). Fig. 31 shows the sectional view and appearance of the brake. As shown in the left drawing of Fig. 31, this brake consists of multi-layered disks. ER fluid is filled between the

rotor-disks and stator-disks. As a result, six layers of ER fluid generate brake torque with the change of the fluid. Piston mechanism works for the prevention of liquid spill with thenexpansion of the fluid. We can control the brake torque form 0.1 [Nm] to 4.0 [Nm] with applied electric field from 0.0 [kV/mm] to 3.0 [kV/mm]. Additionally, response time of torque is several milliseconds.

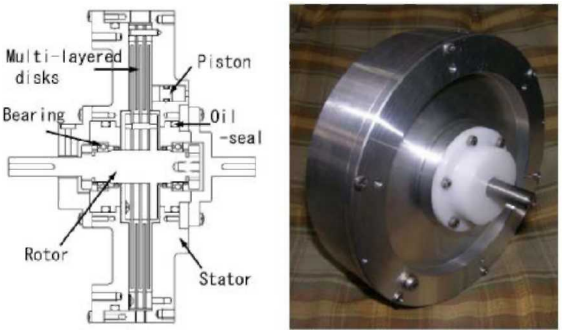

Fig. 31. ER Brake: sectional view (left) and picture (right).

Fig. 32 shows a passive force display using ER brakes (IEEE Virtual Reality 2001) in previous research (Furusho, Sakaguchi et al., 2002). In the research, we established control methods with a passive force display system on 2-D space. On the basis of this technology, we developed basic structure and control method of PLEMO.

Fig. 32. Passive force display using ER brakes (PLEMO-P-Prototype).

5.3 Quasi-3-DOF Rehabilitation System for Upper Limbs, "PLEMO"

Based on the technology of PLEMO-P-Prototype, we developed Ouasi-3D Rehabilitation System PLEMO-P series, PLEMO-P1,PLEMO-P2,PLEMO-P3 and so on. Fig. 33 shows the rehabilitation system of PLEMO-P3 (Furusho., Ozaw et al., 2009). The angle of working plane can be adjusted according to the rehabilitation program. We named this system "Quasi-3-DOF Rehabilitation System for Upper Limb" or "PLEMO". PLEMO is a combination of "pleasant" and "motivation". This word includes our hope that this system gives patents a pleasant experience of recovery and motivation for rehabilitation trainings. This system is safe for human because it use only brakes. Force control unit consist of the two ER brakes and the brake torque generates output-force on a handle by a parallel

linkage. Working area of PLEMO is 0.6 [m] (W) * 0.5 [m] (D). Adjustable angle of the inclination is from -30 to 90 degree. Plemo-Pl realizes from vertical training to horizontal training by only one system. Total size of the system is 1.0 [m] (W) * 0.6 [m] (D) * 0.7 [m] (H), except for the display. This is similar to the size of general desks. Not to use any actuator contributes to make this system more compact, simple, and reasonable for cost.
We developed new sensing device for detecting abnormal symptoms and aim to build an appropriate evaluation system for stroke patients with information of abnormal symptoms. Fig. 34 shows mechanisms of our former and current handle.

Fig. 33. PLEMO-P3

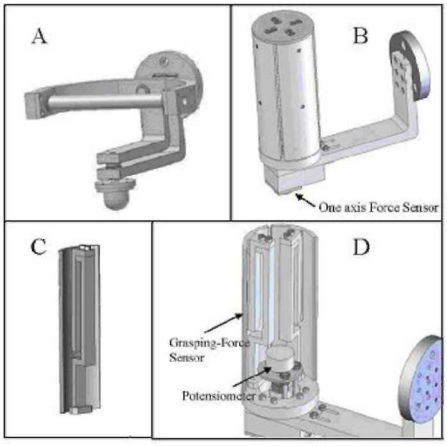

Fig. 34. Sensor grip device: (A) Former handle (passive gimbal), (B) Current handle (sensor grip), (C) A part of grip force sensor, (D) inner mechanism of the grip device

5.4 Software of PLEMO

We develop a rehabilitation software shown in Fig. 35. This is a tracking test program. An operator grips the handle and moves it to track a target ball. The position of operating handle is displayed as red sphere. The target ball is moving along the target track. White zone in this figure means smooth area without any force-feedback. Blue zone means sticky area; operator feels virtual force like moving his hand in the viscous fluid. It is easy to change kinds of the virtual forces and its area. Data of position, velocity and operating force are saved in the output files and we can evaluate accuracy of poison and velocity, range of motion, cognitive faculty and so on. We should make decision of the training protocol and evaluating method depending on the symptom of patient individually.

We have developed an evaluation program for reaching/pulling movements (Shown in Fig. 36(A); this software is similar to conventional 'reaching/pulling training'. Moreover, symptoms of patient's synergic movements can be detected during training. In this program, a patient is instructed to the position of target point (sphere shape in this figure) with each numbers in the monitor. The position of the hand is shown as the small white dot, which is moved depending on the movement of the end-effecter. The task starts when a patient operates his/her hand to the start position displayed as the yellow small dot in Fig. 36. The subjects are six stroke patients with different Brunnstrom stages and twenty-seven healthy volunteers. PLEMO was used to measure the moving features of the healthy subjects and stroke patients (Brunnstrom stage 3, 4, 5). The experimental results show big difference between the stroke patients and the healthy people. We construed the difference is based on the synergy movement of stroke. Now, we are trying to make an appropriate evaluation system of stroke patients based on these differences.

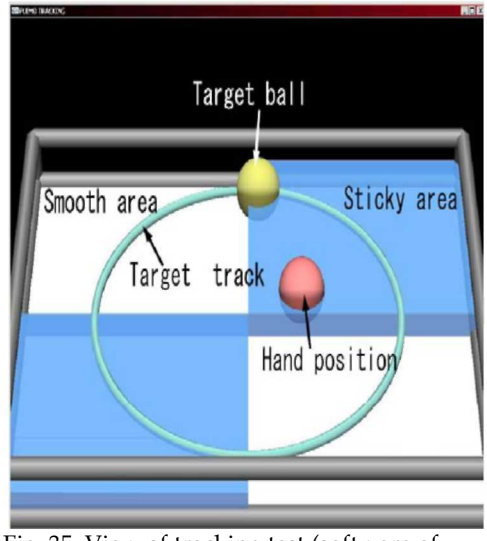

Fig. 35. View of tracking test (software of PLEMO-P1,PLEMO-P2,PLEMO-P3)

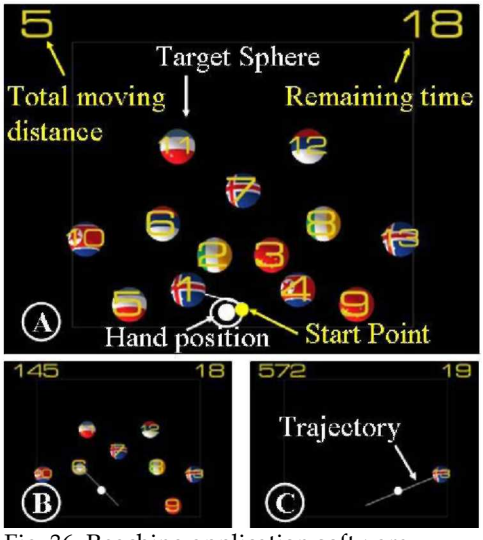

Fig. 36. Reaching application software (PLEMO-P3)

5.5 Hybrid-PLEMO (Jin , Kikuchi et al.,2008)

"Hybrid-PLEMO" is one type of PLEMO, which can switch active type and passive type (see Fig. 37). To generate haptic force on the end-effector, we use double-shaft ER Brake (shown in Fig. 38) as ER clutch. Fig. 39 shows the mechanism of Input parts of actuator box. In order to transmit forces from the Er clutches to the end-effector, we take direct-drive mechanism by using parallel linkage mechanism(shown in Fig. 40)

We suggest two types of reaching program with Hybrid-PLEMO system (shown in Fig. 41). search target trajectory with only force information and trace it. In active mode, PLEMO system generates outgoing- vector force of 5N from target trajectory. On the other hand, in passive mode, the system generates a distribution of resistant force (0N or 3N or 5N). The nearer to the target the hand position is, the stronger the resistance is. The start position was same (X = 0cm) in every experiment. The target changes its X position (X = -20, -10, 0, 10, 20cm) in a random manner. In order to evaluate simply the effect of force information, we hide any visual information on display. Fig. 42 show experimental results of same target position (X = 10cm) with active/passive mode. An operator is healthy person. Broken lines show the target trajectory, and black dots show the starting position of the handle. As shown in the left side of Fig. 42, operator can recognize the target position smoothly with active-type force guidance. On the other hand, as shown in the right side of Fig. 42, it took more time to recognize the target position with passive-type force guidance than active mode. The reason of this delay is thought that, in passive mode, the operator needs more time to understand the distribution of force field with his own motion, and recognize correct direction toward the target. In future works, we must clarify effects and roles of active / passive force feedback for human's sense, motion and rehabilitation.

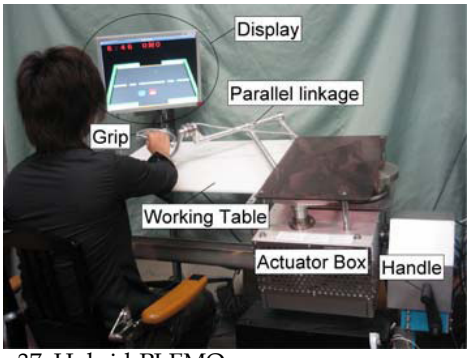

Fig. 37. Hybrid-PLEMO

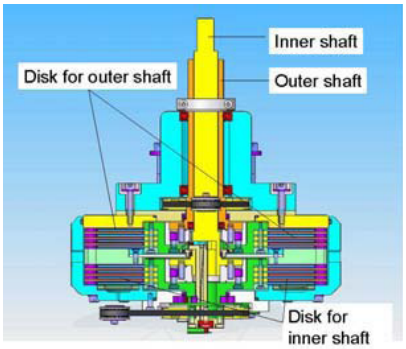

Fig. 38. Double-shaft ER brake/clutch

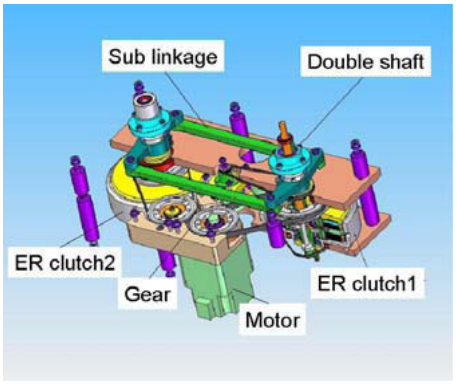

Fig. 39. Input parts of actuator box

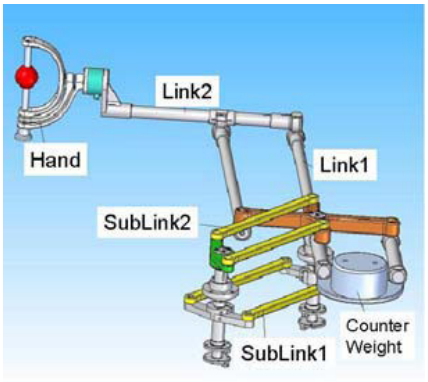

Fig. 40. Parallel linkage mechanism

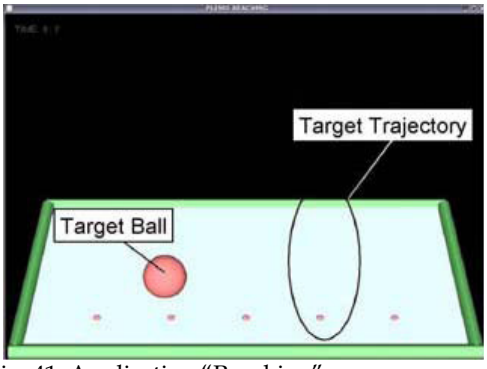

Fig. 41. Application "Reaching"

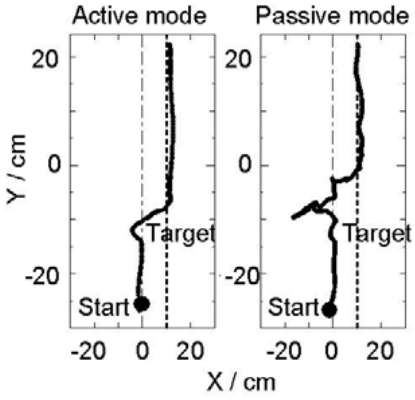

Fig. 42. Experimental Results

6. 2-DOF Passive-type force Display and Rehabilitation System with Redundant Brakes (Jin, Kikuchi et al., 2009)

6.1 Introduction

We have developed "Hybrid-PLEMO" system with another concept for safety. It has only 2-DOF force feedback function on working plane for downsizing and low-cost, its working plane can be adjusted the inclination, and it can be switched between active type and passive type.

However, there are some directions and link positions that are difficult to display the force when Hybrid-PLEMO works at passive type. To solve this problem, Davis and Book (Davis & Book, 1997) studied a passive manipulator with a redundant actuation scheme by using redundant electromagnetic brakes. However, the controllability and response time of electromagnetic brakes and power brakes are not good for using force display system. The various methodologies for performance evaluation of haptic device have been introduced through diverse researches (Lawrence & Chape, 1994 and Jinung & Kwon, 2002). However, there are no succinct performance evaluation methods that are common to any haptic

passive device with redundant brakes. In our study, a novel method is presented for performance evaluation of a passive-type force display system with redundant brakes. Using this method, we evaluate the performance of a 2-DOF passive-type force display system with and without redundant brakes. Experimental results show that it is good to add redundant brakes to the passive-type force display and rehabilitation system.

6.2 2-DOF Passive-type force Display & Rehabilitation System with Redundant Brakes

Fig. 43 shows the force display system with redundant couple of brakes (Koyanagi, Morita et al., 2005) (Furusho, Jin et al., 2009). It has three ER fluid brakes and one ER fluid clutch, i.e., it is a passive system with couple of redundant brakes.

All connections between brakes and links are by belt-pulley systems with timing belts (toothed belts). It has advantages in high power-transmitting ratio and little backlash. Link 1 (angle θ_1) and Link 2 (angle θ_2) are connected to ER fluid brake 1 and ER fluid brake 2 by belt-pulley respectively. Rotate angle of ER fluid brake 3 is θ_3 ($\theta_3 = \theta_1 + \theta_2$) and rotate angle of ER fluid clutch is θ_4 ($\theta_4 = -\theta_1 + \theta_2$).

The system has high-resolution encoders to detect the link posture or the handle position. The length of Link 1 and Link 3 is 0.25 [m]. The handle has a force sensor to detect the force from the operator. The size of the base part (excluding the links and the handle) is approximately 0.60x0.60x0.35 [m].

6.3 Performance Evaluation Method of Passive-Type Force Display and Rehabilitation System with Redundant Brakes

A: Definition of Lower bound angle a1 and upper bound angle a2 of resistance forcing angle

As shown in Fig. 44, let us consider resistance force that could be represented in the 2-DOF passive-type force display system. The hatching shows the range of resistance force when the velocity of handle is V. The opposite direction to the motion V' is assumed to be a standard direction of resistance force and anti-clockwise is assumed to be a positive direction. The forcing angle α is defined with the angle between resistance force and V'. The lower bound angle within the range of resistance forces is assumed to be a_1 and the upper bound angle is assumed to be $\alpha 2$. Obviously $\alpha 1 < \alpha 2$. The relationship between resistance forces and $\alpha 1$, $\alpha 2$ is shown in Table 4. Resistance force with two sides can be displayed only when $\alpha 1 < 0$ and $\alpha 2 > 0$. Moreover, the greater a difference between upper bound angle $\alpha 2$ and lower bound angle $\alpha 1$ is, the wider the range of resistance force that can be displayed is.

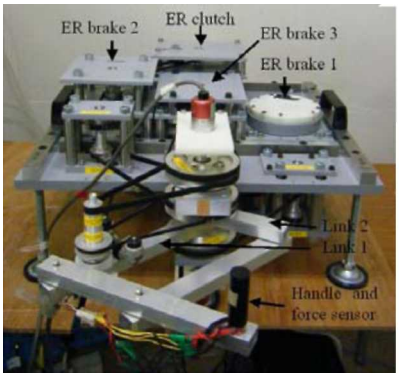

Fig. 43. 2-DOF passive-type force display system with redundant brakes.

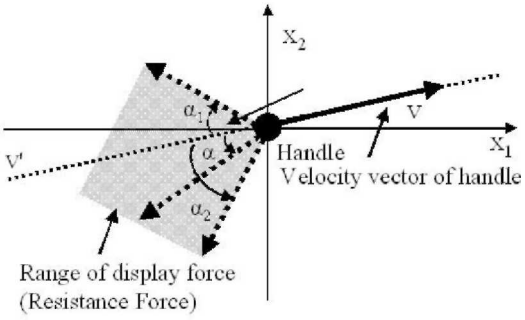

Fig. 44. Resistance force in 2-DOF passivetype force display system.

	$\alpha_2<0$	$\alpha_2>0$
$\alpha_1<0$	Resistance force with only one side can be displayed.	Resistance force with two sides can be displayed.
$\alpha_1>0$	NONE.	Resistance force with only one side can be displayed.

Table 4. Relation between Resistance Force and α_1, α_2

B: Performance Evaluation Method

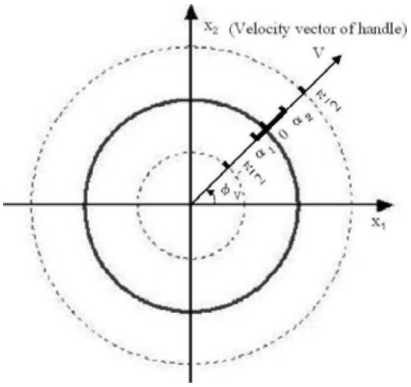

Fig. 45. Angle Graph of a_1, a_2.

Lower bound angle a_1 and upper bound angle a_2 is demonstrated in Fig. 45. Circle 0 means a =0 (radian), i.e., the direction 0 (radian) is the opposite direction to the motion (as shown in Fig. 45). Circle - $\pi/2$ and circle $\pi/2$ mean $a = \pi/2$ and $a = -\pi/2$ respectively, i.e., the direction

is vertical to the motion. Resistance force is drawn as the solid line, and the range of resistance force is between c_{ti} and a_2, i.e., a_2-a_i.

C: Simulation

1) ER fluid brake 1 and ER fluid brake 2 working without redundant brakes Fig. 46 shows the simulation results when handle is at the position of (0.0, 0.45). The opposite direction to the motion cannot be displayed with two side when handle is at the sections of A, B, C or D. Fig. 47 shows the simulation results when handle is at (0.1,0.25), (0.1,0.45), (-0.1,0.25), and (-0.1,0.45) respectively. We can see that it is impossible for resistance force to be displayed with two sides in all direction of handle.

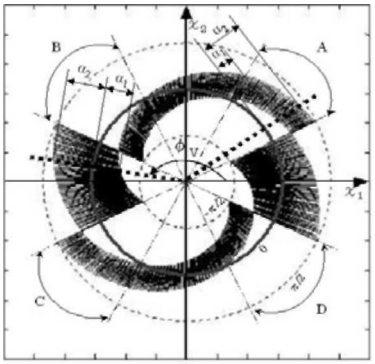

Fig. 46. Angle graphs(x_1=0m, x_2=0.45m;without redundant brake)

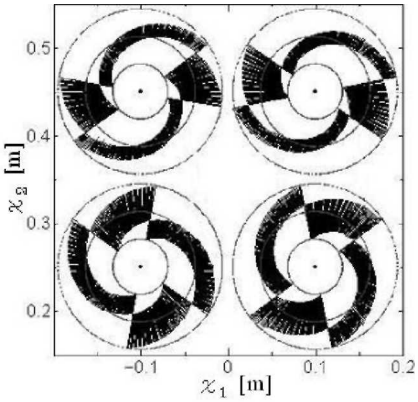

Fig. 47. Angle graphs (without redundant brake)

2) ER fluid brake 1 and ER fluid brake 2 working with redundant brake 3

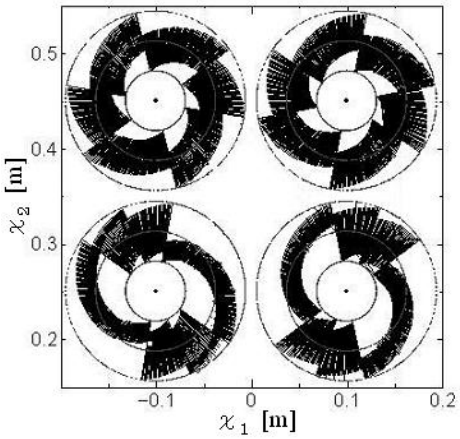

Fig. 48. Angle graphs (with one redundant brakes

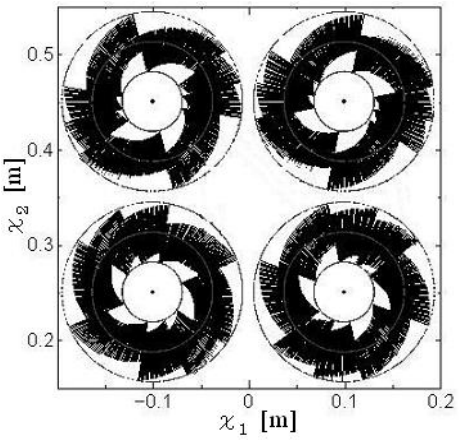

Fig. 49. Angle graphs (with two redundant brakes)

Fig. 48 shows the simulation results when handle is at (0.1,0.25), (0.1,0.45), (-0.1,0.25), and (-0.1,0.45) respectively. It is impossible for resistance force to be displayed with two sides in all direction of handle when handle is at the position of (-0.1,0.25), and (-0.1,0.45). ER fluid brake 1 and ER fluid brake 2 working with redundant ER fluid brake 3and ER fluid clutch
Fig. 49 shows the simulation results when handle is at (0.1,0.25), (0.1,0.45), (-0.1,0.25), and (-0.1,0.45). We can see that it is possible for resistance force to be displayed with two sides in all direction of handle when handle is at the position of (-0.1,0.25), and (-0.1,0.45), (-0.1,0.25), and (-0.1,0.45).

7. Isokinetic Exercise System Using High Performance MR Fluid Brake

7.1 Introduction

IN recent year, several kinds of training method, for example, "isometric", "isotonic", and "isokinetic" exercise are used in muscle strengthening training depending on the contractile types of their muscles (Verrill, Shoup et al., 1992).
In an isometric contraction, the angle of a joint is fixed, and the length of muscle is also fixed constantly. At specific angle of joint, subjects is required to generate their maximal muscle strength. In this type, we can measure maximal torque of muscles, but can not measure dynamic properties of them. On the other side, in the isotonic contraction, constant weights are loaded on the muscle. In this type, we can measure dynamic properties of muscles but can not measure maximal torque. In order to solve this problem, isokinetic exercise was suggested. We can measure maximal torque at any angle of joint dynamically, because in this method, subjects required to generate maximal torque during whole range of motion under the restriction of velocity with special training machine which can develop exact velocity control.
As mentioned above, we need the isokinetic exercise machine to develop exact isokinetic exercise. Conventionally, actuator-type (Bohannon, 1991 and Kelli & Baltzopoulos, 1996) was used in clinical field, but these system cost expensive depending on its actuation device (actuator is usually servomotor with high torque) and safety system.
In order to develop an isokinetic exercise machine with low-cost, high safety and high performance, we have developed isokinetic exercise machine using ER Fluid Brake (Furusho, Sakaguchi et al., 2002) (Kikuchi & Furusho, 2003). In this brake-type machine, driving force is generated from human itself, and velocity control is conducted with only braking torque of the controllable brake. We could reduce its inertia and realized very high speed isokinetic exercise at 800deg/s with this system. However, we had to change reduction ratio depending on the target velocity because of a loss of dynamic range of the ER Fluid Brake.
In this report, we describe development of isokinetic exercise system using a MR fluid brake. By the contribution of wide dynamic range of MR fluid brake, we can conduct wide range of the training velocity (from 0 to more than 800deg/s). At the same time, we can conduct the velocity control with high accuracy thanks to the high performance (time constant of torque is about 5 milliseconds) of the MRF brake.
Additionally, we suggest iso-contractile mode using this system. Basic idea of this mode and experimental result is presented at the end part of this section.

7.2 Muscle Exercise Machine Using Brake

A: MR Fluid

Magneto-Rheological (MR) fluid is a kind of functional fluids that are attracting much attention these days. This fluid is composite material of non-colloidal solution and magnetic metal particles (e.g., iron particles). The diameter of the particle is 1-10 micrometers. The fluid changes its apparent viscosity (a rheological characteristic) when a magnetic field is applied to it (Carlson & Jolly, 2000). The response of changing the viscosity is very rapid (about several milliseconds). The MR Fluid used in this study is MRF-132DG, which is developed by LORD Co., USA.

Fig. 50 shows how the shear stress changes with the shear rate as the magnetic field in the MR fluid. The fluid presents the characteristics of Newtonian fluid when no magnetic field is applied (H = 0), as shown by the dashed line in Fig. 50. When the magnetic field is applied (H # 0), the fluid has its viscosity greatly changed, presenting the characteristics of Bingham fluid, as shown by the solid line in Fig. 50. In particular, the shear stress is almost independent of the shear rate, but changes with the magnitude of the magnetic field. In other words, the magnetic field generates a force between two plates, which can be represented by a Coulomb friction model. Making use of this characteristic, we developed a brake and a clutch-type actuator (Takesue, Furusho, et al., 2004).

B: High Performance MR Fluid Brake (Kikuchi, Furusho et al., 2006) (Oda, Isozumi et al., 2009)

An MR Fluid Brake (or MRF brake) consists of discs with an output shaft, MR fluid (or MRF), electromagnetic coil, and a fixed cover as shown in Fig. 51. When a current is applied to the coil, the magnetic field is generated in the MRF, and then the viscosity of the fluid increases. This increase of viscosity generates the braking torque and reduces the rotational speed.

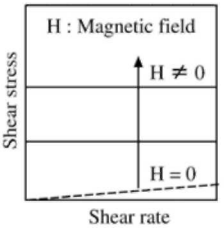

Fig. 50. Characteristics of MR fluid

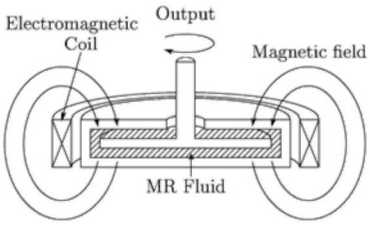

Fig. 51. Basic structure of MR fluid brake.

The MRF brake has high response because MRF has high response itself. Moreover, MRF brake has good back-drivability. In off-stage of the magnetic field, MRF brake generates little force because of the off-state characteristics of MR fluid.

In this study, four C- type yokes were built around the disc of the MRF brake. The coils were rolled around each yokes. The yokes became the main path of magnetic flux. However, when the magnetic flux density passing through the electric conductor changes, electromotive force is induced and the eddy current passes through the conductor. Due to the eddy current, a counter-magnetic field that opposes the change in flux is produced and the response becomes slower. The magnitude of eddy current depends on the width of the conductor as shown in Fig. 52. In order to reduce eddy current, we use the yoke that is laminated thin silicon steel sheets as shown in Fig. 53. Each sheet is insulated from others.

The structure and specification of the MRF brake are shown in Fig. 54 and Table 5, respectively.

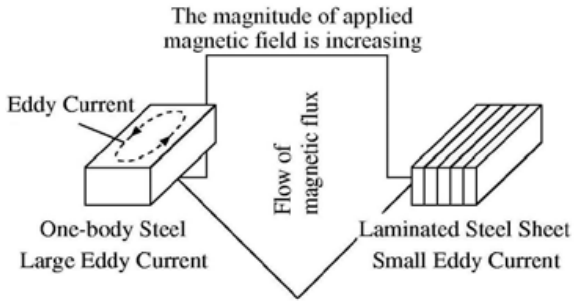

Fig. 52. Magnitude of eddy current depends on the width of conductor.

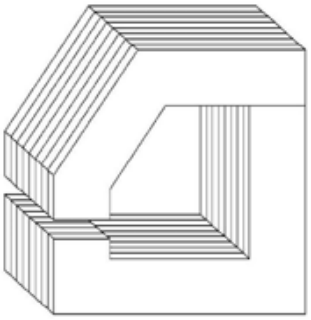

Fig. 53. C-Type yoke laminated silicon steel sheet.

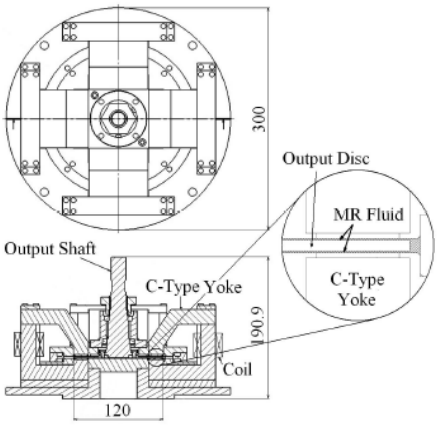

Fig. 54. Structure of MRF brake.

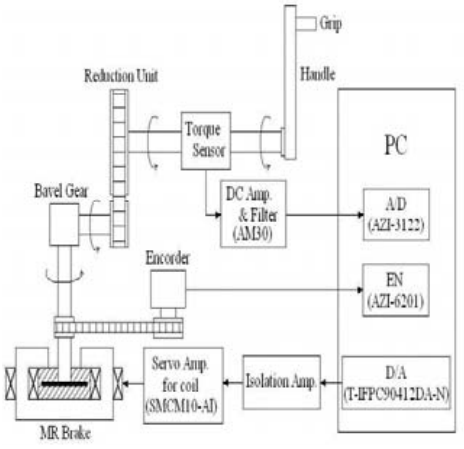

Fig. 55. Diagram of the training system.

Parameter	Value
Diameter of casing	300mm
Diameter of output disc	120mm
Height	190.9mm
Disc gap	0.4mm
Mass	26.4kg
Num. of yoke	4
Turn num. of coil	400turn
Max. input current	2A
Max. braking torque	27.5Nm (at 2A)

Table 5. Specification of MR Brake.

C: Muscle Exercise Machine Using MRF Brake

We have developed an isokinetic exercise system using an ERF brake (Kikuchi, Furusho et al., 2003). In this section, we develop an isokinetic exercise system using MRF brake. The diagram of the basic system is shown in Fig. 55, and shows its appearance. By using this system, isometric, isotonic and isokinetic exercises can be conducted. Moreover, at these exercises, we can conduct both directions, that are flexion or extension, for both hands; right or left.

As shown in Table 6, we can control the load of 27.5Nm directly using the MRF brake, but it will not be enough for whole range of training. Therefore we determined to install a reduction system between the brake and an operation section. The reduction system was designed using a belt-pulley mechanism. The reduction ratio of this system was decided as 1/4.41 to generate more than 90Nm. This goal was made based on the data of an average of 19-year-old men from a human-database (Shuppan, 1992).

This machine is very safe because any active device is not used for its velocity control. Driving force is generated from human itself, and rotational velocity is controlled with the braking torque of the MRF brake accurately. Specifications of the system are shown in Table 6.

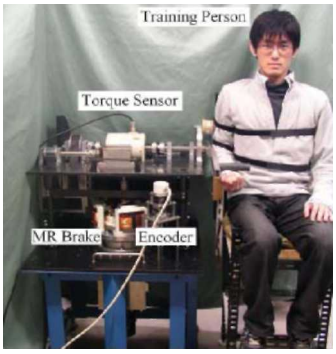

Fig. 56. Appearance of MEM-MRB.

Parameters	Definition
Reduction ratio	4.41
Max. breaking torque	120Nm
Training direction	Both(flexion, extension)
Training side of band	Both(right, left)

Table 6. Specification of the system

7.3 Characteristics on Isokinetic Mode

A: Motivation and theory

It is known that the relation called a force-velocity curve is established between the output force of a muscle and a joint velocity. The model drawing of the force-velocity curve is shown in Fig. 57.

The case of the zero joint velocity is called an "isometric contraction." In the isometric contraction, the joint is fixed but inside the muscle, muscle fibers are shortened and elastic sites such as a tendon are extended.
The case of the negative velocity of the joint while generating the force, that is to say, the state of the joint movement toward an opposite direction of the output force is called an "eccentric contraction." This corresponds to the negative zone of the velocity in Fig. 57. The maximum muscle force in the eccentric contraction is larger than the maximum muscle force in the isometric contraction, but forcing the joint to elongate leads to a rupture of the muscle fiber and a destruction of the joint.
On the other hand, the case of the positive velocity of the joint while generating the force, that is to say, the state of the joint movement toward the same direction with the direction of the output force is called a "concentric contraction." This corresponds to the positive zone of the velocity in Fig. 57. In the case of the concentric contraction, the output force decreases with the increase of the joint velocity and exceeding certain joint velocity leads to the zero output force. This curve under the concentric contraction is formulated by A.V.Hill (Hill, 1939) as:

$$V = b(P0 - P) / (P + a) \quad (1)$$

where P is the force, V is the velocity of a contraction of a muscle, P0 is the force at the isometric contraction, and a and b are parameters depending on each muscle. This equation is called "Hill's equation" or "Hill's curve".
As such a relationship holds between the output force of the muscle and the joint velocity, a quantitative evaluation is possible if the maximum output force of the muscle at each joint velocity could be measured under the isokinetic mode.

B: Control method

The control system for the isokinetic mode is shown in Fig. 58. PI controller was used for its velocity control. KP and KI mean a proportional gain [Nm's/rad] and an integral gain [Nm/rad], respectively, and G(s) means a transfer function of the controlled object (MRF brake). TO, TB, and ω mean an operation torque [Nm], the brake torque [Nm], and the angular velocity of elbow [rad/s], respectively.
The output torque acts toward only an opposite direction to the rotational direction, and if the operator gives enough torque during the training, the output torque direction required for the brake is an opposite direction of the rotational direction.

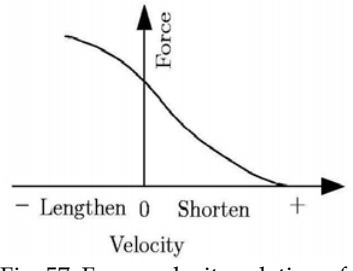

Fig. 57. Force-velocity relation of muscle.

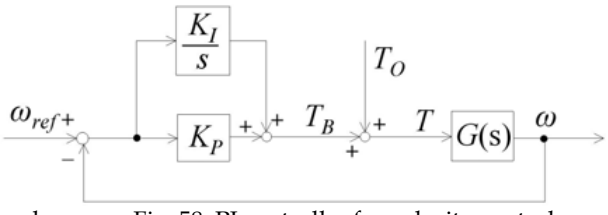

Fig. 58. PI controller for velocity control.

7.4 Suggestion for the Iso-contractile Mode

A: Motivation and Model

In conventional researches about the isokinetic exercise, only angular velocity of joints was controlled (or kept constant). But in basic experiments of muscles, for example Hill's experiments (Hill, 1939), the velocity-force relationship under the linear contraction have been measured. We have to control the linear contractile velocity of muscles if we want to reveal the real velocity-force relationship in vivo.

When we rotate a joint, several muscles work concurrently during its motion. At the same time, joint movements are generally complex because they include both of rolling action and sliding action. Therefore, it is difficult to control velocities of particular muscles with controls of single joints. However, if we focus on the elbow flexion, we can approximately control the contractile velocity of a biceps brachii muscle. The reasons are as follows:

(1) In the elbow flexion, three muscles (biceps brachii, brachialis and brachioradialis) work concurrently. However, the contraction force of the biceps brachii is overwhelmingly larger than others.

(2) Basically, the biceps brachii is a two-joint muscle corresponding to an elbow joint and a shoulder joint. However, if we fix the angle of the shoulder joint, the biceps brachii works as a one-joint muscle corresponding to only the elbow joint.

(3) Elbow joints are exactly single-axis joint without sliding actions

Due to these reasons, we can make a simple model of the elbow flexion as shown in Fig. 59. In this figure, 0 and a mean an elbow angle and an angular velocity of elbow, respectively. Additionally, L and r mean a length and lever arm of biceps brachii, respectively. Under this assumption, L and a can be calculated as following equations;

$$L = \sqrt{R^2 + r^2 - 2Rr\cos\theta} \tag{2}$$

$$\omega = \frac{-Rr\sin\theta}{\sqrt{R^2 + r^2 + 2Rr\cos\theta}} \frac{dL}{dt} \tag{3}$$

In conventional isokinetic exercises, a was kept constant with the velocity control of instruments. But we can control the contractile velocity of the biceps brachii muscle *(dL/dt)* with equation (3). We call this mode "iso-contractile" mode in this section.

B: Basic method for Iso-Contractile Control

Iso-contractile control can be simply conducted with the velocity control of our muscle exercise machine and a reference angular velocity curve which calculated from equation (3). Fig. 60 shows an example of the reference velocity curve of the constant contractile velocity of 200mm/s. In this case, R and r of Fig. 59 were set to 0.3m, 0.03m, respectively. A dashed line means a contractile velocity of the biceps brachii. As you see it, the contractile velocity is constant. On the other hand, a solid line means a reference velocity of the elbow joint. As you see in this line, the reference velocity becomes a concaved curve.

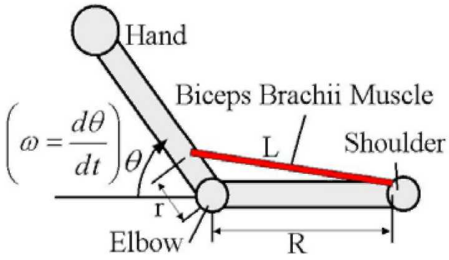

Fig. 59. Simple model of the elbow flexion.

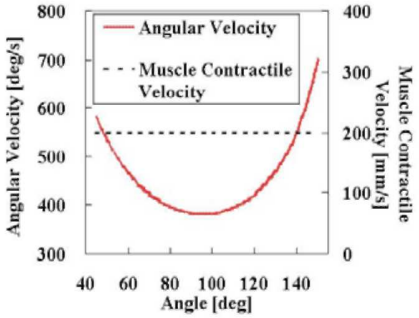

Fig. 60. Reference curve of angular velocity at the muscle contractile velocity of 200mm/s

8. Intelligently-Controlled Prosthetic Ankle Joint Using MR Fluid

We realized the first walking with kick action in biped robots using "BLR-G"(shown in Fig. 61) (Furush&Sano,1990). In this robot the ankle torque was sophisticatedly controlled. At present we are studying the control of ankle torque of prosthesis and orthosis.All prosthesis users need "foot" part. This part moves so frequently and widely that it needs to be as light as possible. It also must be silent and strong because it is used in daily life. If stiffness or spring characteristics of prosthesises can be changed according to the timing of walking and dorsiflection can be kept adequately, it will be much easier for users to walk and run. Now, shapes of prosthetic sockets have been improved and the range of actions of prosthesis has varied. Also, a lot of intelligent prosthetic knees have been developed and are sold on the market. But none of prosthesis that can control the ankle was on the market. Fig. 62 shows an example of a prosthetic "foot" part. It is composed of a prosthetic ankle joint and a foot-ankle unit. Energy of movement stored at the elastic part (rubber) of the prosthetic ankle joint is relieved when kicking, producing driving force. This rubber can also absorb shocks when the heel hits on the ground, and changing the angle smoothly. After kicking back, a leg leaves from the ground and swings forward during swing phase. Then the rubber goes back to its balanced midpoint, which makes the ankle turns instantly from the dorsal direction (deflecting a tiptoe upward, as shown in Fig. 62 (a)) to the plantar direction (swaging a tiptoe underneath, as shown in Fig. 62 (c)).

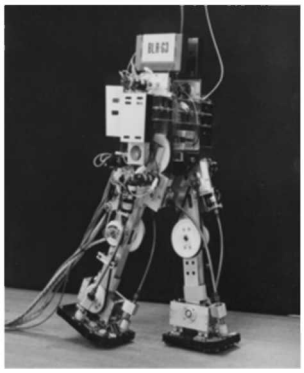

Fig. 61. Biped Locomotion Robot BLR-G

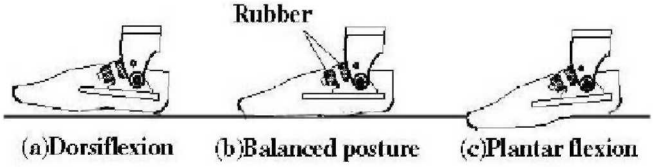

Fig. 62. Prosthetic foot.

Since there is a problem that the tiptoe of the prosthesis tends to collide on the ground (shown in Fig. 63), users have to walk paying attention to lifting legs in order not to tumble. This is why users walk unnaturally causing to use unnecessary energy. To solve this problem, we suggest setting a linear brake at "foot" part.

The MR (Magnetorheological) fluid has been used for the linear brakes. Fig. 64 shows a schematic of MR Linear Brake (MRLB). MRLB consists of a piston composed of two rods, a bobbin sandwiched by the rods on both sides, and MR fluid inside a cylinder. When electric current is applied to the coil which rolls the bobbin, magnetic field is generated in loops as follows; Bobbin^MR fluid^Cylinder^MR fluid ^Bobbin.

We developed two prototypes of the intelligent prosthetic ankle joint using MR brakes (Furusho, Takesue et al., 2004), (Li, Furusho et al., 2006), (Li, Tokuda, Furusho et al., 2006). Fig. 65 shows the 2nd prototypes. Fig. 66 and Fig. 67 show the series of static images extracted from moving images of the walking experiments. Circles around the ankle in these figures show the test subject's left leg (a swinging leg).

Fig. 63. Walking appearance of prosthetic foot during swing phase.

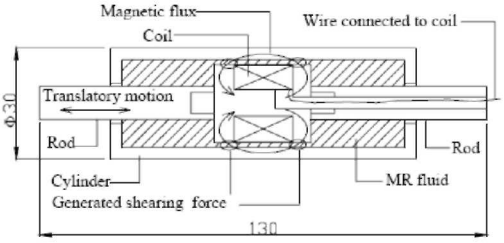

Fig. 64. Construction of MR Linear Brake.

Fig. 65. 2nd prototype.

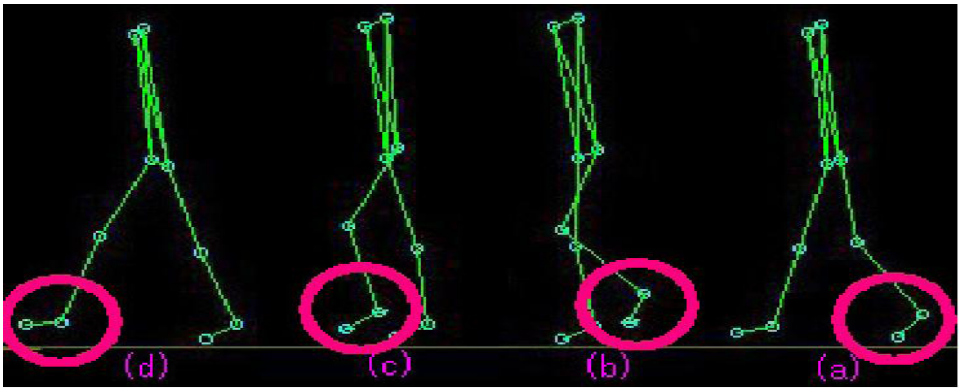

Fig. 66. Walking positions with brake control.

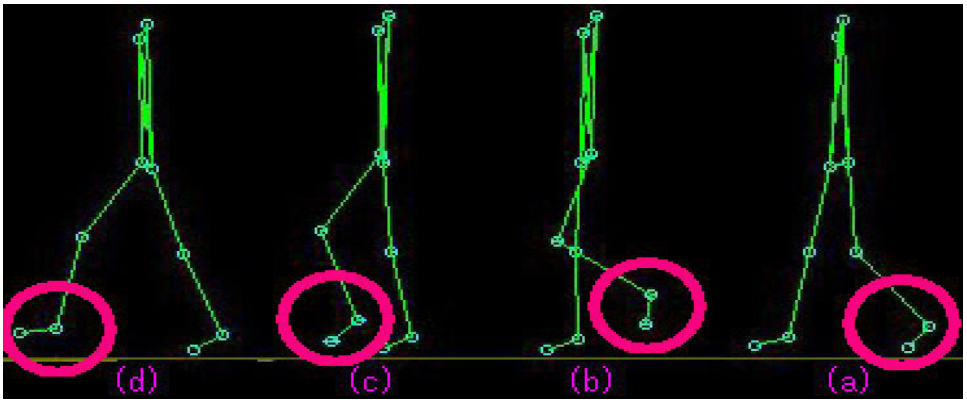

Fig. 67. Walking positions without brake control.

The subject's impressions of experiments with 2nd prototype are as follows: "I felt easier to walk by keeping dorsiflexion. I didn't care the total weight only for some hours, but if I use it in my daily life all day, it will be a load for me ".

9. Intelligent Ankle-Foot Orthosis with Shear-type MR Fluid Brake

Recently, as habits of people has changed, stroke patients tend to increase. There are many cases of the hemiplegia as aftereffects of a stroke. Stroke patient with hemiplegia show difference in the degree by a part and a range of a lesion caused by a disease, however rehabilitation is indispensable to restore functional disorder of lower limbs. We are developing intelligent ankle-foot orthoses using shear-type MR fluid brakes in a 3-year NEDO project (Furusho, Li et al., CME2007) (Furusho, Kikuchi et al., ICORR2007). Fig. 68 shows a conceptual illustration of shear-type MR fluid brakes. A coil rolled round a shaft give an MR fluid a magnetic field. Scroll number of coils and spindle diameter are decided by performing magnetic field analysis. As for materials of each part, magnetism materials are used in a magnetic circuit part. In addition, a housing is made of a nonmagnetic body, to avoid the magnetic flux from leaking.

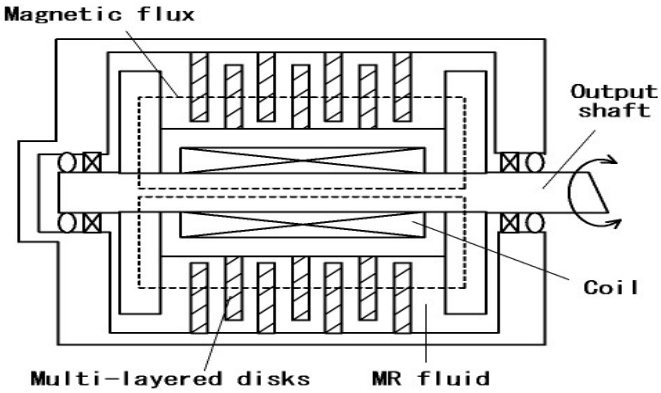

Fig. 68. Structure of MRB.

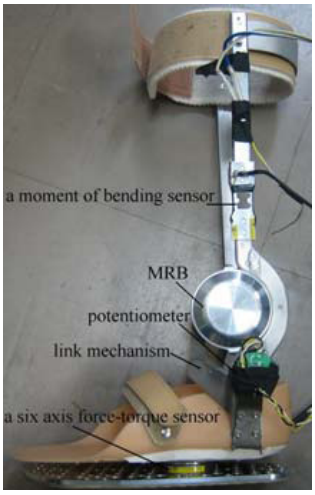

Fig. 69. Ankle-foot orthosis.

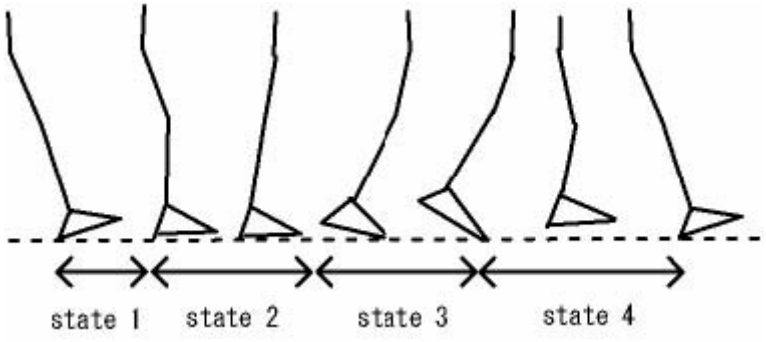

Fig. 70. Walking State.

Fig. 69 shows the second Prototype of intelligent ankle-foot orthosis using the shear-type MR fluid brake. We obtain the maximum torque of 24 [Nm] with the idling torque of 0.1[Nm]. We use four sensors: potentiometer on the ankle, 6-axis force-torque sensor at the center of a foot bottom, a moment of bending sensor and an acceleration sensor on the prop part of an orthosis side. We divide a walking step into four; into heel reaching the ground, tiptoe reaching the ground, heel leaving ground, tiptoe leaving ground (shown in Fig. 70). These states are detected by using the above sensors, and then the brake torque is controlled in accordance with each state.

10. Intelligently Controllable Ankle Foot Orthosis (I-AFO) and its application for a Patient of Guillain-Barre Syndrome

10.1 Introduction

LOCOMOTION is most important skill of the activity of daily living (ADL) for human. Therefore gait training is made a high priority in rehabilitative training.

Normal gait is cyclic and can be characterized by timing of foot contact with the ground; an entire sequence of functions by one limb is identified as a gait cycle (Cappozzo, 1984 and Inman, Ralston et al., 1981) (shown in Fig. 71). Each gait cycle has two basic components: "stance phase," which designates the duration of foot contact with the ground, and "swing phase," the period during which the foot is in the air for the purpose of limb advancement. The swing phase can be further divided into three functional subphases: "initial swing," "mid swing" and "terminal swing." In the same manner, the stance phase can be partitioned into five functional subphases: "initial contact," "loading response," "midstance," "terminal stance" and "preswing" (Bampton, 1979 and Esquenazi & Hirai, 1991). In the normal gait, initial contact becomes "initial contact (or heel-contact)," appropriately. And in the initial swing (or "toe-off"), normal subjects can keep appropriate clearance from the ground to prevent a malfunctional interaction with the ground. For patients who have dysfunction of ankles, for example hemiplegia, central nerve injury, polio or peroneal nerve palsy, it is difficult to control their ankle by themselves. This problem causes "equinus foot" or "drop foot", which are lacks of ankle dorsiflexion during the swing phase. In many case, they can not prevent from tripping their toe on even small steps on the ground. Additionally, they have a tendency to incline their body more than healthy persons because of the rough motion to prevent from stumbling of the toe. It causes undesired energy-loss in walking.

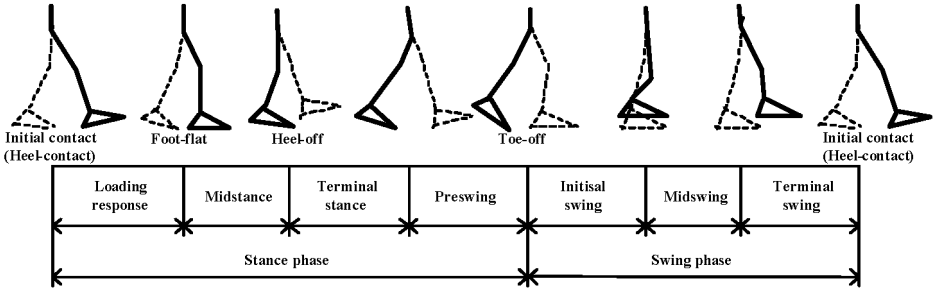

Fig. 71. Normal gait cycle.

An orthosis is defined as a device attached or applied to an external surface of a body to improve functions, restrict or enforce, or support a body segment (Redford, 1984). In order to improve the gait of the patients, lower limb orthoses are applied to them. In order to assist their ankle function, ankle-foot orthoses (AFOs) are often used to restrict their involuntary plantarflexion and so on.

Recently, powered AFOs have been focused on. Some kinds of the powered AFO were reported (Aaron & Hugh, 2007) by using several types of actuators, e.g. pneumatic actuation system (Keith & Daniel, 2007), ball screw drive system (Bashir & Arafat, 2006), series elastic actuator (Joaquin & Hugh, 2004), and so on.

In this study, we suggest the passive controllable AFO with a compact brake devise for a dynamic gait control. In particular, the control of drop-foot can be realized by only using passive devices. The passive controllable AFO also have a great advantage for cost, safety and downsizing. In our previous research (Furusho, Kikuchi et al., 2007), we developed some kinds of intelligently controlled AFO (I-AFO) which can control ankle torque with compact magneto-rheological fluid brakes (MRB) (Carlson & Jolly, 2000). In this paper, we describe the gait-control tests with the I-AFO for a patient of the Guillain-Barre syndrome.

10.2 Intelligently Controllable AFO (I-AFO)

A: Components of I-AFO

Fig. 72 (a) shows the I-AFO reported in the previous report (Furusho, Kikuchi et al., 2007). This I-AFO was developed for the gait control of hemiplegic patients. As shown in this picture, this AFO system has three types of sensing devices as follows;

(1) A potentiometer at the ankle position,
(2) A 6-axis force sensor under a sole,
(3) A bending moment sensor built in a brace.

This system has great advantage to measure several types of information during walking. In previous report, we detected the initial contact (heal contact) with the force (or torque) information. However, the weight of the total system exceeded 1.5kg, and lightening of the weight is strongly demanded for.

In order to lighten the weight, we improve the sensing system of the I-AFO shown in Fig. 72 (b). In the new sensing system, we detect the initial contact (or other states) with ON/ OFF-states information from two foot switches attached on the heel side and MP (metatarsophalangeal) joint of the sole (see Fig. 73). The reason why we attached a foot switch on the MP joint is because the subject always used the plastic orthosis that was cut out from MP joint to toe.

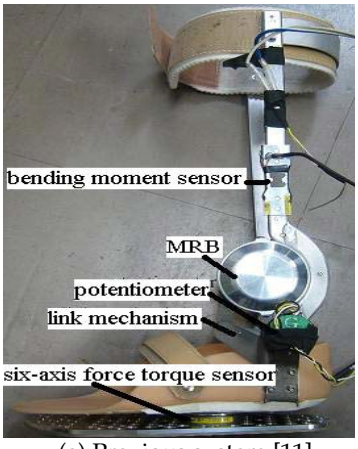

(a) Previous system [11]

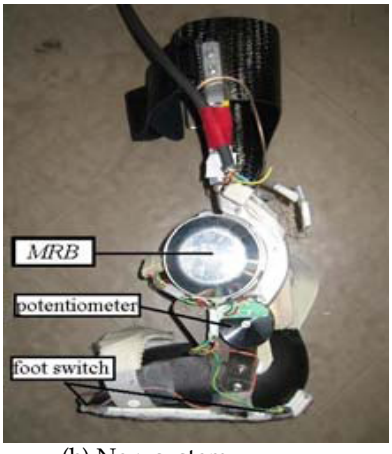

(b) New system

Fig. 72. I-AFO with a MR fluid brake.

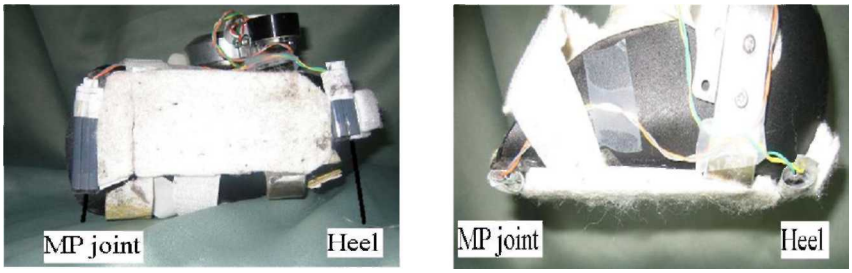

(a) Bottom view (b)Side view

Fig. 73. Foot switches for contact detection.

In this sensing system, we can not measure the force information, e.g. GRF (Ground Reaction Force) by itself. But in experiments, we measured GRF with a reaction force plate as mentioned at section 3. As result, the weight was decreased from 1.5kg to 1.1kg. Additionally, in the same way of the previous system, an ankle angle is measured with a potentiometer attached on the ankle joint and the ankle torque is controlled with MRB (MR brake). The maximum ankle torque is 12 Nm with applying the electric current of 1A.

B: Control System

Fig. 74 shows a picture and signal flow diagram of the control system of the I-AFO. A laptop computer attached with a multi-functional card (A/D and D/A) was used as a controller of this system. The braking torque was controlled by an electric current from a current amplifier in the circuit box. A reference signal to the current amplifier was outputted from the controller (laptop). The signals from tow types of sensors (a potentiometer and foot switches) ware inputted through the A/D card into the controller. The battery provided energy for the sensors and amplifier. Sampling frequency was 125[Hz].

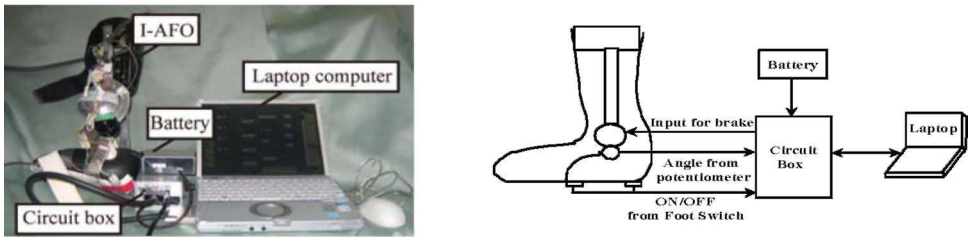

(a) Appearance (b) Signal flow diagram

Fig. 74. Control system for I-AFO.

C: Control Method

Main purposes of the control of the I-AFO are as follows:

(1) To prevent the drop foot in the swing phase and,
(2) To prevent a slap foot and a knee buckling at initial contact.

For convenience, we rename the phases of the gait cycle (shown in Fig. 71) for the control method as following four states;

(1) State 1: from initial contact (IC) to loading response (LR)
(2) State 2: from LR to terminal stance (TSt)
(3) State 3: from TSt to initial swing (ISw)

(4) State 4: from ISw to IC

Fig. 75 shows a flow diagram of the control method. In the Fig. 75, "MS" means the state of the foot switch on the MP joint and "HS" means the state of that on the heel side. The ON/OFF-states of the foot switches decide the state mentioned above. In a normal gait, control state will shift from "state 1" to "state 4" cyclically as shown in this figure. However, if a subject walks with an abnormal gait, it is possible to pass some states, for example directly changing from "state 2" to "state 4".

Fig. 76 shows a reference signal for the brake torque of the I-AFO corresponding to each state of Fig. 75. At the instant of the initial contact, MR brake generates rapid and strong torque to keep dorsiflexion. After that, the brake torque is gradually decreased during "state 1". In the "state 2", brake torque is not generated to facilitate smooth movement to forward direction. At the instant of the TSt, the brake generates its torque to keep dorsiflexion. And this torque is kept during "state 3" and "state 4".

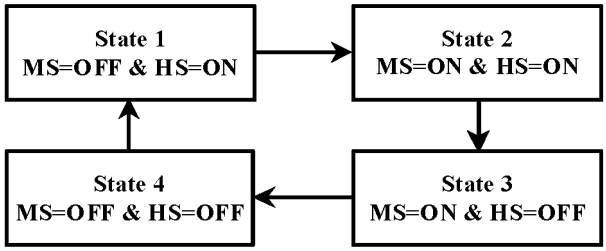

Fig. 75. Flow chart diagram for gait control (normal state)

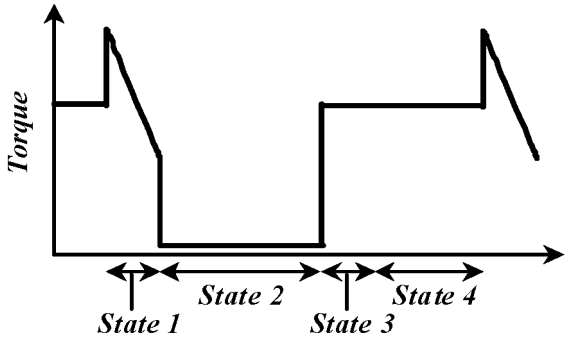

Fig. 76. Reference signal of brake torque.

10.3 Method

A: Subject

The subject was one male patient of the Guillain-Barre syndrome (height: 183.0cm, weight: 83.1kg). The subject has difficulty with voluntary movement of the peripheral part of the inferior limb, especially ankle joints and toes of both lower limbs. He attaches a plastic AFO in the daily life, for assisting functions of ankle joint. He shows the drop foot in walking. In addition, the disuse muscle atrophy is presented remarkably, too.

The ROM of the ankle joint of the plantar flexion is 45 degrees. That of the dorsiflexion is 0 degrees. He has restrictions of the dorsiflexion, especially.

B: Data collection

We made gait experiments on a flat floor and measured it with a three-dimensional movement analysis device (Video Locus 3D: Anima Co. Ltd. Japan) and a reaction force plate (MG2090: Anima Co. Ltd., Japan). The subject walked in three conditions: it is 1) a bare foot walk, 2) a walk with I-AFO (or "I-AFO walk"), 3) a walk with plastic orthosis (or "P-AFO walk"). In each condition, the subject performed it at normal walking speed (Walking cycle 1.30sec, Walking rate 92steps / min), fast speed (Walking cycle 1.03sec, Walking rate 116steps / min), and slow speed (Walking cycle 1.72sec, Walking rate 69steps / min). Walking cycle was adjusted with a metronome. Consequently, we measured with nine conditions in total. Before the measurements, the subject performs ambulatory exercise. The subject walked 5m from the 3 meter front of the reaction force plate with looking at the front naturally.

Fig. 77 shows the experimental environment. In this set, we installed two infrared cameras in the left side of the subject and captured a view from a sagittal plane. In addition, the reaction force plate was arranged to be put by only left foot. Furthermore, we photographed the gait using a digital video camera (DM - FM M20: Canon Co. Ltd., Japan) from his left side.

The markers for the three-dimensional movement analysis device were put on as shown in Fig. 78 and five markers were used for analyses; I) anterior superior iliac spine (marker 3), II) trochanter major (marker 4), III) knee joint fissure (marker 5), IV) lateral malleolus (marker 6) and V) basis ossis of the fifth metatarsalis (marker 7). We calculated hip joint angle from the infrared marker I), II), III) and knee joint angle from II), III), IV) and ankle joint angle from III), IV), V).

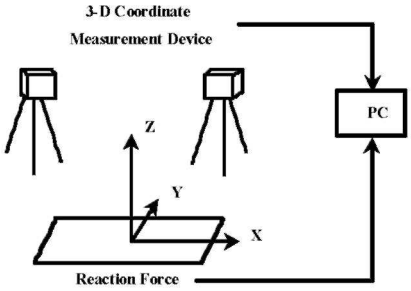

Fig. 77. Experimental environment

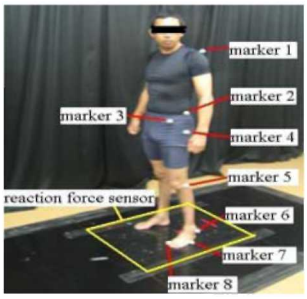

Fig. 78. Subject and markers

About the ethical consideration, we performed informed consent based on its form and managed the personal information severely.

11. Conclusion

High safety rehabilitation systems using functional fluid , Robotherapist and other rehabilitation system swere introduced. Robotherapist is a 6-dofrehabilitation system for upper limbs including wrists in the 2-year NEDO Project (2004-2005). EMUL were made in

the 5-year NEDO project, and they were transferred from NEDO to Furusho Laboratory of Osaka University. We continue clinical evaluation of 3-D rehabilitation system and quasi-3-DOF rehabilitation system by using EMUL, Robotherapist and PLEMO.
We have been studying rehabilitation robotics mainly from the standpoint of mechatronics and virtual reality. Hereafter, we would like to study it also from the standpoint of physical therapy and motion control of human beings.

12. References

Aaron M. Dollar, Hugh Herr. (2007). Active Orthoses for the Lower-Limbs: Challenges and State of the Art, Proceedings of the 2007 IEEE 10the International Conference on Rehabilitation Robotics, pp.968-977.

Akai H, Jin Y, Kikuchi T, Fukushima K and Furusho J (2008) ,Study on Development of Active-Passive Rehabilitation System for Upper Limbs, "Hybrid-PLEMO", Proceedings of The 7th International Conference on Machine Automation, pp.67-70.

Bampton S.(1979). A guide to the visual examination of pathological gait, Philadelphia, Temple University-Moss Rehabilitation Hospital.

Bashir M.Y. Nouri and Arafat Zaidan. (2006). Conputer control of a powered two degree freedom reciprocating gait orthosis, ISA Transaction, vol.45, No. 2, pp.249-258.

Bohannon, R.W. (1991). Correlation of knee extension force and torque with gait speed in patients with stroke, Physiotherapy Theory and Practice, Vol.7, No.3, pp.185-190.

Bossis, G. (2002). Ed., Proceedings of the eighth International conference on Electrorheological fluids and Magnetorheological Suspensions. World Scientific

Burgar, C. G. ; Lum, P.S. ; Shor, P. C. & der Loos, H. M. V. (2000). Development of robots for rehabilitation therapy : The palo alto va/ stanford experience, Jurnal of Rehabilitation Reseach and Development, Vol. 37, No.6, 663-673

Cappozzo A.(1984). Gait analysis methodology, Hum. Mov. Sci., vol.3, pp.27-50.

Carlson, J. D. and Jolly, M. R. (2000). MR fluid, foam and elastomer devices, Mechatronics, Vol.10, pp. 555-569.

Charles, S. ; Krebs, H. I. ; Volpe, B. T. ; Lynch, D. & Hogan, N. (2005). Wrist rehabilitation following stroke:Initial clinical results, Proceedings of the 2005 IEEE 9th International Conference on Rehabilitation Robotics, 13-16 D.A. Lawrence and J.D. Chapel. (1994). "Performance Trade-offs for Hand Controller Design" Proc. of the 1994 IEEE Conference on Robotics and Automation, San Diego, CA, pp. 3211-3216.

D.E.Voss, M.K.Ionta, B.J.Myers, "proprioceptive neuromuscular facilitation, patterns and techniques,'' Third Edition, Sedgwick Mead.

Demeurisse, G. et al. (1980). Motor evaluation in vascular hemiplegia, Eur, Neurol., Vol.19, 382-389 Fugel-Meyer A. R. et al. (1975). The post-stroke hemiplegic patient1, a method for evaluation of physical perpormance, Scand. J. Rahabil. Med., Vol.7, 13-31

Esquenazi A. and Hirai B.(1991). Assessment of gait and orthotic prescription, Phys Med Rehabil Clin North Am, vol.2, pp.473-485.

Fugl-Meyer A. R. et al., (1975), The post-stroke hemiplegic patient1, a method for evaluation of physical performance, Scand. J. Rahabil. Med., vol. 7, 13-31.

Furusho, J. & Kikuchi, T. (2006). Collaboration of medical engineering and fluid power (Review paper), Journal of the Japan Fluid Power System Society, Vol.37, No.5, 272276 (In Japanese)

Furusho, J. & Masubuchi, M. (1987). A theoretically motivated reduced order model for the control of biped locomotion, Trans. ASME, Journal of Dynamic Systems, Measurement and Control, Vol.109, 155-163

Furusho, J. & Sakaguchi, M. (1999). New actuators using ER fluid and their applications to force display devices in virtual reality and medical treatments, International Journal of Modern Physics B, Vol.13, No.14, 15 & 16, 2151-2159

Furusho, J. & Sano, A. (1990). Sensor-based control of a nine-link biped, The International Journal of Robotics Research, Vol.9, No.2, 83-98

Furusho, J. & Takesue, N. et al. (2004). Development of intelligent prosthetic ankle joint (1st report, development of linear-type MR-fluid brake), Transactions of the Japan Society of Mechanical Engineers (C), Vol.70, No.695, 275-282

Furusho, J. (2001). Mechatronics system using ER fluids (review paper), Journal of Japan Hydraulics and Pneumatic Society, Vol. 32, No .6, 390-395 (In Japanese)

Furusho, J.; Hu, X.; Kikuchi, T.; Nakayama, K.; Yamaguchi, Y.; Li, C.; Shichi, N.; Inoue, A. & Ryu, U. (2006). Development of a 6-DOF force display system using ER actuator with high-safety, Proceedings of the ACM International Conference on Virtual Reality Continuum and Its Applications 2006 (CD-ROM), 405-408

Furusho, J.; Jin, Y, Oda K, Haraguchi M, Kikuchi,T, Akai H, (2009)A Performance Evaluation Method of a Passive-Type Force Display and Rehabilitation System with Redundant Brakes, Proceedings of The 2009 IEEE 11th International Conference on Rehabilitation Robotics (in press).

Furusho, J.; Kikuchi, T., Tokuda .M.; Kakehashi, T.; Ikeda, K.; Morimoto, S.; Hashimoto,Y.; Tomiyama, H.; Nakagawa, A. & Akazawa, Y.(2007). Development of Shear Type Compact MR Brake for the Intelligent Ankle-Foot Orthosis and Its Control (Research and Development in NEDO for Practical Application of Human Support Robot), Proceedings of IEEE International Conference on Rehabilitation Robotics.

Furusho, J.; Kikuchi, T.; Oda, K.; Ohyama, Y.; Morita, T.; Shichi, N.; Jin, Y. & Inoue, A.(2007). A 6-DOF Rehabilitation Support System for Upper Limbs including Wrists "Robotherapist" with Physical Therapy, Proceedings of IEEE International Conference on Rehabilitation Robotics.

Furusho, J.; Koyanagi, K.; Imada, Y.; Fujii, Y.; Nakanishi, K.; Domen, K.; Miyakoshi, K. U. Ryu, S. Takenaka, A, Inoue. (2005). A 3-D Rehabilitation system for Upper Limbs Developed in a 5-year NEDO Project and its Clinical Testing, Proceedings of the 2005 IEEE 9th International Conference on Rehabilitation Robotics , 53-56

Furusho, J.; Koyanagi, K.; Kataoka, J. Ryu, U.; Inoue, A. & Takenaka, S. (2005). Development of 3-D rehabilitation system for upper limb -1st report: development of mechanism including ER actuators and whole system -, Journal of the Robotics Society of Japan, Vol.23, No.5, 629-636 (In Japanese)

Furusho, J.; Li, C.; Morimoto, S.; Tokuda, M.; Kikuchi, T. & Hashimoto, Y. (2007). Development of Shear-type MR Brakes and their Application to Ankle-Foot Orthoses, Proceedings of the International Conference on Complex Medical Engineering (CD-ROM), 1283-1287.

Furusho, J.; Sakaguchi, M.; Takesue, N. & Koyanagi, K. (2002). Development of ER brake A 6-DOF Rehabilitation System for Upper Limbs "Robotherapist" and Other Rehabilitation Systems with High Safety 39 and its application to passive force display, Journal of Intelligent Material Systems and Structures, Vol. 13, No. 7/8, 425-429

Furusho, J.; Wei, Z. & Koga, S. (1995). Development of an actuator with low inertia using electro-rheological fluid and its application to virtual reality, Proceeding of the 72nd JSME Spring Annual Meeting, Vol.4, 265-266

Furusho,J, Sakaguchi,M.and Takesue,N. (2002) Basic Study for Development of Muscular-Strength Estimation and Training System Using ER Brake, Journal of Robotics Society of Japan,Vol.20,No.1,pp.77-84

Furusho,J., Ozaw,T. & Kikuchi,T (2009). Study and Development of Quasi-3D Rehabilitation System for Upper Limbs "PLEMO-P3", Proc. of 46th Annual Meeting of the Japanese Association of Rehabilitation Medicine (in Press).

Gihodo Shuppan. (1992). The handbook of the characteristics value and equation on human engineering , pp.128-130,(in Japanese).

H. Davis and W. Book. (1997). "Torque control of a redundantly actuated passive type force manipulator," Proceeding of American Control Conference, pp.959-963.

Hill A.V. (1939). The heat of shortening and the dynamic constants of muscle. Proc. Roy. Soc. B. 126, pp.136-195.

Inman V., Ralston H. and Todd F.(1981). Human walking, Baltimore, Williams & Wilkins.

Ishikawa, T. (2000). Basic Study on the Development of a Rehabilitation Training System, Master's Thesis of Osaka Univesity.

ISO10218 (1992). Manipulating industrial robots-safty.

Jin Y, Kikuchi T, Fukushima K, Akai H, Furusho J (2008), Quasi-3DOF Active-Passive Hybrid Rehabilitation System for Upper Limbs "Hybrid-PLEMO", The Journal of the Japan Society of Mechanical Engineers, Vol.74, No.745, pp.2099-2106 (in Japanese).

Jin Y, Kikuchi T, Furusho J, Akai H (2009), A Basic Study on a Passive-Type Force Display System with Redundant Brakes (Performance Evaluation Methods and Force Display in Collision), The Journal of the Japan Fluid Power System Society （in Japanese）(in press).

Jinung An and Dong-Soo Kwon. (2002). Haptic Experimentation on a Hybrid Active/Passive Force Feedback Device, Proceedings of the 2002 IEEE International Conference on Robotics Automation,pp4218-4222

Joaquin A. Blaya and Hugh Herr. (2004). Adaptive Control of a Variable-Impedance Ankle-Foot Orthosis to Assist Drop-Foot Gait, IEEE Transactions on Neural Systems and Rehabilitation Engineering, vol.12, No.1, pp.24-31.

K. Koyanagi, T. Morita and J. Furusho. (2005). "Basic Algorithm of Controlling Passive Force Display System with Redundant Brakes", Proceedings of the 2005 IEEE International Conference on Robotics & Automation, pp.1767-1772.

Keith E. Gordon and Daniel P. Ferris. (2007). Learning to walk with a robotic ankle exoskeleton, Journal of Biomechanics, vol.40, pp.2636-2644.

Kelli, E. and Baltzopoulos, V. (1996). Agonist and antagonist moment and EMB-angle relationship during isokinetic eccentric and concentric exercise, Isokinetics and Exercise Science, Vol.6, No.2, pp.79-87.

Kikuchi, T. Furusho, J., and Oda K. (2003). Development of Isokinetic Exercise Machine Using ER Brake, Proceedings of the 2003 IEEE International Conference on Robotics & Automation, pp.214-219.

Kikuchi, T., Furusho, J., Yamaguchi, Y. and Kimura, S.(2006). Design of the highperformance MR brake and its characteristics, Proceedings of the 10th International Conference on ER Fluids and MR Suspensions, p667-673.

Kikuchi, T.; Furusho, J.; Jin, Y.; Hu, X.; Fukushima, K. & Inoue, A. (2007). Development of the quasi-3-DOF rehabilitation system for upper limbs, "PLEMO", The Japanese Journal for Medical Virtual Reality, Vol.5, No.1, 24-31

Krebs, H. I.; Volpe, B. T.; Aisen, M. L. & Hogan, N. (2000). Increasing productivity and quality of care : Robot-aided neuro rehabilitation, Jurnal of Rehabilitation Research and Development, Vol. 37, No.6, 639-652

Li C. & Furusho, J. et al. (2006) Developement of intelligent prosthetic ankle joint (2nd report, development of the 1st prototype with intelligent prosthetic ankle joint), Transactions of the Japan Society of Mechanical Engineers (C), Vol.72, No.714, 493-498

Li, C.; Miwa, T.; Furusho, J.; Morimoto, S.; Koyanagi, K.; Nakagawa, A.; Akazawa, Y. & Hashimoto, Y. (2006). Research and developement of the intelligently-controlled prosthetic ankle joint, Proceedings of 2006 IEEE International Conference on Mechatronics and Automation, 1114-1119

Miyakoshi K, Domen K, Koyama T, Furusho J, and Koyanagi K (2006), The effect of Robotaided training on motor recovery following stroke, The Japanese Journal of Rehabilitation Medicine, vol.43, No.6, 47-352.

Oda K, Isozumi S, Ohyama Y, Tamida K, Kikuchi T, Furusho J(2009), Development of Isokinetic and Iso-contractile Exercise Machine "MEM-MRB" Using MR Brake, Proceedings of The 2009 IEEE 11th International Conference on Rehabilitation Robotics (in press).

Redford JB. (1984). "Orthoses," In: Basmajian JV., and Kirby RL., eds., Medical rehabilitation, Baltimore, Williams & Wilkins, pp.101.

Sakaguchi, M.; Furusho, J. & Genda, E. (1999). Basic study in rehabilitation training system using ER actuators, Proceeding of 1999 IEEE International Conference on Systems, Man, and Cybernetics, 135-140 (in Japanese)

T. Flash and N. Hogan (1985). "The Coordination of Arm Movements: An Experimentally Confirmed Mathematical Model", the Journal of Neurosciecne, Vol.5, No.7, pp.1688-1703.

Takesue, N., Furusho, J. and Kiyota, Y.(2004). Fast Response MR-Fluid Actuator, JSME International Journal, Series C, Vol.47, No.3, pp.783-791.

Verrill, D., Shoup, E., McElveen, G., Witt, K. and Bergey, D.(1992).Resistive Exercise Training in Cardiac Patients (Review Article), Sports Medicine, Vol.13, No.3, pp.171-193.